(12) INTERNATIONAL APPLICATION PUBLISHED UNDER THE PATENT COOPERATION TREATY (PCT)

(19) World Intellectual Property Organization
International Bureau

(43) International Publication Date
27 February 2025 (27.02.2025)

WIPO | PCT

(10) International Publication Number
WO 2025/040887 A1

(51) International Patent Classification:
A61K 47/54 (2017.01) *C12Q 1/68* (2018.01)
B82Y 5/00 (2011.01) *C12Q 1/6869* (2018.01)
B82Y 10/00 (2011.01) *G06N 3/00* (2023.01)
C07D 401/14 (2006.01)

(21) International Application Number:
PCT/GB2024/052165

(22) International Filing Date:
16 August 2024 (16.08.2024)

(25) Filing Language: English

(26) Publication Language: English

(30) Priority Data:
2312709.5 18 August 2023 (18.08.2023) GB

(71) Applicant: **OXFORD UNIVERSITY INNOVATION LIMITED** [GB/GB]; Buxton Court, 3 West Way, Oxford Oxfordshire OX2 0JB (GB).

(72) Inventors: **WANG, Xingzao**; Chemistry Research Laboratory, 12 Mansfield Road, Oxford Oxfordshire OX1 3TA (GB). **QING, Yujia**; Chemistry Research Laboratory, 12 Mansfield Road, Oxford Oxfordshire OX1 3TA (GB). **BAYLEY, Hagan**; Chemistry Research Laboratory, 12 Mansfield Road, Oxford Oxfordshire OX1 3TA (GB).

(74) Agent: **J A KEMP LLP**; 80 Turnmill Street, London Greater London EC1M 5QU (GB).

(81) Designated States *(unless otherwise indicated, for every kind of national protection available)*: AE, AG, AL, AM, AO, AT, AU, AZ, BA, BB, BG, BH, BN, BR, BW, BY, BZ, CA, CH, CL, CN, CO, CR, CU, CV, CZ, DE, DJ, DK, DM, DO, DZ, EC, EE, EG, ES, FI, GB, GD, GE, GH, GM, GT, HN, HR, HU, ID, IL, IN, IQ, IR, IS, IT, JM, JO, JP, KE, KG, KH, KN, KP, KR, KW, KZ, LA, LC, LK, LR, LS, LU, LY, MA, MD, MG, MK, MN, MU, MW, MX, MY, MZ, NA, NG, NI, NO, NZ, OM, PA, PE, PG, PH, PL, PT, QA, RO, RS, RU, RW, SA, SC, SD, SE, SG, SK, SL, ST, SV, SY, TH, TJ, TM, TN, TR, TT, TZ, UA, UG, US, UZ, VC, VN, WS, ZA, ZM, ZW.

(84) Designated States *(unless otherwise indicated, for every kind of regional protection available)*: ARIPO (BW, CV, GH, GM, KE, LR, LS, MW, MZ, NA, RW, SC, SD, SL, ST, SZ, TZ, UG, ZM, ZW), Eurasian (AM, AZ, BY, KG, KZ, RU, TJ, TM), European (AL, AT, BE, BG, CH, CY, CZ, DE, DK, EE, ES, FI, FR, GB, GR, HR, HU, IE, IS, IT, LT, LU, LV, MC, ME, MK, MT, NL, NO, PL, PT, RO, RS, SE, SI, SK, SM, TR), OAPI (BF, BJ, CF, CG, CI, CM, GA, GN, GQ, GW, KM, ML, MR, NE, SN, TD, TG).

(54) Title: NANOPORE

Fig. 1

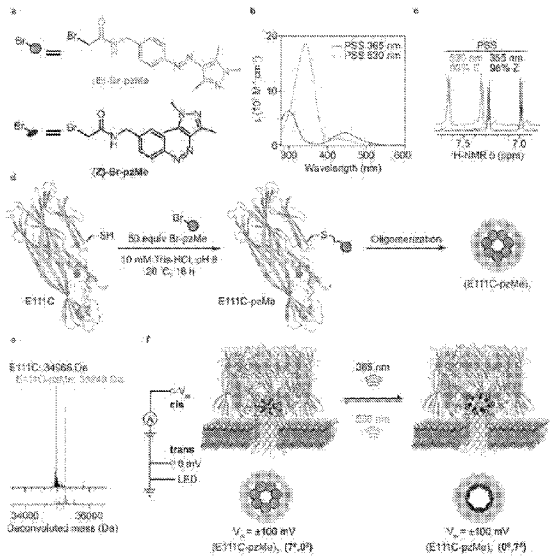

(57) Abstract: Described is a nanopore that is selectively convertible between an open form and a closed form using light, a method for producing such a nanopore, a method of modulating the flow of one or more substances through the nanopore, the use of the nanopore in modulating ionic flow across an amphiphilic membrane, a device comprising the nanopore, use of the nanopore as an ionotronic component, use of the nanopore in bio-computation and/or bioionotronics, a method of transmitting information using the nanopore, and method of receiving information comprising the nanopore, and an ionotronic component comprising the nanopore.

WO 2025/040887 A1

[Continued on next page]

Published:
— *with international search report (Art. 21(3))*
— *with sequence listing part of description (Rule 5.2(a))*

NANOPORE

Field

The present disclosure relates to a nanopore that is selectively convertible between an open form and a closed form using light, a method for producing such a nanopore, a method of modulating the flow of one or more substances through the nanopore, the use of the nanopore in modulating ionic flow across an amphiphilic membrane, a device comprising the nanopore, use of the nanopore as an ionotronic component, use of the nanopore in bio-computation and/or bioionotronics, a method of transmitting information using the nanopore, and method of receiving information comprising the nanopore, and an ionotronic component comprising the nanopore. The present disclosure also provides kits suitable for providing the nanopores of the invention, a protein particularly amenable to functionalisation (for instance, with one or more photoisomerisable groups), the use of the nanopore in drug delivery, a transmitter comprising the nanopore and a receiver comprising the nanopore.

Background

Molecular tools for the remote modulation of transmembrane ionic communication are widely utilized in biomedical sciences. Among them, optically active tools have garnered attention because of their advantageous features, including spatiotemporal control, reversibility, minimal invasiveness, and multiplexing capability.
Light-controlled ion flux across membranes is usually mediated by photoswitchable chromophores, being membrane-embedded or protein-bound. Proteinaceous light-gated ion transporters, such as microbial rhodopsins, generate or dissipate electrochemical gradient when their cognate chromophores (e.g., all-trans retinal) are activated by light. This enables the regulation of the electrical activity of rhodopsin-expressing cells in vitro and in vivo, which allows basic biological activities, such as calcium signalling and neuronal firing, to be dissected or manipulated. These optogenetic tools also function as integrable parts of bioelectronic systems with therapeutic potentials, such as cardiac arrhythmia or vision restorage. In parallel, synthetic alternatives have been devised to recapitulate the light-activating passive ion transportation, either directly or indirectly. Macromolecular ion transporters, activated by built-in photoswitches (e.g., azobenzene), move ions down the

gradient to offer therapeutic potential for channelopathies. Similarly, synthetic photochromic binders have been developed as photopharmacological drugs targeting ligand-gated ionotropic receptors, such as potassium channel, TRPV, and GABA, to adjust ionic signalling.

In bottom-up synthetic biology, naturally occurring ion transporters (e.g., rhodopsins) have been reconstituted into artificial membranes for optical control over ion flux. Care must be taken in selecting protein constructs activatable by the desired wavelength, promoting directional insertion into the bilayer, and providing continuous irradiation to achieve sustained ion-conducting effects for diverse applications. Light-activating protein nanopores represent an alternative class of optical tools, featuring robust channel-forming ability upon engineering, the ease of handling soluble monomers, and the potential for controlled molecular transmission. Previous studies have focused on engineering α-hemolysin (αHL) and fragaceatoxin C (FraC) monomers with photo-cages, which, upon prolonged UV irradiation (~10-30 minutes), release to trigger irreversible channel formation for permanently activated ionic signalling.

As such there remains a need to provide nanopores that may be reversibly activated by light. In particular, there is a need to provide photoreversible ON-OFF nanopores (such as protein nanopores) that are able to control ionic flow with a low background current in the OFF state and a long channel lifetime in the ON state.

Summary

The disclosure relates to a nanopore that is selectively convertible between an open form and a closed form using light. Such a nanopores may be termed a “photopores”. Preferably, the nanopores have one or more photoisomerisable groups (“photoswitches”) within the lumen of the nanopore. The photoisomerisable groups have desirable photostationary properties, enabling the nanopore (or “photopore”) to demonstrate diode-like or resistor-like behaviour under light control.

By way of summary, the present inventors have developed nanopores that are selectively convertible between an open form and a closed form using light. Nanopores of the invention provide:

- excellent photoreversibility (exhibiting robust switching over tens of cycles)
- a useful spectral working range (Switch ON: 365 nm; Switch OFF: 455 or 530 nm)

- excellent resistance to photobleaching (photoswitching lasts for hours under irradiation)
- good lifetime properties (for example, a preferred nanopore of the invention having a diazene photoisomerisable group provides an E isomer lifetime of more than a day for (7E,0Z))
- a good response time of switching (e.g. around 1 s with 30 mW/cm^2 irradiation)
- excellent current control (under reverse bias, the photopore can gate 95% current). Current gating = 1 − (I530nm − I365nm)

Further beneficial properties of specific nanopores according to the invention are:

• Photopore at 530 nm is a diode and it is a resistor at 365 nm.
• Photopore is compatible ion flow of concentration gradient.
• Photoswitching is compatible with synthetic tissue.
• Photopore can be used as a biotronic logic component.

Thus, the present invention is a nanopore that is selectively convertible between an open form and a closed form using light. Thus, the nanopore of the invention may be converted, using light, between a form that permits the flow of one or more substances through the nanopore (open form), and a form in which the one or more substances are restricted from being able to move though the nanopore (closed form). Preferably, the closed form (i.e. form in which the one or more substances are restricted from being able to move though the nanopore) restricts the flow of the one or more substances, relative to the flow of the one or more substances though the open form, by 10% or more, such as 20% or more, 30% or more, 40% or more, 50% or more, 60% or more, 70% or more. In a preferred embodiment, when the nanopore is in the closed form, substantially no substances are able to move through the nanopore, meaning that the closed form (i.e. form in which the one or more substances are restricted from being able to move though the nanopore) restricts the flow of the one or more substances, relative to the flow of the one or more substances though the open form by 80% or more, preferably by 90% or more, preferably 95% or more, more preferably still by 99% or more. Most preferably, the closed form (i.e. form in which the one or more substances are restricted from being able to move though the nanopore) restricts the flow of the one or more substances, relative to the flow of the one or more substances though the open form, by 100%. Said another way,

most preferably, when the nanopore is in the closed form, no substances are able to move through the nanopore.

Accordingly, provided herein is a photoactivatable nanopore or ion channel which is capable of being switched between an active state and an inactive state by application of light. In one embodiment the active state is an open state. In the open state the nanopore or ion channel is wholly or substantially open. In one embodiment the inactive state a closed state. In the closed state the nanopore or ion channel is wholly or substantially closed. An open pore is typically capable of operably bridging between two compartments such that one or more chemical species can pass between the compartments through the pore. A closed pore may be used to insulate between the two compartments, and typically does not allow one or more chemical species can pass between the compartments through the pore

Typically, the nanopore has one or more photoisomerisable groups within the lumen of the nanopore, wherein the one or more photoisomerisable groups are each independently groups of formula (I):

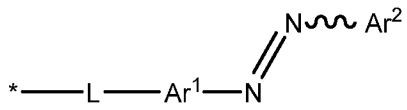

(I)

wherein:

* denotes the point of attachment to the nanopore;

L is a linker; and

Ar^1 and Ar^2 are each independently selected from an optionally-substituted aryl group and an optionally substituted heteroaryl group. Preferably, at least one of Ar^1 and Ar^2 is an optionally substituted heteroaryl group.

Most preferably, the one or more photoisomerisable groups are each independently groups of chemical formula (IC):

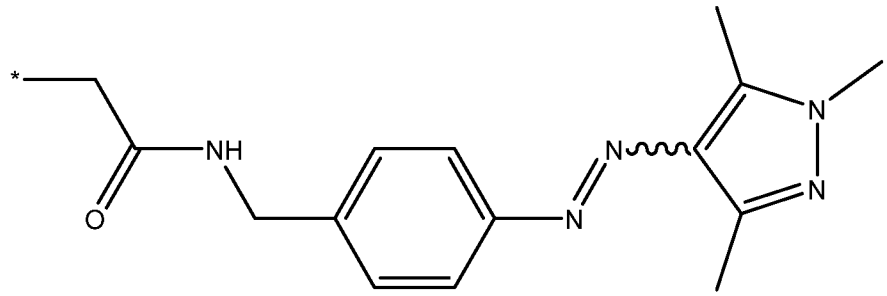

(IC)

wherein:

* denotes the point of attachment to the nanopore.

Preferably, the nanopore is a transmembrane protein pore that is an alpha hemolysin (αHL) pore, preferably an αHL pore formed of seven αHL monomers. Most preferably, the αHL pore comprises a E111C substitution.

The present invention also provides a method for producing the nanopore according to the invention, the method comprising introducing one or more photoisomerisable groups into a nanopore.

The present invention also provides a method for modulating the flow of one or more substances through a nanopore according to the invention, the method comprising irradiating the nanopore with light. Most preferably, the or more substances are ions.

The present invention also provides the use of a nanopore according to the invention in modulating ionic flow across an amphiphilic membrane.

The present invention also provides a device comprising an amphiphilic membrane-enclosed vesicle, wherein the vesicle lumen contains one or more pharmaceutical agents and wherein the amphiphilic membrane contains a nanopore according to the invention.

The present invention also provides the use of the nanopore according to the invention as an iontronic component photoswitchable between a resistor and diode.

The present invention also provides the use of the nanopore according the invention in bio-computation and/or bioiontronics.

The present invention also provides a method of transmitting information, the method comprising:

irradiating the nanopore according to the invention with a plurality of pulses of light, each pulse comprising light having one of a predetermined set of wavelengths.

The present invention also provides a method of receiving information, the method comprising:

measuring an ionic current through the nanopore according to the invention during irradiating of the nanopore with a plurality of pulses of light, each pulse comprising light having one of a predetermined set of wavelengths.

The present invention also provides an iontronic component comprising the nanopore according to the invention.

Brief Description of the Figures

Fig. 1 | Construction and characterization of a non-limiting example of a photopores with seven ON-OFF switches. **a**, The bromoacetyl azopyrazole (Br-pzMe) photoswitch exhibited either as an E isomer (green, upper) or a Z isomer (purple, lower). **b**, UV/Vis spectra of E or Z isomers of Br-pzMe in DMSO at room temperature. **c**, The photostationary state (PSS) of Br-pzMe determined by the 1H-NMR chemical shifts of the aromatic protons in DMSO. **d**, The α-hemolysin (αHL) monomer containing a cysteine at position 111 was functionalized with an azopyrazole group through a bromoacetamide handle before heptamerization to form an (E111C-pzMe)7 photopore. **e**, A total ion chromatogram confirming the complete modification of αHL monomer with Br-PzMe. **f**, The remote modulation of ionic current passing through a single or multiple photopores was assayed using voltage–clamp electrical recording, where a transmembrane potential (Vm) was applied to the cis side of a planar lipid bilayer while the trans side was grounded. LED light was collimated and irradiated onto the bilayer from the trans side. Irradiation at 530 nm or 365 nm isomerized azopyrazole groups within individual pores, thereby populating photopores at either the state in which all seven photoswitches adopted the E configuration, (7E,0Z), or the Z configuration, (0E,7Z).

Fig. 2 | Reversible ON-OFF switching of photopores. **a**, Optical control of ionic flow passing through a single photopore. Irradiation at 365 nm (purple) converted a photopore towards the (0E,7Z) state, while irradiation at 530 nm (green) towards the (7E,0Z) state. **b**, ON-OFF switching of a single photopore effected by cycles of UV (365 nm)-dark-green (530 nm)-dark irradiation. The moving average of the ionic current (grey) was shown in black, which was generated with Savitzky–Golay filter. **c**, Zoom-in of the grey box in b. Each step decrease in the current was attributed to the isomerization of a

photoswitch. **d-e**, In dark, the ionic current remained stable. Under continuous 530-nm irradiation, the current fluctuated as the photopore frequently switched between (7E,0Z) and the neighbouring (6E,1Z) state. **f**, Optical control of ionic flow through a collection of photopores. **g**, ON-OFF switching of >2000 photopores at −100 mV. Number of pores was estimated assuming each pore at PSS365 contributed 50 pA. **h**, ON-OFF switching of a collection of photopores with the Nernst potential generated by asymmetrical KCl concentration across the membrane in the absence of externally applied transmembrane potential. **i**, Gating efficiency in a single, double, and ensemble pores without and with 355-nm and 532 nm in-line filters (n = 3, standard deviations shown as error bars). The current traces were recorded at −100 mV and filtered using a 20 Hz Bessel filter. Recording conditions: 2 M KCl, 10 mM Tris-HCl, 0.1 mM EDTA, pH 8.5, 24 ± 1 °C.

Fig. 3 | Diode properties of photopores. **a**, The current–voltage (I–V) characterization of a single (E111C-pzMe)7 photopore under 365-nm or 530-nm irradiation revealed diode behaviour at negative potentials (0 to −200 mV) and resistor behaviour at positive potentials (0 to +200 mV). The 95% confidence interval (n = 3) is shown as shaded areas. **b**, The wavelength-dependent I-V characteristics of a group of (E111C-pzMe)7 photopores were attributed to the seven pzMe photoswitches within individual photopores adopting different dominant combinatorial states. Current in each I–V graph was normalized assuming that each pore contributed 50 pA at +100 mV. The number of pores ranges from 60 to 904 (n = 7). **c**, The percentage of pzMe photoswitches present in the Z configuration at the photostationery state calculated under the wavelength of 365 nm, 405 nm, 455 nm, or 530 nm. **d**, Voltage and wavelength dependence of the gating efficiency (GP = 1 − IOFF/ION). **e**, The rectification was speculated to result from the opposite orientations of pzMe photoswitches along the pore axis within the electroosmotic flow of opposite directions, which was determined by the polarity of the transmembrane potential (See Supplementary Fig. XX). **f**, Voltage dependence of the rectification ratio of a single or multiple (E111C-pzMe)7 photopores. The rectification ratio was defined as the ratio of absolute currents at +100 mV and −100 mV (n = 3, standard deviations shown as error bars). **g**, Current passing through a group of (E111C-pzMe)7 photopores in response to an applied alternating potential. h, Truth table for photopore logic.

Fig. 4 | Effects of light intensity and wavelength on photopore conductance. **a**, The rate of transition from the low-conductance state to the high-conductance state of (E111C-pzMe)7 pores decreased as the light intensity (Q%) was lowered. The drifted baseline was caused by the gradual depletion of AgCl on electrodes when recording current at the nA scale for minutes. **b**, After 228 photopores reached an equilibrium state of fully ON (ION = –11.4 nA) or OFF (IOFF = –1.8 nA) under continuous irradiation at 530 nm (green) or 365 nm (purple), reducing the light intensity from the maximum LED output (Q% = 100%) did not result in any further changes in the conductance level. **c**, The equilibrium current level was determined by the irradiation wavelength, with a fully OFF state achieved by irradiation at 530 nm (green), a fully ON state achieved by irradiation at 365 nm (purple), and intermediate current levels at 405 nm (violet) and 455 nm (blue). **d**, The mixed-wavelength irradiation with varying ratios of 365-nm and 455-nm light in 3-min steps allowed fine-control of the PSS of a group of photopores, enabling access to intermediate equilibrium current states. The current traces were recorded at −100 mV and filtered using a 20 Hz Bessel filter. Recording conditions: 2 M KCl, 10 mM Tris-HCl, 0.1 mM EDTA, pH 8.5, 24 ± 1 °C.

Fig. 5 | Remote signal transmission with photopores. **a**, Image or text messages were encoded as light sequences to generate ionic current output through (E111C-pzMe)7 photopores. Using the provided keys, the ionic current data were deconvoluted to reconstruct the original messages. **b**, Transmission of binary pixel pattern. A representative segment of the output trace was shown with the binary current levels. **c**, Transmission of three-state pixel art ravelled to a 1D light sequence. The pixel figure was generated from PDB: 7AHL. **d**, Transmission of three-state morse code. Blue box is the deciphered morse code from the current trace, and the purple box the translated text. The light sequence was input at wavelengths of 365 nm, 455 nm or mixed 365/455 nm at a rate of 20 s per bit to generate a current pattern consisting of three levels with a group of photopores.

Fig. 6 | What is a Photopore? A photopore is a photoreversible nanopore1 that switches between two states: iontronic resistor and diode, according to the wavelength of incident UV-Vis irradiation. When reverse-biased, 95% current is reduced by photoswitching. Optical control of transmembrane ionic communication is achieved using photopore that shows robust and reversible photoswitching.

Fig. 7 | Applications of photopores. Ionic flow with asymmetrical KCl concentration across the lipid bilayer is controlled by photopore (neuron sciences). Photoswitching is observed in a 3D-bioprinted droplet network with droplet interface bilayer (smart drug or photopharmacology). Information encrypted as light pulses is converted to an ionic signal and deconvoluted (bio-computation and bio-iontronics).

Fig. 8 | Analysis of photoswitching pathway. A photopore has seven azobenzene photoswitches that isomerize stepwisely. It was wondered how each photoswitch contributed to the conductance. Besides, the isomerisation pathway is not clear due to the complexity of isomers—the configurational, conformational and axial-enantiomeric isomers. Here this question was approached with a simple graph theory analysis.

Fig. 9 | Example 2 Fig. 1 - Construction and characterization of the $(E111C\text{-}pzMe)_7$ photopore. **a**, The α-hemolysin (αHL) monomer containing a cysteine at position 111 was modified with (E)- bromoacetyl arylazopyrazole (Br-pzMe) before oligomerization to form the $(E111C\text{-}pzMe)_7$ photopore. **b**, The Br-pzMe exists either as the E isomer (green) or the Z isomer (purple). **c**, Deconvoluted mass of E111C and E111C-pzMe monomer confirming quantitative modification of the αHL monomer with pzMe. **d**, UV/Vis spectra of E (green) or Z isomers (purple) of Br-pzMe in DMSO at room temperature. **e**, The photostationary states (PSS) of Br-pzMe examined by the ^1H NMR chemical shifts of the aromatic protons in DMSO-*d6*. **f**, The modulation of ionic current passing through single or multiple photopores was evaluated by using voltage–clamp electrical recording, in which a transmembrane potential (V_m) was defined as one in which positive charge moved through the bilayer from the trans side of the pore to the cis. LED light was collimated and projected onto the bilayer from the trans side. Irradiation at 530 nm or 365 nm isomerized arylazopyrazole groups within individual pores, thereby populating photopores in either E or Z states. When all seven arylazopyrazoles adopted the E or Z configuration, such configurations were named as $(7^E,0^Z)$ or $(0^E,7^Z)$.

Fig. 10 | Example 2 Fig. 2 - Reversible ON-OFF switching of $(E111C\text{-}pzMe)_7$ photopore. **a,** Optical control of ionic flow through an ensemble of ~1839 photopores. Irradiation at 365 nm (purple) converted photopores to an ON state, while irradiation at 530 nm (green) produced an OFF state. The current trace demonstrates ON-OFF switching of the photopore ensemble effected by cycles of UV (365 nm) → dark → green (530 nm) → dark. **b,** Optical control through a single photopore switching between $(0^E,7^Z)$ and

(7^E,0^Z) states. The same light cycle as in **a** was applied. The moving average of the ionic current (grey) is shown in black, which was smoothed with a Savitzky–Golay filter (400 ms window length). During 365 nm irradiation, the photopore switched constantly, causing the black downwards events. By contrast, in the dark, these events stopped. **c,** Zoom-in of the dashed-line box in **b**. Each stepwise decrease in the current was attributed to the isomerization of one or more pzMe photoswitches. **d-e,** Ionic current under continuous irradiation. The current fluctuated due to switching between the (7^E,0^Z) and neighboring (6^E,1^Z) states at 530 nm in panel **d** or between the (0^E,7^Z) and neighboring (1^E,6^Z) states at 365 nm in panel **e**. **f,** Ionic current in the dark. The current remained stable with occasional upward bursts of seconds in duration. Such a dark event was irrelevant to the photoisomerization. **g,** Percent gated current ($I_{gate\%}$) in bilayers containing one, two, or an ensemble of pores (n = 4, standard deviations shown as error bars). In-line filters (355-nm filter for 365 nm LED; 532-nm filter for 530 nm LED) were applied to an ensemble of pores with little effect on $I_{gate\%}$. **h,** ON-OFF switching of an ensemble of photopores under the electrochemical driving force generated by an asymmetrical KCl concentration across the membrane in the absence of an externally applied transmembrane potential. The current traces were recorded at +100 mV at 25 kHz sampling frequency and filtered using a 5 kHz in-line Bessel filter and a 20 Hz digital Bessel filter. Recording conditions: 2 M KCl (**a-f**), 0.2 M KCl (cis)/2 M KCl (trans) (**h**), 10 mM Tris-HCl, 0.1 mM EDTA, pH 8.5, 24 ± 1 °C. The number of pores in ensemble experiments was estimated, assuming each (0^E,7^Z) pore contributed +64 pA at +100 mV.

Fig. 11 | Example 2 Fig. 3 - Diode properties of $(E111C\text{-}pzMe)_7$ photopore. **a,** The current–voltage (I–V) curves of a single $(E111C\text{-}pzMe)_7$ after 365-nm or 530-nm irradiation reveals photoswitchable resistor and diode behaviors. The 95% confidence interval (N = 3 photopores) is shaded. **b,** The I-V responses of ensembles of $(E111C\text{-}pzMe)_7$ recorded after irradiation at four wavelengths (365 nm, 405 nm, 455 nm, and 530 nm) and normalized according to the number of pores. Each pore was assumed to contribute +64 pA at +100 mV after 365-nm irradiation. The number of pores in each experiment ranged from 60 to 904 (N = 7 experiments). The 95% confidence intervals are shaded. **c,** Voltage- and wavelength-dependences of the percent gated current [$I_{gate\%} = (1 - I_{OFF}/I_{ON}) \times 100\%$], where I_{ON} is the current after 365-nm irradiation and I_{OFF} is the current at the wavelength of interest. The right schematic shows an estimated distribution of

intermediate states at PSS of four wavelengths. **d,** Voltage-dependence rectification ratio (I_-/I_+) of a single or multiple (E111C-pzMe)$_7$ photopores (N = 3 experiments, standard deviations shown as error bars). **e,** Current passing through an ensemble of (E111C-pzMe)$_7$ photopores in response to an alternating potential. The curves from the top to bottom are the applied voltage, and the current responses at 365 nm and at 530 nm. **f,** A truth table for the NAND logic achieved using photopores. High and low current levels are achieved by combinations of the input wavelength (λ) and the applied potential. The current I–V curves were recorded with a 5 kHz in-line Bessel filter at 25 kHz sampling frequency, and a 20 Hz digital Bessel filter was used for data analysis. Recording conditions: 2 M KCl, 10 mM Tris-HCl, 0.1 mM EDTA, pH 8.5, 24 ± 1 °C.

Fig. 12 | Example 2 Fig. 4 - Effects of light intensity and wavelength on the conductance of (E111C-pzMe)$_7$ ensembles. **a,** Reduced rate of transition from the low-conductance state (I_{OFF}) to the high-conductance state (I_{ON}) due to reductions in the intensity of 365 nm irradiation (purple). The light irradiance (Q) is shown above the light sequence. The baseline drift is caused by the degradation of Ag/AgCl electrodes when recording for minutes at the nA level. **b,** Insensitivity of output current to light intensity after an equilibrium state is reached. When photopores reached equilibrium states of I_{ON} = 11.4 nA (530 nm, green) or I_{OFF} = 1.8 nA (365 nm, purple) (purple), reductions in the light intensity from high to low Q did not cause further changes in the current. **c,** At equilibrium, wavelengths of continuous irradiation result in: an ON state at 365 nm (purple), partially OFF states at 405 nm (violet) and 455 nm (blue) and a fully OFF state at 530 nm (green). **d,** Intermediate current levels can be accessed by polychromic light. Mixed-wavelength irradiation over 3-min intervals with various ratios of 365-nm and 455-nm light allowed fine-control of the PSS ratios with >200 photopores. The current traces were recorded at +100 mV using a 5 kHz in-line Bessel filter at 25 kHz sampling frequency, and a 20 Hz digital Bessel filter was used for data analysis. Recording conditions: 2 M KCl, 10 mM Tris-HCl, 0.1 mM EDTA, pH 8.5, 24 ± 1 °C.

Fig. 13 | Example 2 Fig. 5 - Light-to-current signal conversion. **a,** Overview. Image or text data were encoded as light sequences that produced ionic current responses from (E111C-pzMe)$_7$. By using predetermined keys to assign the current levels, the ionic currents were deciphered to reconstruct the original data. **b,** Transmission of a binary pixel pattern with monochromic 365- and 455-nm irradiation. **c,** Transmission of a three-state

pixel art in a light sequence. The image of the αHL pore was generated from PDB: 7AHL and converted to three-color pixel art. Each pixel was assigned to 0, 1 or 2 based on the color. The matrix of pixels was flattened to 1D to produce the light sequence. **d,** Transmission of three-state Morse code. The blue box is the Morse code from the deciphered current trace, and the purple box is the translated text. The light sequence was the input at wavelengths of 365 nm, 455 nm or mixed 365/455 nm at a rate of 20 s per bit to generate a current pattern consisting of three levels. The current traces were recorded at +100 mV using a 5 kHz in-line Bessel filter at 25 kHz sampling frequency, and a 20 Hz digital Bessel filter was used for data analysis. Currents from $(E111C\text{-}pzMe)_7$ ensembles were recorded in 150 mM KCl, 20 mM Tris-HCl, 0.1 mM EDTA, pH 8.5, 24 ± 1 °C.

Fig. 14 | Example 2 Supplementary Fig. 1 - $(E111C\text{-}fAzo)_7$ and $(E111C\text{-}pzH)_7$ photopores. **a,** The fAzo or pzH photoswitches were covalently attached to the cysteine residues at position 111 (E111C) through thioether bond formation. The photoswitches are shown as E isomers. The electrical traces with ensembles of wild-type (WT) α-hemolysin (αHL) (**b**), unmodified $(E111C)_7$ (**c**), $(E111C\text{-}fAzo)_7$ (**d**), and $(E111C\text{-}pzH)_7$ (**e**) were recorded under alternating light cycles. Wavelengths of irradiation are color-coded: 365 nm, burgundy; 405 nm, purple; 530 nm, green; dark, grey. The WT αHL and $(E111C)_7$ were not photoresponsive. The ensembles of $(E111C\text{-}fAzo)_7$ and $(E111C\text{-}pzH)_7$ responded to irradiation by E/Z isomerization. The percentage gated current $I_{gate\%}$ was around ~20%. For $(E111C\text{-}fAzo)_7$, irradiation at 405 nm closed the pore, and 530 nm opened the pore. In contrast, for $(E111C\text{-}pzH)_7$, irradiation at 530 nm closed the pore, and irradiation at 365 nm opened the pore. The current traces were recorded at +100 mV using a 5 kHz in-line Bessel filter at 25 kHz sampling frequency, and a 20 Hz digital Bessel filter was used for data analysis. Recording conditions: 2 M KCl, 10 mM Tris-HCl, 0.1 mM EDTA, pH 8.5, 24 ± 1 °C.

Fig. 15 | Example 2 Supplementary Fig. 2 - Photopores with pzMe modification in the αHL β barrel. **a,** Representation of the αHL pore and residues in the β barrel. The grey semi-transparent structure of the αHL heptamer was generated from PDB: 7AHL with PyMOL The grey solid dumbbell model showing the protein channel volume was retrieved from ChannelsDB [43]. Electrical traces from ensembles of $(E111C\text{-}pzMe)_7$ (**b**), $(T115C\text{-}pzMe)_7$ (**c**), $(T125C\text{-}pzMe)_7$ (**d**) and $(T129C\text{-}pzMe)_7$ (**e**) were recorded under alternating light cycles. Wavelengths of irradiation are color-coded: 365 nm, burgundy; 530 nm,

green; dark, grey. The (E111C-pzMe)$_7$ showed the largest percentage gated current ($I_{gate\%}$) at 82% in the illustrated trace. All pzMe photopores showed the following correlation—Z, ON; E, OFF. The current traces were recorded at +100 mV using a 5 kHz in-line Bessel filter at 25 kHz sampling frequency, and a 20 Hz digital Bessel filter was used for data analysis. Recording conditions: 2 M KCl, 10 mM Tris-HCl, 0.1 mM EDTA, pH 8.5, 24 ± 1 °C.

Fig. 16 | Example 2 Supplementary Fig. 3 - Structural models for pzMe-modified αHL at position 111. **a,** Top views of a single pzMe group, in either the Z or E state, covalently attached to the E111C position and extended into the central lumen of an αHL pore. **b,** Side views of a single pzMe group in the E state pointing towards either the cis vestibule or the trans opening of the β barrel. c. Top views of seven pzMe groups inside an αHL pore, oriented towards the trans opening of the β barrel. Models were created and modified manually from PDB: 7AHL.

Fig. 17 | Example 2 Supplementary Fig. 4 - LC–MS characterization of E111C monomers before and after chemical modification. The left panels are total ion current chromatograms. The right panels are deconvoluted ESI–MS spectra in the range of 30-40 kDa. **a,** E111C-D_8H_6 monomer: mass = 34966 (calculated) and 34966 (observed). **b,** E111C-pzMe-D_8H_6 monomer: mass = 35249 (calculated) and 35249 (observed). **c,** E111C-fAzo-D_8H_6 monomer: mass = 35289 (calculated) and 35289 (observed). **d,** E111C-pzH-D_8H_6 monomer: mass = 35221 (calculated) and 35221 (observed).

Fig. 18 | Example 2 Supplementary Fig. 5 - LC–MS characterization of photopores obtained by modification with Br-pzMe. The left panels are total ion current chromatograms. The right panels are deconvoluted ESI–MS spectra in the range of 30-40 kDa. **a,** T115C-pzMe-D_8H_6 monomer: mass = 35277 (calculated) and 35277 (observed). **b,** T125C-pzMe-D_8H_6 monomer: mass = 35277 (calculated) and 35277 (observed). **c,** T129C-pzMe-D_8H_6 monomer: mass = 35277 (calculated) and 35277 (observed).

Fig. 19 | Example 2 Supplementary Fig. 6 - Quantitative photoswitching of Br-pzMe. **a,** UV/Vis absorption spectra of Br-pzMe in photostationary states (PSS) in DMSO. **b,** The ratio of Br-pzMe extinction coefficients (ε) between 365 and 530 nm calculated from the data in **a**. The higher ε of the E isomer of Br-pzMe at 365 nm biased the equilibrium towards the Z isomer at PSS 365 nm. Similarly, the Z isomer of pzMe exhibited higher ε at 530 nm, which favored isomerization to the E isomer at PSS 530 nm.

c, ^{1}H NMR signal of the aryl protons (green) of Br-pzMe in DMSO-d_6. **d,** UV/Vis absorption spectra of Br-pzH in the dark after heating and at PSS 365 nm. The right panel shows parts of the ^{1}H NMR spectra of Br-pzH at PSS 365 and 530 nm. **e,** UV/Vis absorption spectra of Br-fAzo in the dark after heating and at PSS 530 nm. The right panel shows the parts of the ^{1}H NMR spectra of Br-fAzo at PSS 405 and 530 nm. The UV/Vis spectra and ^{1}H NMR were recorded in DMSO-d_6 at 298 K.

Fig. 20 | Example 2 Supplementary Fig. 7 - Custom recording chamber for planar lipid bilayer (PLB) experiments under irradiation. **a,** A recording chamber for photopore characterization. An electrical potential was applied across the PLB with Ag/AgCl electrodes (yellow wires). The cis electrode was grounded, and the compartment with the trans electrode was connected to an optical fiber (Ø 1000 µm, NA = 0.39). **b,** Technical schematic of the chamber. The front hole was attached to a collimator and an optical window (not shown). Electrodes were inserted into buffer-containing compartments contained 1 mL buffer each. **c,** Components of the chamber. The fiber-coupled LED projected light to a Teflon film between the compartments. When adjusted, a collimated beam was projected onto the aperture (Ø ~100 µm). **d,** Measurement of light intensity. The irradiance of the light was measured with a power meter by replacing the trans part of the chamber. The collimated light was masked by a Ø 300 µm pinhole. The beam profile through the pinhole was approximately the same as that through the aperture in the Teflon. **e,** Irradiance values of LEDs measured at 365 nm, 405 nm, 455 nm and 530 nm. The irradiance was calculated from the intensity through the pinhole. Irradiance (Q) = Intensity / Pinhole area.

Fig. 21 | Example 2 Supplementary Fig. 8 - Photopore preparation and characterization. (E111C-pzMe)$_7$ is described as an example, but the procedures apply to other photopores. **a,** To obtain homoheptamers, monomers were incubated with sodium deoxycholate (DOC) buffer after 530 nm irradiation. Remaining monomer was removed by anion exchange chromatography (IEX). The purified homoheptamer was examined by electrical recording at the single-molecule level. A population of ON-state currents (I_{ON}) was examined by observing the stepwise insertion of homoheptamers generated with DOC and irradiated at 365 nm. The OFF-state current was not pursued as each pore only contributed few pA, which was indistinguishable from noise. For ensemble characterization, monomers irradiated at 530 nm were added directly to the recording

chamber. **b,** Monitoring the IEX purification by gel electrophoresis. Each monomer had a D_8H_6 tag. The homoheptamer in lanes 5 and 6 was used for recording. Anion IEX conditions: 20 mM Tris-HCl, pH 7.5, NaCl gradient 0.2→0.6 M. Gel: 10% SDS-PAGE with Tris-Glycine SDS buffer.

Fig. 22 | Example 2 Supplementary Fig. 9 - Stepwise insertion of $(E111C\text{-}pzMe)_7$ irradiated at 365-nm. **a,** Insertion of $(E111C\text{-}pzMe)_7$ in the $(0^E,7^Z)$ state in the dark. $(E111C\text{-}pzMe)_7$ was irradiated at 365 nm for 30 minutes and then introduced into the cis compartment. **b,** Histogram of the current steps produced by pore insertions in **a**. The current units in pA were converted to conductance units in nS consistent with the recording conditions. $(WT\text{-}H_6)_7$ exhibited a mono-disperse distribution of conductance values. In contrast, the distribution of $(E111C\text{-}pzMe)_7$ conductance values was broader. **c,** Pore conductance values. The mean unitary conductance of $(WT\text{-}H_6)_7$ was three times that of $(E111C\text{-}pzMe)_7$ after 365 nm irradiation. The current trace was recorded at +100 mV using a 5 kHz in-line Bessel filter at 25 kHz sampling frequency, and a 20 Hz digital Bessel filter was used for data analysis. Recording conditions: 2 M KCl, 10 mM Tris-HCl, 0.1 mM EDTA, pH 8.5, 24 ± 1 °C.

Fig. 23 | Example 2 Supplementary Fig. 10 - ON-OFF switching of $(E111C\text{-}pzMe)_7$. **a,** Illustrative scheme for the single-channel recording of pre-heptamerized $(E111C\text{-}pzMe)_7$ pore. ON-state current (I_{ON}), OFF-state current (I_{OFF}) and percentage gated current ($I_{gate\%}$) were determined by the current traces recorded with pre-formed homoheptamer. **b,** ON-OFF switching performance of individual pre-formed homoheptamers. Each repeat refers to a new pore, and the data are sorted with descending I_{ON}. Despite the diverse values of I_{ON} (0.51 ± 0.31 nS, n = 21 repeats), which are consistent with the stepwise insertion results, the mean value of $I_{gate\%}$ is more tightly defined. The seventh repeat was with the pore used to collect the 40-minute recording of ON-OFF switching (Fig. 10b/Example 2 Fig. 2b). **c,** Illustrative scheme for an $(E111C\text{-}pzMe)_7$ ensemble generated by the insertion of monomers. The ensemble was characterized with a pair of in-line filters to shift the LED irradiation wavelengths from 365/530 nm to 355/532 nm. The filter also narrowed the spectral bandwidth from 9/30 nm to 10/4 nm while reducing the output intensity. **d-e,** ON-OFF switching of the ensemble without and with the filters. The current and $I_{gate\%}$ values were calculated from traces recorded at +100 mV

using a 5 kHz in-line Bessel filter at 25 kHz sampling frequency. Recording conditions: 2 M KCl, 10 mM Tris-HCl, 0.1 mM EDTA, pH 8.5, 24 ± 1 °C.

Fig. 24 | Example 2 Supplementary Fig. 11 - Representative determinations of $I_{gate\%}$ values for single $(E111C\text{-}pzMe)_7$ pores. The moving averages of the ionic currents (grey traces) were generated with a Savitzky–Golay filter and shown in black. The top bar shows the irradiation cycle of dark→365 nm→dark→530 nm→dark. The $I_{gate\%}$ of all traces is >90%, suggesting that $I_{gate\%}$ appears to be consistent regardless of the absolute current (I_{ON} and I_{OFF}). The current traces were recorded at +100 mV using a 5 kHz in-line Bessel filter at 25 kHz sampling frequency, and a 20 Hz digital Bessel filter was used for data analysis. Recording conditions: 2 M KCl, 10 mM Tris-HCl, 0.1 mM EDTA, pH 8.5, 24 ± 1 °C.

Fig. 25 | Example 2 Supplementary Fig. 12 - Prolonged trace of ON-OFF cycles recorded with a single $(E111C\text{-}pzMe)_7$ pore. Ten cycles were recorded over 40 minutes. Fig. 10d/Example 2 Fig. 2d was taken from the region between the two grey dashed lines at 6.5 and 18.5 min. The current trace was recorded at +100 mV using a 5 kHz in-line Bessel filter at 25 kHz sampling frequency, and a 20 Hz digital Bessel filter was used for data analysis. Recording conditions: 2 M KCl, 10 mM Tris-HCl, 0.1 mM EDTA, pH 8.5, 24 ± 1 °C.

Fig. 26 | Example 2 Supplementary Fig. 13 - Multiple current levels arise from the single $(1^E,6^Z)$ combination of the $(E111C\text{-}pzMe)_7$ pore. **a,** Overlay of ten Z-to-E transitions recorded with a single $(E111C\text{-}pzMe)_7$ pore. The transitions consistently started from the 64 pA level (ON) and ended at 1.6 pA (OFF). The inset histogram summarizes the all the current levels observed during the ten transitions from ON to OFF. The green and purple dots are the OFF and ON states. **b-c,** Heatmaps of all transitions observed with a single $(E111C\text{-}pzMe)_7$ pore under continuous 530-nm (**b**) or 365-nm (**c**) irradiation. The color bar on the right indicates the number of events (N). **d**, Overlay of transitions between current levels above 30 pA. Four dominant transitions are present between $(0^E,7^Z)$ and $(1^E,6^Z)$. According to the permutational isomer model (**e**), only one $(1^E,6^Z)$ state is expected. Therefore, a convincing model based simply on E/Z isomerization cannot be built.

Fig. 27 | Example 2 Supplementary Fig. 14 - Prolonged recording with a single ON-state $(E111C\text{-}pzMe)_7$ pore in the dark. A single $(E111C\text{-}pzMe)_7$ photopore was switched on by 365-nm irradiation at 1 min. The ON-state current level was 98 pA at +100 mV. Subsequently, the light was turned off and the electrical recording of the ON-state

$(E111C\text{-}pzMe)_7$ photopore, with photoswitches in the Z state, was conducted for 1 hour. The current level remained stable in the dark, with occasional reversible events up to ~110 pA (purple asterisks) and infrequent gating events to almost 0 pA (blue arrows). The gating was reversed automatically or by briefly applying -100 mV. No pore closure caused by Z-to-E thermal relaxation was observed. The photopore was switched off by 530-nm irradiation at 59 min. The current trace was recorded at +100 mV at 25 kHz sampling frequency using a 5 kHz in-line Bessel filter and a 20 Hz digital Bessel filter. Recording conditions: 2.0 M KCl, 10 mM Tris-HCl, 0.1 mM EDTA, pH 8.5, 24 ± 1 °C.

Fig. 28 | Example 2 Supplementary Fig. 15 - Estimation of the $I_{gate\%}$ values for an ensemble of $(E111C\text{-}pzMe)_7$ based on single-channel recording. **a,** Under 530-nm continuous irradiation, the photopore remained in the complete OFF state (green line) for 74% of the time (N = 84 transitions between OFF and partially ON states). For 26% of the time, the photopore was partially ON (black line) with an average percent residual current ($I_{res\%} = I/I_{ON}$) of 21%. **b,** Under 365-nm continuous irradiation, the photopore remained in the complete ON state (purple line) for 70% of the time (N = 349 transitions between ON and partially ON states). For 30% of the time, the photopore was partially ON (black line) with an average $I_{res\%}$ of 64%. **c**, The incomplete closure under 530 nm and the incomplete opening under 365 nm reduced the macroscopic gating efficiency. Based on single-channel observations, the ensemble $I_{gate\%}$ was estimated to be 100% − 12%/89% = 86%, which aligns with the experimental value of a mean $I_{gate\%}$ of 85% (Fig. 10g/Example 2 Fig. 2g). Recording conditions: 2.0 M KCl, 10 mM Tris-HCl, 0.1 mM EDTA, pH 8.5, 24 ± 1 °C.

Fig. 29 | Example 2 Supplementary Fig. 16 - Charge selectivity of $(E111C\text{-}pzMe)_7$. **a,** Transmembrane potential generated by an asymmetric KCl concentration across the lipid bilayer. The reversal potential (V_r) is defined as the potential required to bring the current flow to zero. **b**, I–V characterization of an ensemble of $(E111C\text{-}pzMe)_7$. The reversal potential was measured after 530- and 365-nm irradiation. The shading around the curves represents the 95% confidence interval after three repeats. The measured V_r suggests anion selectivity. **c-d,** Currents driven by a KCl concentration gradient. The values of $I_{gate\%}$ in **c** and **d** was consistent with the voltage-dependence of $I_{gate\%}$ reported in Fig. 11c/Example 2 Fig. 3c. The experiment was recorded at 25 kHz sampling frequency and filtered using a 5 kHz in-line Bessel filter. Recording conditions: (**b**, **c**) 2 M / 0.2 M KCl, (**d**) 0.2 M / 2 M KCl, 10 mM Tris-HCl, 0.1 mM EDTA, pH 8.5, 24 ± 1 °C.

Fig. 30 | ^{1}H NMR Spectrum of **S2** (Chloroform-*d*, 298 K).

Fig. 31 | ^{1}H NMR Spectrum of **S3** (Chloroform-*d*, 298 K).

Fig. 32 | ^{1}H NMR Spectrum of **S5** (Chloroform-*d*, 298 K).

Fig. 33 | ^{1}H NMR Spectrum of **S6** (Chloroform-*d*, 298 K).

Fig. 34 | ^{1}H NMR Spectrum of **S7** (Chloroform-*d*, 298 K).

Fig. 35 | ^{1}H NMR Spectrum of **S8** (Chloroform-*d*, 298 K).

Fig. 36 | ^{1}H NMR Spectrum of **S10** (Chloroform-*d*, 298 K).

Fig. 37 | ^{13}C NMR Spectrum of **S10** (Chloroform-*d*, 298 K).

Fig. 38 | HSQC NMR Spectrum of **S10.** (Chloroform-*d*, 298 K).

Fig. 39 | HMBC NMR Spectrum of **S10** (Chloroform-*d*, 298 K).

Fig. 40 | ^{1}H NMR Spectrum of **S11** (MeOH-*d4*, 298 K).

Fig. 41 | ^{13}C NMR Spectrum of **S11** (MeOH-*d4*, 298 K).

Fig. 42 | HSQC NMR Spectrum of **S11.** (MeOH-*d4*, 298 K).

Fig. 43 | HMBC NMR Spectrum of **S11.** (MeOH-*d4*, 298 K).

Fig. 44 | ^{1}H NMR Spectrum of **Br-pzMe** (DMSO-*d6*, 298 K).

Fig. 45 | ^{13}C NMR Spectrum of **Br-pzMe** (DMSO-*d6*, 298 K).

Fig. 46 | HSQC NMR Spectrum of **pzMe.** (DMSO-*d6*, 298 K).

Fig. 47 | HSQC NMR Spectrum of **pzMe.** (DMSO-*d6*, 298 K).

Fig. 48 | ^{1}H NMR Spectrum of **S13** (Chloroform-*d*, 298 K).

Fig. 49 | ^{13}C NMR Spectrum of **S13** (Chloroform-*d*, 298 K).

Fig. 50 | ^{1}H NMR Spectrum of **S14** (MeOD-d_4, 298 K).

Fig. 51 | ^{13}C NMR Spectrum of **S14** (MeOD-d_4, 298 K).

Fig. 52 | ^{1}H NMR Spectrum of **Br-pzH** (DMSO-d_6, 298 K).

Fig. 53 | ^{13}C NMR Spectrum of **Br-pzH** (DMSO-d_6, 298 K).

Fig. 54 | ^{1}H NMR spectrum of **S20.** (Chloroform-*d*, 298 K).

Fig. 55 | ^{13}C NMR spectrum of **S20.** (Chloroform-*d*, 298 K).

Fig. 56 | ^{1}H NMR spectrum of **Br-fAzo.** (*Z*)**-Br-fAzo** signals labelled as *. (Chloroform-*d*, 298 K).

Fig. 57 | ^{13}C NMR spectrum of **Br-fAzo.** (*Z*)**-Br-fAzo** signals labelled as *. (Chloroform-*d*, 298 K). **Fig. 58** | HRMS spectrum of **S10**. HRMS-EI (m/z) Calculated for $C_{18}H_{26}N_5O_2$ $[M+H]^+$, 344.2081; found 344.2084.

Fig. 59 | HRMS spectrum of **S10**. HRMS-EI (m/z) Calculated for C13H18N5 $[M+H]^+$, 244.1557; found 244.1557.

Fig. 60 | HRMS spectrum of **Br-pzMe**. HRMS-EI (m/z) Calculated for C15H19N5OBr $[M+H]^+$, 364.0767; found 364.0763.

Fig. 61 | HRMS spectrum of **S14**. HRMS-EI (m/z) Calculated for $C_{11}H_{14}N_4$ $[M+H]^+$, 216.1244; found 216.1245.

Fig. 62 | HRMS spectrum of **Br-pzH**. HRMS-EI (m/z) Calculated for $C_{13}H_{15}N_5OBr$ $[M+H]^+$, 336.0454; found 336.0457.

Fig. 63 | HRMS spectrum of **S20**. HRMS-EI (m/z) Calculated for $C_{28}H_{20}N_3O_2F_4$ $[M+H]^+$, 506.1486; found 506.1488.

Fig. 64 | HRMS spectrum of **Br-fAzo**. HRMS-ESI (m/z) Calculated for $C_{15}H_{11}ON_3BrF_4$ $[M+H]^+$, 404.0016; found 404.0017**Fig. 65** | Partial ^1H NMR spectrum of **pzMe** in the dark (Bottom), 530 nm and 365 PSS states. (DMSO-*d6*, 298 K). With NMR sample (4 mM).

Fig. 66 | UV-vis Spectra of **pzMe** (DMSO-*d6*, 298 K).

Fig. 67 | Deconvoluted spectrum of (*E*)-**pzMe** (DMSO-*d6*, 298 K).

Fig. 68 | Deconvoluted spectrum of (*Z*)-**pzMe** (DMSO-*d6*, 298 K).

Detailed Description

The present invention will be described with respect to particular embodiments and with reference to certain drawings but the invention is not limited thereto but only by the claims. Any reference signs in the claims shall not be construed as limiting the scope. Of course, it is to be understood that not necessarily all aspects or advantages may be achieved in accordance with any particular embodiment of the invention. Thus, for example those skilled in the art will recognize that the invention may be embodied or carried out in a manner that achieves or optimizes one advantage or group of advantages as taught herein without necessarily achieving other aspects or advantages as may be taught or suggested herein.

The invention, both as to organization and method of operation, together with features and advantages thereof, may best be understood by reference to the following detailed description when read in conjunction with the accompanying drawings. The

aspects and advantages of the invention will be apparent from and elucidated with reference to the embodiment(s) described hereinafter. Reference throughout this specification to "one embodiment" or "an embodiment" means that a particular feature, structure or characteristic described in connection with the embodiment is included in at least one embodiment of the present invention. Thus, appearances of the phrases "in one embodiment" or "in an embodiment" in various places throughout this specification are not necessarily all referring to the same embodiment, but may. Similarly, it should be appreciated that in the description of exemplary embodiments of the invention, various features of the invention are sometimes grouped together in a single embodiment, figure, or description thereof for the purpose of streamlining the disclosure and aiding in the understanding of one or more of the various inventive aspects. This method of disclosure, however, is not to be interpreted as reflecting an intention that the claimed invention requires more features than are expressly recited in each claim. Rather, as the following claims reflect, inventive aspects lie in less than all features of a single foregoing disclosed embodiment.

It should be appreciated that “embodiments” of the disclosure can be specifically combined together unless the context indicates otherwise. The specific combinations of all disclosed embodiments (unless implied otherwise by the context) are further disclosed embodiments of the claimed invention.

In addition as used in this specification and the appended claims, the singular forms “a”, “an”, and “the” include plural referents unless the content clearly dictates otherwise. Thus, for example, reference to “a photoisomerisable group” includes two or more photoisomerisable groups.

All publications, patents and patent applications cited herein, whether supra or infra, are hereby incorporated by reference in their entirety.

Definitions

Where an indefinite or definite article is used when referring to a singular noun e.g. "a" or "an", "the", this includes a plural of that noun unless something else is specifically stated. Where the term "comprising" is used in the present description and claims, it does not exclude other elements or steps. Furthermore, the terms first, second, third and the like in the description and in the claims, are used for distinguishing between similar elements and not necessarily for describing a sequential or chronological order. It is to be

understood that the terms so used are interchangeable under appropriate circumstances and that the embodiments of the invention described herein are capable of operation in other sequences than described or illustrated herein. The following terms or definitions are provided solely to aid in the understanding of the invention. Unless specifically defined herein, all terms used herein have the same meaning as they would to one skilled in the art of the present invention.

"Nucleotide sequence", "DNA sequence" or "nucleic acid molecule(s)" as used herein refers to a polymeric form of nucleotides of any length, either ribonucleotides or deoxyribonucleotides. This term refers only to the primary structure of the molecule. Thus, this term includes double- and single-stranded DNA, and RNA. The term "nucleic acid" as used herein, is a single or double stranded covalently-linked sequence of nucleotides in which the 3' and 5' ends on each nucleotide are joined by phosphodiester bonds. The polynucleotide may be made up of deoxyribonucleotide bases or ribonucleotide bases. Nucleic acids may be manufactured synthetically in vitro or isolated from natural sources. Nucleic acids may further include modified DNA or RNA, for example DNA or RNA that has been methylated, or RNA that has been subject to post-translational modification, for example 5'-capping with 7-methylguanosine, 3'-processing such as cleavage and polyadenylation, and splicing. Nucleic acids may also include synthetic nucleic acids (XNA), such as hexitol nucleic acid (HNA), cyclohexene nucleic acid (CeNA), threose nucleic acid (TNA), glycerol nucleic acid (GNA), locked nucleic acid (LNA) and peptide nucleic acid (PNA). Sizes of nucleic acids, also referred to herein as "polynucleotides" are typically expressed as the number of base pairs (bp) for double stranded polynucleotides, or in the case of single stranded polynucleotides as the number of nucleotides (nt). One thousand bp or nt equal a kilobase (kb). Polynucleotides of less than around 40 nucleotides in length are typically called "oligonucleotides" and may comprise primers for use in manipulation of DNA such as via polymerase chain reaction (PCR).

The term "amino acid" in the context of the present disclosure is used in its broadest sense and is meant to include organic compounds containing amine (NH_2) and carboxyl (COOH) functional groups, along with a side chain (e.g., a R group) specific to each amino acid. In some embodiments, the amino acids refer to naturally occurring L α-amino acids or residues. The commonly used one and three letter abbreviations for naturally occurring amino acids are used herein: A=Ala; C=Cys; D=Asp; E=Glu; F=Phe; G=Gly; H=His;

I=Ile; K=Lys; L=Leu; M=Met; N=Asn; P=Pro; Q=Gln; R=Arg; S=Ser; T=Thr; V=Val; W=Trp; and Y=Tyr (Lehninger, A. L., (1975) Biochemistry, 2d ed., pp. 71-92, Worth Publishers, New York). The general term "amino acid" further includes D-amino acids, retro-inverso amino acids as well as chemically modified amino acids such as amino acid analogues, naturally occurring amino acids that are not usually incorporated into proteins such as norleucine, and chemically synthesised compounds having properties known in the art to be characteristic of an amino acid, such as β-amino acids. For example, analogues or mimetics of phenylalanine or proline, which allow the same conformational restriction of the peptide compounds as do natural Phe or Pro, are included within the definition of amino acid. Such analogues and mimetics are referred to herein as "functional equivalents" of the respective amino acid. Other examples of amino acids are listed by Roberts and Vellaccio, The Peptides: Analysis, Synthesis, Biology, Gross and Meiehofer, eds., Vol. 5 p. 341, Academic Press, Inc., N.Y. 1983, which is incorporated herein by reference.

The terms "polypeptide", and "peptide" are interchangeably used herein to refer to a polymer of amino acid residues and to variants and synthetic analogues of the same. Thus, these terms apply to amino acid polymers in which one or more amino acid residues is a synthetic non-naturally occurring amino acid, such as a chemical analogue of a corresponding naturally occurring amino acid, as well as to naturally-occurring amino acid polymers. Polypeptides can also undergo maturation or post-translational modification processes that may include, but are not limited to: glycosylation, proteolytic cleavage, lipidization, signal peptide cleavage, propeptide cleavage, phosphorylation, and such like. A peptide can be made using recombinant techniques, e.g., through the expression of a recombinant or synthetic polynucleotide. A recombinantly produced peptide it typically substantially free of culture medium, e.g., culture medium represents less than about 20 %, more preferably less than about 10 %, and most preferably less than about 5 % of the volume of the protein preparation.

The term "protein" is used to describe a folded polypeptide having a secondary or tertiary structure. The protein may be composed of a single polypeptide, or may comprise multiple polypeptides that are assembled to form a multimer. The multimer may be a homooligomer, or a heterooligmer. The protein may be a naturally occurring, or wild type protein, or a modified, or non-naturally, occurring protein. The protein may, for example,

differ from a wild type protein by the addition, substitution or deletion of one or more amino acids.

A “variant” of a protein encompass peptides, oligopeptides, polypeptides, proteins and enzymes having amino acid substitutions, deletions and/or insertions relative to the unmodified or wild-type protein in question and having similar biological and functional activity as the unmodified protein from which they are derived. The term "amino acid identity" as used herein refers to the extent that sequences are identical on an amino acid-by-amino acid basis over a window of comparison. Thus, a "percentage of sequence identity" is calculated by comparing two optimally aligned sequences over the window of comparison, determining the number of positions at which the identical amino acid residue (e.g., Ala, Pro, Ser, Thr, Gly, Val, Leu, Ile, Phe, Tyr, Trp, Lys, Arg, His, Asp, Glu, Asn, Gln, Cys and Met) occurs in both sequences to yield the number of matched positions, dividing the number of matched positions by the total number of positions in the window of comparison (i.e., the window size), and multiplying the result by 100 to yield the percentage of sequence identity.

For all aspects and embodiments of the present invention, a “variant” has at least 50%, 60%, 70%, 80%, 90%, 95% or 99% complete sequence identity to the amino acid sequence of the corresponding wild-type protein. Sequence identity can also be to a fragment or portion of the full length polynucleotide or polypeptide. Hence, a sequence may have only 50 % overall sequence identity with a full length reference sequence, but a sequence of a particular region, domain or subunit could share 80 %, 90 %, or as much as 99 % sequence identity with the reference sequence.

The term “wild-type” refers to a gene or gene product isolated from a naturally occurring source. A wild-type gene is that which is most frequently observed in a population and is thus arbitrarily designed the “normal” or “wild-type” form of the gene. In contrast, the term “modified”, “mutant” or “variant” refers to a gene or gene product that displays modifications in sequence (e.g., substitutions, truncations, or insertions), post-translational modifications and/or functional properties (e.g., altered characteristics) when compared to the wild-type gene or gene product. It is noted that naturally occurring mutants can be isolated; these are identified by the fact that they have altered characteristics when compared to the wild-type gene or gene product. Methods for introducing or substituting naturally-occurring amino acids are well known in the art. For instance, methionine (M)

may be substituted with arginine (R) by replacing the codon for methionine (ATG) with a codon for arginine (CGT) at the relevant position in a polynucleotide encoding the mutant monomer. Methods for introducing or substituting non-naturally-occurring amino acids are also well known in the art. For instance, non-naturally-occurring amino acids may be introduced by including synthetic aminoacyl-tRNAs in the IVTT system used to express the mutant monomer. Alternatively, they may be introduced by expressing the mutant monomer in *E. coli* that are auxotrophic for specific amino acids in the presence of synthetic (i.e. non-naturally-occurring) analogues of those specific amino acids. They may also be produced by naked ligation if the mutant monomer is produced using partial peptide synthesis. Conservative substitutions replace amino acids with other amino acids of similar chemical structure, similar chemical properties or similar side-chain volume. The amino acids introduced may have similar polarity, hydrophilicity, hydrophobicity, basicity, acidity, neutrality or charge to the amino acids they replace. Alternatively, the conservative substitution may introduce another amino acid that is aromatic or aliphatic in the place of a pre-existing aromatic or aliphatic amino acid. Conservative amino acid changes are well-known in the art and may be selected in accordance with the properties of the 20 main amino acids as defined in Table 1 below. Where amino acids have similar polarity, this can also be determined by reference to the hydropathy scale for amino acid side chains in Table 2.

Table 1 - Chemical properties of amino acids

Ala	aliphatic, hydrophobic, neutral	Met	hydrophobic, neutral
Cys	polar, hydrophobic, neutral	Asn	polar, hydrophilic, neutral
Asp	polar, hydrophilic, charged (-)	Pro	hydrophobic, neutral
Glu	polar, hydrophilic, charged (-)	Gln	polar, hydrophilic, neutral
Phe	aromatic, hydrophobic, neutral	Arg	polar, hydrophilic, charged (+)
Gly	aliphatic, neutral	Ser	polar, hydrophilic, neutral
His	aromatic, polar, hydrophilic, charged (+)	Thr	polar, hydrophilic, neutral
Ile	aliphatic, hydrophobic, neutral	Val	aliphatic, hydrophobic, neutral
Lys	polar, hydrophilic, charged(+)	Trp	aromatic, hydrophobic, neutral
Leu	aliphatic, hydrophobic, neutral	Tyr	aromatic, polar, hydrophobic

Table 2 - Hydropathy scale

Side Chain	Hydropathy
Ile	4.5
Val	4.2
Leu	3.8
Phe	2.8
Cys	2.5
Met	1.9
Ala	1.8
Gly	-0.4
Thr	-0.7
Ser	-0.8
Trp	-0.9
Tyr	-1.3
Pro	-1.6
His	-3.2
Glu	-3.5
Gln	-3.5
Asp	-3.5
Asn	-3.5
Lys	-3.9
Arg	-4.5

A mutant or modified protein, monomer or peptide can also be chemically modified in any way and at any site. A mutant or modified monomer or peptide is preferably chemically modified by attachment of a molecule to one or more cysteines (cysteine linkage), attachment of a molecule to one or more lysines, attachment of a molecule to one or more non-natural amino acids, enzyme modification of an epitope or modification of a terminus. Suitable methods for carrying out such modifications are well-known in the art. The

mutant of modified protein, monomer or peptide may be chemically modified by the attachment of any molecule. For instance, the mutant of modified protein, monomer or peptide may be chemically modified by attachment of a dye or a fluorophore.

A photoisomerisble group (also known herein as a photoswitch) is a group that undergoes isomerisation (here, E-/Z- isomerisation) under light irradiation. Preferred photoisomerisable groups are defined further below.

"Optionally substituted" means that one or more hydrogen atoms present in the group indicated as being "optionally substituted" may be replaced with another chemical group, for instance selected from the lists provided for R^1 and R^2 further below. However, for instance, any one or more optional substituents may be selected from the group consisting of C_{1-6} alkyl optionally substituted with COO^-, SO_3^-, or $NR^3_3^+$; C_{5-10} cycloalkyl optionally substituted with C_{1-6} alkyl, halogen, COO^-, SO_3^-, or $NR^3_3^+$; C_{6-10} aryl optionally substituted with C_{1-6} alkyl, halogen, COO^-, SO_3^-, or $NR^3_3^+$; 5-10 membered heteroaryl or heterocycle having 1-4 ring heteroatoms independently selected from N, O and S, optionally substituted with C_{1-6} alkyl, halogen, COO^-, SO_3^-, or $NR^3_3^+$; C_{2-6} alkenyl optionally substituted with COO^-, SO_3^-, or $NR^3_3^+$; C_{2-6} alkynyl optionally substituted with COO^-, SO_3^-, or $NR^3_3^+$; halogen; OH; CN; NO_2; C_{1-6} haloalkyl; C_{1-6} alkoxy optionally substituted with COO^-, SO_3^-, or $NR^3_3^+$; C_{1-6} haloalkoxy; $COOC_{1-6}$ alkyl optionally substituted with COO^-, SO_3^-, or $NR^3_3^+$; $CONH_2$; $CONR^4C_{1-6}$ alkyl optionally substituted with COO^-, SO_3^-, or $NR^3_3^+$; $CSNH_2$; $CSNR^4C_{1-6}$ alkyl optionally substituted with COO^-, SO_3^-, or $NR^3_3^+$; NR^4COC_{1-6} alkyl optionally substituted with COO^-, SO_3^-, or $NR^3_3^+$; SO_2NH_2; $SO_2NR^4C_{1-6}$ alkyl optionally substituted with COO^-, SO_3^-, or $NR^3_3^+$; $NR^4SO_2C_{1-6}$ alkyl optionally substituted with COO^-, SO_3^-, or $NR^3_3^+$; COO^-, SO_3^-, or $NR^3_3^+$; wherein each R_3 is independently H or C_{1-6} alkyl and each R^4 is independently H or C_{1-6} alkyl. More typically, the one or more optional substituents may be selected from the group consisting of C_{1-6} alkyl; C_{5-10} cycloalkyl; C_{6-10} aryl; 5-10 membered heteroaryl or heterocycle having 1-4 ring heteroatoms independently selected from N, O and S; C_{2-6} alkenyl; C_{2-6} alkynyl; halogen; OH; CN; NO_2; C_{1-6} haloalkyl; C_{1-6} alkoxy; C_{1-6} haloalkoxy; $COOC_{1-6}$ alkyl; $CONH_2$; $CONR^4C_{1-6}$ alkyl; $CSNH_2$; $CSNR^4C_{1-6}$ alkyl; NR^4COC_{1-6} alkyl; SO_2NH_2; $SO_2NR^4C_{1-6}$ alkyl; $NR^4SO_2C_{1-6}$ alkyl; COO^-, SO_3^-, or $NR^3_3^+$; wherein each R^4 is independently H or C_{1-6} alkyl. Even more typically, the one or more optional substituents may be selected from the group consisting of C_{1-3} alkyl; halogen; OH; CN; NO_2; C_{1-3}

haloalkyl; C_{1-3} alkoxy; C_{1-3} haloalkoxy. Even more typically, the one or more optional substituents may be selected from the group consisting of methyl; F, Cl, Br, OH, CN, CF_3 OCH_3 and OCF_3.

Alkyl means a linear of branched monovalent hydrocarbon group of having the general formula C_nH_{2n+1}, wherein the group is optionally contains one or two heteroatoms in the chain (i.e. O or S, or NR, wherein R is H or C_{1-6} alkyl). Preferably, alkyl means a linear of branched hydrocarbon group of having the general formula C_nH_{n+1}. Unless otherwise defined, the alkyl group is a C_{1-20} alkyl group. Preferably, any alkyl is a C_{1-6} alkyl group, more preferably a C_{1-3} alkyl group, most preferably methyl.

Alkylene means a linear or branched divalent hydrocarbon group of having the general formula C_nH_{2n}, wherein the group is optionally contains one or two heteroatoms in the chain (i.e. O or S, or NR, wherein R is H or C_{1-6} alkyl). Preferably, alkyl means a linear of branched hydrocarbon group of having the general formula C_nH_{2n}. Unless otherwise defined, the alkylene group is a C_{1-20} alkylene group. Preferably, any alkylene is a C_{1-6} alkylene group, more preferably a C_{1-3} alkylene group, most preferably methylene.

Alkenyl means a carbon-carbon double bond attached to an alkyl group as defined above where the alkenyl group is an alkenyl group of C_3 or higher. Unless otherwise defined, the alkylene group is a C_{2-20} alkenyl group.

Alkynyl means a carbon-carbon triple bond attached to an alkyl group as defined above where the alkenyl group is an alkenyl group of C_3 or higher. Unless otherwise defined, the alkylene group is a C_{2-20} alkenyl group.

The “substances” that flow through the nanopore are chemical substances and may be independently selected from ions, water, sugars, inorganic salts, lipids, amino acids, peptides, nucleotides, nucleic acids, metabolites, neurotransmitters, labels and pharmaceutical agents (i.e. drugs). Most typically, the substances that move through the nanopore are ions. Additionally or alternatively, the substances may be one or more substances that are imported into or exported from cells.

The one or more substances may comprise ions. The ions may be cations, such as metal cations. The cations may be selected from potassium (K^+), sodium (Na^+) and/or calcium (Ca^{2+}). The ions may be anions. The anions may be chloride (Cl^-).

The one or more substances may comprise nucleic acids, i.e. polynucleotides. The polynucleotides may be double-stranded or single-stranded. Typically when the one or

more substances comprise nucleic acids, the nucleic acid is single stranded, such as cDNA or RNA. The polynucleotides may comprise DNA and/or RNA. Nucleic acids are negatively charged. A nucleic acid is a macromolecule comprising two or more nucleotides. The nucleotides can be naturally occurring or artificial. A nucleotide typically contains a nucleobase, a sugar and at least one phosphate group. The nucleobase is typically heterocyclic. Nucleobases include, but are not limited to, purines and pyrimidines and more specifically adenine, guanine, thymine, uracil and cytosine. The sugar is typically a pentose sugar. Nucleotide sugars include, but are not limited to, ribose and deoxyribose. The nucleotide is typically a ribonucleotide or deoxyribonucleotide. The nucleotide typically contains a monophosphate, diphosphate or triphosphate. Phosphates may be attached on the 5' or 3' side of a nucleotide. Suitable nucleotides include, but are not limited to, adenosine monophosphate (AMP), adenosine diphosphate (ADP), adenosine triphosphate (ATP), guanosine monophosphate (GMP), guanosine diphosphate (GDP), guanosine triphosphate (GTP), thymidine monophosphate (TMP), thymidine diphosphate (TDP), thymidine triphosphate (TTP), uridine monophosphate (UMP), uridine diphosphate (UDP), uridine triphosphate (UTP), cytidine monophosphate (CMP), cytidine diphosphate (CDP), cytidine triphosphate (CTP), cyclic adenosine monophosphate (cAMP), cyclic guanosine monophosphate (cGMP), deoxyadenosine monophosphate (dAMP), deoxyadenosine diphosphate (dADP), deoxyadenosine triphosphate (dATP), deoxyguanosine monophosphate (dGMP), deoxyguanosine diphosphate (dGDP), deoxyguanosine triphosphate (dGTP), deoxythymidine monophosphate (dTMP), deoxythymidine diphosphate (dTDP), deoxythymidine triphosphate (dTTP), deoxyuridine monophosphate (dUMP), deoxyuridine diphosphate (dUDP), deoxyuridine triphosphate (dUTP), deoxycytidine monophosphate (dCMP), deoxycytidine diphosphate (dCDP) and deoxycytidine triphosphate (dCTP). The nucleotides are usually selected from AMP, TMP, GMP, UMP, dAMP, dTMP, dGMP or dCMP.

The one or more substances may comprise peptides, such as polypeptides. The polypeptide may be a protein or a fragment thereof. The polypeptide can be naturally-occurring or non-naturally-occurring. The polypeptide can include within it synthetic or modified amino acids. A number of different types of modification to amino acids are known in the art. The peptide may be a polymer of from about 2 to about 50 amino acids or may be a longer polymer of amino acids. Proteins are typically polypeptides that are

folded into a functional conformation or form part of a functional complex. For example, the polypeptide may be from about 2 to about 1000 amino acids, such as from about 5 to about 500 amino acids, e.g. from about 10 to about 100 amino acids, such as from about 20 to about 60 amino acids e.g. from about 30 to about 50 amino acids. Suitable polypeptides include, but are not limited to, proteins such as enzymes, antibodies, hormones, growth factors or growth regulatory proteins, such as cytokines; or fragments of such proteins. The polypeptide may be bacterial, archaeal, fungal, viral or derived from a parasite. The polypeptide may be derived from a plant. The polypeptide is typically mammalian, more usually human.

The one or more substances may comprise sugars, such as polysaccharides. A polysaccharide is a polymeric carbohydrate molecule composed of chains of monosaccharide units bound together by glycosidic linkages. A polysaccharide may be linear or branched. A polysaccharide may be homogeneous (comprising only one repeating unit) or heterogeneous (containing modifications of the repeating unit). Polysaccharides include callose or laminarin, chrysolaminarin, xylan, arabinoxylan, mannan, fucoidan and galactomannan. A polysaccharide may be produced by a bacterium such as a pathogenic bacterium. The polysaccharide may be a capsular polysaccharide having a molecular weight of 100–2000 kDa. The polysaccharide may be synthesized from nucleotide-activated precursors (called nucleotide sugars). The polysaccharide may be a lipopolysaccharide. The polysaccharide may be a therapeutic polysaccharide. The polysaccharide may be a toxic polysaccharide. The polysaccharide may be suitable for use as a vaccine. The polysaccharide may be for example bacterial or derived from a plant. The polysaccharide may be useful as an antibiotic, such as streptomycin, neomycins, paromomycine, kanamycin, chalcomycin, erythromycin, magnamycin, spiramycin, oleandomycin, cinerubin and amicetin, or a derivative of any one of the preceding compounds. A polysaccharide, the polysaccharide may comprise from about 2 to about 1000 monosaccharide units, such as from about 5 to about 500 monosaccharide units, e.g. from about 10 to about 100 monosaccharide units, such as from about 20 to about 60 monosaccharide units e.g. from about 30 to about 50 monosaccharide units.

The one or more substances may comprise neurotransmitters. The neurotransmitter may be selected from glutamate, glycine, serotonin, epinephrine, dopamine, opioids, ATP,

GBP, nitric oxide, carbon monoxide, γ-aminobutyric acid (GABA), acetylcholine, and norepinephrine.

The one or more substances may further comprise large charged substances, such as sulfo-Cy5 and FMN.

Nanopore

As discussed above, the nanopore of the invention is a nanopore that is selectively convertible between an open form and a closed form using light. Thus, the nanopore of the invention may be converted, using light, between a form that permits the flow of one or more substances through the nanopore (open form), and a form in which the one or more substances are restricted from being able to move though the nanopore (closed form). Preferably, the closed form (i.e. form in which the one or more substances are restricted from being able to move though the nanopore) restricts the flow of the one or more substances, relative to the flow of the one or more substances though the open form, by 10% or more, such as 20% or more, 30% or more, 40% or more, 50% or more, 60% or more, 70% or more, or 80% or more. Preferably, the closed form (i.e. form in which the one or more substances are restricted from being able to move though the nanopore) restricts the flow of the one or more substances, relative to the flow of the one or more substances though the open form, by 90% or more, preferably 95% or more, more preferably by 99% or more. Most preferably, the closed form (i.e. form in which the one or more substances are restricted from being able to move though the nanopore) restricts the flow of the one or more substances, relative to the flow of the one or more substances though the open form, by 100%. Said another way, most preferably, when the nanopore is in the closed form, no substances are able to move through the nanopore.

Definition of nanopore for use in the invention

A nanopore typically comprises a channel through which substances, preferably ions, may pass. The channel is otherwise known as the lumen of the nanopore. As discussed below, typically, nanopore of the invention has nanopore has one or more photoisomerisable groups within the lumen of the nanopore.

Any suitable nanopore can be used. The nanopore may be a transmembrane nanopore. A transmembrane pore is a structure that crosses the membrane to some degree. It permits hydrated ions driven by an applied potential to flow across or within the

membrane. The transmembrane pore typically crosses the entire membrane so that hydrated ions may flow from one side of the membrane to the other side of the membrane. However, the transmembrane pore does not have to cross the membrane. It may be closed at one end. For instance, the pore may be a well, gap, channel, trench or slit in the membrane along which or into which hydrated ions may flow.

The nanopore may a protein pore, a DNA origami pore, a solid-state pore or a polymer-based pore. For example, the nanopore may be a transmembrane protein pore, a transmembrane DNA origami pore or a transmembrane solid-state pore. The nanopore is preferably a transmembrane protein pore.

The pore may be a monomer or an oligomer, *i.e.* comprising two or more monomers. For example, a transmembrane protein pore may be a monomer or may be an oligomer, *i.e.* may comprise two or more protein subunits/monomers. The pore may be a homo-oligomer (all monomer units identical) or a hetero-oligomer (two or more different types of monomer). The pore may comprise linked monomers, for example dimers that assemble into the oligomeric structure of the pore. The monomers may be connected in the same polypeptide strand, i.e. genetically fused.

The pore may comprise at least one dimer and 1, 2, 3, 4, 5, 6, 7 8, 9, 10, 11, 12, 13 or 14 monomers. The pore may comprise two, three, four or more dimers. Such pores further comprise sufficient monomers to form the pore. A further pore comprises only dimers, for example a pore may comprise 4, 5, 6, 7 or 8 dimers. A specific pore for use according to the inventions comprises four dimers. The dimers may oligomerise into a pore with a structure such that only one monomer of a dimer contributes to the barrel or vestibule of the pore. Typically the other monomers of the construct will be on the outside of the barrel or vestibule of the pore. For example, a pore may comprise 5, 6, 7 or 8 dimers where the barrel or vestibule comprises 8 monomers.

Each monomer of the nanopore may comprise at least one of the photoisomerisable groups. For example, where the nanopore is an αHL pore comprising seven αHL monomers, preferably each αHL monomer comprises at least one of the photoisomerisable groups. Each monomer of the nanopore may comprise two or more of the photoisomerisable groups.

A transmembrane pore suitable for use in the invention may be a solid state pore. A solid-state nanopore is typically a nanometer-sized hole formed in a synthetic

membrane. Suitable solid state pores include, but are not limited to, silicon nitride pores, silicon dioxide pores and graphene pores. Solid state nanopores may be fabricated e.g. by focused ion or electron beams, so the size of the pore can be tuned freely. Suitable solid state pores and methods of producing them are discussed in US Patent No. 6,464,842, WO 03/003446, WO 2005/061373, US Patent No. 7,258,838, US Patent No. 7,466,069, US Patent No. 7,468,271 and US Patent No. 7,253,434, each of which is incorporated by reference in their entirety.

A transmembrane pore may be a DNA origami pore as disclosed in Langecker et al., Science, 2012; 338: 932-936 and in WO 2013/083983, each of which is incorporated by reference in their entirety. A transmembrane pore may be a scaffold based pore, such as a DNA-scaffold protein nanopore as disclosed in E. Spruijt, Nat. Nanotechnol. 2018, incorporated by reference.A transmembrane protein pore is a polypeptide, or one or more polypeptides, that permit substances to pass within, along, or though the pore.

A transmembrane pore may be a polymer-based pore. Suitable pores can be made from polymer-based plastics such as a polyester e.g. polyethylene terephthalate (PET) via track etching.

A transmembrane pore suitable for use in the invention may be a transmembrane protein pore. A transmembrane protein pore is a polypeptide or a collection of polypeptides that permits ions driven by an applied potential to flow from one side of a membrane to the other side of the membrane. Transmembrane protein pores are particularly suitable for use in the invention.

A transmembrane protein pore may be isolated, substantially isolated, purified or substantially purified. A pore is isolated or purified if it is completely free of any other components, such as lipids or other pores. A pore is substantially isolated if it is mixed with carriers or diluents which will not interfere with its intended use. For instance, a pore is substantially isolated or substantially purified if it present in a form that comprises less than 10%, less than 5%, less than 2% or less than 1% of other components, such as lipids or other pores. The pore is typically present in a membrane, for example a lipid bilayer or a synthetic membrane e.g. a block-copolymer membrane.

A transmembrane protein pore may be a monomer or an oligomer. A transmembrane protein pore is often made up of several repeating subunits (otherwise known as monomers), such as at least 6, at least 7, at least 8, at least 9, at least 10, at least

11, at least 12, at least 13, at least 14, at least 15, or at least 16 subunits. The pore is typically a hexameric, heptameric, octameric, nonameric, or tetradecameric pore.

A transmembrane protein pore may typically comprises a barrel or channel through which the ions may flow. The subunits of the pore typically surround a central axis and contribute strands to a transmembrane β barrel or channel or a transmembrane α-helix bundle or channel. The transmembrane protein pore can be derived from a β-barrel pore or α-helix bundle pore.

Suitable transmembrane pores for use in accordance with the invention can be β-barrel pores, α-helix bundle pores or solid state pores. β-barrel pores comprise a barrel or channel that is formed from β-strands. Suitable β-barrel pores include, but are not limited to, β-toxins, such as α-hemolysin, anthrax toxin and leukocidins, and outer membrane proteins/porins of bacteria, such as Mycobacterium smegmatis porin (Msp), for example MspA, MspB, MspC or MspD, CsgG, outer membrane porin F (OmpF), outer membrane porin G (OmpG), outer membrane phospholipase A and Neisseria autotransporter lipoprotein (NalP) and other pores, such as lysenin. α-helix bundle pores comprise a barrel or channel that is formed from α-helices. Suitable α-helix bundle pores include, but are not limited to, inner membrane proteins and α outer membrane proteins, such as Wza (e.g. see K. R. Mahendran, Nat. Chem. 2016, incorporated by reference) and ClyA toxin. For example, the transmembrane pore may be derived from or based on Msp, α-hemolysin (α-HL), lysenin, Phi29, CsgG, CgsF, ClyA, Sp1, aerolysin and haemolytic protein fragaceatoxin C (FraC).

The transmembrane protein pore, e.g. one or more, such as all, of the subunits of the transmembrane protein pore, typically comprise a nucleophilic amino acid. The nucleophilic amino acid is capable of forming, or forms, a covalent bond with the photoisomerisable group. The nucleophilic amino acid is preferably an amino acid facing the lumen of the nanopore, *i.e.* is an amino acid on the lumenal surface of the nanopore. The nucleophilic amino acid may cysteine, lysine, histidine, tyrosine or other natural or non-natural nucleophilic acids. Preferably, the nucleophilic amino acid is cysteine.

The transmembrane protein nanopore may comprise a porin, a pore-forming protein or a channel protein.

The transmembrane protein pore may be a porin. Porins are β-barrel proteins that typically cross a membrane and act as a pore. The porin may be a porin selected from

porin superfamily I, porin superfamily II (MspA superfamily), protein superfamily III, protein superfamily IV and porin superfamily V. The porin may be a *Mycobacterium smegmatis* porin (Msp), for example MspA, MspB or MspC, outer membrane phospholipase A, *Neisseria* autotransporter lipoprotein (NalP) or a pore from the Omp family (e.g. Omp F, OmpG etc).

The transmembrane protein pore may be a pore-forming protein. Pore-forming proteins are typically produced by bacteria and other organisms typically to induce lysis of targeted cells. The pore-forming protein may be an alpha-pore-forming toxin (such as a protein of the hemolysin E family, actinoporins (such as fragaceatoxin C), corynebacterial porin B, cytolysin A of *E. coli*), a β-barrel pore-forming toxin (such as α-hemolysin (αHL), Panton-Valentine leucocidin), a large β-barrel pore-forming toxin (such as MACPF and Cholesterol-dependent cytolysins (CDCs), and gasdermin), a binary toxin (such as anthrax toxin, pleurotolysin) or a small pore-forming toxin (such as gramicidin A). The pore-forming protein is preferably an α-hemolysin (αHL).

The transmembrane protein pore may be a channel protein. The channel protein may be an ion channel. Ion channels are pore-forming proteins that allow ions to pass through the channel pore. The ion channel may be a voltage-gated ion channel, a ligand-gated ion channel, a lipid-gated ion channel. The ion channel may be a chloride channel, a potassium channel, a sodium channel, a calcium channel, a proton channel or a non-selective cation channel.

A voltage-gated ion channel may be a voltage-gated sodium channel, a voltage-gated calcium channel, a voltage-gated potassium channel, a voltage-gated chloride channel, a transient receptor potential (TRP) channel, a hyper-polorisation cyclic nucleotide-gated channel, or a voltage-gated proton channel. The voltage-gated potassium channel may be a Shaker potassium channel.

A ligand-gated ion channel may be a cys-loop receptor. The cys-loop receptor may be an acetylcholine receptor, a serotonin receptor, a glycine receptor, a glutamate receptor or a γ-aminoutyric acid (GABA) receptor. The ligand-gated ion channel may be a cationic cys-loop receptor, such as a cationic serotonin receptor, a cationic nicotinic acetylcholine receptor (nAChR), or a cationic zinc-activated ion channel. The ligand-gated ion channel may be an anionic cys-loop receptor, such as a GABA receptor or a glycine receptor. The ligand-gated ion channel may be an ionotropic glutamate receptor, such as

an α-amino-3-hydroxy-5-methyl-4-isoxazolepropionic acid (AMPA) receptor, a kainite receptor, an N-methyl-D-aspartate (NMDA) receptor or an orphan ionotropic glutamate receptor. The ligand-gated ion channel may be an ATP-gated channel, such as a P2X channel.

A lipid-gated ion channel may be an inward-rectifier potassium channel or a two-pore domain potassium channel. A lipid-gated ion channel may be a Phosphatidylinositol 4,5-bisphosphate (PIP_2)-gated channel, such as a K_{ir} channel, a K_v7 channel or a TRP channel. A lipid-gated ion channel may be a phosphatidic acid (PA)-gated channel, such as a K_{2p} channel, a nAChR, or a Kv channel. A lipid-gated ion channel may be a Phosphatidylglycerol (PG)-gated channel.

The transmembrane protein pore is preferably derived from an α-hemolysin (αHL). The wild type αHL pore is formed of seven identical monomers or subunits (i.e. it is heptameric). The transmembrane protein pore preferably comprises seven monomers derived from αHL. The sequence of one wild-type monomer or subunit of αHL (WT αHL) is shown in SEQ ID NO: 1.

SEQ ID NO: 1

ADSDINIKTGTTDIGSNTTVKTGDLVTYDKENGMHKKVFYSFIDDKNHNKKLLVIR
TKGTIAGQYRVYSEEGANKSGLAWPSAFKVQLQLPDNEVAQISDYYPRNSIDTKE
YMSTLTYGFNGNVTGDDTGKIGGLIGANVSIGHTLKYVQPDFKTILESPTDKKVG
WKVIFNNMVNQNWGPYDRDSWNPVYGNQLFMKTRNGSMKAADNFLDPNKASS
LLSSGFSPDFATVITMDRKASKQQTNIDVIYERVRDDYQLHWTSTNWKGTNTKDK
WTDRSSERYKIDWEKEEMTN

Amino acids 1, 7 to 21, 31 to 34, 45 to 51, 63 to 66, 72, 92 to 97, 104 to 111, 124 to 136, 149 to 153, 160 to 164, 173 to 206, 210 to 213, 217, 218, 223 to 228, 236 to 242, 262 to 265, 272 to 274, 287 to 290 and 293 of SEQ ID NO: 1 form loop regions. Residues 111, 113 and 147 of SEQ ID NO: 1 form part of a constriction of the barrel or channel of α-HL.

The pore preferably comprises seven proteins or monomers each comprising the sequence shown in SEQ ID NO: 1 or a variant thereof. The transmembrane protein may be (a) formed of seven identical subunits as shown in SEQ ID NO: 1 or (b) a variant thereof in which one or more of, or all of, the seven subunits is a variant of SEQ ID NO: 1 and which retains pore activity. 1, 2, 3, 4, 5, 6 or 7 of the subunits may be variants. The variants in a

pore may be the same or different. The seven subunits may be the same (homoheptamer) or different (heteroheptamer).

A variant of SEQ ID NO: 1 is a protein that has an amino acid sequence which varies from that of SEQ ID NO: 1 and which retains its pore forming ability. The ability of a variant to form a pore can be assayed using any method known in the art. For instance, the variant may be inserted into an amphiphilic layer, such as a lipid bilayer, along with other appropriate subunits and its ability to oligomerise to form a pore may be determined. Methods are known in the art for inserting subunits into amphiphilic layers, such as lipid bilayers. For example, subunits may be suspended in a purified form in a solution containing a lipid bilayer such that it diffuses to the lipid bilayer and is inserted by binding to the lipid bilayer and assembling into a functional state. Alternatively, subunits may be directly inserted into the membrane using the "pick and place" method described in M.A. Holden, H. Bayley. J. Am. Chem. Soc. 2005, 127, 6502-6503 and International Application No. PCT/GB2006/001057 (published as WO 2006/100484).

The αHL may comprise one or more nucleophilic amino acids exposed to the lumen of the αHL pore. The αHL may comprise one or more nucleophilic amino acids in the constriction of the αHL pore. The αHL may comprise a nucleophilic amino acid at position 111, 113 and/or 147 of SEQ ID NO: 1, preferably at position 111 of SEQ ID NO: 1. The αHL may comprise a nucleophilic amino acid at a position corresponding to position 111, 113 and/or 147 of SEQ ID NO: 1, preferably at a position corresponding to 111 of SEQ ID NO: 1. The nucleophilic amino acid may be histidine, serine, threonine, tyrosine or cysteine, and is preferably cysteine. The αHL may comprise a cysteine at position 111, 113 and/or 147 of SEQ ID NO: 1. The αHL may comprise an E111C, an M113C or a K147C substitution. Preferably, the αHL comprises an E111C substitution. The αHL may comprise a cysteine at position corresponding to position 111, 113 and/or 147 of SEQ ID NO: 1. The αHL may comprise a substitution corresponding to a E111C, an M113C or a K147C substitution of SEQ ID NO: 1. Preferably, the αHL comprises a substitution corresponding to a E111C substitution of SEQ ID NO: 1.

In another embodiment, αHL may comprise a nucleophilic amino acid at position 111, 115, 125 and/or 129 of SEQ ID NO: 1, preferably at position 111 and/or 115 of SEQ ID NO: 1, most preferably at position 111 of SEQ ID NO: 1. The αHL may comprise a nucleophilic amino acid at a position corresponding to position 111, 115, 125 and/or 129 of

SEQ ID NO: 1, preferably at a position corresponding to position 111 and/or 115 of SEQ ID NO: 1, most preferably at a position corresponding to position 111 of SEQ ID NO: 1. The nucleophilic amino acid may be histidine, serine, threonine, tyrosine or cysteine, and is preferably cysteine. The αHL may comprise a cysteine at position 111, 115, 125 and/or 129 of SEQ ID NO: 1. The αHL may comprise an E111C, a T115C, a T125C or a T129C substitution. Preferably, the αHL comprises an E111C or a T115C substitution, most preferably an E111C substitution. The αHL may comprise a cysteine at position corresponding to position 111, 115, 125 and/or 129 of SEQ ID NO: 1. The αHL may comprise a substitution corresponding to a E111C, a T115C, a T125C or a T129C substitution of SEQ ID NO: 1. Preferably, the αHL comprises a substitution corresponding to an E111C substitution or a T115C substitution of SEQ ID NO: 1, most preferably an E111C substitution of SEQ ID NO: 1.

The variant may be a naturally occurring variant which is expressed naturally by an organism, for instance by a *Staphylococcus* bacterium. Alternatively, the variant may be expressed *in vitro* or recombinantly by a bacterium such as *Escherichia coli*. Variants also include non-naturally occurring variants produced by recombinant technology. The variant may include non-naturally occurring amino acids or other molecules that can be introduced by native or non-native chemical ligation. The variant may also include non-covalent modifications such as the use of cyclodextrin as adapters; these modifications include molecules that bind tightly to the pore.

Over the entire length of the amino acid sequence of SEQ ID NO: 1, a variant will preferably be at least 50% homologous to that sequence based on amino acid identity. More preferably, the variant may be at least 55%, at least 60%, at least 65%, at least 70%, at least 75%, at least 80%, at least 85%, at least 90% and more preferably at least 95%, 97% or 99% homologous based on amino acid identity to the amino acid sequence of SEQ ID NO: 1 over the entire sequence. There may be at least 80%, for example at least 85%, 90% or 95%, amino acid identity over a stretch of 200 or more, for example 230, 250, 270 or 280 or more, contiguous amino acids ("hard homology").

Standard methods in the art may be used to determine homology. For example the UWGCG Package provides the BESTFIT program which can be used to calculate homology, for example used on its default settings (Devereux *et al* (1984) *Nucleic Acids Research* **12**, p387-395). The PILEUP and BLAST algorithms can be used to calculate

homology or line up sequences (such as identifying equivalent residues or corresponding sequences (typically on their default settings)), for example as described in Altschul S. F. (1993) J Mol Evol 36:290-300; Altschul, S.F *et al* (1990) J Mol Biol 215:403-10. Software for performing BLAST analyses is publicly available through the National Center for Biotechnology Information (http://www.ncbi.nlm.nih.gov/).

Amino acid substitutions may be made to the amino acid sequence of SEQ ID NO: 1 in addition to those discussed above, for example up to 1, 2, 3, 4, 5, 10, 20 or 30 substitutions. Conservative substitutions replace amino acids with other amino acids of similar chemical structure, similar chemical properties or similar side-chain volume. The amino acids introduced may have similar polarity, hydrophilicity, hydrophobicity, basicity, acidity, neutrality or charge to the amino acids they replace. Alternatively, the conservative substitution may introduce another amino acid that is aromatic or aliphatic in the place of a pre-existing aromatic or aliphatic amino acid. Conservative amino acid changes are well-known in the art and may be selected in accordance with the properties of the 20 main amino acids as defined in Table 1 below. Where amino acids have similar polarity, this can also be determined by reference to the hydropathy scale for amino acid side chains in Table 2. Non-conservative replacements can be made too while the protein pore retains its structure and function.

One or more amino acids of the amino acid sequence of SEQ ID NO: 1 may additionally be deleted from the polypeptides described above. Up to 1, 2, 3, 4, 5, 10, 20 or 30 residues may be deleted, or more.

Variants may include fragments of SEQ ID NO: 1. Such fragments retain pore forming activity. Fragments may be at least 50, 100, 200 or 250 amino acids in length. Such fragments may be used to produce the pores. A fragment preferably contains the pore forming domain of SEQ ID NO: 1. Fragments typically include residues 111, 119, 121, 135, 113 and 139 of SEQ ID NO: 1.

One or more amino acids may be alternatively (insertions) or additionally added to the polypeptides described above. An extension may be provided at the amino terminal or carboxy terminal of the amino acid sequence of SEQ ID NO: 1 or polypeptide variant or fragment thereof. The extension may be quite short, for example from about 1 to about 10 amino acids in length. Alternatively, the extension may be longer, for example up to about 50 or about 100 amino acids.

As discussed above, a variant is a polypeptide that has an amino acid sequence which varies from that of SEQ ID NO: 1 and which retains its ability to form a pore. A variant typically contains the regions of SEQ ID NO: 1 that are responsible for pore formation. The pore forming ability of α-HL, which contains a β-barrel, is provided by β-strands in each subunit. These segments can be shortened making the β-barrel shorter but still retaining the ability to form a pore in the membrane. A variant of SEQ ID NO: 1 typically comprises the regions in SEQ ID NO: 1 that form β-strands. One or more modifications can be made to the regions of SEQ ID NO: 1 that form β-strands as long as the resulting variant retains its ability to form a pore. Specific modifications that can be made to the β-strand regions of SEQ ID NO: 1 are discussed above.

A variant of SEQ ID NO: 1 preferably includes one or more modifications, such as substitutions, additions or deletions, within its a-helices, β strands and/or loop regions. Amino acids that form a-helices and loops are discussed above.

As will be apparent from the above discussion, nanopores for use in the disclosed methods typically have a first opening, a second opening and a solvent-accessible channel therebetween.

Also provided in an array of nanopores as described herein, e.g. an array of nanopores having one or more photoisomerisable groups within the lumen of the nanopore as described herein. The methods and uses described herein may be carried out using the array of nanopores. The use of an array of pores may allow the monitoring of the method by monitoring a signal such an electrical or optical signal. The optical detection of analytes using an array of nanopores can be conducted using techniques known in the art, such as those described by Huang et al, Nature Nanotechnology (2015) 10: 986-992.

Photoisomerisable groups

In a preferred embodiment, the nanopore has one or more photoisomerisable groups within the lumen of the nanopore. Suitably, it is the photoisomerization of the photoisomerisable groups that converts the nanopore of the invention between an open form and a closed form using light. Thus, the nanopore of the invention may be converted, using light, between a form that permits the flow of one or more substances through the nanopore (open form), and a form in which the one or more substances are restricted from

being able to move though the nanopore (closed form). Preferably, the closed form (i.e. form in which the one or more substances are restricted from being able to move though the nanopore) restricts the flow of the one or more substances, relative to the flow of the one or more substances though the open form, by 10% or more, such as 20% or more, 30% or more, 40% or more, 50% or more, 60% or more, 70% or more. In a preferred embodiment, when the nanopore is in the closed form, substantially no substances are able to move through the nanopore, meaning that the closed form (i.e. form in which the one or more substances are restricted from being able to move though the nanopore) restricts the flow of the one or more substances, relative to the flow of the one or more substances though the open form by 80% or more, preferably by 90% or more, preferably 95% or more, more preferably still by 99% or more. Most preferably, the closed form (i.e. form in which the one or more substances are restricted from being able to move though the nanopore) restricts the flow of the one or more substances, relative to the flow of the one or more substances though the open form, by 100%. Said another way, most preferably, when the nanopore is in the closed form, no substances are able to move through the nanopore.

In the invention, preferably, the one or more photoisomerisable groups are each independently groups of formula (I):

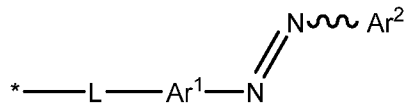

(I)

wherein:

* denotes the point of attachment to the nanopore;

L is a linker; and

Ar^1 and Ar^2 are each independently selected from an optionally-substituted aryl group and an optionally substituted heteroaryl group.

Where the photoisomerisable group is a group of formula (I), it is the isomerisation of the Z form to the E form that provides converts the nanopore of the invention from the open form to the closed form. Correspondingly, it is the isomerisation of the E form to the Z form that converts the nanopore of the invention from the closed form to the open form.

In a preferred embodiment, the group of formula (I) is further defined in that:

- said optionally substituted aryl group is a 6-10 membered aryl group that is optionally substituted with from 1-4 R^1; and
- said optionally substituted heteroaryl group is a 5-10 membered heteroaryl group having 1-4 ring heteroatoms independently selected form the group consisting of N, O and S; the 5-10 membered heteroaryl group being optionally substituted with from 1-4 R^2; and
- R^1 and R^2 are each independently selected from the group consisting of C_{1-6} alkyl optionally substituted with COO^-, SO_3^-, or $NR^3_3^+$; C_{2-6} alkenyl optionally substituted with COO^-, SO_3^-, or $NR^3_3^+$; C_{2-6} alkynyl optionally substituted with COO^-, SO_3^-, or $NR^3_3^+$; halogen; CN; NO_2; C_{1-6} haloalkyl; OH; C_{1-6} alkoxy optionally substituted with COO^-, SO_3^-, or $NR^3_3^+$; C_{1-6} haloalkoxy; $COOC_{1-6}$ alkyl optionally substituted with COO^-, SO_3^-, or $NR^3_3^+$; $CONH_2$; $CONR^4C_{1-6}$ alkyl optionally substituted with COO^-, SO_3^-, or $NR^3_3^+$; NR^4COC_{1-6} alkyl optionally substituted with COO^-, SO_3^-, or $NR^3_3^+$; SO_2NH_2; $SO_2NR^4C_{1-6}$ alkyl optionally substituted with COO^-, SO_3^-, or $NR^3_3^+$; $NR^4SO_2C_{1-6}$ alkyl optionally substituted with COO^-, SO_3^-, or $NR^3_3^+$; COO^-, SO_3^-, or $NR^3_3^+$; wherein each R^3 is independently H or C_{1-6} alkyl, and each R^4 is independently H or C_{1-6} alkyl.

Typically, the optionally substituted aryl group is optionally substituted with from 1-3 R^1. More preferably, the optionally substituted aryl group is optionally substituted with 1 or 2 R^1. More preferably still, the optionally substituted aryl group is optionally substituted with 1 R^1. Most preferably, the aryl group is unsubstituted.

Typically, the optionally substituted heteroaryl group is optionally substituted with from 1-3 R^2. More preferably, the heteroaryl group is substituted with 1-3 R^2. More preferably still, the heteroaryl group is substituted with 2 or 3 R^2. Most preferably, the heteroaryl group is substituted with 3 R^2.

Typically, the aryl group is a napthyl group or a phenyl group. Most preferably, the aryl group is a phenyl group.

Typically, the heteroaryl group is a 5 or 6 membered heteroaryl group having 1-4 ring heteroatoms independently selected form the group consisting of N, O and S. Preferably, the heteroaryl group is a 5 or 6 membered heteroaryl group having 1-4 ring heteroatoms independently selected form the group consisting of N and O. More preferably, the heteroaryl group is a 5 membered heteroaryl group having 1-4 ring

heteroatoms independently selected form the group consisting of N and O. More preferably, the heteroaryl group is a 5 membered heteroaryl group having 1-3 ring heteroatoms independently selected form the group consisting of N and O. More preferably still, the heteroaryl group is a group of the following formulae:

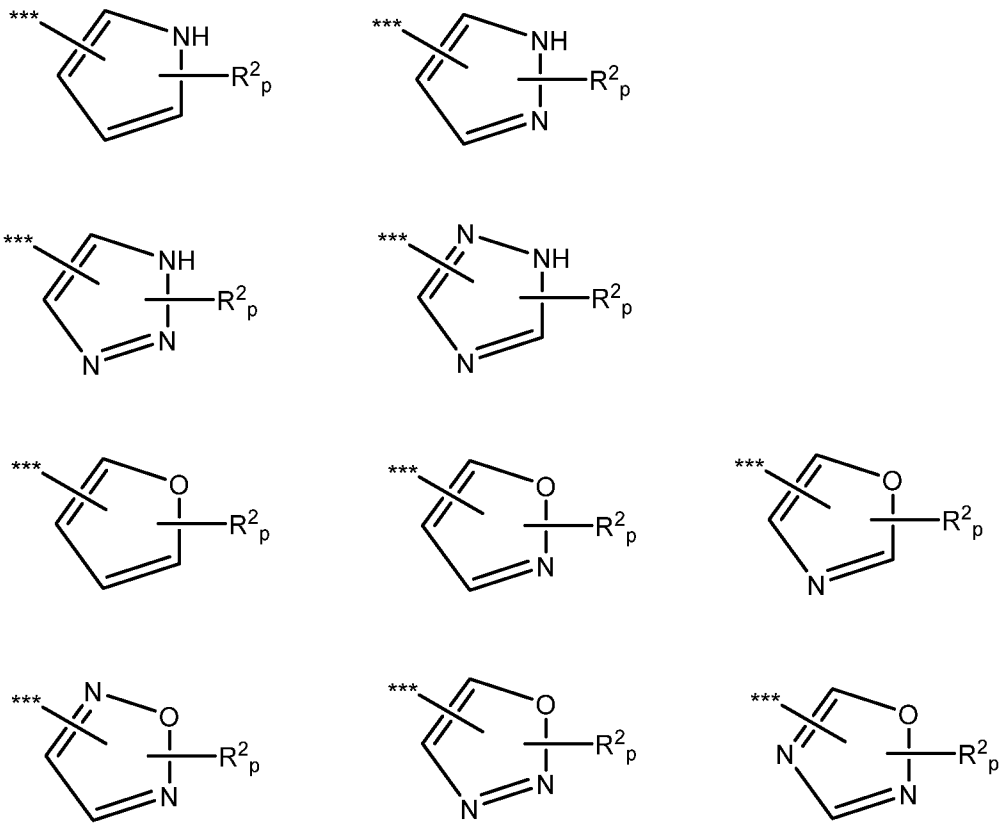

wherein:

*** denotes the point of attachment to the azo group;

R^2 is as defined above (and below);

p is an integer from 0 to 3, preferably 1 to 3, more preferably 2 or 3, most preferably 3.

Even more preferably still, the heteroaryl group is a group of the following formulae:

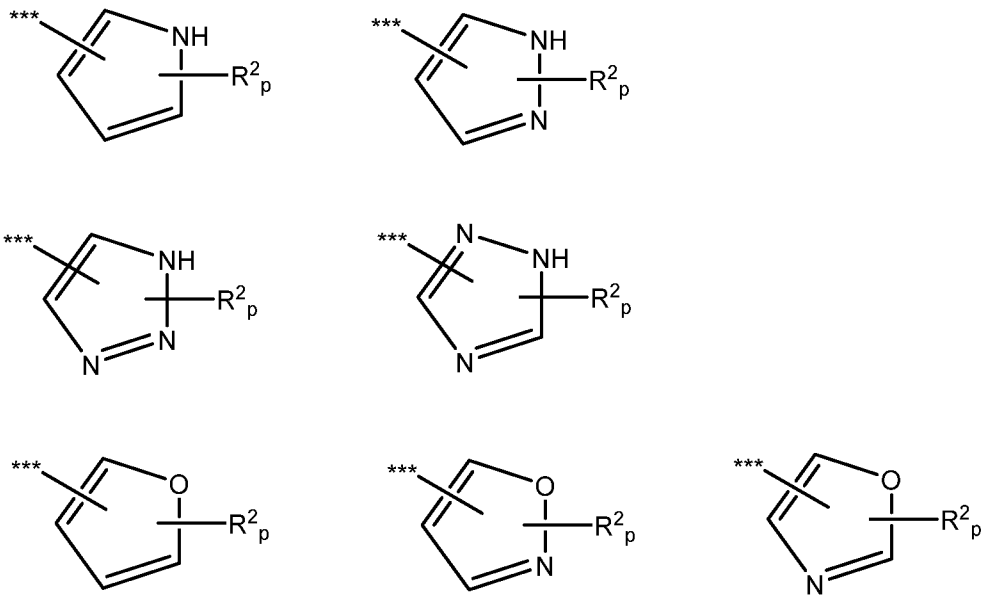

wherein:

*** denotes the point of attachment to the azo group;

R^2 is as defined above (and below);

p is an integer from 0 to 3, preferably 1 to 3, more preferably 2 or 3, most preferably 3.

Even more preferably still, the heteroaryl group is a group of the following formulae:

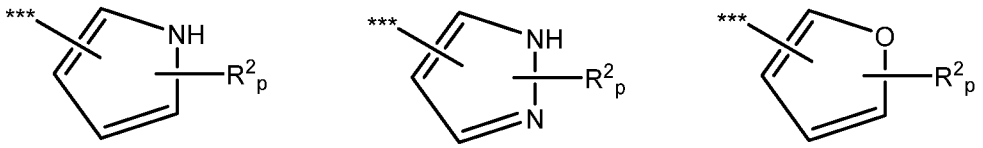

wherein:

*** denotes the point of attachment to the azo group;

R^2 is as defined above (and below);

p is an integer from 0 to 3, preferably 1 to 3, more preferably 2 or 3, most preferably 3.

Even further preferably still, the heteroaryl group is a group of the following formulae:

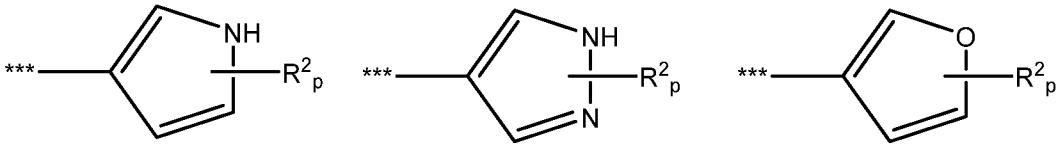

wherein:

*** denotes the point of attachment to the azo group;

R^2 is as defined above (and below);

p is an integer from 0 to 3, preferably 1 to 3, more preferably 2 or 3, most preferably 3.

Even further preferably still, the heteroaryl group is a group of the following formulae:

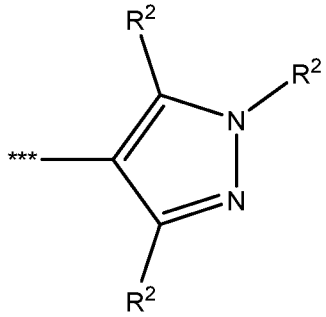

wherein:

*** denotes the point of attachment to the azo group;

R^2 is as defined above (and below).

R^1 and R^2 are each independently selected from the group consisting of C_{1-6} alkyl optionally substituted with COO^-, SO_3^-, or $NR^3_3^+$; C_{2-6} alkenyl optionally substituted with COO^-, SO_3^-, or $NR^3_3^+$; C_{2-6} alkynyl optionally substituted with COO^-, SO_3^-, or $NR^3_3^+$; halogen; C_{1-6} haloalkyl; OH; C_{1-6} alkoxy optionally substituted with COO^-, SO_3^-, or $NR^3_3^+$; C_{1-6} haloalkoxy; $CONH_2$; $CONR^4C_{1-6}$ alkyl optionally substituted with COO^-, SO_3^-, or $NR^3_3^+$; NR^4COC_{1-6} alkyl optionally substituted with COO^-, SO_3^-, or $NR^3_3^+$; SO_2NH_2; $SO_2NR^4C_{1-6}$ alkyl optionally substituted with COO^-, SO_3^-, or $NR^3_3^+$; $NR^4SO_2C_{1-6}$ alkyl optionally substituted with COO^-, SO_3^-, or $NR^3_3^+$; COO^-, SO_3^-, or $NR^3_3^+$; wherein each R^3 is independently H or C_{1-6} alkyl, and each R^4 is independently H or C_{1-6} alkyl.

More preferably R^1 and R^2 are each independently selected from the group consisting of C_{1-3} alkyl optionally substituted with COO^-, SO_3^-, or $NR^3_3^+$; C_{2-3} alkenyl optionally substituted with COO^-, SO_3^-, or $NR^3_3^+$; C_{2-3} alkynyl optionally substituted with COO^-, SO_3^-, or $NR^3_3^+$; halogen; C_{1-6} haloalkyl; OH; C_{1-3} alkoxy optionally substituted with COO^-, SO_3^-, or $NR^3_3^+$; C_{1-3} haloalkoxy; $CONH_2$; $CONR^4C_{1-3}$ alkyl optionally substituted with COO^-, SO_3^-, or $NR^3_3^+$; NR^4COC_{1-3} alkyl optionally substituted with COO^-, SO_3^-, or $NR^3_3^+$; SO_2NH_2; $SO_2NR^4C_{1-3}$ alkyl optionally substituted with COO^-, SO_3^-, or $NR^3_3^+$;

$NR^4SO_2C_{1-3}$ alkyl optionally substituted with COO^-, SO_3^-, or $NR^3_3^+$; COO^-, SO_3^-, or $NR^3_3^+$; wherein each R^3 is independently H or C_{1-3} alkyl, and each R^4 is independently H or C_{1-3} alkyl.

More preferably, R^1 and R^2 are each independently selected from the group consisting of C_{1-3} alkyl; halogen; C_{1-3} haloalkyl; $NHCOC_{1-3}$ alkyl optionally substituted with COO^-, SO_3^-, or $NR^3_3^+$; $NHSO_2C_{1-3}$ alkyl optionally substituted with COO^-, SO_3^-, or $NR^3_3^+$, COO^-, SO_3^-, or $NR^3_3^+$; wherein each R_3 is independently C_{1-3} alkyl.

More preferably still, R^1 and R^2 are each independently selected from the group consisting of C_{1-3} alkyl; F; Cl; Br; and CF_3; such as the group consisting of C_{1-3} alkyl; Cl; Br; and CF_3. Most preferably still, R^1 and R^2 are each methyl. In an embodiment, Ar^1 is an optionally substituted aryl group (as defined above). More preferably, the groups of formula (I) are groups of formula (IA'):

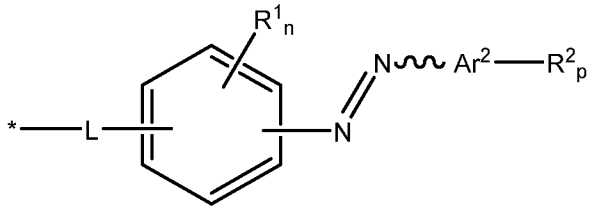

(IA')

Wherein:

L is as defined above (and below),

Ar^2 is an optionally substituted aryl group or an optionally substituted heteroaryl group (as defined above),

R^1 and R^2 are as defined above,

n is an integer from 0 to 4, preferably 0 to 3, more preferably 0 to 2; and

p is an integer from 0 to 4, and is preferably as defined above.

In one specific example of such an embodiment, the groups of formula (I) are groups of formula (IA''):

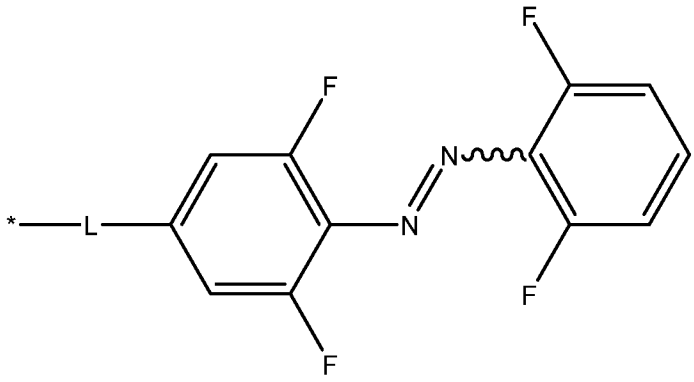

(IA'')

Preferably, however, at least one of Ar^1 and Ar^2 is an optionally substituted heteroaryl group (as defined above). More preferably, one of Ar^1 and Ar^2 is an optionally substituted heteroaryl group (as defined above). More preferably still, the groups of formula (I) are groups of formula (IA):

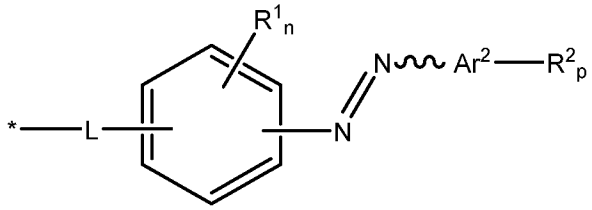

(IA)

Wherein:

L is as defined above (and below),

Ar^2 is an optionally substituted heteroaryl group (as defined above),

R^1 and R^2 are as defined above,

n is an integer from 0 to 4, preferably 0 to 3, more preferably 0 to 2, more preferably 0 or 1, most preferably 0; and

p is an integer from 0 to 4, and is preferably as defined above.

Thus, in a preferred embodiment, the groups of formula (I) are groups of formula (IA):

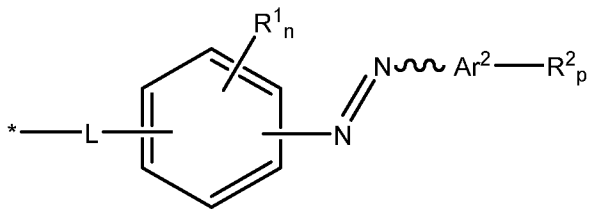

(IA)

Wherein:

L is as defined above (and below),

Ar^2 is a heteroaryl group is a 5 membered heteroaryl group having 1-3 ring heteroatoms independently selected form the group consisting of N and O; and

R^1 and R^2 are each independently selected from the group consisting of C_{1-3} alkyl; halogen; C_{1-3} haloalkyl; $NHCOC_{1-3}$ alkyl optionally substituted with COO^-, SO_3^-, or NR_3^+; SO_2NH_2; $NHSO_2C_{1-3}$ alkyl optionally substituted with COO^-, SO_3^-, or NR_3^+, COO^-, SO_3^-, or NR_3^+; wherein each R_3 is independently H or C_{1-3} alkyl.

In one specific example of such an embodiment, the groups of formula (I) are groups of formula (IB'):

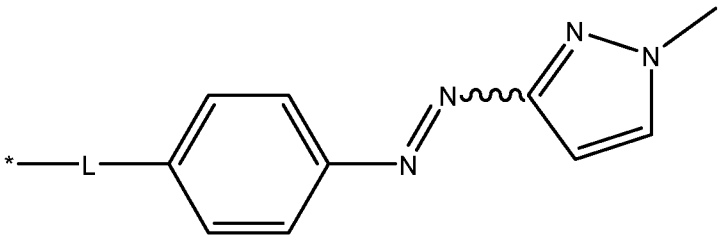

(IB')

More preferably, however, the groups of formula (I) are groups of formula (IB):

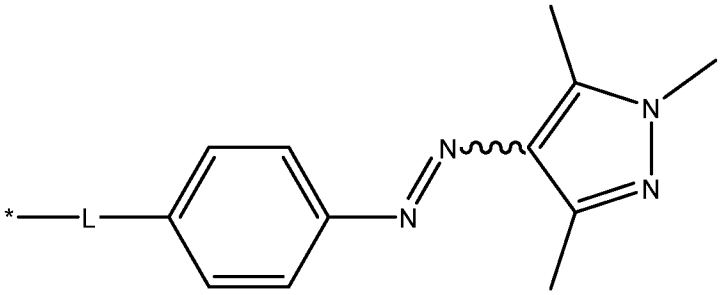

(IB)

The linker may be any divalent group capable of attaching the diaryl azo moiety to the nanopore. Suitable linker chemistry is well known to the person skilled in the art, particularly the persons skilled in preparing (e.g.) antibody-drug conjugates.

Preferably, the linker is a linker of the structure (L1);

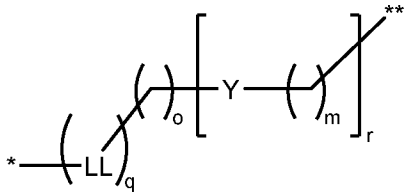

(L1)

wherein:

* denotes the point of attachment to the nanopore,

** denotes the point of attachment to Ar^1,

LL is an optionally substituted 5-10 membered carbocylic or an optionally substituted 5 - 10 membered heterocyclic ring;

Y is independently C_{1-20} alkylene group optionally substituted with halogen, OH, or C_{1-6} alkyl; an amide group (-$CONR^5$- or NR^5CO-); a sulfonamide group (-SO_2NR^5- or NR^5SO_2-); an ester group; a thioester group; an ether group; a thioether group; and an amine group (-NR^5-), wherein each R^5 is independently H or C_{1-6} alkyl;

q is 0 or 1; and

m, o and r are each independently an integer from 0 to 5.

Where q is 0, the linker has the structure (L2):

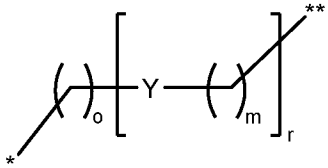

(L2)

wherein *, **, Y, o, m and r are as defined above (or below).

Where q is 1, LL is suitably an optionally substituted 5 or 6 membered carbocylic (i.e. 5 or 6 member cycloalkyl, or phenyl, preferably phenyl) or an optionally substituted 5 or 6 heterocyclic ring having from 1 to 4 heteroatoms (preferably 1 to 3, more preferably 1 or 2, most preferably 1), selected from O, N and S, preferably O and N, more preferably N. The heterocyclic ring may be aromatic or non-aromatic, but is preferably non-aromatic. There may be from 1 to 3 optional substituents, and the optional substituents may be as defined for R^1 and R^2 above. However, when the carbocylic or heterocyclic ring is non-aromatic, the ring is preferably substituted with at least one oxo group. Most preferably, the LL is a succinmide ring. Therefore, in one embodiment, the linker may have the structure (L3)

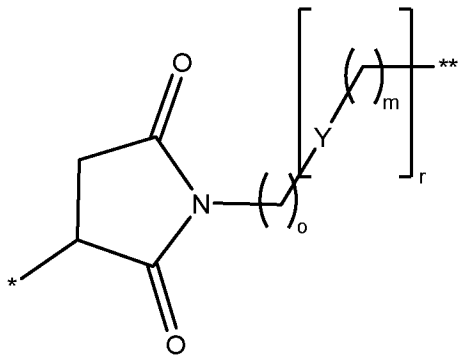

(L3)

wherein *, **, Y, o, m and r are as defined above (or below).

In each of L1 to L3, Y is preferably independently selected from C_{1-6} alkylene, optionally substituted with OH; an amide group (-$CONR^5$- or NR^5CO-), a sulfonamide group (-SO_2NR^5- or NR^5SO_2-), wherein each R^5 is independently H or C_{1-6} alkyl. Y is more preferably an amide group (-$CONR^5$- or NR^5CO-), a sulfonamide group (-SO_2NR_5- or NR_5SO_2-), wherein each R^5 is independently H or methyl. Y is more preferably still an amide group (-CONH- or NHCO-), a sulfonamide group (-SO_2NH- or $NHSO_2$-); more preferably an amide group (-CONH- or NHCO-), and most preferably is an amide group (-CONH-).

In one embodiment, m, o and r are each independently an integer from 0 to 3. Preferably, m, o and r are each independently an integer from 0 to 2. Preferably, m, o and r are each 1 or 0. Typically, at least one, and preferably both, of m and o is 1, and r is 1.

In a particularly preferred embodiment, the linker is linker of the structure (L4):

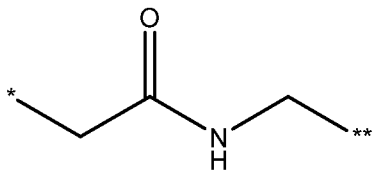

(L4)

wherein:

* denotes the point of attachment to the nanopore,

** denotes the point of attachment to Ar^1.

Thus, in an embodiment of the invention, the one or more photoisomerisable groups are each independently groups of chemical formula (IC') or are each independently groups of chemical formula (IC''):

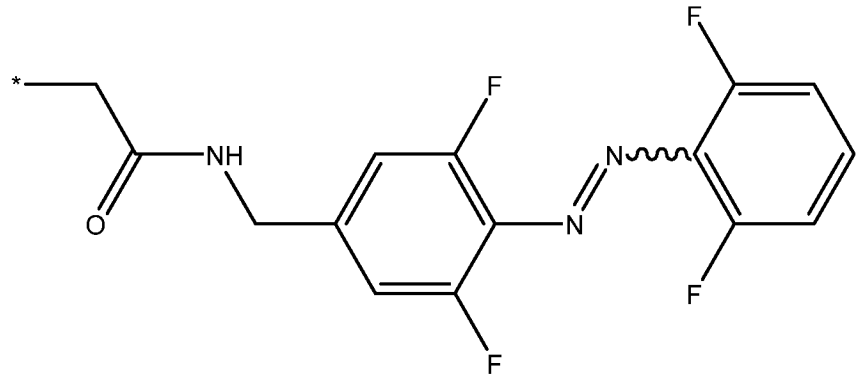

(IC')

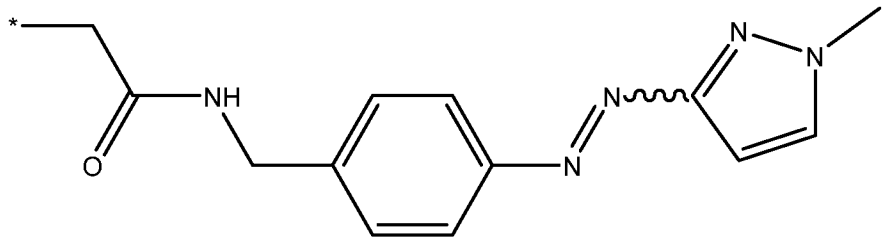

(IC'')

However, in a particularly preferred embodiment of the invention, the one or more photoisomerisable groups are each independently groups of chemical formula (IC):

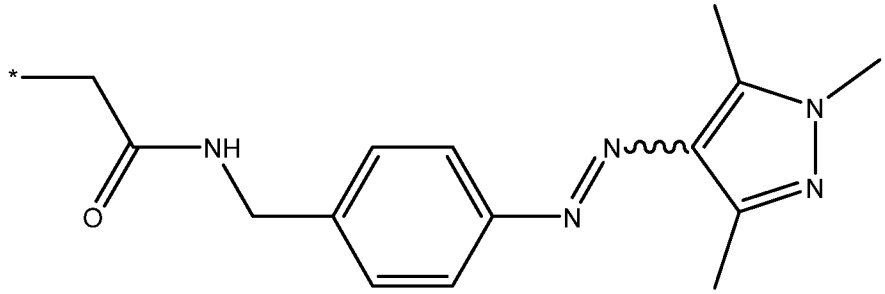

(IC)

wherein:

* denotes the point of attachment to the nanopore.

The photoisomerisable group of chemical formula (IC) is particularly advantageous as the photostationary state (PSS) has a higher proportion of one isomer over the other.

Advantageously, the one or more photoisomerisable groups are covalently attached to the nanopore. Thus, preferably, the one more photoisomerisable groups are covalently

attached to a nucleophilic amino acid exposed to the lumen of the nanopore (as defined further above). Most preferably, the wherein, further preferably:

- the nucleophilic amino acid is a cysteine.

photoisomerisable grops. I.e. most preferably, the one more photoisomerisable groups are covalently attached to a nucleophilic amino acid exposed to the lumen of the nanopore, wherein the nucleophilic acid is a cysteine.

Membrane

Typically, the nanopore is typically present in a membrane. Any suitable membrane may be used in the system. In one embodiment, a multiplicity of nanopores (i.e. an ensemble/array of nanopores) are present in a membrane.

Suitable membranes are well-known in the art. The membrane is typically an amphiphilic layer. An amphiphilic layer is a layer formed from amphiphilic molecules, such as phospholipids, which have both at least one hydrophilic portion and at least one lipophilic or hydrophobic portion. The amphiphilic layer may be a monolayer or a bilayer. The amphiphilic molecules may be synthetic or naturally occurring. Non-naturally occurring amphiphiles and amphiphiles which form a monolayer are known in the art and include, for example, block copolymers (Gonzalez-Perez et al., Langmuir, 2009, 25, 10447-10450).

In some embodiments the membrane comprises one or more archaebacterial bipolar tetraether lipids or mimcs thereof. Such lipids are generally found in extremophiles such as that survive in harsh biological environments, thermophiles, halophiles and acidophiles. Their stability is believed to derive from the fused nature of the final bilayer. It is straightforward to construct block copolymer materials that mimic these biological entities by creating a triblock polymer that has the general motif hydrophilic-hydrophobic-hydrophilic. This material may form monomeric membranes that behave similarly to lipid bilayers and encompass a range of phase behaviours from vesicles through to laminar membranes.

Block copolymers are polymeric materials in which two or more monomer sub-units polymerized together create a single polymer chain. Block copolymers typically have properties that are contributed by each monomer sub-unit. However, a block copolymer may have unique properties that polymers formed from the individual sub-units do not possess. Block copolymers can be engineered such that one of the monomer sub-

units is hydrophobic (i.e. lipophilic), whilst the other sub-unit(s) are hydrophilic whilst in aqueous media. In this case, the block copolymer may possess amphiphilic properties and may form a structure that mimics a biological membrane. The block copolymer may be a diblock (consisting of two monomer sub-units), but may also be constructed from more than two monomer sub-units to form more complex arrangements that behave as amphipiles. The copolymer may be a triblock, tetrablock or pentablock copolymer. Typically the copolymer is a triblock copolymer comprising two monomer subunits A and B in an A-B-A pattern; typically the A monomer subunit is hydrophilic and the B subunit is hydrophobic.

The amphiphilic layer is typically a planar lipid bilayer or a supported bilayer.

The amphiphilic layer is typically a lipid bilayer. Lipid bilayers are models of cell membranes and serve as excellent platforms for a range of experimental studies. For example, lipid bilayers can be used for *in vitro* investigation of membrane proteins by single-channel recording. Alternatively, lipid bilayers can be used as biosensors to detect the presence of a range of substances. The lipid bilayer may be any lipid bilayer. Suitable lipid bilayers include, but are not limited to, a planar lipid bilayer, a supported bilayer or a liposome. The lipid bilayer is usually a planar lipid bilayer. Suitable lipid bilayers are disclosed in WO 2008/102121, WO 2009/077734 and WO 2006/100484).

Any lipid composition that forms a lipid bilayer may be used. Lipids typically comprise a head group, an interfacial moiety and two hydrophobic tail groups which may be the same or different. Suitable head groups include, but are not limited to, neutral head groups, such as diacylglycerides (DG) and ceramides (CM); zwitterionic head groups, such as phosphatidylcholine (PC), phosphatidylethanolamine (PE) and sphingomyelin (SM); negatively charged head groups, such as phosphatidylglycerol (PG); phosphatidylserine (PS), phosphatidylinositol (PI), phosphatic acid (PA) and cardiolipin (CA); and positively charged headgroups, such as trimethylammonium-Propane (TAP). Suitable interfacial moieties include, but are not limited to, naturally-occurring interfacial moieties, such as glycerol-based or ceramide-based moieties. Suitable hydrophobic tail groups include, but are not limited to, saturated hydrocarbon chains, such as lauric acid (*n*-Dodecanolic acid), myristic acid (*n*-Tetradecononic acid), palmitic acid (*n*-Hexadecanoic acid), stearic acid (*n*-Octadecanoic) and arachidic (*n*-Eicosanoic); unsaturated hydrocarbon chains, such as oleic acid (*cis*-9-Octadecanoic); and branched hydrocarbon chains, such as phytanoyl. The

length of the chain and the position and number of the double bonds in the unsaturated hydrocarbon chains can vary. The length of the chains and the position and number of the branches, such as methyl groups, in the branched hydrocarbon chains can vary. The hydrophobic tail groups can be linked to the interfacial moiety as an ether or an ester. The lipids may be mycolic acid.

The lipids can also be chemically-modified. The head group or the tail group of the lipids may be chemically-modified. Suitable lipids whose head groups have been chemically-modified include, but are not limited to, PEG-modified lipids, such as 1,2-Diacyl-sn-Glycero-3-Phosphoethanolamine-N -[Methoxy(Polyethylene glycol)-2000]; functionalised PEG Lipids, such as 1,2-Distearoyl-sn-Glycero-3 Phosphoethanolamine-N-[Biotinyl(Polyethylene Glycol)2000]; and lipids modified for conjugation, such as 1,2-Dioleoyl-sn-Glycero-3-Phosphoethanolamine-N-(succinyl) and 1,2-Dipalmitoyl-sn-Glycero-3-Phosphoethanolamine-N-(Biotinyl). Suitable lipids whose tail groups have been chemically-modified include, but are not limited to, polymerisable lipids, such as 1,2-bis(10,12-tricosadiynoyl)-sn-Glycero-3-Phosphocholine; fluorinated lipids, such as 1-Palmitoyl-2-(16-Fluoropalmitoyl)-sn-Glycero-3-Phosphocholine; deuterated lipids, such as 1,2-Dipalmitoyl-D62-sn-Glycero-3-Phosphocholine; and ether linked lipids, such as 1,2-Di-O-phytanyl-sn-Glycero-3-Phosphocholine. The lipids may be chemically-modified or functionalised to facilitate coupling of the polynucleotide.

Other components that affect the properties of the amphiphilic layer may be incorporated, such as fatty acids, such as palmitic acid, myristic acid and oleic acid; fatty alcohols, such as palmitic alcohol, myristic alcohol and oleic alcohol; sterols, such as cholesterol, ergosterol, lanosterol, sitosterol and stigmasterol; lysophospholipids, such as 1-Acyl-2-Hydroxy-sn- Glycero-3-Phosphocholine; and ceramides.

Methods for forming lipid bilayers are known in the art. Suitable methods are disclosed in the Example. Lipid bilayers are commonly formed by the method of Montal and Mueller (Proc. Natl. Acad. Sci. USA., 1972; 69: 3561-3566), in which a lipid monolayer is carried on aqueous solution/air interface past either side of an aperture which is perpendicular to that interface. The method of Montal & Mueller is popular because it is a cost-effective and relatively straightforward method of forming good quality lipid bilayers that are suitable for protein pore insertion. Other common methods of bilayer formation include tip-dipping, painting bilayers and patch-clamping of liposome bilayers.

The lipid bilayer may be formed as described in WO 2009/077734. A lipid bilayer may also be a droplet interface bilayer formed between two or more aqueous droplets each comprising a lipid shell such that when the droplets are contacted a lipid bilayer is formed at the interface of the droplets.

In another preferred embodiment, the membrane is a solid state layer. A solid-state layer is not of biological origin. In other words, a solid state layer is not derived from or isolated from a biological environment such as an organism or cell, or a synthetically manufactured version of a biologically available structure. Solid state layers can be formed from both organic and inorganic materials including, but not limited to, microelectronic materials, insulating materials such as Si_3N_4, $A1_2O_3$, and SiO, organic and inorganic polymers such as polyamide, plastics such as Teflon® or elastomers such as two-component addition-cure silicone rubber, and glasses. The solid state layer may be formed from monatomic layers, such as graphene, or layers that are only a few atoms thick. Suitable graphene layers are disclosed in WO 2009/035647. The nanopore may in some embodiments be present in an amphiphilic membrane or layer contained within the solid state layer, for instance within a hole, well, gap, channel, trench or slit within the solid state layer. Suitable systems are disclosed in WO 2009/020682 and WO 2012/005857. Any of the amphiphilic membranes or layers discussed above may be used.

Advantageously, the photoisomerisable groups may be potentially orientated in a favourable conformation by the electroosmotic flow present within the charge-selective protein scaffold (i.e. of the nanopore). The present invention therefore further provides the use of orientating forces in the preparation or the application stage of future photopores. Such orientating forces may be osmotic flow or electrophoretic force (on highly charged photoswitches), or even by using facilitating molecules.

Method for producing nanopore

As discussed above, the present invention also provides a method for producing the nanopore according to the invention, the method comprising introducing one or more photoisomerisable groups into a nanopore. For the avoidance of doubt, the nanopores into which the photoisomerisable group is to be introduced as as defined above in relation to the nanopores of the invention.

Typically, in the method for producing the nanopore, the one or more photoisomerisable groups are introduced into the nanopore by treating the nanopore with a compound of formula (II):

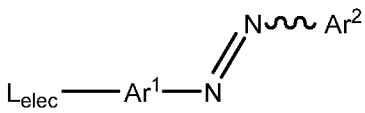

(II)

wherein:

Ar^1 and Ar^2 are as defined above in connection with formula (I), including all preferred features; and

L_{elec} corresponds the linker of as defined above except that the atom that is to be attached to the nanopore is an electrophilic atom capable of undergoing reaction with a nucleophile, preferably as defined further below.

Accordingly, the one or more photoisomerisable groups may be introduced into the nanopore by treating the nanopore with a compound of formula (IIA'):

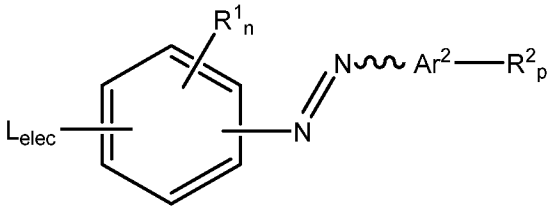

(IIA')

Wherein R^1, Ar^2, R^1, R^2, n or p are as defined above in connection with formula (IA'), including all preferred features; and

L_{elec} corresponds the linker of as defined above except that the atom that is to be attached to the nanopore is an electrophilic atom capable of undergoing reaction with a nucleophile, preferably as defined further below.

In one specific example the one or more photoisomerisable groups are introduced into the nanopore by treating the nanopore with a compound of formula (IIA''):

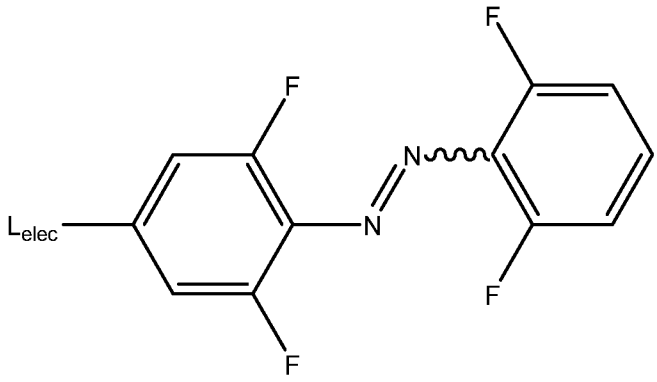

(IIA'')

More preferably, however, the one or more photoisomerisable groups are introduced into the nanopore by treating the nanopore with a compound of formula (IIA):

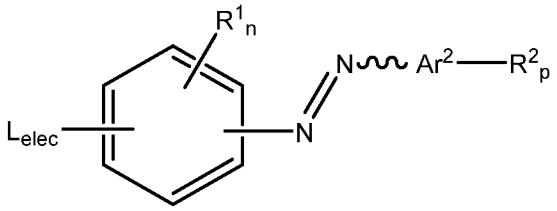

(IIA)

Wherein R^1, Ar^2, R^1, R^2, n or p are as defined above in connection with formula (IA), including all preferred features; and

L_{elec} corresponds the linker of as defined above except that the atom that is to be attached to the nanopore is an electrophilic atom capable of undergoing reaction with a nucleophile, preferably as defined further below.

Thus, in one specific example, the one or more photoisomerisable groups are introduced into the nanopore by treating the nanopore with a compound of formula (IIB'):

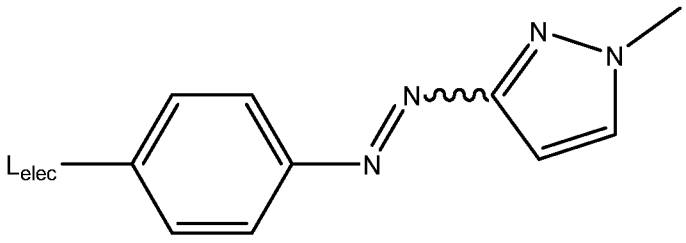

(IIB')

However, more preferably still, the one or more photoisomerisable groups are introduced into the nanopore by treating the nanopore with a compound of formula (IIB):

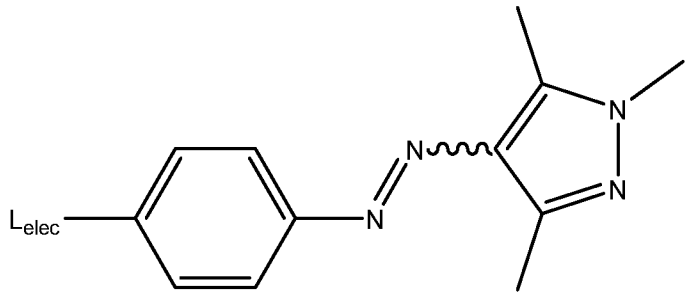

(IIB)

wherein L_{elec} corresponds the linker of as defined above except that the atom that is to be attached to the nanopore is an electrophilic atom capable of undergoing reaction with a nucleophile, preferably as defined further below.

Typically, L_{elec} is of the structure ($L_{elec}1$) or ($L_{elec}1'$);

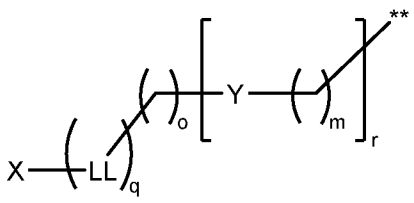

($L_{elec}1$)

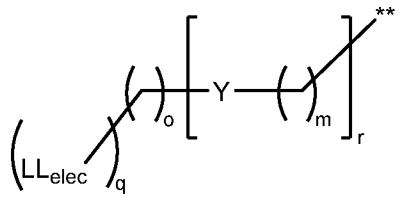

($L_{elec}1'$)

wherein:

** denotes the point of attachment to Ar^1,

LL is as defined above in relation to (L1), including preferred features;

Y is as defined above in relation to (L1), including preferred features;

q, m, o and r are as defined above in relation to (L1) including preferred features;

X is a leaving group as understood by the person skilled in the art, and is typically a halogen (such as F, Cl, Br or I, most preferably Br), or an a sulfonate (preferably tosylate or trifluoromethanesulfonate), most preferably Br; and

LL_{elec} is an analogue of LL as defined above in relation to (L1) that is capable of undergoing nucleophilic addition (i.e. having a double bond conjugated to an electron-withdrawing group, such as a carbonyl). Most preferably LL_{elec} is a maleimide.

Where q is 0, L_{elec} preferably has the structure ($L_{elec}2$):

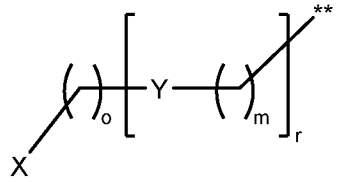

($L_{elec}2$)

wherein ** denotes the point of attachment to Ar^1,

Y is as defined above in relation to (L2), including preferred features;

m, o and r are as defined above in relation to (L2) including preferred features;

X is a leaving group as defined above.

Where q is 1, L_{elec} preferably has the structure ($L_{elec}3$)

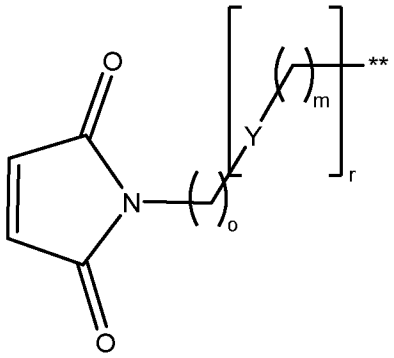

(L3)

wherein ** denotes the point of attachment to Ar^1,

Y is as defined above in relation to (L3), including preferred features;

m, o and r are as defined above in relation to (L3) including preferred features..

In a particularly preferred embodiment, the L_{elec} of the structure ($L_{elec}4$):

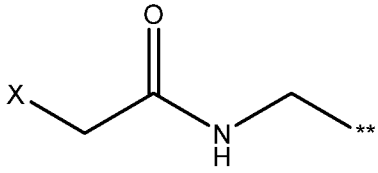

($L_{elec}4$)

wherein:

** denotes the point of attachment to Ar^1, and

X is a leaving group as defined above.

Accordingly, in an embodiment of the invention, the compound is a compound of formula (IIC') or (IIC''):

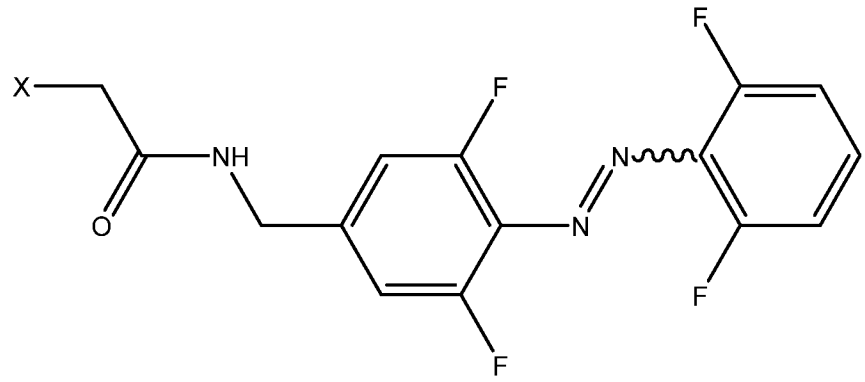

(IIC')

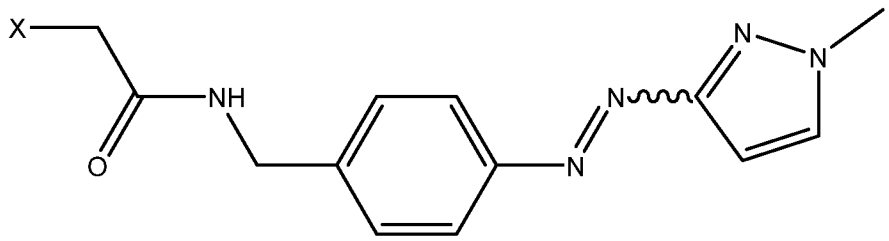

(IIC'')

wherein X is a leaving group, preferably a group selected from a halogen (preferably F, Cl, Br or I) and a sulfonate group (preferably tosylate or trifluoromethanesulfonate), most preferably Br. Accordingly, the compound may be 2-bromo-N-(4-((2,6-difluorophenyl)diazenyl)-3,5-difluorobenzyl)acetamide or 2-bromo-N-(4-((1-methyl-1H-pyrazol-3-yl)diazenyl)benzyl)acetamide.

However, in a most preferred embodiment, the compound is the compound of formula (IIC):

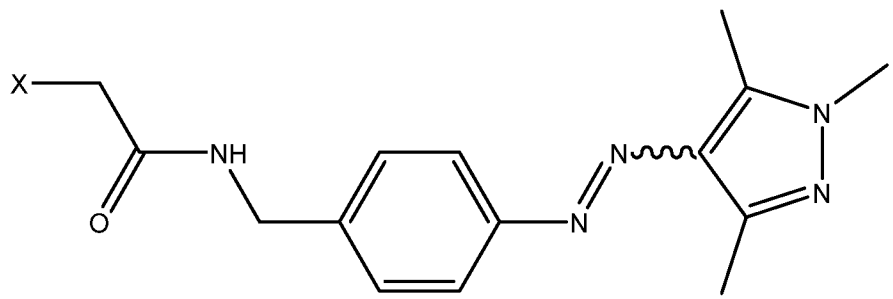

(IIC)

wherein X is a leaving group, preferably a group selected from a halogen (preferably F, Cl, Br or I) and a sulfonate group (preferably tosylate or trifluoromethanesulfonate), most preferably Br. Thus, most preferably, the compound is 2-bromo-N-(4-((1,3,5-trimethyl-1H-pyrazol-4-yl)diazenyl)benzyl)acetamide.

In the method of the invention it is preferred that the one or more photoisomerisable groups are introduced into the nanopore by treating monomers of the nanopore with a compound of formula (II), (IIA), (IIA'), (IIA''), (IIB), (IIB'), (IIC), (IIC') or (IIC'') (preferably (II), (IIA), (IIB) or (IIC)) as defined above. Further preferably, the one or more photoisomerisable groups are introduced into the nanopore by treating monomers of the nanopore with a compound of formula (II), (IIA), (IIA'), (IIA''), (IIB), (IIB'), (IIC), (IIC') or (IIC'') (preferably (II), (IIA), (IIB) or (IIC)) as defined above and then oligomerising the monomers to provide the nanopore.

Typically, the photoisomerisable groups are introduced into the nanopore by treating the nanopore (preferably the monomers of the nanopore) with a compound of formula (II), (IIA), (IIA'), (IIA''), (IIB), (IIB'), (IIC), (IIC') or (IIC'') (preferably (II), (IIA), (IIB) or (IIC)) present as 1-100 equivalents of the compound (for instance from 10-90, 20-80, 30-70, 40-60, most preferably around 50 equivalents of the compound) per monomer to be functionalised.

Typically, the treatment occurs where the nanopore is held in membrane. Typically, the treatment occurs under buffer conditions, where, preferably, the buffer buffers the solution at pH 6-9, preferably pH 7 or 8, more preferably pH 8. Preferably the buffer is Tris-HCl.

Typically, the monomers assemble to provide the nanopore *in situ*.

Alternatively, the treatment occurs *in vitro* in a detergent (for instance, deoxycholate), and the nanopore is separated by chromatography (for instance, ion exchange chromatography)

Compounds

The present invention also provides compounds of formulae (IIA), (IIA'), (IIA''), (IIB), (IIB'), (IIC), (IIC') or (IIC'') as defined above (preferably compounds of formulae (IIA), (IIB) and (IIC) as defined above), and 2-bromo-N-(4-((1,3,5-trimethyl-1H-pyrazol-

4-yl)diazenyl)benzyl)acetamide, 2-bromo-N-(4-((2,6-difluorophenyl)diazenyl)-3,5-difluorobenzyl)acetamide, and 2-bromo-N-(4-((1-methyl-1H-pyrazol-3-yl)diazenyl)benzyl)acetamide (preferably 2-bromo-N-(4-((1,3,5-trimethyl-1H-pyrazol-4-yl)diazenyl)benzyl)acetamide) *per se*.

Kit

The present disclosure also provides kit of parts comprising:

(a) a nanopore to be functionalised, and

(b) a compound of any one of formulae (IIA), (IIA'), (IIA''), (IIB), (IIB'), (IIC), (IIC') or (IIC'') as defined above (preferably a compounds of any one of formulae (IIA), (IIB) or (IIC) as defined above), or 2-bromo-N-(4-((1,3,5-trimethyl-1H-pyrazol-4-yl)diazenyl)benzyl)acetamide, 2-bromo-N-(4-((2,6-difluorophenyl)diazenyl)-3,5-difluorobenzyl)acetamide, or 2-bromo-N-(4-((1-methyl-1H-pyrazol-3-yl)diazenyl)benzyl)acetamide (preferably 2-bromo-N-(4-((1,3,5-trimethyl-1H-pyrazol-4-yl)diazenyl)benzyl)acetamide).

For the avoidance of doubt, the he nanopore to be functionalised may be a nanopore as defined above in the section describing the nanopore of the invention.

Method of modulating the flow of one or more substances through the nanopore

As discussed above, the present invention also provides a method for modulating the flow of one or more substances through a nanopore according to the present invention, the method comprising irradiating the nanopore with light.

In a preferred embodiment of the method, the nanopore of the present invention is a nanopore containing a photoisomerisable group as discussed above. Thus, where the photoisomerisable group is a group of formula (I) (or (IA), (IA'), (IA''), (IB), (IB'), (IC), (IC'), (IC'') etc, preferably (IA), (IB), (IC), etc), it is the isomerisation of the Z form to the E form that provides converts the nanopore of the invention from the open form to the closed form (thereby preventing flow of one of more substances through the nanopore). Correspondingly, it is the isomerisation of the E form to the Z form that converts the nanopore of the invention from the closed form to the open form (thereby permitting flow of one or more substances.

Preferably, the light is light having wavelength of from 355 to 550 nm.

In a preferred embodiment, the method comprises irradiating the nanopore with a first wavelength of light and a second wavelength of light. Preferably, the first wavelength of light isomerises the photoisomerisable group into its Z form, and the second wavelength of light isomerises the photoisomerisable group into its E form. However, the first and second wavelengths of light may be reversed.

The wavelengths of light are thus preferably chosen to bias isomerisation of the photoisomerisation groups towards the E form or towards the Z form, selectively.

Thus, in the present invention, the first wavelength of light is preferably a wavelength of light capable of isomerising the photoisomerisable group into its Z form. Similarly, the second wavelength of light is preferably a wavelength of light capable of isomerising the photoisomerisable group into its E form.

Suitably, the first wavelength of light is a wavelength of light in the UV/Vis spectrum where the ratio εE/εZ is the greatest, and the second wavelength of light is the wavelength in the UV/Vis spectrum where the ratio εZ/εE is the greatest, wherein:

εE is the molar extinction coefficient of the E form of the photoisomerisable group, and

εZ is the molar extinction coefficient of the Z form of the photoisomerisable group.

Suitably, εE and εZ are determined using an UV/Vis spectrophotometer.

Thus, typically, for the photoisomerisable group is a group of formula (I) (or (IA), (IA'), (IA''), (IB), (IB'), (IC), (IC'), (IC'') etc, preferably (IA), (IB), (IC), etc), the first wavelength of light is around 320-400 nm (preferably 350-380 nm, more preferably 360-370, and most preferably around 365 nm) and wherein the second wavelength of light is from 420-550 nm, typically 440-540, preferably around 455 nm or around 530 nm, most preferably around 530 nm.

Other wavelengths of light may be conveniently chosen is it desired to achieve an intermediate level of flow of the one or more substances. For example, to bias 50% flow, a wavelength of light may be chosen where the ratio of εZ/εE is approximately 1.

Any intensity of light may be chosen to induce photoisomerisation. For instance, the intensity of light may be grater that 1 mW/cm^2, for instance greater than 5 mW/cm^2, for instance greater than 10 mW/cm^2, for instance greater than 20 mW/cm^2. Conveniently, the intensity may be around 30 mW/cm^2.

The irradiation may be for any length of time, for example from 1 ms to 1 day, 10 ms to 1 hour, 50 ms to 10 minutes, 500 ms to 1 minute, for instance around 1 second.

The one or substances may be any of the one or more substances described in the definitions section above. As such, the one or more substances maty be independently selected from ions, water, sugars, inorganic salts, lipids, amino acids, peptides, nucleotides, nucleic acids, metabolites, neurotransmitters, and pharmaceutical agents. Most preferably, the one or more substances are ions, preferably cations, such as metal cations. The cations may be selected from potassium (K^+), sodium (Na^+) and/or calcium (Ca^{2+}). The ions may be anions. The anions may be chloride (Cl^-). Advantageously, the ions are both anions and cations, typically K^+ and Cl^-.

Use in modulating ion flow

As discussed above, the present invention also provides the use in modulating ionic flow across a membrane, such an amphiphilic membrane. For the avoidance of doubt, the membrane/amphiphilic membrane may be as defined in the section concerning the nanopores of the invention. Preferably the ions are as defined above.

In one embodiment, the ion flow is the flow of ions form a high concentration side of the membrane to a low concentration side of the membrane. The opening and closing of the nanopore modulates the flow of the ions from the high concentration side to the low concentration side, leading to a change in the ionic current. Advantageously, the modulation of the flow of ions is between and ON state (where the nanopore is open) and an OFF state (where the nanopore is closed).

Advantageously, the flow of ions is only permitted (in the ON/open state) in one direction, such that the open nanopore functions as a diode. In the OFF/closed state, no ion flow takes place in either direction, such that the nanopore functions as a resistor.

Advantageously, the use in modulating ion flow of the present invention may be applied in neuron sciences, for instance to induce — using light — an action potential in neurons having nanopores of the invention contained in their cell membranes (i.e. by allowing rapid influx of ions).

Use in modulating the flow of one or more substances

The present disclosure also provides the use of the nanopore of the invention in modulating the flow of one or more substances across a membrane, such an amphiphilic membrane. For the avoidance of doubt, the membrane/amphiphilic membrane may be as defined in the section concerning the nanopores of the invention. The substances are preferably as defined above.

In one embodiment, the flow is the flow of substances form a high concentration side of the membrane to a low concentration side of the membrane. The opening and closing of the nanopore modulates the flow of the substances from the high concentration side to the low concentration side, leading to a change in the delivery rate of the substances. Advantageously, the modulation of the flow is between and ON state (where the nanopore is open) and an OFF state (where the nanopore is closed).

In one embodiment, when the one or more the substances are oligomeric or polymeric (for instance, in the case of polynucleotides, polypeptides, and polysaccharides) then the use in modulating the flow of one or more substances may be in the context of characterising the one or more substances as analytes. Accordingly, in one aspect, the present invention provides the use of the nanopore of the invention in characterising one or more analytes, wherein the one or more analytes are preferably one or more substances as defined herein, such as polynucleotides, polypeptides, and polysaccharides (more preferably polynucleotides or polypeptides, most preferably polynucleotides).

Device

As discussed above, the present invention also provides comprising an amphiphilic membrane-enclosed vesicle, wherein the vesicle lumen contains one or more pharmaceutical agents and wherein the amphiphilic membrane contains a nanopore according to the invention. For the avoidance of doubt, the amphiphilic membrane may be as defined above in connection with nanopore of the invention.

The pharmaceutical agent may be any pharmaceutical agent, but may beneficially be a pharmaceutical agent for targeting a disease state occurring in a specific part of the body. Particularly beneficially, the pharmaceutical agent may be a chemotherapeutic agent. The device of the invention could be triggered to release the therapeutic agent using light in a target region. Advantageously, a non-target region could be irradiated with a wavelength of light to prevent/stop release of the therapeutic agent.

Thus, the present application further provides the use of the nanopore of the invention in drug delivery.

System

The nanopore may be provided as part of a system comprising the nanopore and a light source. The light source may be configured to emit light to irradiate the nanopore to convert the nanopore between the open form and the closed form. The light source may be a variable wavelength light source. This allows the light source to be used to convert the nanopore both from the open form to the closed form and from the closed form to the open form by varying the wavelength of light used. The light source may be configured to emit light of at least the first wavelength and/or the second wavelength. The light source may be configured to emit light of plural wavelengths simultaneously. The light source may be a pulsed light source configured to emit pulses of light. This can be used to encode information as discussed further below. The light source may be configured to emit pulses of varying length. The pulses may have a length of at least 0.5s, optionally at least 1s, optionally at least 5s, optionally at least 10s. The pulses may have a length of at most 1 minute, optionally at most 30s. The light source may have an intensity of at least 5mW/cm^2, optionally at least 10 mW/cm^2, optionally at least 20 mW/cm^2, optionally at least 30 mW/cm^2.

The system may comprise a plurality of nanopores, for example in an array. The light source may be configured to irradiate the plurality of nanopores with light. The light source may be configured to irradiate the plurality of nanopores simultaneously with substantially the same wavelength and/or intensity of light.

Use as an iontronic component

As discussed above, the present invention also provides the use of a nanopore as described above as an iontronic component. The nanopore is selectively convertible between an open form and a closed form using light. This is achieved by irradiating the nanopore with light, as discussed above. The conductive properties of the nanopore differ between the open and closed states. This allows for the use of the nanopore as a photoswitchable iontronic component. The conductive properties in this context refers to the resistance of the nanopore to an ionic current that flows through the nanopore.

In the closed form, the conductive properties of the nanopore are asymmetric with respect to applied voltage across the nanopore and/or the direction of ionic current flow through the nanopore. An ionic current through the nanopore for a first applied voltage across the nanopore differs from an ionic current through the nanopore for a second applied voltage across the nanopore, where the second applied voltage has equal magnitude but opposite direction to the first applied voltage. The resistance of the nanopore to ionic current flowing in a first direction through the nanopore is different to the resistance of the nanopore to ionic current flowing through the nanopore in a second direction that is opposite to the first direction. It is possible that some asymmetry of the conductive properties may exist in the open form as well, but the asymmetry in the closed form is greater than the asymmetry in the open form.

In the open form, the nanopore allows ionic current to flow through the nanopore in both the first direction and the second direction. In the closed form, the nanopore allows ionic current to flow through the nanopore in the first direction, but blocks a majority, optionally substantially all, of the ionic current flowing through the nanopore in the second direction. An ionic current flowing through the nanopore in the closed form in the second direction for a first applied voltage across the nanopore may be at most 30% of an ionic current flowing through the nanopore in the open form in the second direction for the first applied voltage, optionally at most 20%, optionally at most 10%, optionally at most 5%. An ionic current flowing through the nanopore in the closed form in the second direction for a first applied voltage across the nanopore may be at most 30% of an ionic current flowing through the nanopore in the closed form in the first direction for a second applied voltage equal and opposite to the first applied voltage, optionally at most 20%, optionally at most 10%, optionally at most 5%.

This asymmetry of the conductive properties in the closed form means that the nanopore may be used as an iontronic resistor in the open form and an iontronic diode in the closed form. The nanopore may be used as an iontronic component photoswitchable between a resistor and diode. The nanopore may further be used as a photoswitchable switch. Thereby, the present invention also provides a iontronic component comprising the nanopore.

The iontronic component may be a resistor, diode, or photoswitchable switch. Other iontronic components analogous to conventional electrical circuit components can

also be constructed. Using the diode properties of the nanopore, a suitable arrangement of the nanopore can be used for rectification. Consequently, the iontronic component may be a half-wave rectifier.

The iontronic component may comprise a plurality of the nanopores, for example arranged in an array. Using a plurality of nanopores may, for example, improve the ability of the iontronic component to handle larger currents.

Since the iontronic component exhibits switching properties, it can be used as a logic component, for example a logic gate. Consequently, the present invention also provides the use of the nanopore in bio-computation and/or bioiontronics.

An iontronic component comprising a plurality of the nanopores may be used as a variable resistor. The variable resistor may be configured to be settable to at least three different resistance values. Resistance in this context is a resistance to ionic current flowing through the nanopore.

As discussed above, irradiating the nanopore with light having the first wavelength causes the nanopore to convert to the open form. Irradiating the nanopore with light having the second wavelength causes the nanopore to convert to the closed form. Ionic current flowing through the nanopore in the second direction experiences a much higher resistance when the nanopore is in the closed form compared to when the nanopore is in the open form.

A plurality of the nanopores may be illuminated simultaneously with light having the first wavelength and light having the second wavelength. Without wishing to be bound by theory, it is believed this creates a dynamic equilibrium between nanopores switching from the open form to the closed form and vice versa. By varying a relative intensity of light having the first wavelength and light having the second wavelength, the equilibrium point can be adjusted. This means that the overall resistance of the plurality of nanopores to ionic current flowing in the second direction can be varied by varying the relative intensity of light having the first wavelength and light having the second wavelength.

The resistance of the iontronic component comprising the plurality of nanopores can also be varied by varying the wavelength of the incident light between the first wavelength and the second wavelength. The relative rate at which nanopores of the plurality of nanopores convert from the open form to the closed form and vice versa will

also vary depending on the wavelength as the rate of conversion from one form to the other varies.

Method of transmitting information

As discussed above, the present invention also provides a method of transmitting information. As demonstrated in Fig. 5 and Fig. 7, information can be transmitted by modulating the flow of substances, for example an ionic current, through the nanopore using incident light on the nanopore.

The method comprises irradiating the nanopore with a plurality of pulses of light. Each pulse comprises light having one of a predetermined set of wavelengths. The predetermined set of wavelengths is chosen so that pulses comprising light having different wavelengths of the predetermined set of wavelengths cause conversion of the nanopore into different ones of the open or closed forms. Each pulse may consist of light having only one of the predetermined set of wavelengths.

When the nanopore is irradiated with pulses of light having different wavelengths of the predetermined set of wavelengths, the resistance of the nanopore to ionic current flowing through the nanopore in the second direction will vary as the nanopore is converted between the open form and the closed form. This variation in current can be used to encode information. The method may comprise encoding the information into the pulses of light.

The predetermined set of wavelengths may consist of two different wavelengths, for example the first wavelength of light and the second wavelength of light as discussed above. This can allow the information to be encoded as binary data, where the two binary states are represented by the open form and the closed form of the nanopore and the corresponding resistance to ionic current flowing through the nanopore. Fig. 5b demonstrates the encoding of information as binary data.

To implement the method of transmitting information, the present invention provides a transmitter. The transmitter comprises the nanopore of the present invention. The transmitter further comprises a light source configured to emit the pulses of light, and a controller configured to control the light source to irradiate the nanopore with the pulses of light. The controller may be configured to encode the information into the pulses of light.

A plurality of nanopores may be used to transmit information. In this case, the method of transmitting information comprises illuminating the plurality of nanopores with the pulses of light, and the transmitter comprises a plurality of nanopores. As discussed above, a plurality of nanopores can be used as a component having a variable resistance with three or more values of resistance. These three or more values can be used to encode information as ternary data, quaternary data, etc. depending on the number of resistance values that can be provided by the plurality of nanopores.

Where a plurality of nanopores are used, the the irradiating of the plurality of nanopores may comprise simultaneously irradiating the nanopores with pulses of light having different ones of the predetermined set of wavelengths. That is, some of the pulses of light may consist of light having only one wavelength of the predetermined set of wavelengths, while others of the pulses of light may comprise light having plural ones of the predetermined set of wavelengths. As discussed above, this can be used to produce further resistance states that can encode data with three or more states. Fig. 5c and Fig. 5d demonstrate the encoding of information into three states using three types of pulses of light: 1) pulses consisting of light of the first wavelength, 2) pulses consisting of light of the second wavelength, 3) pulses comprising light having both the first wavelength and the second wavelength.

As discussed for the variable resistor, three or more states may also be encoded by using pulses of light having a wavelength intermediate between the first wavelength and the second wavelength, instead of using pulses of light comprising a mixture of light having the first wavelength and light having the second wavelength. In this case, the predetermined set of wavelengths may further comprise a third wavelength intermediate between the first wavelength and the second wavelength.

Method of receiving information

As discussed above, the present invention also provides a method of receiving information. The method comprises measuring an ionic current through the nanopore during irradiating of the nanopore with a plurality of pulses of light. As discussed above, each pulse comprises light having one of a predetermined set of wavelengths. The ionic current through the nanopore will varying depending on the wavelength of light with which the nanopore is irradiated as the nanopore converts between the open form and the closed form.

A plurality of nanopores may be used, in which case the measuring of the ionic current comprises measuring the current through the plurality of nanopores. The current is measured as an overall current through the plurality of nanopores as an ensemble. Measurement are not necessarily made of the ionic current through each individual nanopore of the plurality of nanopores.

The measurements of the ionic current can be decoded to determine the information according to a predetermined key. The predetermined key indicates what levels of ionic current correspond to each of a plurality of states. The plurality of states may consist of two states in which case the information is encoded as binary data. Where a plurality of nanopores is used, the plurality of states may comprise three or more states.

To implement the method of receiving information, the present disclosure also provides a receiver. The receiver comprises the nanopore of the invention. The receiver further comprises a measurement circuit configured to measure an ionic current through the nanopore, and a controller configured to decode information from the measured ionic current according to the predetermined key.

The present invention also provides the use of the nanopore of the invention as a two-in-one sensor, enabling the same analyte to be characterised by individual nanopores to generate two types of signals under light control. This would be of interest to nanopore sequencing and biomolecule sensing in general, as snapshots taken from different angles would be more informative.

EXAMPLES

Example 1

Molecular tools for the remote modulation of transmembrane ionic communication are widely utilized in biomedical sciences. Among them, optically active tools have garnered attention because of their advantageous features, including spatiotemporal control, reversibility, minimal invasiveness, and multiplexing capability.

Light-controlled ion flux across membranes is usually mediated by photoswitchable chromophores, being membrane-embedded or protein-bound. Proteinaceous light-gated ion transporters, such as microbial rhodopsins, generate or dissipate electrochemical gradient when their cognate chromophores (e.g., all-trans retinal) are activated by light. This

enables the regulation of the electrical activity of rhodopsin-expressing cells in vitro and in vivo, which allows basic biological activities, such as calcium signalling and neuronal firing, to be dissected or manipulated. These optogenetic tools also function as integrable parts of bioelectronic systems with therapeutic potentials, such as cardiac arrhythmia or vision restorage. In parallel, synthetic alternatives have been devised to recapitulate the light-activating passive ion transportation, either directly or indirectly. Macromolecular ion transporters, activated by built-in photoswitches (e.g., azobenzene), move ions down the gradient to offer therapeutic potential for channelopathies. Similarly, synthetic photochromic binders have been developed as photopharmacological drugs targeting ligand-gated ionotropic receptors, such as potassium channel, TRPV, and GABA, to adjust ionic signalling.

In bottom-up synthetic biology, naturally occurring ion transporters (e.g., rhodopsins) have been reconstituted into artificial membranes for optical control over ion flux. Care must be taken in selecting protein constructs activatable by the desired wavelength, promoting directional insertion into the bilayer, and providing continuous irradiation to achieve sustained ion-conducting effects for diverse applications. Light-activating protein nanopores represent an alternative class of optical tools, featuring robust channel-forming ability upon engineering, the ease of handling soluble monomers, and the potential for controlled molecular transmission. Previous studies have focused on engineering α-hemolysin (αHL) and fragaceatoxin C (FraC) monomers with photo-cages, which, upon prolonged UV irradiation (~10-30 minutes), release to trigger irreversible channel formation for permanently activated ionic signalling.

Here, we construct photoreversible ON-OFF protein nanopores to control ionic flow with a low background current in the OFF state and a long channel lifetime in the ON state. Our approach involves covalent modification of the pore-forming monomers of αHL with photoswitches of desirable photostationary properties. Individual photopores have been characterized at both the single-molecule or ensemble levels to showcase their diode-like or resistor-like behaviour under light control, which has been further exploited for signal processing.

Details of Example 1 are provided in Figures 1 to 5. The Figure legends are provided below.

Fig. 1 | Construction and characterization of a non-limiting example of a photopores with seven ON-OFF switches. **a**, The bromoacetyl azopyrazole (Br-pzMe) photoswitch exhibited either as an E isomer (green, upper) or a Z isomer (purple, lower). **b**, UV/Vis spectra of E or Z isomers of Br-pzMe in DMSO at room temperature. **c**, The photostationary state (PSS) of Br-pzMe determined by the 1H-NMR chemical shifts of the aromatic protons in DMSO. **d**, The α-hemolysin (αHL) monomer containing a cysteine at position 111 was functionalized with an azopyrazole group through a bromoacetamide handle before heptamerization to form an (E111C-pzMe)7 photopore. **e**, A total ion chromatogram confirming the complete modification of αHL monomer with Br-PzMe. **f**, The remote modulation of ionic current passing through a single or multiple photopores was assayed using voltage–clamp electrical recording, where a transmembrane potential (Vm) was applied to the cis side of a planar lipid bilayer while the trans side was grounded. LED light was collimated and irradiated onto the bilayer from the trans side. Irradiation at 530 nm or 365 nm isomerized azopyrazole groups within individual pores, thereby populating photopores at either the state in which all seven photoswitches adopted the E configuration, (7E,0Z), or the Z configuration, (0E,7Z).

Fig. 2 | Reversible ON-OFF switching of photopores. **a**, Optical control of ionic flow passing through a single photopore. Irradiation at 365 nm (purple) converted a photopore towards the (0E,7Z) state, while irradiation at 530 nm (green) towards the (7E,0Z) state. **b**, ON-OFF switching of a single photopore effected by cycles of UV (365 nm)-dark-green (530 nm)-dark irradiation. The moving average of the ionic current (grey) was shown in black, which was generated with Savitzky–Golay filter. **c**, Zoom-in of the grey box in b. Each step decrease in the current was attributed to the isomerization of a photoswitch. **d-e**, In dark, the ionic current remained stable. Under continuous 530-nm irradiation, the current fluctuated as the photopore frequently switched between (7E,0Z) and the neighbouring (6E,1Z) state. **f**, Optical control of ionic flow through a collection of photopores. **g**, ON-OFF switching of >2000 photopores at –100 mV. Number of pores was estimated assuming each pore at PSS365 contributed 50 pA. **h**, ON-OFF switching of a collection of photopores with the Nernst potential generated by asymmetrical KCl concentration across the membrane in the absence of externally applied transmembrane potential. **i**, Gating efficiency in a single, double, and ensemble pores without and with 355-nm and 532 nm in-line filters (n = 3, standard deviations shown as error bars). The

current traces were recorded at −100 mV and filtered using a 20 Hz Bessel filter. Recording conditions: 2 M KCl, 10 mM Tris-HCl, 0.1 mM EDTA, pH 8.5, 24 ± 1 °C.

Fig. 3 | Diode properties of photopores. **a**, The current–voltage (I–V) characterization of a single (E111C-pzMe)7 photopore under 365-nm or 530-nm irradiation revealed diode behaviour at negative potentials (0 to −200 mV) and resistor behaviour at positive potentials (0 to +200 mV). The 95% confidence interval (n = 3) is shown as shaded areas. **b**, The wavelength-dependent I-V characteristics of a group of (E111C-pzMe)7 photopores were attributed to the seven pzMe photoswitches within individual photopores adopting different dominant combinatorial states. Current in each I–V graph was normalized assuming that each pore contributed 50 pA at +100 mV. The number of pores ranges from 60 to 904 (n = 7). **c**, The percentage of pzMe photoswitches present in the Z configuration at the photostationery state calculated under the wavelength of 365 nm, 405 nm, 455 nm, or 530 nm. **d**, Voltage and wavelength dependence of the gating efficiency (GP = 1 − IOFF/ION). **e**, The rectification was speculated to result from the opposite orientations of pzMe photoswitches along the pore axis within the electroosmotic flow of opposite directions, which was determined by the polarity of the transmembrane potential (See Supplementary Fig. XX). **f**, Voltage dependence of the rectification ratio of a single or multiple (E111C-pzMe)7 photopores. The rectification ratio was defined as the ratio of absolute currents at +100 mV and −100 mV (n = 3, standard deviations shown as error bars). **g**, Current passing through a group of (E111C-pzMe)7 photopores in response to an applied alternating potential. h, Truth table for photopore logic.

Fig. 4 | Effects of light intensity and wavelength on photopore conductance. **a**, The rate of transition from the low-conductance state to the high-conductance state of (E111C-pzMe)7 pores decreased as the light intensity (Q%) was lowered. The drifted baseline was caused by the gradual depletion of AgCl on electrodes when recording current at the nA scale for minutes. **b**, After 228 photopores reached an equilibrium state of fully ON (ION = –11.4 nA) or OFF (IOFF = –1.8 nA) under continuous irradiation at 530 nm (green) or 365 nm (purple), reducing the light intensity from the maximum LED output (Q% = 100%) did not result in any further changes in the conductance level. **c**, The equilibrium current level was determined by the irradiation wavelength, with a fully OFF state achieved by irradiation at 530 nm (green), a fully ON state achieved by irradiation at 365 nm (purple),

and intermediate current levels at 405 nm (violet) and 455 nm (blue). **d**, The mixed-wavelength irradiation with varying ratios of 365-nm and 455-nm light in 3-min steps allowed fine-control of the PSS of a group of photopores, enabling access to intermediate equilibrium current states. The current traces were recorded at −100 mV and filtered using a 20 Hz Bessel filter. Recording conditions: 2 M KCl, 10 mM Tris-HCl, 0.1 mM EDTA, pH 8.5, 24 ± 1 °C.

Fig. 5 | Remote signal transmission with photopores. **a**, Image or text messages were encoded as light sequences to generate ionic current output through (E111C-pzMe)7 photopores. Using the provided keys, the ionic current data were deconvoluted to reconstruct the original messages. **b**, Transmission of binary pixel pattern. A representative segment of the output trace was shown with the binary current levels. **c**, Transmission of three-state pixel art ravelled to a 1D light sequence. The pixel figure was generated from PDB: 7AHL. **d**, Transmission of three-state morse code. Blue box is the deciphered morse code from the current trace, and the purple box the translated text. The light sequence was input at wavelengths of 365 nm, 455 nm or mixed 365/455 nm at a rate of 20 s per bit to generate a current pattern consisting of three levels with a group of photopores.

Example 2 - ON-OFF nanopores for optical control of transmembrane ionic communication

Summary

Nanoscale photoswitchable proteins could facilitate precise spatiotemporal control of transmembrane communication and support studies in synthetic biology, neuroscience, and bioelectronics. Through covalent modification of the α-hemolysin protein pore with arylazopyrazole photoswitches, we have produced "photopores" that transition between iontronic resistor and diode modes in response to irradiation at orthogonal wavelengths. In the diode mode, a low-leak OFF-state nanopore exhibits a reversible increase in unitary conductance of more than 20-fold upon irradiation at 365 nm. A rectification ratio of >5 was achieved with photopores in the diode state by either direct or alternating voltage input. Unlike conventional electronic phototransistors with intensity-dependent photoelectric responses, the photopores regulated current output solely based on the

wavelength(s) of monochromatic or dual-wavelength irradiation. Dual-wavelength irradiation at various relative intensities allowed graded adjustment of photopore conductance. By using these properties, photonic signals were converted into ionic signals, highlighting the potential applications of photopores as components of smart devices in synthetic biology.

Introduction

Remote control of transmembrane ionic communication can be facilitated by various molecular tools that respond to external stimuli (e.g. light [1–5] , temperature [6], magnetic [7] or electrical fields [8]). Among them, optically activated devices fitted with photo-responsive functional groups have garnered attention, which leverage light inputs to achieve spatiotemporal modulation of ionic signaling across membranes [9–11].

In top-down synthetic biology, ion fluxes across cell membranes can be modulated by nanodevices containing photoswitchable chromophores. For example, natural light-driven ion transporter proteins, such as microbial rhodopsins [12,13], generate or dissipate electrochemical gradients through chromophores such as all-trans retinal. This enables regulation of the electrical activities of cells in which rhodopsin expression has been introduced, thereby allowing basic biological activities, such as calcium signalling [14,15] and neuronal firing [16,17], to be manipulated. These optogenetic tools can also function as integral parts of miniaturized bioelectronic systems [18,19]. Optical control can also be introduced into natural ion channels through the use of synthetic photoisomerizable allosteric ligands that regulate the opening (ON) and closing (OFF) of ligand-gated receptors, such as ionotropic glutamate receptors [20], transient receptor potential channels [21], and voltage-gated K^+ or Ca^{2+} channels [5,22].

In bottom-up synthetic biology, to modulate transmembrane ionic signaling, there is a strong demand for photoresponsive devices featuring modular design, ease of assembly, immediate and reversible ON-OFF responses, sustained ON and complete OFF states, and the potential to respond to additional input stimuli. Fully synthetic systems offer broad scopes of designs and applications, but face challenges in affording efficient, real-time and light-actuated ion movements across membranes. For example, DNA nanopores equipped with a photoisomerizable lid strand were optically activated or deactivated before inserting

into lipid bilayers [23]. Synthetic ion transporters with built-in photoswitches moved ions down a transmembrane gradient one at a time [24,25]. Semi-synthetic approaches are also pursued to leverage the natural ON-OFF machinery of protein channels. Chemical engineering of proteins with photoswitches enabled transient light-activated opening of mechanosensitive channels4 or timed irreversible formation of protein nanopores [26,27]. New designs are required to achieve prolonged activation and reversible ionic responses to light.

Here, we describe reversible ON-OFF photopores, which exhibit a long open lifetime in the ON state and a low background current in the OFF state. The ON-OFF machinery has been engineered into a protein construct that was not evolved to open and collapse and can be activated in real time when embedded in membranes. This was achieved by covalent modification of α-hemolysin (αHL) monomers with arylazopyrazoles that exhibit almost quantitative photoswitching between E and Z isomers and exhibit high thermal stability in both states. The photopores have been characterized at both the single-molecule and ensemble levels to showcase their ability to permit or restrict transmembrane ionic current in response to light. The pores exhibit behaviors analogous to both electronic diodes (i.e. one-way current flow) and light-tunable resistors (i.e. current modulation) depending on the wavelength of irradiation. The properties of the photopores have been exploited to generate light-to-ionic signal conversion.

Results and discussion

Construction of photoreversible nanopores

To construct photopores, we functionalized α-hemolysin (αHL), a heptameric protein nanopore, with photoisomerizable chemical groups on the interior of the channel (Fig. 9/Example 2 Fig. 1). The αHL monomers containing a single cysteine residue at position 111, 115, 125 or 129 were separately modified with one of the three types of photoswitches—o-fluoroazobenzene (fAzo) [28], arylazopyrazole (pzH) [29], or methyl arylazopyrazole (pzMe) [30] —by using thiol-specific chemistry (Figs. 9a,b, 14 and 15/Example 2 Fig. 1a,b, Supplementary Figs. 1 and 2). Upon assembly into heptamers, the side chains of these residues project into the lumen of the transmembrane β barrel [31].

The modification of αHL monomers (Fig. 16/Example 2 Supplementary Fig. 3) with one molecule of either fAzo, pzH, or pzMe was confirmed by liquid chromatography-mass spectrometry (LC-MS) (Figs. 9c, 17 and 18/ Example 2 Fig. 1c, Supplementary Figs. 4 and 5). Modified monomers with these photoswitches self-assembled to form homoheptameric pores when introduced into a synthetic lipid bilayer consisting of 1,2-diphytanoyl-sn-glycero-3-phosphocholine (DPhPC) or in the presence of sodium deoxycholate (Fig. 9a/Example 2 Fig. 1a).

The fAzo, pzH, and pzMe photoswitches were reported to exhibit high E/Z or Z/E isomer ratios at photostationary states (PSSs) as well as thermal stability in the Z state. [28,29] Determined by ultraviolet/visible (UV/Vis) and proton nuclear magnetic resonance (1H NMR) spectroscopy, the bromoacetamide derivative of pzMe (Br-pzMe) demonstrated the highest isomer ratios at PSSs generated by 'orthogonal' wavelengths (Fig. 9d,e/Example 2 Fig. 1d,e). Upon LED irradiation at 365 nm, Br-pzMe was converted primarily to the Z isomer (PSS365 = 96% Z), while when irradiated at 530 nm, Br-pzMe was present predominantly as the E isomer (PSS530 = 93% E) (Figs. 9e and 19/Example 2 Fig. 1e and Supplementary Fig. 6). By contrast, Br-fAzo was 85% in the E form at PSS405 and 91% in the Z form at PSS530, while Br-pzH was 65% E at PSS365 and 85% Z at PSS530 (Fig. 19/ Example 2 Supplementary Fig. 6). High isomer ratios were expected to produce tight control of ionic communication through modified nanopores.

Reversible ON-OFF photopores

The photoreversible modulation of ionic current passing through αHL nanopores containing fAzo, pzH, or pzMe photoswitches was first characterized by ensemble electrical recordings in planar lipid bilayers (PLB), i.e. in bilayers containing hundreds or thousands of pores. A bespoke poly(methyl methacrylate) (PMMA) chamber was made, equipped with a collimated fiber-coupled LED, for electrical recording under illumination over a range of intensities from the grounded side (trans) of the bilayer (Figs. 9f and 20/ Example 2 Fig. 1f and Supplementary Fig. 7). To align with the convention of reporting current through αHL pores, we defined a positive current as one in which positive ions moved through the bilayer from the trans side of the pore to the cis (i.e. from the bottom of

the barrel towards the vestibule). The transmembrane potential (Vm) was given as the potential on the trans side relative to the cis side.

Interconversion between a high-current level (ION) and a low-current level (IOFF) was recorded at +100 mV with pores equipped with fAzo, pzH, or pzMe under alternating wavelengths (365 nm/530 nm for pzH and pzMe, or 405 nm/530 nm for fAzo) (Figs. 10a, 14 and 15/Example 2 Fig. 2a and Supplementary Figs. 1 and 2). We refer to the lower-current state as the OFF state, in which the ionic flow is partially or almost completely restricted, by comparison with the highest obtainable current level, which is the ON state. In general, the photoreversible nanopores switched to the ON state after irradiation at the shorter wavelength (photoswitches in the Z state), and to the OFF state following irradiation at the longer wavelength (photoswitches in the E state).

Of the homoheptamers modified at position 111 with fAzo, pzH, or pzMe, (E111C-pzMe)7 produced the largest percent gated current [Igate% = (1 − IOFF/ION) × 100%] of 85% at the ensemble level, whereas the other two photoswitches produced low Igate% values of ~20% (Fig. 15/Example 2 Supplementary Fig. 2). When the pzMe modification was moved to positions 115, 125, or 129, a decrease in Igate% was recorded. Without further investigating the mechanism underlying the position- and photoswitch-dependent efficiency of current gating, we proceeded to characterize the (E111C-pzMe)7 photopore and explore its applications.

We investigated the photochemistry underlying the ON-OFF behavior of (E111C-pzMe)7 photopores at the single-channel level (Fig. 2b-f). Sequential insertions of pre-formed heptamers, pre-irradiated at 365 nm, revealed that the ON-state conductance of individual photopores ranged from 0.12 to 1.27 nS. The average conductance of a pore (0.62 ± 0.30, N = 42 pores) was three times smaller than wild type αHL (1.81 ± 0.17 nS, N = 17 pores) (Figs. 21-22/Example 2 Supplementary Figs. 8-9). Nevertheless, an $I_{gate\%}$ of 95 ± 2.5% (N = 21) was consistently recorded at the single-channel level across all the (E111C-pzMe)7 photopores observed (Fig. 23-24/Example 2 Supplementary Figs. 10-11). Reversible photogating was observed by voltage–clamping individual single photopores and exposing them to ten repeats of UV (365 nm) → dark → green (530 nm) → dark (Figs. 10b and 25/Example 2 Fig. 2b and Supplementary Fig. 12). Upon UV irradiation, a photopore switched from ON to OFF with a mean response time of 1.8 ± 0.8 s (N = 9 transitions), and the OFF-to-ON transition occurred on average within 31.4 ± 7.7 s (N = 9 transitions) under

the green light. The LED irradiance values (365 nm: 36.2 mW/cm^2; 530 nm: 30.3 mW/cm^2) were derived from measurements of light intensities in microwatts through a 300 μm-diameter pinhole in place of the bilayer (See Fig. 20/Example 2 Supplementary Fig. 7). The intermediate current levels between I_{ON} and I_{OFF} were likely produced by the stepwise isomerization of individual pzMe molecules (Fig. 10c/Example 2 Fig. 2c). Based on the number of pzMe switches in either the E or Z state within a photopore, we designated the configuration of an ON-state photopore as (0E, 7Z), the photopore at the maximum OFF state as (7E, 0Z), and a partially OFF pore as one ranging from (1E, 6Z) to (6E, 1Z) (Fig. 10b/Example 2 Fig. 2b). Notably, the intermediate current levels recorded with a single photopore during its ON-to-OFF or OFF-to-ON transitions differed from one transition to another (Fig. 26/Example 2 Supplementary Figs. 13). For example, during the stepwise reduction of the current recorded through an (E111C-pzMe)$_7$ photopore under 530-nm irradiation, more than 10 distinct current levels were recorded across multiple transitions (Fig. 26a/Example 2 Supplementary Fig. 13a). The complexity was attributed to both the combinatorial possibilities of the E/Z configurations of the seven photoswitches [32], as well as the conformations of the photoswitches. For example, in the (5E, 2Z) state, there are three possible arrangements of the two pzMe photoswitches in the Z configuration around the central axis of the pore (Fig. 26b/ Example 2 Supplementary Fig. 13b). Once a single photopore reached a terminal ON or OFF state, the current level exhibited fluctuations under continuous irradiation, while remaining relatively stable in the dark (Fig. 10d-f/Example 2 Fig. 2d-f). This was expected as continuous irradiation would drive the reversible isomerization of photoswitches within an (E111C-pzMe)$_7$ photopore: for example, switching between (0E, 7Z) and (1E, 6Z) states under 365 nm or (7E, 0Z) and (6E, 1Z) states under 530 nm. In the dark, (E111C-pzMe)$_7$ photopore was locked in a single configuration; no Z-to-E thermal relaxation was observed for at least 1 hour after the irradiation was turned off (Fig. 27/ Example 2 Supplementary Fig. 14).

The behavior of the (E111C-pzMe)$_7$ photopores at the ensemble level was compared to that at the single-channel level (Fig. 10g/Example 2 Fig. 2g). We found that the $I_{gate\%}$ value was ~10% lower with multiple pores compared to that of a single pore. This was likely caused by the presence of photopores in partially ON configurations as predicted by the single-channel observations (Fig. 28/Example 2 Supplementary Fig. 15). The incorporation of in-line bandpass filters to reduce the LED bandwidths to 10 nm did not improve the

$I_{gate\%}$ value. By employing an asymmetric KCl concentration across a membrane to establish a physiologically relevant membrane potential (Fig. 29/ Example 2 Supplementary Fig. 16), the photoswitching behavior was reproduced in the absence of an externally applied transmembrane potential (Fig. 10h/Example 2 Fig. 2h).

Switchable iontronic diode properties of (E111C-pzMe)$_7$ photopores

The ON-OFF behavior of the (E111C-pzMe)$_7$ photopore was further demonstrated in a broader range of applied potential by ramping the voltage from −200 mV to +200 mV at 10 mV per step. We characterized the current-voltage (I–V) behavior of a single (E111C-pzMe)$_7$ photopore in the dark after reaching the ON at 365 nm or the OFF state at 530 nm (Fig. 11a/Example 2 Fig. 3a). After irradiation at 530 nm, the photopore exhibited a diode-like non-linear I–V response; almost no current passed through the pore at positive potentials (0 to +200 mV, Vm applied on trans side, Fig. 9f/Example 2 Fig. 1f), whereas the current demonstrated resistor-like behavior at negative potentials (G = I/V = 0.32 ± 0.11 nS at −100 mV, N = 3 pores) (Fig. 11a/Example 2 Fig. 3a). After irradiation at 365 nm, a less obvious rectification was observed (G = I/V = 0.46 ± 0.06 nS at +100 mV and 0.58 ± 0.12 nS at −100 mV, N = 3 pores) (Fig. 11a/Example 2 Fig. 3a). In other words, the photopore functioned as a photoresistor after irradiation at 365 nm and as an iontronic diode after irradiation at 530 nm. We speculate that the voltage-dependent behavior of (E111C-pzMe)$_7$ photopores arises from the biased orientation of photoswitches confined within an asymmetric nanopore. The orientation of these charge-neutral photoswitches could be influenced by electroosmotic flow, which is directionally dependent on the applied voltage. Depending on their orientations, the seven photoswitches could adopt various configurations, promoted by the surrounding protein environment, thereby altering the ionic flow.

The dual-mode feature (i.e., diode and photoresistor) demonstrated with single pores was reproduced with hundreds of pores in ensemble experiments (N = 8 experiments, 100 to 600 pores per experiment) under 365-nm and 530-nm irradiation (Fig. 11b/Example 2 Fig. 3b). Irradiation at wavelengths of 405 nm and 455 nm was also tested; these wavelengths generated current levels between those produced by 365 nm and 530 nm at all applied potentials (Fig. 11b/Example 2 Fig. 3b). To give an overview of the voltage-dependent

behavior in the ensemble, $I_{gate\%}$ was calculated following $I_{gate\%} = (1 - I_{OFF}/I_{ON}) \times 100\%$, where the current level after 365-nm irradiation was I_{ON} and that after 405 nm, 455 nm, or 530 nm was I_{OFF} (i.e. $I_{gate\%(405\ nm)} = (1 - I_{405}/I_{365}) \times 100\%$) (Fig. 11c/Example 2 Fig. 3c). Between −150 mV to +100 mV, $I_{gate\%}$ increased with decreasing negative potential and increasing positive potential for all three wavelengths. From +100 mV to +200 mV, $I_{gate\%}$ plateaued at ~85% for 530 nm, ~80% for 455 nm, and ~60% for 405 nm (Fig. 11c/Example 2 Fig. 3c). Under negative potentials, $I_{gate\%}$ plateaued at ~20% for 405 nm and 455 nm, and ~35% for 530 nm when approaching −200 mV (Fig. 11c/Example 2 Fig. 3c). The difference in PSS ratios associated with irradiation wavelengths was the primary reason for the wavelength dependence of $I_{gate\%}$. Moreover, the voltage dependence should be ascribed to the relative population of the strongly rectifying (7E, 0Z) state. The rectification ratio of $(E111C\text{-}pzMe)_7$ (RR = I_-/I_+, the ratio of currents recorded under opposite polarities at the same potential) scaled almost linearly with the amplitude of the applied potential up to ±150 mV (Fig. 11d/Example 2 Fig. 3d), and was 5.5 ± 0.7 at ±100 mV in the diode mode after 530-nm irradiation (Fig. 11d/Example 2 Fig. 3d).

Nanopore diodes can be used in soft devices as half-wave rectifiers [33] to convert alternating current to direct current. We tested our photopore as a switchable iontronic diode to effect a unidirectional current across a synthetic bilayer under an alternating voltage at 0.03 Hz (Fig. 11e/Example 2 Fig. 3e). After 530-nm irradiation, an ensemble of ~900 $(E111C\text{-}pzMe)_7$ photopores functioned as a half-wave rectifier and conducted currents only under a negative potential. After 365-nm irradiation, the current flow replicated the sinusoidal shape of the alternating voltage input, albeit weakly rectified. At higher input frequencies, the capacitive current caused by the bilayer would override the resistive current through the pore, diminishing the rectification. The ionic current output through $(E111C\text{-}pzMe)_7$ photopores was therefore determined by both the wavelength and the applied potential, resembling the NAND Boolean function. This NAND logic gate leveraged the switchable diode properties of $(E111C\text{-}pzMe)_7$ photopores, with the irradiation wavelength as input 1 (0 = 365 nm, 1 = 530 nm) and the applied potential as input 2 (0 = −100, 1 = +100 mV). A low current output only occurs at +100 mV after irradiation at 530 nm (Fig. 11f/Example 2 Fig. 3f).

Light-to-ionic signal conversion with $(E111C\text{-}pzMe)_7$ photopores

The rate of photoisomerization of a photoswitch is typically proportional to the light intensity [5,34,35]. Accordingly, 365-nm irradiation of more than 600 $(E111C\text{-}pzMe)_7$ pores at 36.2, 28.2 and 13.4 mW/cm^2 (Fig. 20/Example 2 Supplementary Fig. 7) increased the duration of OFF-ON transition from 5.8 ± 0.5 s to 7.1 ± 0.6 s, and then to 11.4 ± 2.6 s (N = 4 ensembles, Fig. 12a/Example 2 Fig. 4a). After the equilibrium current level was reached under a given wavelength of irradiation, a reduction in the light intensity led to no change in the current level of an ensemble (Fig. 12b/Example 2 Fig. 4b). In contrast, common electronic components and optogenetic tools often exhibit transient current responses that vary with light intensity.

An ionic signal conducted by multiple $(E111C\text{-}pzMe)_7$ photopores at an intermediate current level between I_{ON} and I_{OFF} could be achieved by switching off the irradiation immediately after reaching the desired current level during an ON-OFF transition at a given wavelength. However, it was challenging to reproducibly capture a transient current level of interest during rapid ON-OFF transitions. An alternative strategy was devised using polychromic light to produce an equilibrium current level as determined by the PSS of photoswitches (Fig. 12c,d/Example 2 Fig. 4c,d). To investigate whether mixed-wavelength irradiation could yield equilibrium current levels unattainable by continuous irradiation at either one of the wavelengths, light from 365-nm and 455-nm LEDs was combined through a fiber-coupler. The graded modulation of ionic signal was demonstrated by varying the relative intensity of the 365-nm and 455-nm irradiation projected onto the multiple $(E111C\text{-}pzMe)_7$ pores in 3-minute steps. Ionic signal levels between those recorded at PSS365 and PSS455 were obtained (Fig. 12d/Example 2 Fig. 4d). This approach allowed for finer control over the graded modulation of ionic current through $(E111C\text{-}pzMe)_7$ photopores.

Inspired by the slow thermal relaxation of arylazopyrazole and the graded modulation of the ionic signal, we proposed light-to-ionic signal conversion by an ensemble of iontronic photopores. We first encrypted information-bearing binary data within light sequences that alternated between 365-nm and 455-nm radiation (Fig. 13a/Example 2 Fig. 5a). Functioning as a light-to-current converter, the $(E111C\text{-}pzMe)_7$ photopores translated the light sequences into two-level current patterns (Fig. 13a/Example 2 Fig. 5a), as illustrated by a representative segment of a trace with an input rate of 20 s/bit (Fig. 13b/Example 2

Fig. 5b). Higher input rates were achieved with increased light intensities, reaching 1.5 s/bit at 365 nm and 1.9 s/bit at 455 nm using the maximum LED outputs. Over a 90-minute experiment, no photobleaching was observed. By associating the ON-state with a black pixel and the OFF state with a white pixel, a pixel art spelling "OXFORD" was reconstructed from a binary light message. Furthermore, adding mixed irradiation at both 365 nm (36.2 mW/cm^2) and 455 nm (56.3 mW/cm^2) expanded the alphabet to a three-state system, which was applied to demodulate a pixel art representation of a protein nanopore and a text message written in Morse code (Fig. 13c,d/Example 2 Fig. 5c,d). In principle, by using mixed-wavelength irradiation, the $(E111C\text{-}pzMe)_7$ photopores could output a series of current levels, between the levels at PSS365 and PSS530, as the basis of complex encoding systems. With our equipment, the current levels fluctuate ± 0.3% in the dark after a 20 Hz digital filter, and the $I_{gate\%}$ was 0~85%. Thus, an upper-level estimate for the number of assignable levels would be ~300.

Conclusions

In this work, we constructed protein nanopores with unitary conductance values that changed under remote light control. Among the tested photopores, we achieved quantitative, prolonged, and reversible modulation of ionic currents within $(E111C\text{-}pzMe)_7$ pores following irradiation at 365 nm (ON, high conductance) and 530 nm (OFF, low conductance). Notably, when an $(E111C\text{-}pzMe)_7$ pore in the ON state was switched OFF at +100 mV, a >95% reduction in the unitary conductance was observed. Similarly, a current reduction of >85% was observed when multiple $(E111C\text{-}pzMe)_7$ pores were used in ensemble experiments. This sustained ON state and the almost complete OFF state is highly advantageous for real-time control over transmembrane ionic communication in nanotechnology or synthetic biology applications.

The photopores described here differ from previously described photoregulated nanopores in two aspects. First, the photoswitches controlled the conductance of a fully assembled nanopore reversibly, rather than the process of irreversible nanopore assembly [27]. Second, the current-voltage characteristics of $(E111C\text{-}pzMe)_7$ exhibited two switchable states: a resistor-like ON-state, after 365-nm irradiation, and a diode-like OFF-state, after 530-nm irradiation. In the diode mode, there is no delay in the rectification of (E111C-

pzMe)$_7$ after the reversal of the polarity of the applied potential, in contrast to the previous (non-photoswitchable) arginine-rich αHL diode [33].

One impact of photopores in the field of nanoscale iontronics might be in light-to-ionic current signaling. In the case of the (E111C-pzMe)$_7$ pore, we have used the ability to produce multiple output current levels, such as the three-state system (blue, mixed, and UV), to demonstrate the ability to reconstruct images or text encoded in light pulses. It follows that by hosting light-modulated nanopores in a 2D array of lipid bilayers, an artificial retina might be created to detect colored images. Our previous work on droplet-hydrogel-bilayer bio-pixels reported a related approach for monochromic 530 nm light [36].

The photopores might also be incorporated into 3D-printed droplet-based synthetic tissues where the spatiotemporal control of communication between compartments is key to the control of tissue-like behaviour [37,38], There, they could be used, amongst other things, to trigger the release of ions or small molecules [38], mediate shape changes [37] or produce motion [39]. We further envisage the development of additional photopores by the conjugation protocol reported here to gain control over additional properties such as selectivity in the transport of small molecules and the ability to mediate the translocation of biopolymers.

Methods

General information

All chemicals were purchased from Merck and used as received unless otherwise stated. Br-pzMe, Br-fAzo and Br-pzH were prepared (see Synthesis and characterization of photoswitches) and used as 3 mM DMSO stock solutions for bioconjugation experiments. Details of synthesis are available in the synthesis section. The fiber-coupled LEDs were purchased from Thorlabs (M405FP1, M455F3 and M530F2). An optical fiber (Ø1000 μm, 0.39 NA) was supplied by Mightex. LC-MS of αHL monomers were recorded on a benchtop QTOF mass spectrometer (Waters Xevo G2-XS) with a ProSwift RP-2H column (ThermoFisher, linear-gradient acetonitrile/water, 0.1% (v/v) TFA, 10 min), and the results were deconvoluted using MassLynx software (Waters). An Arduino UNO microcontroller

was programmed to trigger and log the time points of irradiation. Molecular modelling was carried out by using open-source PyMol on GitHub (Schrodinger).

Preparation of photopore monomers

Site-directed mutagenesis of αHL cysteine mutants

Genes encoding αHL mutants with a single cysteine residue at position E111, T115, T125 or T129 were prepared from the pT7-αHL-D_8H_6 plasmid by site-directed mutagenesis (QuikChange II XL, Agilent) with the primers listed in Table S1. The template plasmid have been previously reported [40], where the octaaspartate and hexahistidine tag (-D_8H_6) was designed for anion exchange (IEX) and Ni-NTA purification. The polymerase chain reaction was initiated by mixing 5 μL 10 × reaction buffer, 10 ng DNA template, 125 ng forward and reverse primers, 1 μL dNTP mix, 3 μL QuikSolution, 2.5 U PfuUltra HF DNA polymerase and nuclease-free water to make a final volume of 50 μL. After thermal cycling (1 × 95°C:1 min → 18 × 95°C: 50 s, 60°C: 50 s, 68°C: 5 min → 1 × 68°C: 7 min), 1 μL DpnI (10 U) was added and the mixture was incubated for 1 h at 37°C to digest the template DNA. Transformation of *E. coli* was performed by incubating 2 μL of the digested PCR product with 45 μL XL-10 Gold competent cells (Agilent) on ice, followed by 30 s heat shock at 42°C. Subsequently, a Luria-Bertani (LB)-agar plate containing carbenicillin (50 μg mL^{-1}, Merck) was inoculated with the transformed cells. All mutants were verified by DNA sequencing.

Expression and purification of αHL cysteine mutants

BL21(DE3)pLysS *E. coli* cells (Agilent) were transformed with the mutated plasmid and inoculated onto LB-agar plates containing antibiotics (carbenicillin, 50 μg mL^{-1}; chloramphenicol, 34 μg mL^{-1}). A single colony from the plate was picked to inoculate 10 mL LB for the preculture. A 400 mL LB culture containing the same antibiotics was inoculated with 4 mL overnight pre-culture. This expression culture was shaken at 37°C at 250 rpm for approximately 3 h until the OD reached 0.6, when it was cooled 18°C before the addition of 2 mL 0.1 M IPTG (Fluorochem) to induce protein expression. The culture was further shaken at 18°C at 200 rpm overnight. The cells were then harvested by centrifugation in a Beckman J25 centrifuge at 5000 rpm for 20 min at 4°C and resuspended in 10 mL lysis buffer (50 mM Tris-HCl, pH 8.0, 150 mM NaCl, 10 mM imidazole, 0.1%

Triton X-100, 5% glycerol, 2 mM TCEP with an EDTA-free protease-inhibitor tablet (ThermoFisher)). Lysis was then performed by the addition of 250 µL 40 mg/mL lysozyme (ThermoFisher), 2 µL 250 U/µL universal nuclease (ThermoFisher) and 25 µL 2 M $MgCl_2$, and incubation on ice for 1 h. The lysate was sonicated at 40% amplitude for 3 min in a 30 s-ON-30 s-OFF pulse train on ice (VCX 500, Sonics). The supernatant was cleared by centrifugation at 29000 x g for 45 min at 4˚C and transferred to a gravity column containing 1 mL (bed volume) Ni-NTA resin (ThermoFisher). The lysate supernatant and resin mixture was mixed at 4˚C on a platform rotator for 1 h. The column was washed with 2 x 15 mL washing buffer (50 mM Tris-HCl, pH 8.0, 500 mM NaCl, 20 mM imidazole, 2 mM TCEP, 0.1% Triton X-100 and 5% glycerol) and eluted with elution buffer (50 mM Tris-HCl, pH 8.0, 500 mM NaCl, 250 mM imidazole, 2 mM TCEP, 0.1% Triton X-100 and 5% glycerol). The fractions (~10 mL) containing αHL were combined and loaded onto a HiLoad 26/600 Superdex 200pg (Cytiva) SEC column equilibrated with SEC buffer (10 mM Tris-HCl, pH 8.0, 150 mM NaCl, 2 mM TCEP and 5% glycerol) at 4˚C. Fractions containing monomers of αHL cysteine mutants were concentrated to 1 mg/mL and stored at −80˚C as aliquots. The mass of the monomer was verified by LC-MS. On average, 9 mg pure αHL-D_8H_6 monomer after SEC purification was obtained from 400 mL culture.

Conjugation of photoswitches

Br-pzMe, Br-pzH or Br-fAzo (the photoswitches) were dissolved at 3 mM in dimethyl sulfoxide (DMSO). Purified monomers of the αHL cysteine mutants were buffer-exchanged and diluted to 0.5 mg/mL in low TE buffer (10 mM Tris-HCl, pH 8.0, 0.1 mM EDTA). A photoswitch was added to a monomer solution stepwise over 18 h to a final concentration of 750 µM. The mixture was incubated at 20˚C and cooled to 4˚C before the removal of the excessive photoswitch. The extent of reaction was assessed by LC-MS. The conjugated protein solution was passed through a desalting spin column (ThermoFisher) equilibrated in the low TE buffer to remove excess photoswitch and the eluent was stored at −80˚C.

Formation and purification of photopore homoheptamers

The photopore monomer was concentrated with a PES protein concentrator (ThermoFisher) to ~8 mg/mL, and exchanged into low TE buffer (10 mM Tris-HCl, pH

8.0, 0.1 mM EDTA) with a desalting spin column. Heptamerization was performed by adding 10% (w/v) sodium deoxycholate solution to the concentrated protein solution, reaching a final concentration of 6.25 mM. The mixture was incubated at 22°C for 1 h. To separate oligomerized photopores from the remaining monomers, the mixture was loaded onto a membrane-based strong cation exchange spin column (ThermoFisher), which was equilibrated with 20 mM MOPS, pH 7.5. The sample was eluted with the same buffer containing NaCl (0.2, 0.3, 0.4, 0.6, 2 M) (Fig. 21b/Example 2 Supplementary Fig. 8b). The homoheptamer eluted at ~0.3 M NaCl, and fractions were combined and frozen at −80°C. Before electrical recording, the MOPS buffer was exchanged for low TE buffer (10 mM Tris-HCl, pH 8.0, 0.1 mM EDTA).

Electrical recording in the planar lipid bilayers

Custom recording chamber

Planar lipid bilayer recording experiments were performed in a custom poly(methyl methacrylate) (PMMA) recording chamber. The chamber accommodated an LED light source through an adjustable FiberPort collimator (Thorlabs), allowing accurate alignment and direct irradiation of the aperture in the Teflon film (Ø100 µm). Before recording, the collimator was adjusted to achieve consistent projection of the maximum light intensity onto the aperture through a 3-mm-thick sapphire window (Thorlabs). Fiber-coupled LEDs of various wavelengths (365, 405, 455, 530 nm, Thorlabs) were connected to the collimator through a UV-compatible multimode fiber (0.39 NA, Ø1000 µm, Mightex). In the experiments with mixed wavelengths, a bifurcated fiber bundle (0.39 NA, Ø1000 µm, Thorlabs) was connected to two LEDs. Band-pass filters (Thorlabs) were used for the data presented in Fig. 10g/Example 2 Fig. 2g to achieve a narrow bandwidth of 10 nm for 355 nm and 4 nm for 532 nm (Fig. 23c/Example 2 Supplementary Fig. 10c). These filters were loaded onto an integrated in-line reflective fiber optic filter (Thorlabs).

Single-channel and ensemble experiments

The Teflon aperture of the recording chamber was pre-treated with hexadecane (~5 µL 1% in pentane). After 10 min, recording buffer (1 mL, 10 mM Tris-HCl pH 8.5, 2 M KCl, 0.1 mM EDTA) was added to both the cis and trans compartments. A lipid bilayer was formed

on the aperture by adding 1,2-diphytanoyl-3-sn-phosphatidylcholine (DPhPC, Avanti Polar Lipids) to each compartment. A pair of Ag/AgCl electrodes was placed in each compartment through a salt bridge (3 M KCl in 2% (w/v) agarose). The electrodes were covered with black tape to avoid exposure to light from the LED.

To insert a single pore into the bilayer (Fig. 23a/Example 2 Supplementary Fig. 10a), homoheptamer (0.1 µL, 0.2 mg/mL) was added to the cis compartment. Once a pore had inserted and showed photoresponse, the buffer was perfused five times to prevent further insertions. To achieve the stepwise insertion of multiple pores, more homoheptamer (10 µL, 0.2 mg/mL) was used (Fig. 22a/Example 2 Supplementary Fig. 9a).

The characterization of the photopore ensemble was recorded using photopore monomers pre-irradiated at 530 nm for 30 min prior to use to ensure the reproducibility of pore insertion (Fig. 23c/Example 2 Supplementary Fig. 10c). The monomers (~5 µL 0.2~0.5 mg/mL) were added to the cis compartment while 530 nm LED was switched on. Pore insertion occurred under an alternating applied potential of ±20 mV, and the insertion rate slowed down over 15 min. Excess monomers were removed by perfusion of the cis compartment.

Ionic currents were recorded through Ag/AgCl electrodes connected to a patch clamp amplifier (Axopatch 200B, Axon Instruments). The signal was filtered with an in-line 4-pole low-pass Bessel filter (80dB/decade, 5 kHz). A Digidata 1322A digitizer (Molecular Devices) was used to convert the analogue signal to digital form. The data were analyzed with the pCLAMP 10.3 software suite (Molecular Devices). Electrical traces were plotted with Python (3.8.8), Pyabf (2.3.5), Matplotlib (3.3.4) and Seaborn (0.11.1).

$(E111C\text{-}pzMe)_7$ permeability ratios (P_{K+}/P_{Cl-}) and electro-osmotic flow

The current–voltage response of $(E111C\text{-}pzMe)_7$ was measured over an applied potential ranging from −200 mV to + 200 mV in 10 mV increments with an asymmetric KCl gradient: 2 M KCl (cis) / 0.2 M KCl (trans) (Fig. 29/Example 2 Supplementary Fig. 16). The permeability ratio (P_{K+}/P_{Cl-}) was determined from the potential at the zero current intercept (the reversal potential, V_r) by using the Goldman-Hodgkin-Katz (GHK) equation [41]:

$$\frac{P_{K^+}}{P_{Cl^-}} = \frac{[Cl^-]_{trans} - [Cl^-]_{cis} e^{\frac{V_r F}{RT}}}{[K^+]_{trans} e^{\frac{V_r F}{RT}} - [K^+]_{cis}} \quad (1)$$

where F is the Faraday constant; R is the ideal gas constant; T is 298K.

The magnitude of the electro-osmotic flow (J_{EOF}) under symmetrical KCl conditions could then be determined from [42]:

$$J_{EOF} \propto V_m \frac{\frac{P_{K^+}}{P_{Cl^-}} - 1}{\frac{P_{K^+}}{P_{Cl^-}} + 1} \quad (2)$$

where P_{K+}/P_{Cl-} was 0.15 ± 0.01 (530 nm, N = 4 repeats) and 0.20 ± 0.01 (365 nm, N = 4 repeats).

Transmembrane signal transmission by light-to-current conversion

To achieve light-to-current signal conversion, three steps are required. First, the encrypted digital data, as pixel art or text, were converted into a monochromatic or polychromatic 1D light sequence. In the 4 × 25 pixel pattern of the 'OXFORD', the pixel art plotted with Matplotlib was unraveled to a 100 × 1 string of two states (black/white), which were further assigned to '365 nm'/'455 nm' to obtain a light sequence. For example, a list of colors ['black', 'black', 'white', …, 'black'] was converted to a light sequence ['365 nm', '365 nm', '455 nm', …, '365 nm'].

In the αHL pixel art, a snapshot of the PDB:7AHL nanopore model was first converted to a three-color 16 × 16 pixelated image by Adobe Illustrator. The value of each pixel was extracted with Python Imaging Library to generate a 16 × 16 × 3 array, where the 3 was for the RGB color code. This array was unraveled to a 256 × 3 array, and the RGB color code was further replaced by the wavelength. For instance, the RGB color code of white (0,0,0) was assigned to 'mixed (365 + 455) nm'. The assignment of grey and dark grey colors to '455 nm' and '365 nm' lead to a 256 × 1 light sequence. Likewise, the 18-word Morse code sequence (dot/ space/ dash) was converted to the same three wavelengths to generate a light sequence.

In the second step, the 1D light sequence was sent to an Arduino UNO microcontroller to trigger the 365 nm and 455 nm LEDs accordingly. Due to the switching rate of the photopore, each unit of irradiation (a bit) was optimized to last for 20 s to observe the

rectangular signals. A higher rate of data transmission might be obtained at increased light intensities. During the lifetime of a bit, the LEDs were coupled through the bifurcated fiber bundle and switched on or off according to the light sequence to produce a high (365 nm), middle (mixed), or low (455 nm) ionic current response through the photophore.

The final step was to process the electrical recording to visualize and analyze the output signal. The electrical recording trace was processed in reverse from the 1 × N current signal to the pixel image or text. A continuous recording trace sampled at 25 kHz was segmented into bits of 20 s (one 20-second bit = 500000 data points of 0.04 ms), and each bit was denoted as 'high', 'middle' or 'low' state based on the mean value compared to manually chosen thresholds. The state values were further replaced by ('black'/'white' for the 'OXFORD' pattern), ('dark grey'/'white'/'grey' for the αHL pixel art) or ('dot'/'space'/'dash' for the Morse code). Finally, the new array was transformed into the proper dimension and displayed with Matplotlib to visualize the image or text.

Table S1 – Primers used for site-directed mutagenesis

Primers	Forward and reverse primer sequences (5′→3′)
E111C	GAAATTCGATTGATACAAAATGCTATATGAGTACTTTAACTTATGG (SEQ ID NO: 2) CCATAAGTTAAAGTACTCATATAGCATTTTGTATCAATCGAATTTC (SEQ ID NO: 3)
T115C	GATACAAAAGAGTATATGAGTTGCTTAACTTATGGATTCAACGG (SEQ ID NO: 4) CCGTTGAATCCATAAGTTAAGCAACTCATATACTCTTTTGTATC (SEQ ID NO: 5)
T125C	GGATTCAACGGTAATGTTTGTGGTGATGATACAGGAAAAATTGGCGGCC (SEQ ID NO: 6) GGCCGCCAATTTTTCCTGTATCATCACCACAAACATTACCGTTGAATCC (SEQ ID NO: 7)
T129C	GTTACTGGTGATGATTGTGGAAAAATTGGCGGCC (SEQ ID NO: 8) GGCCGCCAATTTTTCCACAATCATCACCAGTAAC (SEQ ID NO: 9)

Primers	Length (nt)	GC %
E111C	44	28
T115C	44	34
T125C	49	45
T129C	34	50

References

1. Bozovic, O., Jankovic, B. & Hamm, P. Using azobenzene photocontrol to set proteins in motion. *Nat. Rev. Chem.* **6**, 112–124 (2022).
2. Emiliani, V. *et al.* Optogenetics for light control of biological systems. *Nat. Rev. Methods Primers* **2**, (2022).
3. Kramer, R. H., Chambers, J. J. & Trauner, D. Photochemical tools for remote control of ion channels in excitable cells. *Nat. Chem. Biol.* **1**, 360–365 (2005).
4. Koçer, A., Walko, M., Meijberg, W. & Feringa, B. L. Chemistry: a light-actuated nanovalve derived from a channel protein. *Science.* **309**, 755–758 (2005).
5. Banghart, M., Borges, K., Isacoff, E., Trauner, D. & Kramer, R. H. Light-activated ion channels for remote control of neuronal firing. *Nat. Neurosci.* **7**, 1381–1386 (2004).
6. Vriens, J., Nilius, B. & Voets, T. Peripheral thermosensation in mammals. *Nat. Rev. Neurosci.* **15**, 573–589 (2014).
7. Huang, H., Delikanli, S., Zeng, H., Ferkey, D. M. & Pralle, A. Remote control of ion channels and neurons through magnetic-field heating of nanoparticles. *Nat. Nanotechnol.* **5**, 602–606 (2010).
8. Catterall, W. A. Ion channel voltage sensors: Structure, function, and pathophysiology. *Neuron* **67**, 915–928 (2010).
9. Hirschi, S., Ward, T. R., Meier, W. P., Muller, D. J. & Fotiadis, D. Synthetic biology: bottom-up assembly of molecular systems. *Chem. Rev.* **122**, 16294–16328 (2022).
10. Ankenbruck, N., Courtney, T., Naro, Y. & Deiters, A. Optochemical control of biological processes in cells and animals. *Angew. Chem. Int. Ed.* **57**, 2768–2798 (2018).
11. SzymaŃski, W., Yilmaz, D., Koçer, A. & Feringa, B. L. Bright ion channels and lipid bilayers. *Acc. Chem. Res.* **46**, 2910–2923 (2013).

12. Govorunova, E. G., Sineshchekov, O. A., Li, H. & Spudich, J. L. Microbial rhodopsins: diversity, mechanisms, and optogenetic applications. *Annu. Rev. Biochem.* **86**, 845–872 (2017).

13. Zhang, F. *et al.* The microbial opsin family of optogenetic tools. *Cell* **147**, 1446–1457 (2011).

14. Maltan, L., Najjar, H., Tiffner, A. & Derler, I. *Deciphering molecular mechanisms and intervening in physiological and pathophysiological processes of Ca^{2+} signaling mechanisms using optogenetic tools. Cells* vol. 10 (2021).

15. Nguyen, N. T. *et al.* CRAC channel-based optogenetics. *Cell Calcium* **75**, 79–88 (2018).

16. Jiang, S., Wu, X., Rommelfanger, N. J., Ou, Z. & Hong, G. Shedding light on neurons: optical approaches for neuromodulation. *Natl. Sci. Rev.* **9**, (2022).

17. Xu, X., Mee, T. & Jia, X. New era of optogenetics: from the central to peripheral nervous system. *Crit. Rev. Biochem. Mol. Biol.* **55**, 1–16 (2020).

18. Nyns, E. C. A. *et al.* An automated hybrid bioelectronic system for autogenous restoration of sinus rhythm in atrial fibrillation. *Sci. Transl. Med.* **11**, 1–12 (2019).

19. Tochitsky, I. *et al.* How azobenzene photoswitches restore visual responses to the blind retina. *Neuron* **92**, 100–113 (2016).

20. Volgraf, M. *et al.* Allosteric control of an ionotropic glutamate receptor with an optical switch. *Nat. Chem. Biol.* **2**, 47–52 (2006).

21. Lam, P. Y. *et al.* TRPswitch - a step-function chemo-optogenetic ligand for the vertebrate trpa1 channel. *J. Am. Chem. Soc.* **142**, 17457–17468 (2020).

22. Fehrentz, T. *et al.* Optical control of L-type Ca^{2+} channels using a diltiazem photoswitch. *Nat. Chem. Biol.* **14**, 764–767 (2018).

23. Offenbartl-Stiegert, D., Rottensteiner, A., Dorey, A. & Howorka, S. A light-triggered synthetic nanopore for controlling molecular transport across biological membranes. *Angew. Chem. Int. Ed.* **61**, (2022).

24. Kerckhoffs, A., Bo, Z., Penty, S. E., Duarte, F. & Langton, M. J. Red-shifted tetra-ortho-halo-azobenzenes for photo-regulated transmembrane anion transport. *Org. Biomol. Chem.* **19**, 9058–9067 (2021).

25. Johnson, T. G., Sadeghi-Kelishadi, A. & Langton, M. J. A Photo-responsive transmembrane anion transporter relay. *J. Am. Chem. Soc.* **144**, 10455–10461 (2022).

26. Mutter, N. L., Volarić, J., Szymanski, W., Feringa, B. L. & Maglia, G. Reversible photocontrolled nanopore assembly. *J. Am. Chem. Soc.* **141**, 14356–14363 (2019).

27. Chang, C., Niblack, B., Walker, B. & Bayley, H. A photogenerated pore-forming protein. *Chem. Biol.* **2**, 391–400 (1995).

28. Bléger, D., Schwarz, J., Brouwer, A. M. & Hecht, S. *O*-fluoroazobenzenes as readily synthesized photoswitches offering nearly quantitative two-way isomerization with visible light. *J. Am. Chem. Soc.* **134**, 20597–20600 (2012).

29. Calbo, J. *et al.* Tuning azoheteroarene photoswitch performance through heteroaryl design. *J. Am. Chem. Soc.* **139**, 1261–1274 (2017).

30. Weston, C. E., Richardson, R. D., Haycock, P. R., White, A. J. P. & Fuchter, M. J. Arylazopyrazoles: azoheteroarene photoswitches offering quantitative isomerization and long thermal half-lives. *J. Am. Chem. Soc.* **136**, 11878–11881 (2014).

31. Walker, B. & Bayley, H. Key residues for membrane binding, oligomerization, and pore forming activity of staphylococcal α-hemolysin identified by cysteine scanning mutagenesis and targeted chemical modification. *J. Biol. Chem.* **270**, 23065–23071 (1995).

32. Braha, O. *et al.* Designed protein pores as components for biosensors. *Chem. Biol.* **4**, 497–505 (1997).

33. Maglia, G. *et al.* Droplet networks with incorporated protein diodes show collective properties. *Nat. Nanotechnol.* **4**, 437–440 (2009).

34. Loudwig, S. & Bayley, H. Photoisomerization of an individual azobenzene molecule in water: an on-off switch triggered by light at a fixed wavelength. *J. Am. Chem. Soc.* **128**, 12404–12405 (2006).

35. Frank, J. A. *et al.* Photoswitchable fatty acids enable optical control of TRPV1. *Nat. Commun.* **6**, (2015).

36. Schild, V. R. *et al.* Light-patterned current generation in a droplet bilayer array. *Sci. Rep.* **7**, 1–9 (2017).

37. Villar, G., Graham, A. D. & Bayley, H. A tissue-like printed material. *Science.* **340**, 48–52 (2013).

38. Booth, M. J., Restrepo Schild, V., Box, S. J. & Bayley, H. Light-patterning of synthetic tissues with single droplet resolution. *Sci. Rep.* **7**, 1–10 (2017).

39. Li, J. *et al.* Metal-organic frameworks as micromotors with tunable engines and brakes. *J. Am. Chem. Soc.* **139**, 611–614 (2017).

40. Pulcu, G. S., Mikhailova, E., Choi, L. S. & Bayley, H. Continuous observation of the stochastic motion of an individual small-molecule walker. *Nat. Nanotechnol.* **10**, 76–83 (2015).

41. Lewis, C. A. Ion-concentration dependence of the reversal potential and the single channel conductance of ion channels at the frog neuromuscular junction. *J. Physiol.* **286**, 417–445 (1979).

42. Gu, L. Q., Cheley, S. & Bayley, H. Electroosmotic enhancement of the binding of a neutral molecule to a transmembrane pore. *Proc. Natl. Acad. Sci. U.S.A.* **100**, 15498–15503 (2003).

43. Pravda, L. *et al.* ChannelsDB: database of biomacromolecular tunnels and pores. *Nucleic Acids Res.* **46**, D399–D405 (2018).

Example 3 – synthesis and characterization of photoswitches

Materials and methods

All reagents and solvents were purchased from commercial sources and used without further purification. Where necessary, solvents were dried by passing through an MBraun MPSP-800 column and degassed with nitrogen. Triethylamine was distilled from and stored over potassium hydroxide. Column chromatography was carried out on Merck® silica gel 60 under a positive pressure of nitrogen. Where mixtures of solvents were used, ratios are reported by volume. NMR spectra were recorded on a Bruker AVIII 400, Bruker AVII 500 (with cryoprobe), Bruker NEO 600 with broadband helium cryoprobe and Bruker AVIII 500 spectrometers. Chemical shifts are reported as δ values in ppm. Mass spectra were carried out on a Waters Micromass LCT and Bruker microTOF spectrometers. UV-Vis spectra were recorded on a V-770 UV-Visible/NIR Spectrophotometer equipped with Peltier temperature controller and stirrer using quartz cuvettes of 1 cm path length. Experiments were conducted at 25°C unless otherwise stated.

PSS Determination and UV/Vis spectra

UV/Vis spectra were determined in the DMSO-d_6 solution. Extinction coefficients were determined by recording UV/Vis spectra for the *E* isomer at 10, 20, 30, 40 μM in DMSO. The absorbance at the maximum of the π - π* transition of the *E*-isomers was

plotted against concentration (Beer-Lambert plot) to determine the molar extinction coefficient ε. For each compound, the *E* isomer sample at 40 μM was irradiated with the desired wavelength of light to generate a photo-stationary state and another spectrum was run. This spectrum was normalized to units of ε and overlaid with the dark (100% *E* isomer) spectrum. Photo-irradiation of liquid samples was carried out using Thorlabs high-power mounted LEDs (models M530L4 (green, 530 nm), M365L2 (UV, 365 nm)) and in-house custom built set-ups using optical components supplied by Thorlabs. Photo-stationary states (PSS) were determined using ^{1}H NMR spectroscopy.

Abbreviations

AcOH: Acetic Acid; Boc: tert-butyloxycarbonyl; DCM: Dichloromethane; DIPA: N,N-Diisopropylamine; DIPEA: N,N-Diisopropylethylamine; DMAP: 4-dimethylaminopyridine; HRMS: High resolution mass spectrometry; MeCN: Acetonitrile; MeOH: Methanol; PhMe: Toluene; Phth: Phthaloyl; PSS: Photo-stationary state; rt: Room temperature; TFA: Trifluoroacetic acid; THF: Tetrahydrofuran; TMS: trimethylsilyl.

Synthesis and characterisation

Synthesis of bromoacetyl azopyrazole (Br-pzMe)

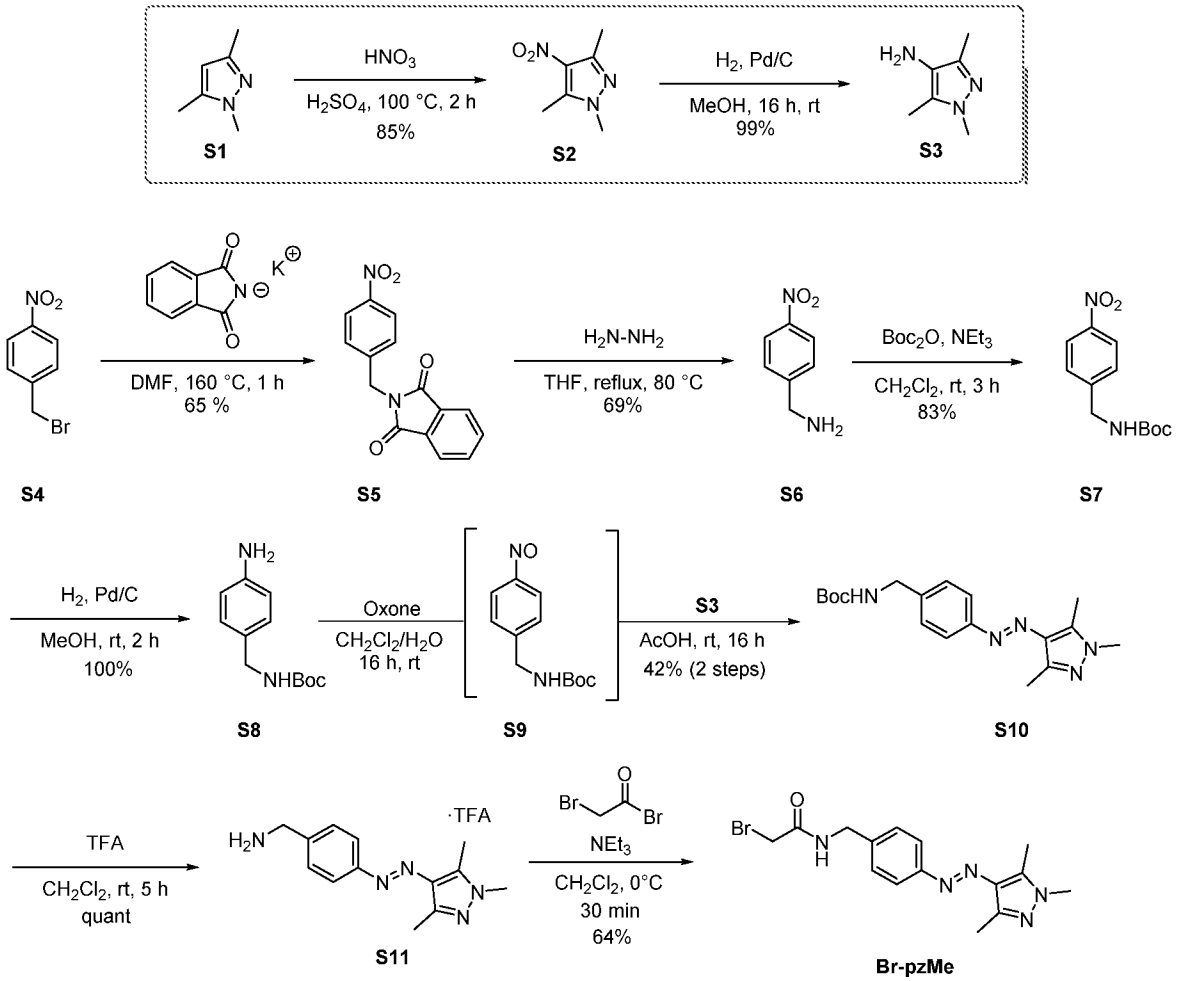

Scheme S1. Preparation of **Br-pzMe**. The synthesis commenced from commercially available **S1**, which was nitrated to **S2** and subsequently hydrogenated to **S3**. The azobenzene scaffold was generated by treatment of **S4** with potassium phthalimide to afford **S5**, which was deprotected to **S6**, reprotected to **S7** and finally hydrogenated to **S8**. This was subjected to a Mills coupling reaction *via* **S9**, which was reacted with **S3** to generate azobenzene **S10** in moderate yields. Boc deprotection to **S11** followed by treatment with bromoacetyl bromide gave rise to **Br-pzMe** in good yields.

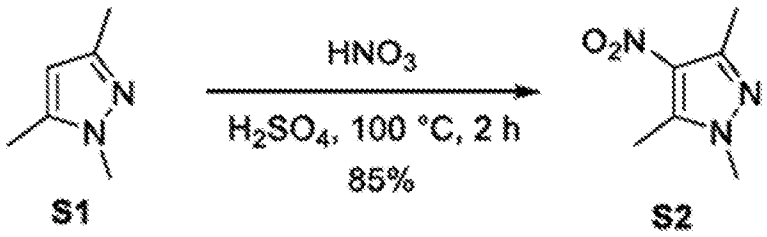

S1 S2

Nitro compound **S2.** Prepared according to a modified literature procedure.[1] Pyrazole **S1** (1.5 g, 13.6 mmol) was dissolved in sulfuric acid (7.5 mL). The solution was cooled to 0 °C, then nitric acid (6 mL, 150 mmol, 11 eq) was added. The solution was heated to 100 °C for 2 hours. The mixture was cooled to room temperature, then poured into ice water. The mixture was slowly basified under ice with NaOH pellets. The precipitated solid was collected via vacuum filtration, washed with water and dried to afford the title compound as an off-white solid (1.8 g, 11.6 mmol, 85%). ^{1}H NMR (400 MHz, CDCl3) δ 3.77 (s, 3H), 2.61 (s, 3H), 2.50 (s, 3H). Data consistent with that given in the literature.[1]

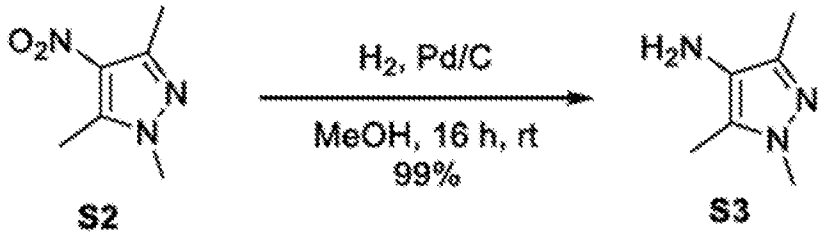

S2 S3

Aniline **S3.** Prepared according to a modified literature procedure.[2] Nitro compound S2 (1.8 g, 11.6 mmol) was dissolved in MeOH (25 mL) and placed under nitrogen. Palladium 10%on carbon (250 mg) was added, then the reaction was stirred under hydrogen atmosphere for 16 hours at room temperature. The reaction was filtered over celite, washed with CH2Cl2. The filtrate was concentrated to afford the title compound as a yellow solid. (1.44 g, 11.5 mmol, 99%). ^{1}H NMR (400 MHz, CDCl3) δ 3.66 (s, 3H), 2.46 – 2.31 (br s, 2H), 2.15 (s, 3H), 2.13 (s,3H). Data consistent with that given in the literature.[2]

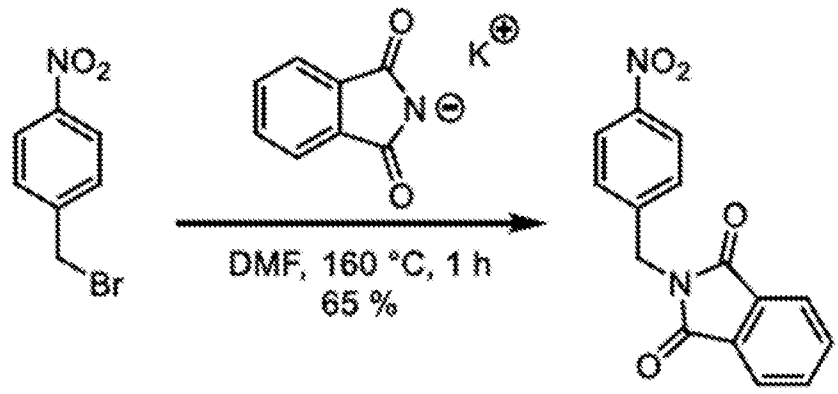

S4 S5

Phthalimide **S5.** Prepared according to a modified literature procedure.[3] *p*-nitrobenzyl bromide **S4** (7 g, 32.40 mmol) was dissolved in DMF (45 mL). Potassium phthalimide (6.3 g, 34 mmol, 1.05 eq) was added and the reaction was stirred at reflux temperature for 1 h. The reaction was cooled, and ice water was added. The filtrate was dissolved in hot EtOAc (300 mL), and allowed to recrystallize for two days at room temperature in a 500 mL flask. The solid was collected and washed with cold EtOAc to afford the title compound as white crystals (5.9 g, 20.9 mmol, 65%). ^{1}H NMR (400 MHz, CDCl3) δ 8.22 – 8.15 (m, 2H), 7.88 (dd, *J* = 5.4, 3.1 Hz, 2H), 7.75 (dd, *J* = 5.5, 3.1 Hz, 2H), 7.62 – 7.56 (m, 2H), 4.93 (s, 2H). Data consistent with that given in the literature.[3]

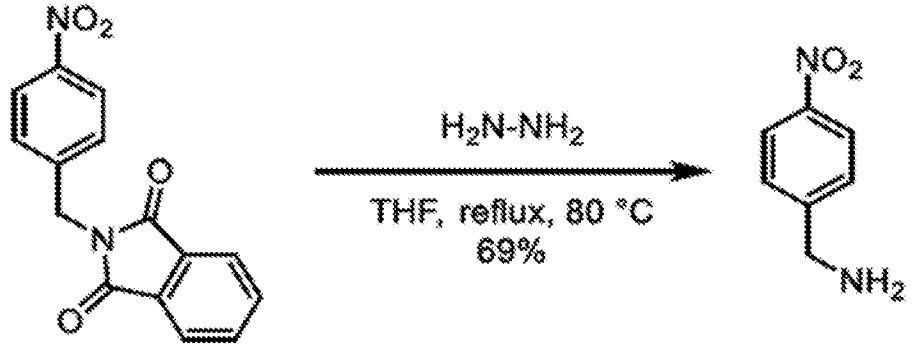

S5 S6

Amine **S6.** Prepared according to a modified literature procedure.[4] Nitro compound **S5** (10 g, 35.43 mmol) was dissolved in THF (100 mL). Hydrazine hydrate (8 mL) was added and the reaction was stirred at reflux temperature for 16 hours. The reaction was concentrated, then taken up in EtOAc. The suspension was filtered over cotton, and the filtrate washed with 1M NaOH. The organic layer was dried, then concentrated to afford

the title compound as a yellow oil (3.7 g, 24.3 mmol, 69%). ^{1}H NMR (400 MHz, CDCl3) δ 8.23 – 8.16 (m, 2H), 7.50 (d, *J* = 8.3 Hz, 2H), 4.01 (s, 2H). Data consistent with that given in the literature.[4]

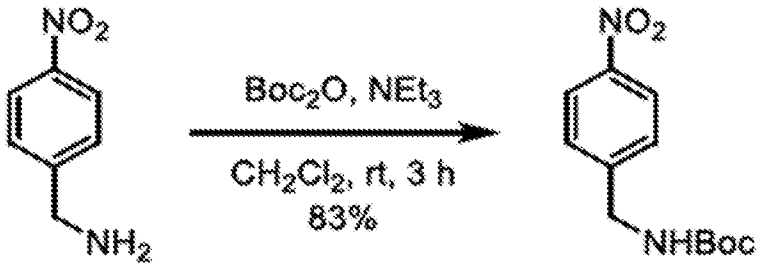

S6 **S7**

Nitro compound **S7.** Prepared according to a modified literature procedure.[5] Amine **S6** (3.7 g, 24.32 mmol) was dissolved in CH2Cl2 (50 mL). NEt3 (10.2 mL, 73 mmol, 3 eq) was added. Then Boc2O (8 g, 36.5 mmol, 1.5 eq) in CH2Cl2 (50 mL) was added dropwise. The reaction was stirred for 3 hours, after which it was poured onto ice water (50 mL). The reaction was recrystalised from isopropyl ether (40 mL) to afford the title compound as a yellow crystalline solid (5.1g, 20.2 mmol, 83%). ^{1}H NMR (400 MHz, CDCl3) δ 8.23 – 8.14 (m, 2H), 7.45 (d, *J* = 8.6 Hz, 2H), 4.99 (s, 1H), 4.42 (d, *J* = 6.3 Hz, 2H), 1.47 (s, 9H). Data consistent with that given in the literature.[5]

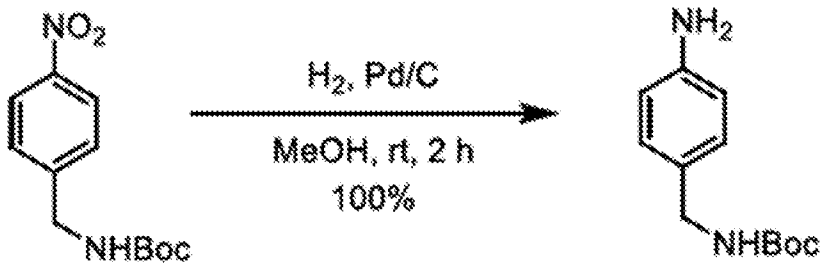

S7 **S8**

Phthalimide **S8.** Prepared according to a modified literature procedure.[5] Nitro compound **S7** (2.42 g, 9.59 mmol) was dissolved in EtOH (40 mL). The reaction was placed under nitrogen, then 10% Pd/C (200 mg) was added. The reaction was stirred under H2 atmosphere for 2 hours, filtered over celite, then concentrated to afford the title compound as a white solid (2.13 g, 9.59 mmol, 100%). ^{1}H NMR (400 MHz, CDCl3) δ 7.07 (d, *J* = 8.0 Hz, 2H), 6.69 – 6.60 (m, 2H), 4.73 (s, 1H), 4.18 (d, *J* = 5.7 Hz, 2H), 1.45 (s, 9H).[5]

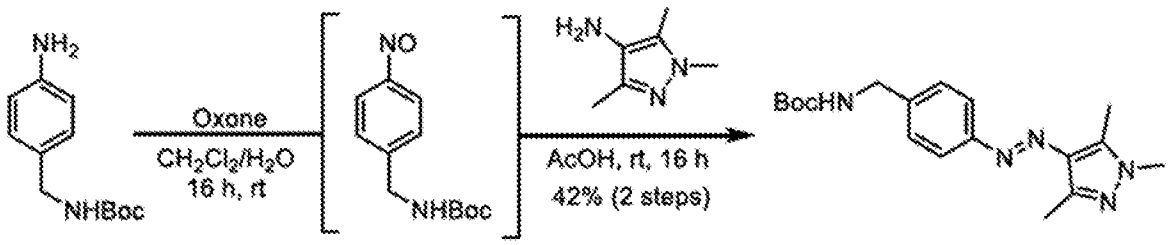

S8 S9 S10

Azobenzene **S10**. A solution of aniline **S8** (554 mg, 2.45 mmol, 1.2 equiv.) in CH_2Cl_2 (40 mL), was treated with a solution of Oxone® (4.9 g, 16 mmol, 6.5 equiv.) in H_2O (40 mL). The biphasic reaction mixture was stirred vigorously at rt for 16 hours. The phases were separated and the aqueous phase extracted with CH_2Cl_2 (20 mL). The combined organic extracts were washed with saturated $NaHCO_3$(aq) solution and H_2O. The washed organic layer was treated with **S3** (260 mg, 2.1 mmol, 1.0 equiv.) and AcOH (30 mL). The CH_2Cl_2 was then removed under reduced pressure at 35 °C and the solution was stirred for 16 hours at rt. The solution was concentrated and purified by flash silica gel chromatography (0 to 10% EtOAc in CH_2Cl_2) to yield the title compound as a yellow solid (300 mg, 0.87 mmol, 42%). ^{1}H NMR (600 MHz, $CDCl_3$) δ 7.74 (d, J = 8.0 Hz, 2H), 7.36 (d, J = 8.0 Hz, 2H), 4.88 (s, 1H), 4.36 (d, J = 6.0 Hz, 2H), 3.78 (s, 3H), 2.57 (s, 3H), 2.49 (s, 3H), 1.47 (s, 9H). ^{13}C NMR (151 MHz, $CDCl_3$) δ 156.03, 153.08, 142.55, 140.31, 138.89, 135.25, 128.13, 122.15, 79.76, 44.58, 36.11, 28.56, 13.91, 10.11. HRMS-EI (m/z) Calculated for $C_{18}H_{26}N_5O_2$ $[M+H]^+$, 344.2081; found 344.2084.

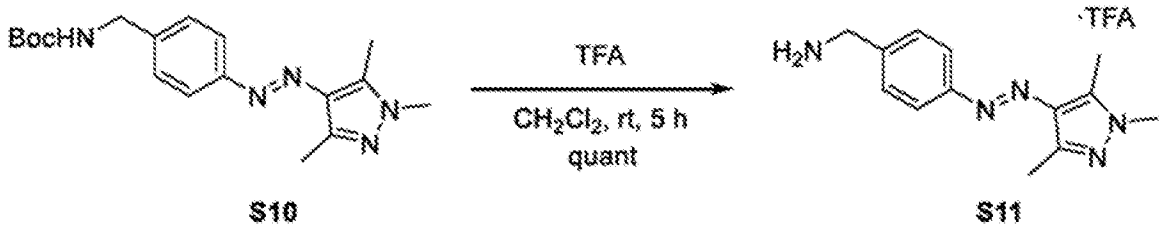

S10 S11

Amine **S11.** To a solution of **S10** (100 mg, 0.29 mmol) in CH_2Cl_2 (5 mL) was added TFA (0.6 mL). The reaction was stirred at room temperature for 5 hours. The TFA was removed under a stream of nitrogen, then the residue was dried in vacuo to afford the title compound as a yellow solid (104 mg, 0.29 mmol, 100%). ^{1}H NMR (600 MHz, MeOD) δ 7.85 – 7.81 (m, 2H), 7.58 – 7.55 (m, 2H), 4.18 (s, 2H), 3.79 (s, 3H), 2.61 (s, 3H), 2.45 (s, 3H).^{13}C NMR (151 MHz, MeOD) δ 155.30, 143.22, 141.59, 136.05, 135.46,

130.82, 123.36, 44.01, 36.13, 13.87, 9.76. HRMS-EI (m/z) Calculated for C13H18N5 $[M+H]^+$, 244.1557; found244.1557.

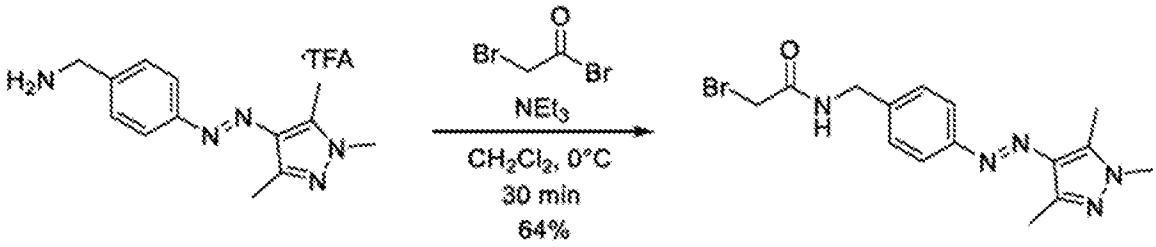

S11 pzMe

Br-pzMe. TFA salt **S11** (98 mg, 0.3 mmol) was suspended in CH_2Cl_2 (2.5 mL). NEt3 (95 µL, 0.69 mmol, 2.5 eq) was added and the solution cooled to 0°C and bromo acetylbromide (37 µL, 0.37 mmol, 1.5 eq) was added and the solution was stirred at 0 °C for 30 minutes. The solution was diluted with CH_2Cl_2, then the volatiles removed by rotary evaporation (35 °C water bath). The residue was purified by flash-column chromatography (15% EtOAc in CH_2Cl_2) to afford the product as a yellow solid (64 mg, 175 µmol, 64%). ^{1}H NMR (600 MHz, DMSO) δ 8.84 (t, *J* = 6.0 Hz, 1H), 7.69 (d, *J* = 8.0 Hz, 2H), 7.39 (d, *J* = 8.0 Hz, 2H), 4.36 (d, *J* = 6.0 Hz, 2H), 3.93 (s, 2H), 3.74 (s, 3H), 2.55 (s, 3H), 2.37 (s, 3H). ^{13}C NMR (151 MHz, DMSO) δ 166.64, 152.55, 140.77, 140.77, 139.94, 134.81, 128.49, 121.87, 42.73, 36.42, 29.91, 14.22, 9.94. HRMS-EI (m/z) Calculated for $C_{15}H_{19}N_5OBr$ $[M+H]^+$, 364.0767; found 364.0763. HMBC shows two peaks at 140.77.

Synthesis of Br-pzH

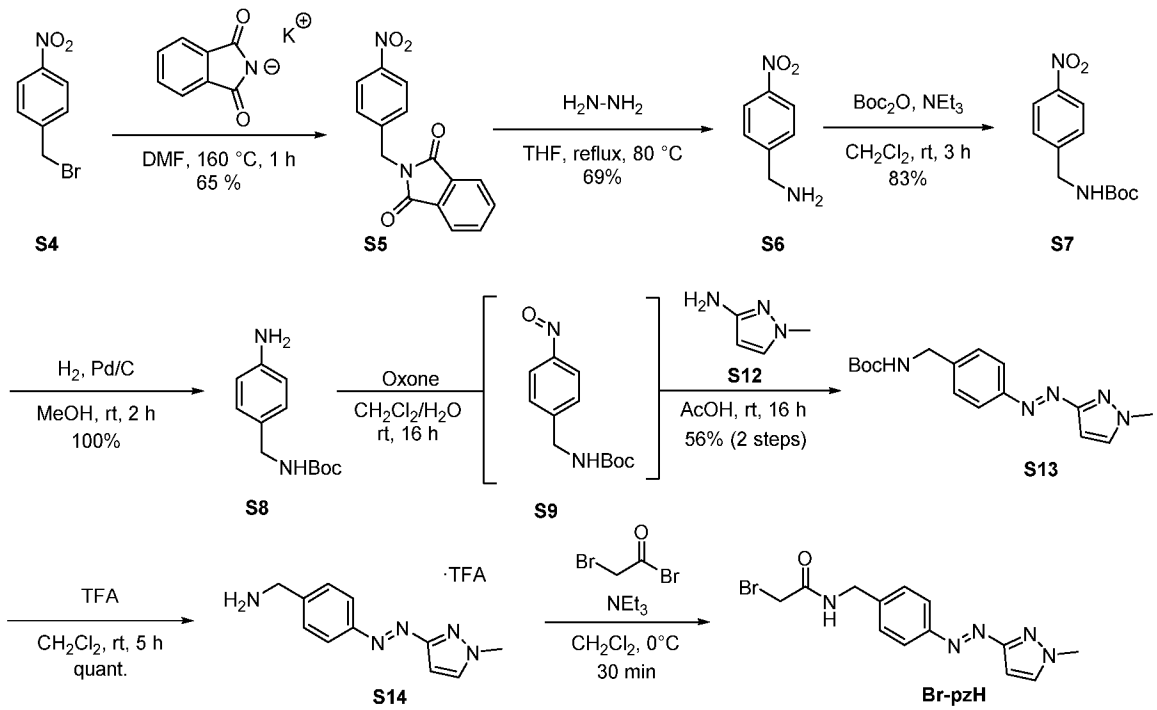

Scheme S2. The synthesis commenced from commercially available **S4**, which was nitrated to **S5** and subjected to hydrazinolysis to **S6**, reprotected to **S7** and finally hydrogenated to **S8**. This was subjected to a Mills coupling reaction *via* **S9**, which was reacted with **S12** to generate azobenzene **S14** in good yields. Boc deprotection to **S14** followed by treatment with bromoacetyl bromide gave rise to **Br-pzH** in good yields.

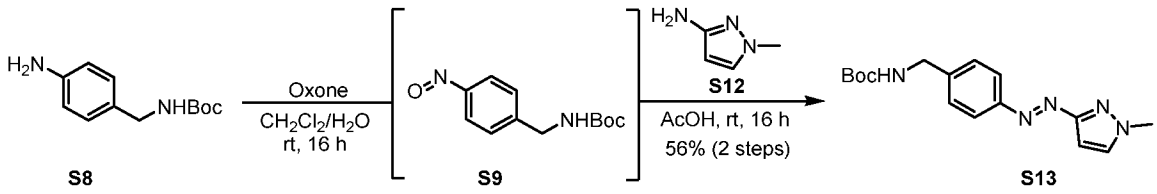

Azobenzene **S13**. A solution of aniline **S8** (452 mg, 2 mmol, 1.2 equiv.) in CH_2Cl_2 (37 mL), was treated with a solution of Oxone® (4 g, 13 mmol, 6.5 equiv.) in H_2O (37 mL). The resulting biphasic reaction mixture was stirred vigorously at room temperature for 16 hours. Subsequently, the phases were separated and the aqueous phase was extracted with CH_2Cl_2 (20 mL). The combined organic extracts were washed sequentially with saturated aqueous sodium bicarbonate solution (50 mL), and H_2O (50 mL). The washed organic layer containing **S9** was treated with **S12** (147 µL, 1.69 mmol, 1.0 equiv.) and AcOH (30 mL). The CH_2Cl_2 was then removed under reduced pressure at 35 °C and the solution was stirred for 16 hours at room temperature. The AcOH was then removed

under reduced pressure. The residue was purified by flash silica gel chromatography (0 to 5% EtOAc in CH_2Cl_2) to yield the title compound as a yellow/brown solid (204 mg, 0.95 mmol, 56%). (*E*)-S13: ^{1}H NMR (400 MHz, $CDCl_3$) δ 7.91 (d, *J* = 8.3 Hz, 2H), 7.45 – 7.35 (m, 3H), 6.65 (d, *J* = 2.4 Hz, 1H), 4.93 (s, 1H), 4.38 (s, 2H), 4.02 (s, 3H), 1.47 (s, 9H). ^{13}C NMR (151 MHz, $CDCl_3$) δ 163.81, 156.06, 152.18, 142.24, 131.98, 128.13, 123.35, 96.38, 79.85, 44.54, 39.80, 28.54. HRMS-EI (m/z) Calculated for $C_{16}H_{22}N_5O_2$ $[M+H]^+$, 316.1768; found 316.1768.

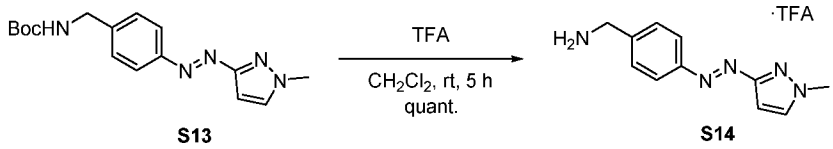

S13 **S14**

Amine **S14**. To a solution of **S13** (100 mg, 0.32 mmol) in CH_2Cl_2 (5 mL) was added TFA (0.6 mL). The reaction was stirred at room temperature for 5 hours. The TFA was removed under a stream of nitrogen, then the residue was dried in vacuo to afford the title compound as a yellow solid (104 mg, 0.32 mmol, 100%). (*E*)-***S14***: ^{1}H NMR (400 MHz, MeOD) δ 7.99 – 7.92 (m, 2H), 7.69 (d, *J* = 2.5 Hz, 1H), 7.66 – 7.60 (m, 2H), 6.64 (d, *J* = 2.5 Hz, 1H), 4.21 (s, 2H), 4.03 (s, 3H). ^{13}C NMR (151 MHz, MeOD) δ 164.83, 154.36, 137.41, 134.28, 130.99, 124.30, 96.25, 43.92, 39.74. HRMS-EI (m/z) Calculated for $C_{11}H_{14}N_4$ $[M+H]^+$, 216.1244; found 216.1245.

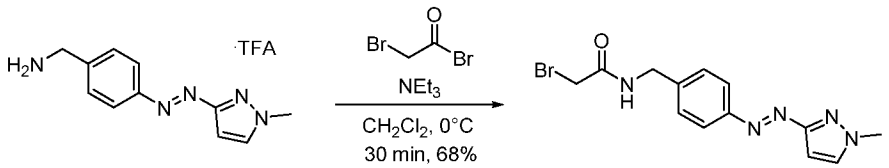

S14 **Br-pzH**

Br-pzH. TFA salt **S14** (98 mg, 0.3 mmol) was suspended in CH_2Cl_2 (2.5 mL). NEt_3 (104 µL, 0.74 mmol, 2.5 eq) was added and the solution cooled to 0 °C and bromo acetylbromide (40 µL, 0.45 mmol, 1.5 eq) was added and the solution was stirred at 0 °C for 30 minutes. The solution was diluted with CH_2Cl_2, then the volatiles removed by rotary evaporation (35 °C water bath). The residue was purified by flash-column chromatography (10% EtOAc in CH_2Cl_2) to afford the product as a yellow solid (68.2 mg, 202 µmol, 68%). (*E*)-**Br-pzH**: ^{1}H NMR (400 MHz, DMSO) δ 8.87 (d, *J* = 6.1 Hz, 1H), 7.83 (d, *J* = 2.4 Hz, 1H), 7.80 (d, *J* = 8.1 Hz, 2H), 7.46 (d, *J* = 8.1 Hz, 2H), 6.53 (d, *J* = 2.4 Hz, 1H), 4.39 (d, *J* = 6.0 Hz, 2H), 3.97 (s, 3H), 3.95 (s, 2H). ^{13}C NMR (151 MHz,

DMSO) δ 166.72, 163.46, 151.56, 143.69, 133.57, 128.64, 122.67, 95.00, 41.83, 40.55, 29.90. HRMS-EI (m/z) Calculated for $C_{13}H_{15}N_5OBr$ $[M+H]^+$, 336.0454; found 336.0457.

Synthesis of Br-fAzo

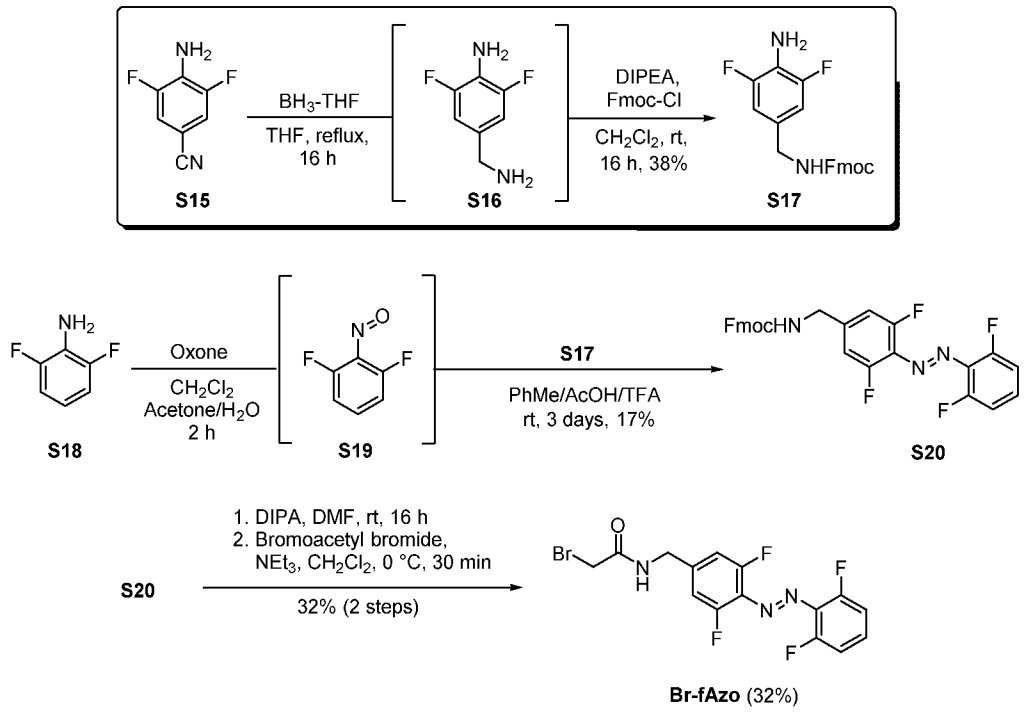

Scheme S3. Preparation of fAzo derivatives. **S15** was reduced to unstable **S16**, followed by Fmoc-protection to **S17**. This was azo coupled to **S18** to generate **S20**, which was deprotected using DIPA and treated with bromoacetyl bromide to afford the **Br-fAzo** derivatives.

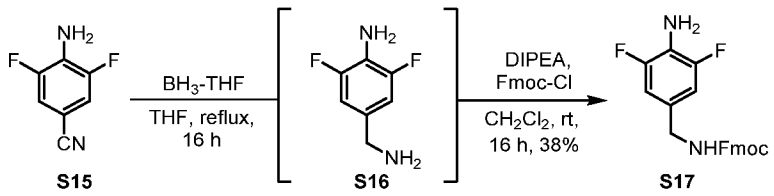

Aniline **S17**. **S15** (1.45 g, 9.41 mmol) was dissolved in THF (20 mL). Borane-THF (1M, 38.4 mL, 38.4 mmol, 4 eq) was added at 0 °C under N_2 atmosphere, and the reaction was stirred at reflux temperature 16 hours. MeOH (5 mL) was added dropwise at this temperature until effervescence stopped, and the reaction was stirred at reflux temperature for 30 minutes. The solvent was removed in vacuo, redissolved in EtOAc and washed

with water. The organic layer was concentrated. The off-white **S16** was redissolved in CH_2Cl_2 (30 mL). DIPEA (1.46 mL, 9.41 mmol, 1 eq) and then Fmoc-Cl (2.43 g, 9.41 mmol, 1 eq) were added and the reaction was stirred for 16 hours at room temperature. The solution was concentrated and purified by silica gel chromatography (6:1 Hexane:Acetone) to afford the title compound as a white solid (1.37 g, 3.60 mmol, 38%). ^{1}H NMR (400 MHz, $CDCl_3$) δ 7.76 (d, J = 7.6 Hz, 2H), 7.59 (d, J = 7.5 Hz, 2H), 7.40 (t, J = 7.5 Hz, 2H), 7.31 (t, J = 7.5 Hz, 2H), 6.75 (d, J = 7.4 Hz, 2H), 5.02 (s, 1H), 4.47 (d, J = 6.8 Hz, 2H), 4.30 – 4.01 (m, 3H), 3.70 (s, 2H). ^{13}C NMR (126 MHz, $CDCl_3$) δ 156.49, 152.05 (dd, J = 242.30 Hz, 8.10 Hz), 143.98, 141.49, 127.86 (t), 127.20, 125.11, 123.24 (t, J = 16.2 Hz), 120.14, 110.28 (dd, J = 15.50 Hz, 6.50 Hz) 66.85, 47.42, 44.28. HRMS-ESI (m/z) Calculated for $C_{22}H_{18}F_2N_2O_2$ $[M+H]^+$, 381.1409; found 381.1408

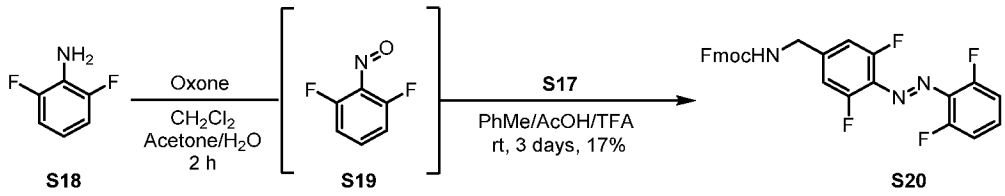

Aniline **S18** (170 mg, 1.31 mmol, 2 eq) was dissolved in CH_2Cl_2 (10 mL). Oxone (5.35 g, 13.1 mmol, 20 eq) in water (20 mL) was added and the biphasic solution was vigorously stirred at room temperature for 16 hours, after which the organic layer turned green. The organic layer was separated, then sequentially washed with 1 N HCl (20 mL), sat. bicarbonate solution (20 mL), water (20 mL). The organic layer was dried and concentrated. The residue was redissolved in 6:6:1 AcOH:Toluene:TFA (20 mL), and **S17** (250 mg, 657 µmol, 1 eq) was added, and the solution was stirred at room temperature for 3 days. The mixture was concentrated, then purified by flash-column chromatography (100% CH_2Cl_2) to afford the title compound as an orange solid and mixture of isomers (66 mg, 133 µmol, 17%). The sample was irradiated with 405 nm to afford 17:1 ratio of *(E)*-**S20** and *(Z)*-**S20** as indicated by ^{1}H NMR analysis. *(E)*-S20: ^{1}H NMR (600 MHz, $CDCl_3$) δ 7.77 (d, J = 7.1 Hz, 2H), 7.60 (d, J = 7.5 Hz, 2H), 7.41 (t, J = 7.6 Hz, 2H), 7.37 (t, J = 8.9 Hz, 1H), 7.33 (t, J = 7.7 Hz, 2H), 7.06 (t, J = 8.9 Hz, 2H), 6.95 (d, J = 10.4 Hz, 2H), 5.16 (t, J = 6.4 Hz, 1H), 4.55 (d, J = 6.5 Hz, 2H), 4.39 (d, J = 6.4 Hz, 2H), 4.24 (t, J = 6.4 Hz, 1H). ^{13}C NMR (151 MHz, $CDCl_3$) δ 156.56, 155.89 (dd, J = 263.0, 4.4 Hz), 155.73 (dd, J = 261.4, 4.0 Hz), 143.97, 143.86, 141.55, 132.01, 131.53 (t, J = 10.3 Hz), 130.78, 127.95, 127.25, 125.04, 120.18, 112.77 (dd, J = 20.1, 3.8 Hz), 111.25 (d, J = 20.9

Hz), 66.94 47.48, 44.34. HRMS-EI (m/z) Calculated for $C_{28}H_{20}N_3O_2F_4$ $[M+H]^+$, 506.1486; found 506.1488.

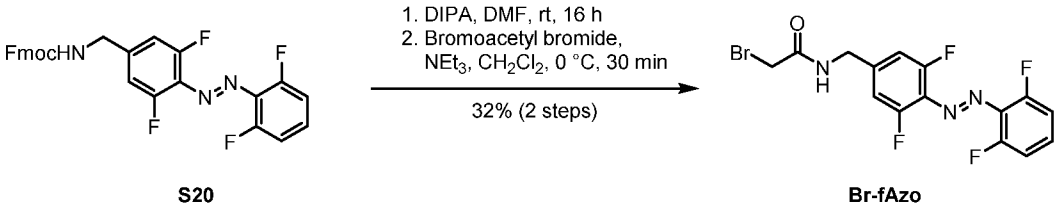

S20 **Br-fAzo**

S20 were dissolved in DMF (66 mg, 131 µmol, 70 mM). DIPA (73 µL, 522 µmol, 4 eq) was added under N_2 and the reaction was stirred for 16 hours at room temperature. The reaction was concentrated, then purified by flash-column chromatography to afford the product as an orange solid. The free amine (16 mg, 56 µmol) was dissolved in CH_2Cl_2 (40 mM). NEt_3 (12 µL, 84 µmol, 1.5 eq) was added and the solution cooled to 0°C and bromoacetylbromide (7 µL, 84 µmol, 1.5 eq) was added and the solution was stirred at 0 °C for 30 minutes. The solution was diluted with CH_2Cl_2, then the volatiles removed by rotary evaporation (35 °C water bath). The residue was purified by flash-column chromatography to afford the product as an orange solid (7.3 mg, 18 µmol, 32%). ***(E)-Br-fAzo***: ^1H NMR (600 MHz, $CDCl_3$) δ 7.37 (tt, J = 8.4, 5.8 Hz, 1H), 7.09 – 7.03 (m, 2H), 7.00 (d, J = 9.8 Hz, 2H), 6.91 (s, 1H), 4.52 (d, J = 6.2 Hz, 2H), 3.98 (s, 2H). ^{13}C NMR (151 MHz, $CDCl_3$) δ 165.72, 155.76 (dd, J = 262.2, 4.7 Hz), 155.63 (dd, J = 261.2, 4.0 Hz), 142.39 (t, J = 9.3 Hz), 131.80 (t, J = 10.0 Hz), 131.54 (t, J = 10.4 Hz), 130.87 (t, J = 9.9 Hz), 112.64 (dd, J = 20.1, 3.8 Hz), 111.49 (dd, J = 21.1, 3.6 Hz), 43.25, 28.88. HRMS-ESI (m/z) Calculated for $C_{15}H_{11}ON_3BrF_4$ $[M+H]^+$, 404.0016; found 404.0017

PSS determination and UV-Vis spectra

UV-vis spectra were determined in DMSO solution. Extinction coefficients were determined by recording a UV-vis spectra for the *E* isomer at 10, 20, 30, 40 µM in DMSO respectively. The absorbance at the maximum of the π - π* transition of the *E*-isomers was plotted against concentration (Beer-Lambert plot) to determine the molar extinction coefficient ε. For each slow relaxing compound, the *E* isomer sample at 40 µM was irradiated with the appropriate wavelength of light to generate the photo-stationary state, and another spectrum was run. This spectrum was normalised to units of ε and overlaid with the dark (100% *E* isomer)spectrum.

Deconvoluted spectra were prepared using Origin Pro 2020b by fitting each λ_{max} to the "Multiple Peak Fit" function.

Photo-irradiation of liquid samples was carried out using Thorlabs high-power mounted LEDs (models M530L4 (green, 530 nm) M365L2 (UV, 365 nm)) ; in-house custom built set-ups using optical components supplied by Thorlabs. Photo-stationary states (PSS) were determined using ^{1}H NMR spectroscopy.

References

[1] E. De Vita, P. Schüler, S. Lovell, J. Lohbeck, S. Kullmann, E. Rabinovich, A. Sananes, B. Heßling, V. Hamon, N. Papo, J. Hess, E. W. Tate, N. Gunkel and A. K. Miller, J Med Chem, 2018, 61, 8859–8874.

[2] P.-Y. Lam, A. R. Thawani, E. Balderas, A. J. P. White, D. Chaudhuri, M. J. Fuchter and R. T. Peterson, J Am Chem Soc, 2020, 142, 17457–17468.

[3] N. Tran-Hoang and T. Kodadek, ACS Comb Sci, 2018, 20, 55–60.

[4] D. P. Nguyen, R. N. Sladek and L. H. Do, Tetrahedron Letters, 2020, 61, 152196.

[5] S. Aït Amiri, C. Deboux, F. Soualmia, N. Chaaya, M. Louet, E. Duplus, S. Betuing, B. Nait Oumesmar, N. Masurier and C. El Amri, J Med Chem, 2021, 64, 5667–5688.

CLAIMS

1. A nanopore that is selectively convertible between an open form and a closed form using light, wherein, when the nanopore is in the closed form, substantially no substances are able to move through the nanopore.

2. The nanopore according to claim 1, wherein the nanopore has one or more photoisomerisable groups within the lumen of the nanopore, wherein the one or more photoisomerisable groups are each independently groups of formula (I):

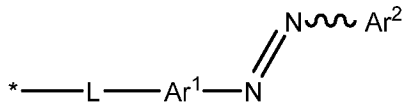

(I)

wherein:

* denotes the point of attachment to the nanopore;

L is a linker; and

Ar^1 and Ar^2 are each independently selected from an optionally-substituted aryl group and an optionally substituted heteroaryl group.

3. The nanopore according to claim 2, wherein:

- said optionally substituted aryl group is a 6-10 membered aryl group that is optionally substituted with from 1-4 R^1; and
- said optionally substituted heteroaryl group is a 5-10 membered heteroaryl group having 1-4 ring heteroatoms independently selected form the group consisting of N, O and S; the 5-10 membered heteroaryl group being optionally substituted with from 1-4 R^2; and
- R^1 and R^2 are each independently selected from the group consisting of C_{1-6} alkyl optionally substituted with COO^-, SO_3^-, or $NR^3{}_3^+$; C_{2-6} alkenyl optionally substituted with COO^-, SO_3^-, or $NR^3{}_3^+$; C_{2-6} alkynyl optionally substituted with COO^-, SO_3^-, or $NR^3{}_3^+$; halogen; CN; NO_2; C_{1-6} haloalkyl; OH; C_{1-6} alkoxy optionally substituted with COO^-, SO_3^-, or $NR^3{}_3^+$; C_{1-6} haloalkoxy; $COOC_{1-6}$ alkyl optionally substituted with COO^-, SO_3^-, or

$NR^3{}_3^+$; $CONH_2$; $CONR^4C_{1-6}$ alkyl optionally substituted with COO^-, SO_3^-, or $NR^3{}_3^+$; NR^4COC_{1-6} alkyl optionally substituted with COO^-, SO_3^-, or $NR^3{}_3^+$; SO_2NH_2; $SO_2NR^4C_{1-6}$ alkyl optionally substituted with COO^-, SO_3^-, or $NR^3{}_3^+$; $NR^4SO_2C_{1-6}$ alkyl optionally substituted with COO^-, SO_3^-, or $NR^3{}_3^+$; COO^-, SO_3^-, or $NR^3{}_3^+$; wherein each R^3 is independently H or C_{1-6} alkyl, and each R^4 is independently H or C_{1-6} alkyl.

4. The nanopore according to claim 3, wherein

- said optionally substituted aryl group is a phenyl group that is optionally substituted with from 1-4 R^1; and
- said optionally substituted heteroaryl group is a 5 membered heteroaryl group having 1-3 ring heteroatoms independently selected form the group consisting of N and O; the 5 membered heteroaryl group being optionally substituted with from 1-3 R^2; and
- R^1 and R^2 are each independently selected from the group consisting of C_{1-3} alkyl; halogen; C_{1-3} haloalkyl; $NHCOC_{1-3}$ alkyl optionally substituted with COO^-, SO_3^-, or $NR^3{}_3^+$; $NHSO_2C_{1-3}$ alkyl optionally substituted with COO^-, SO_3^-, or $NR^3{}_3^+$, COO^-, SO_3^-, or $NR^3{}_3^+$; wherein each R_3 is independently C_{1-3} alkyl.

5. The nanopore according to any one of claims 2 to 4, wherein at least one of Ar^1 and Ar^2 is an optionally substituted heteroaryl group.

6. The nanopore according to claim 5, wherein the one or more photoisomerisable groups are each independently groups of chemical formula (IB):

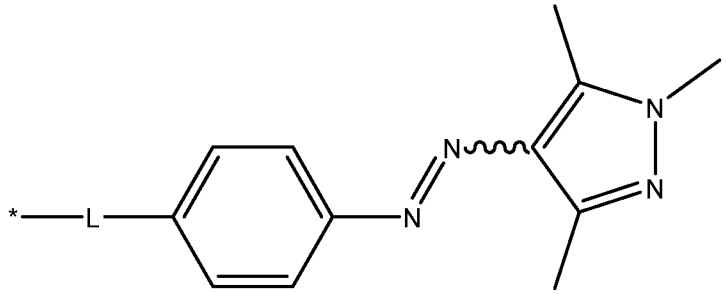

(IB)

wherein:

* denotes the point of attachment to the nanopore; and

L is a linker.

7. The nanopore according to any one of claims 1 to 6, wherein the linker is a linker of the structure (L1),

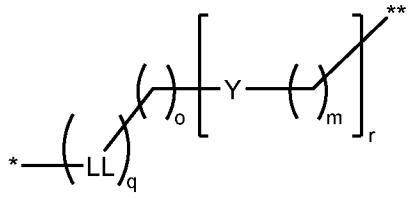

(L1)

wherein:

* denotes the point of attachment to the nanopore,

** denotes the point of attachment to Ar^1,

LL is an optionally substituted 5-10 membered carbocylic or an optionally substituted 5-10 membered heterocyclic ring;

Y is independently C_{1-20} alkylene group optionally substituted with halogen, OH, or C_{1-6} alkyl; an amide group; a sulfonamide group; an ester group; a thioester group; an ether group; a thioether group; and an amine (i.e. $-NR^5-$, wherein R^5 is preferably H or C_{1-6} alkyl) group;

q is 0 or 1; and

m, o and r are each independently an integer from 0 to 5.

8. The nanopore according to claim 7, wherein the linker is a linker of the structure (L4):

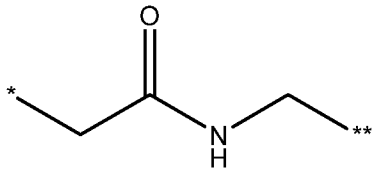

(L4)

wherein:

* denotes the point of attachment to the nanopore,

** denotes the point of attachment to Ar^1.

9. The nanopore according to any one of claim 1 to 8, wherein the one or more photoisomerisable groups are each independently groups of chemical formula (IC):

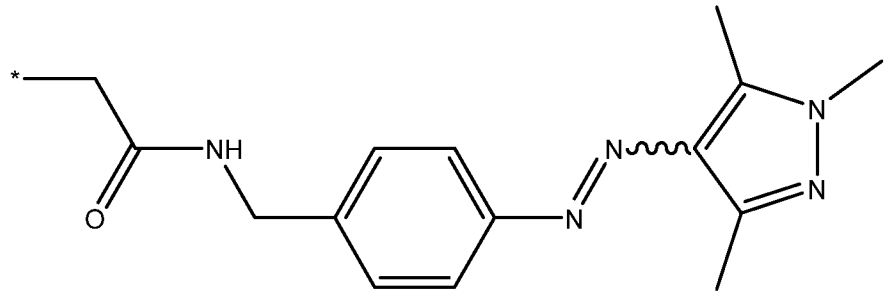

(IC)

wherein:

* denotes the point of attachment to the nanopore.

10. The nanopore according to any one of claims 1 to 9, wherein the nanopore is a transmembrane nanopore; and wherein, preferably

- the transmembrane nanopore is a transmembrane protein pore, a DNA origami pore, a solid-state pore or a polymer-based pore; and, further preferably
- the transmembrane protein pore is a porin, a pore-forming protein or a channel protein; and/or
- the transmembrane protein pore is an alpha hemolysin (αHL) pore, preferably an αHL pore formed of seven αHL monomers.

11. The nanopore according to claim 10, wherein the nanopore has one or more nucleophilic amino acids exposed to the lumen of the pore, wherein, preferably:

- the nanopore is an αHL pore, and the αHL pore preferably comprises a nucleophilic amino acid at a position corresponding to position 111, 113 and/or 147 of SEQ ID NO: 1; and, further preferably
- the αHL pore comprises a substitution corresponding to a E111C, M113C or K147C substitution of SEQ ID NO: 1, most preferably an E111C substitution.

12. The nanopore according to any one of claims 2 to 11, wherein the one or more photoisomerisable groups are covalently attached to the nanopore, wherein, preferably:

- the one more photoisomerisable groups are covalently attached to a nucleophilic amino acid exposed to the lumen of the nanopore, wherein, further preferably:
- the nucleophilic amino acid is a cysteine.

13. The nanopore according to claim 12, wherein the nanopore is αHL and the nucleophilic amino acid is at a position corresponding to position 111, 113 and/or 147 of SEQ ID NO: 1.

14. The nanopore according to any one of claims 1 to 13, wherein the nanopore is an oligomeric nanopore and each monomer of the nanopore comprises at least one of said photoisomerisable groups.

15. The nanopore according to any one of claims 1 to 14, wherein the nanopore is present within an amphiphilic membrane.

16. A method for producing the nanopore according to any one of claims 1 to 15, the method comprising introducing one or more photoisomerisable groups into a nanopore.

17. The method according to claim 16, wherein the one or more photoisomerisable groups are introduced into the nanopore by treating the nanopore with a compound of formula (II):

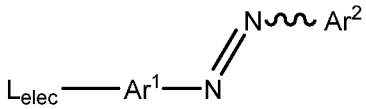

(II)

wherein:

Ar^1 and Ar^2 are as defined in any one of claims 2 to 6; and

L_{elec} corresponds the linker of any one of claims 2, 7 or 8 except that the atom that is to be attached to the nanopore is an electrophilic atom capable of undergoing reaction with a nucleophile.

18. The method according to claim 17, wherein the compound is the compound of formula (IIC):

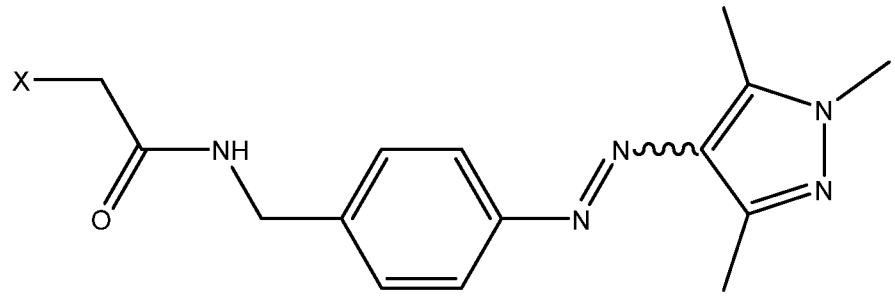

(IIC)

wherein X is a leaving group, preferably a group selected from a halogen (preferably F, Cl, Br or I) and a sulfonate group (preferably tosylate or trifluoromethanesulfonate), most preferably Br.

19. The method according to any one of claims 16 to 18, wherein the one or more photoisomerisable groups are introduced into the nanopore by treating monomers of the nanopore with a compound of formula (II) as defined in claim 17 or the compound of formula (IIC) as defined in claim 18; and, preferably, subsequently oligomerising the monomers to provide the nanopore.

20. A method for modulating the flow of one or more substances through a nanopore according to any one of claims 1 to 15, or obtainable by a method according to any one of claims 16 to 19, the method for modulating comprising irradiating the nanopore with light.

21. The method according to claim 20, wherein the method comprises irradiating the nanopore with a first wavelength of light and a second wavelength of light, wherein, preferably, the nanopore is a nanopore according to any one of claims 2 to 14, and:

- the first wavelength of light isomerises the photoisomerisable group into its Z form, and wherein the second wavelength of light isomerises the photoisomerisable group into its E form, and, further preferably:

- the first wavelength of light is a wavelength of light in the UV/Vis spectrum where the ratio εE/εZ is the greatest, and the second wavelength of light is the wavelength in the UV/Vis spectrum where the ratio εZ/εE is the greatest, wherein:
  εE is the molar extinction coefficient of the E form of the photoisomerisable group, and
  εZ is the molar extinction coefficient of the Z form of the photoisomerisable group, and
  εE and εZ are determined using an UV/Vis spectrophotometer; and/or
- the first wavelength of light is 365 nm and wherein the second wavelength of light is 455 nm or 530 nm, preferably 530 nm.

22. The method according to claim 20 or claim 21, wherein the one or more substances are independently selected from ions, water, sugars, inorganic salts, lipids, amino acids, peptides, nucleotides, nucleic acids, metabolites, neurotransmitters, and pharmaceutical agents, most preferably ions.

23. Use of a nanopore according to any one of claims 1 to 15 in modulating ionic flow across an amphiphilic membrane.

24. A device comprising an amphiphilic membrane-enclosed vesicle, wherein the vesicle lumen contains one or more pharmaceutical agents and wherein the amphiphilic membrane contains a nanopore according to any of claims 1 to 14.

25. Use of the nanopore according to any one of claims 1 to 15 as an iontronic component photoswitchable between a resistor and diode.

26. Use of the nanopore according to any one of claims 1 to 15 in bio-computation and/or bioiontronics.

27. A method of transmitting information, the method comprising:

irradiating the nanopore according to any one of claims 1 to 15 with a plurality of pulses of light, each pulse comprising light having one of a predetermined set of wavelengths.

28. A method of receiving information, the method comprising:

measuring an ionic current through the nanopore according to any one of claims 1 to 15 during irradiating of the nanopore with a plurality of pulses of light, each pulse comprising light having one of a predetermined set of wavelengths.

29. An iontronic component comprising the nanopore according to any one of claims 1 to 15, optionally wherein the component is a logic gate.

Fig. 1

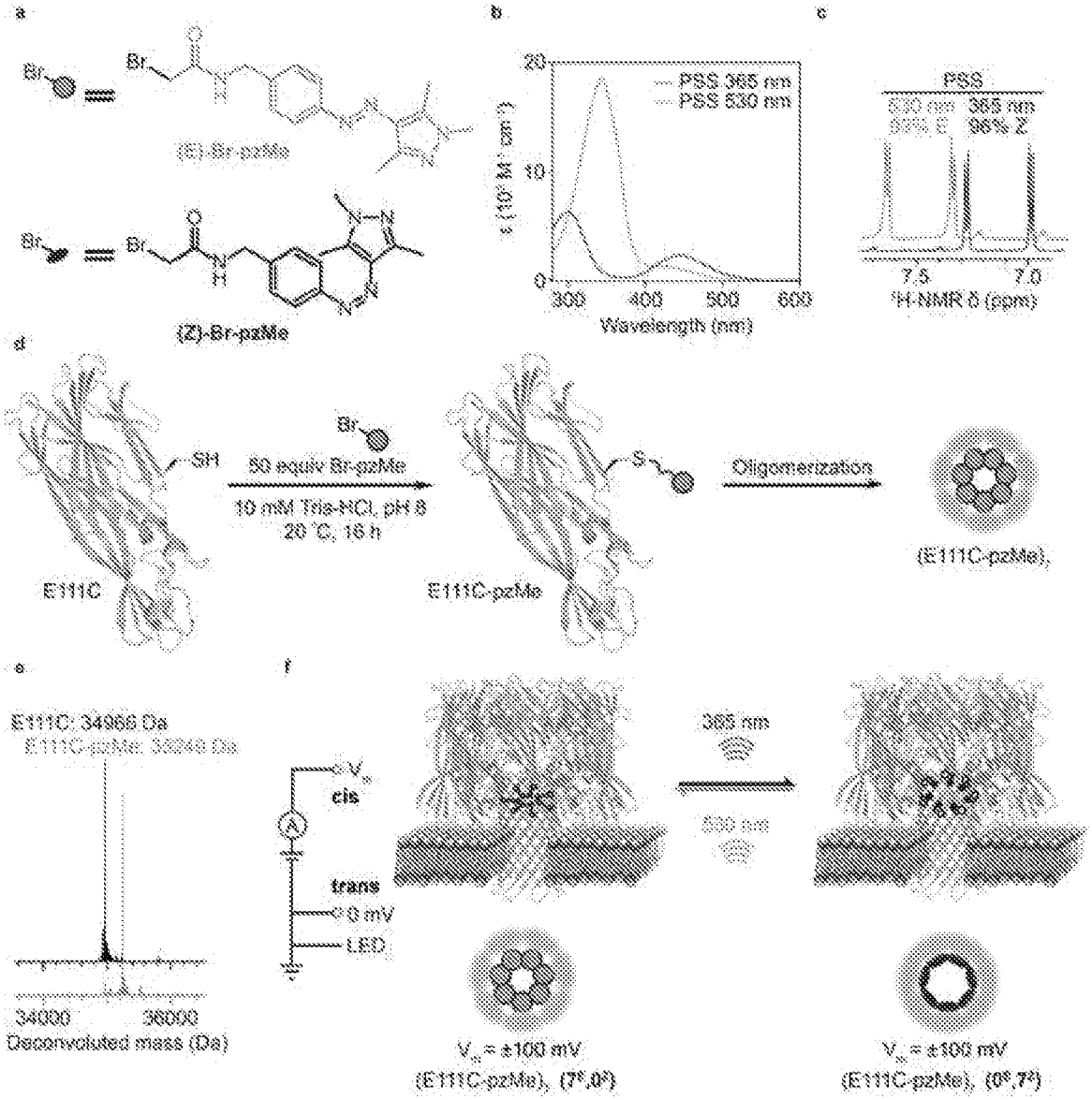
a
(E)-Br-pzMe
(Z)-Br-pzMe
b
PSS 365 nm
PSS 530 nm
ε (10³ M⁻¹ cm⁻¹)
Wavelength (nm)
c
PSS
530 nm
97% E
365 nm
96% Z
¹H-NMR δ (ppm)
d
SH
50 equiv Br-pzMe
10 mM Tris-HCl, pH 8
20 °C, 16 h
E111C
E111C-pzMe
Oligomerization
(E111C-pzMe)n
e
E111C: 34966 Da
E111C-pzMe: 35248 Da
Deconvoluted mass (Da)
f
cis
trans
0 mV
LED
365 nm
530 nm
V_bi = ±100 mV
(E111C-pzMe)n (7*,0*)
V_bi = ±100 mV
(E111C-pzMe)n (0*,7*)

Fig. 2

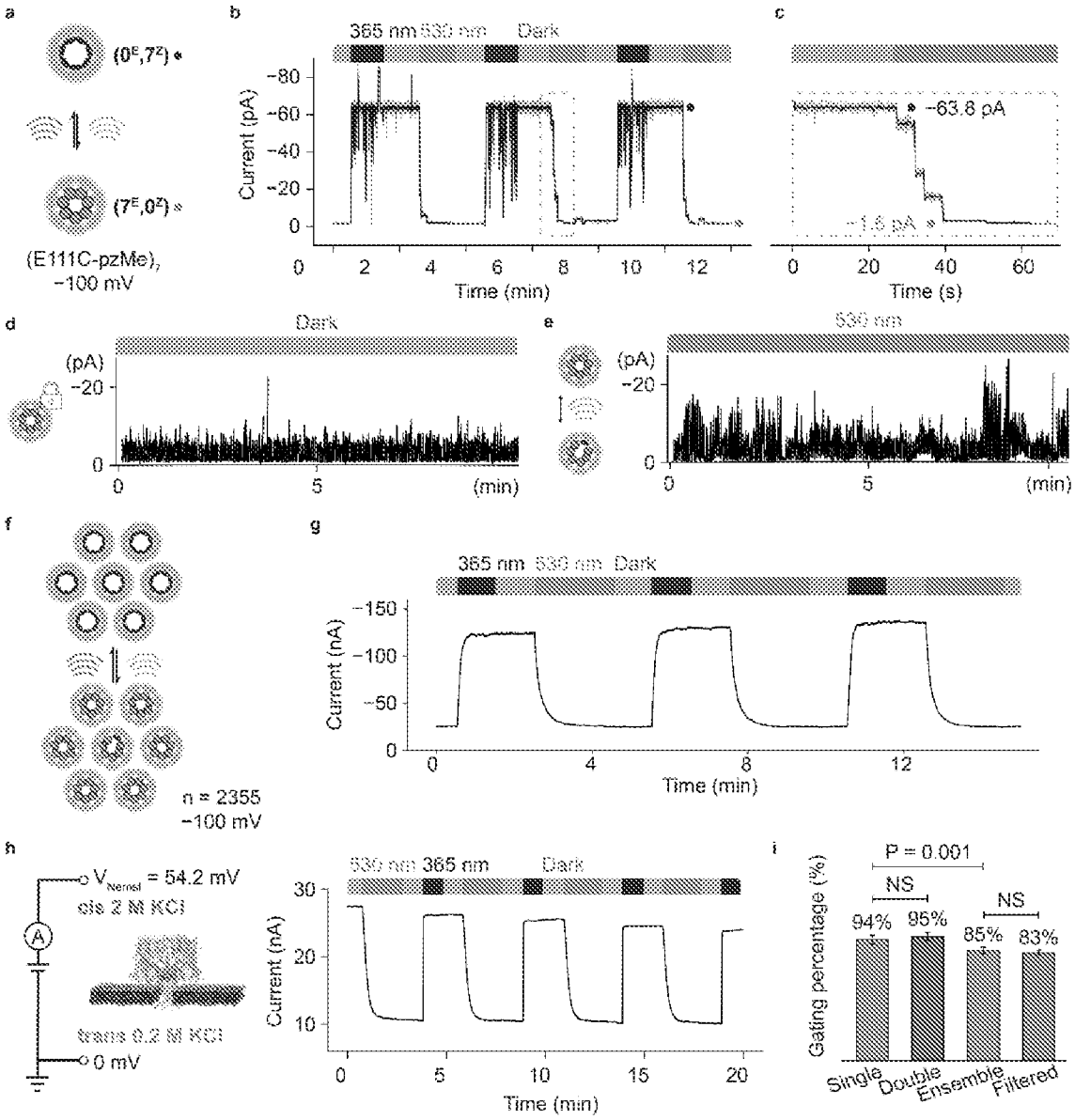
a
(0E,7Z)
(7E,0Z)
(E111C-pzMe),
−100 mV
b
365 nm 530 nm Dark
Current (pA)
−80
−60
−40
−20
0
0 2 4 6 8 10 12
Time (min)
c
−63.8 pA
−1.6 pA
0 20 40 60
Time (s)
d
Dark
(pA)
−20
0
0 5 (min)
e
530 nm
(pA)
−20
0
0 5 (min)
f
n = 2355
−100 mV
g
365 nm 530 nm Dark
Current (nA)
−150
−100
−50
0
0 4 8 12
Time (min)
h
V Nernst = 54.2 mV
cis 2 M KCl
trans 0.2 M KCl
0 mV
530 nm 365 nm Dark
Current (nA)
30
20
10
0 5 10 15 20
Time (min)
i
P = 0.001
NS
NS
Gating percentage (%)
94% 95% 85% 83%
Single Double Ensemble Filtered

Fig. 3

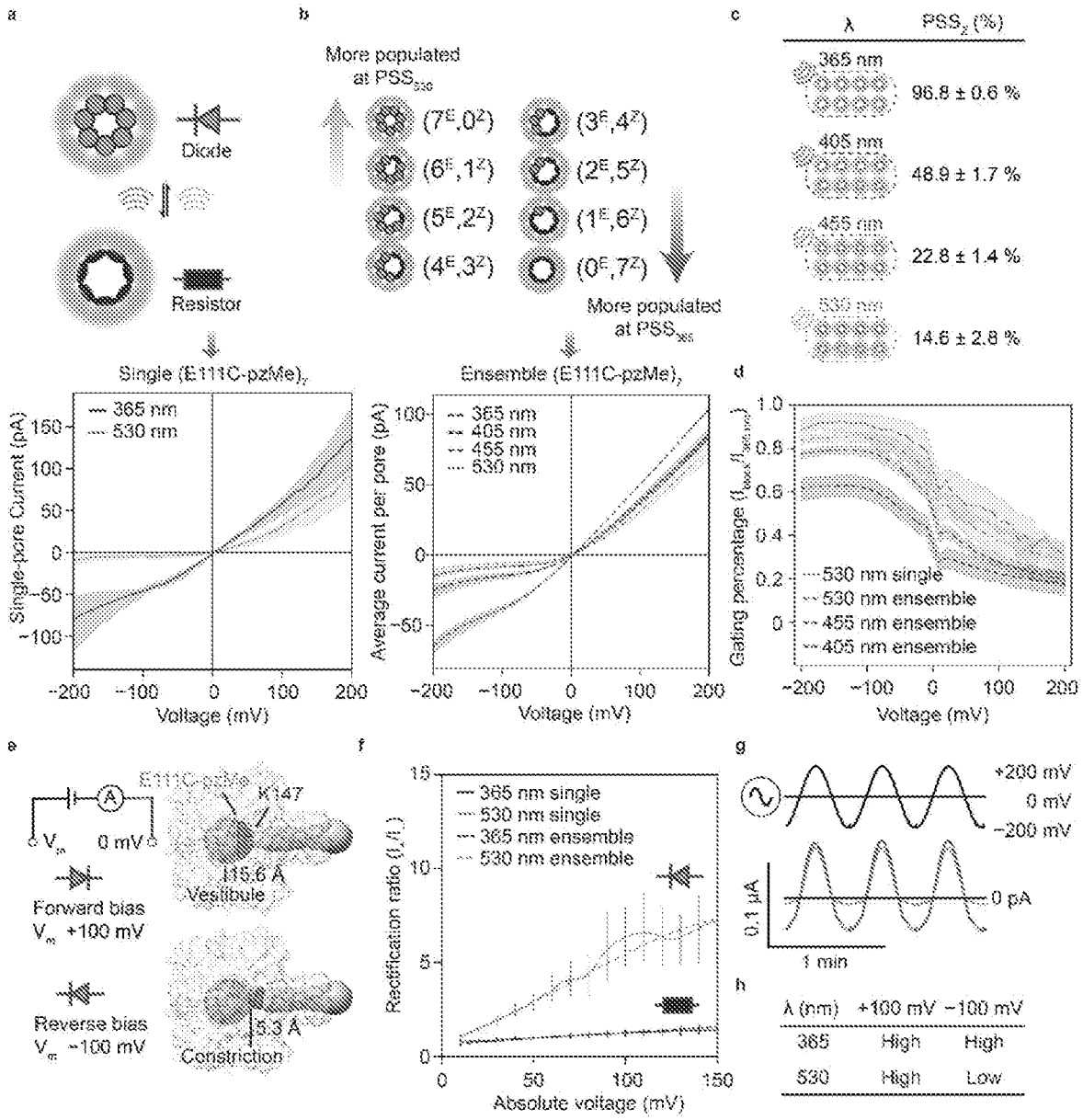
a
Diode
Resistor
b
More populated at PSS530
(7E,0Z)
(6E,1Z)
(5E,2Z)
(4E,3Z)
(3E,4Z)
(2E,5Z)
(1E,6Z)
(0E,7Z)
More populated at PSS365
c
λ
PSS2 (%)
365 nm
96.8 ± 0.6 %
405 nm
48.9 ± 1.7 %
455 nm
22.8 ± 1.4 %
530 nm
14.6 ± 2.8 %
Single (E111C-pzMe)2
Ensemble (E111C-pzMe)2
365 nm
530 nm
405 nm
455 nm
Single-pore Current (pA)
Average current per pore (pA)
Voltage (mV)
d
Gating percentage
530 nm single
530 nm ensemble
455 nm ensemble
405 nm ensemble
e
E111C-pzMe
K147
115.6 Å
Vestibule
5.3 Å
Constriction
Forward bias
Vm +100 mV
Reverse bias
Vm −100 mV
0 mV
f
Rectification ratio (I+/I−)
365 nm single
530 nm single
365 nm ensemble
530 nm ensemble
Absolute voltage (mV)
g
+200 mV
0 mV
−200 mV
0.1 µA
0 pA
1 min
h
λ (nm) +100 mV −100 mV
365 High High
530 High Low

Fig. 4

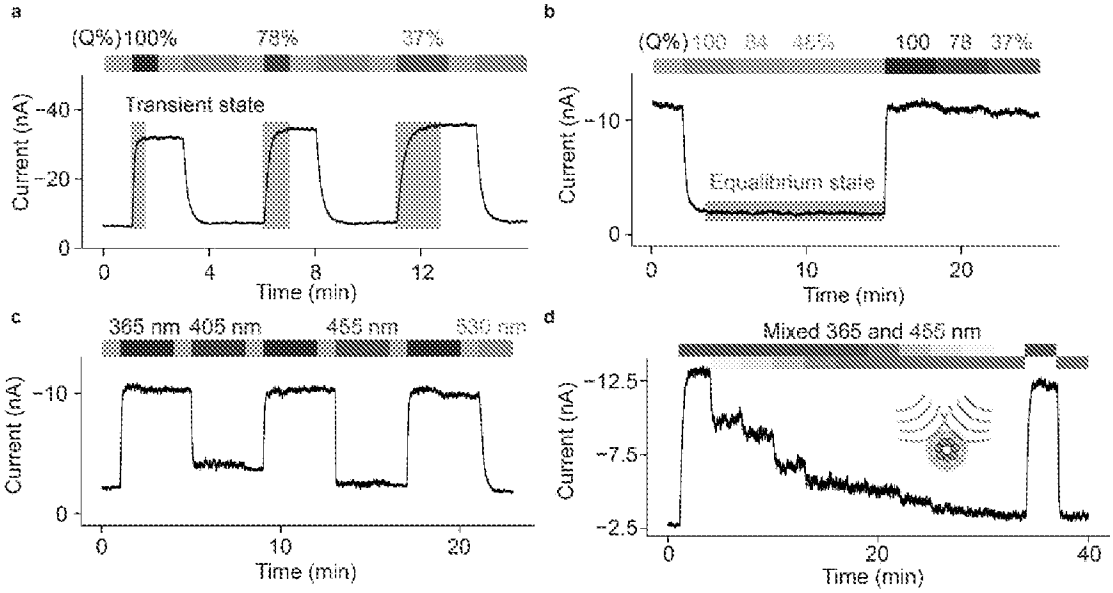
a
(Q%) 100% 78% 37%
Transient state
Current (nA)
Time (min)
b
(Q%) 100 84 46% 100 78 37%
Equilibrium state
Current (nA)
Time (min)
c
365 nm 405 nm 455 nm 530 nm
Current (nA)
Time (min)
d
Mixed 365 and 455 nm
Current (nA)
Time (min)

Fig. 5

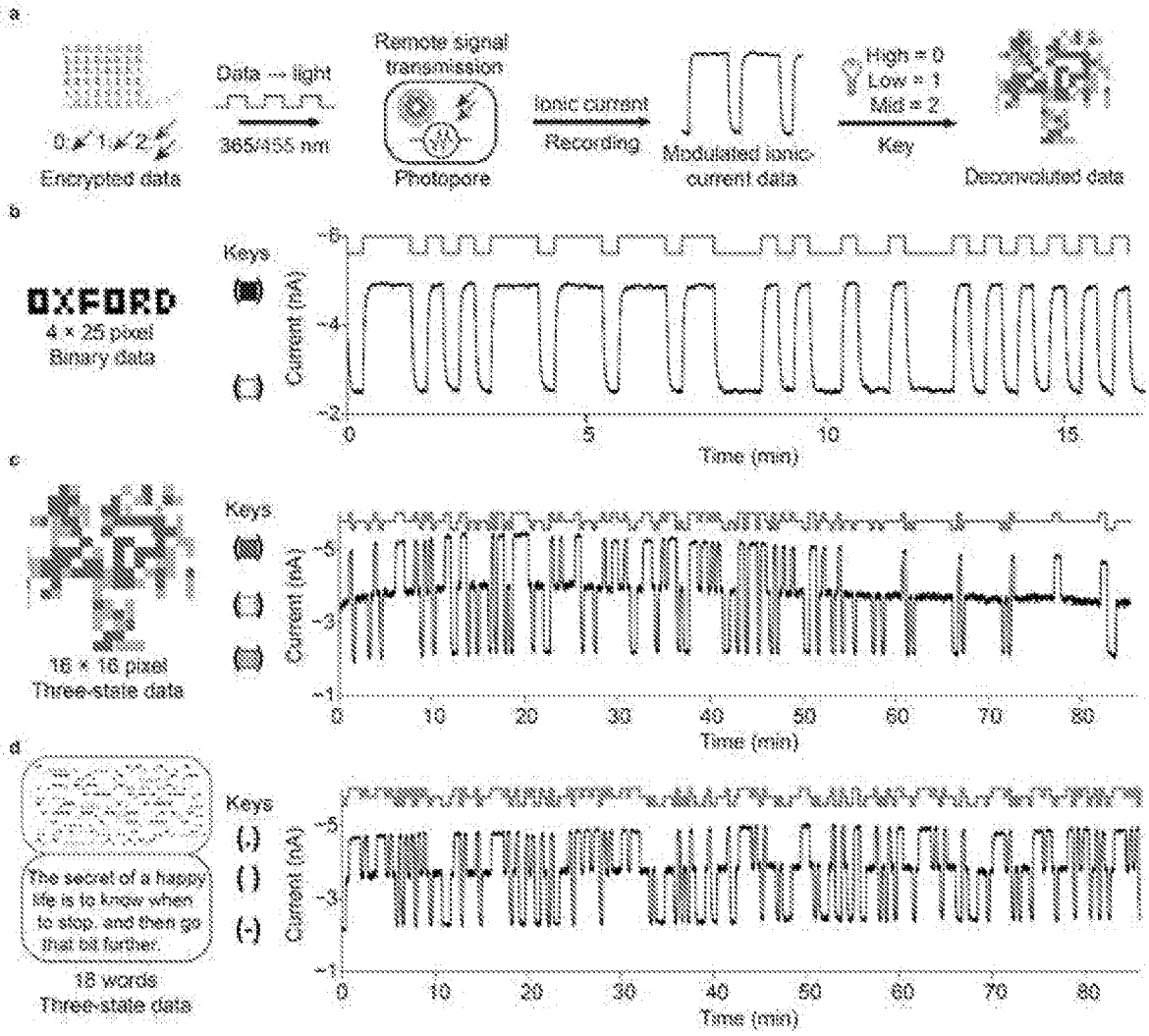
a
Data → light
365/455 nm
Encrypted data
Remote signal transmission
Photopore
Ionic current
Recording
Modulated ionic-current data
High = 0
Low = 1
Mid = 2
Key
Deconvoluted data
b
OXFORD
4 × 25 pixel
Binary data
Keys
Current (nA)
Time (min)
c
16 × 16 pixel
Three-state data
Keys
Current (nA)
Time (min)
d
The secret of a happy life is to know when to stop, and then go that bit further.
18 words
Three-state data
Keys
Current (nA)
Time (min)

Fig. 6

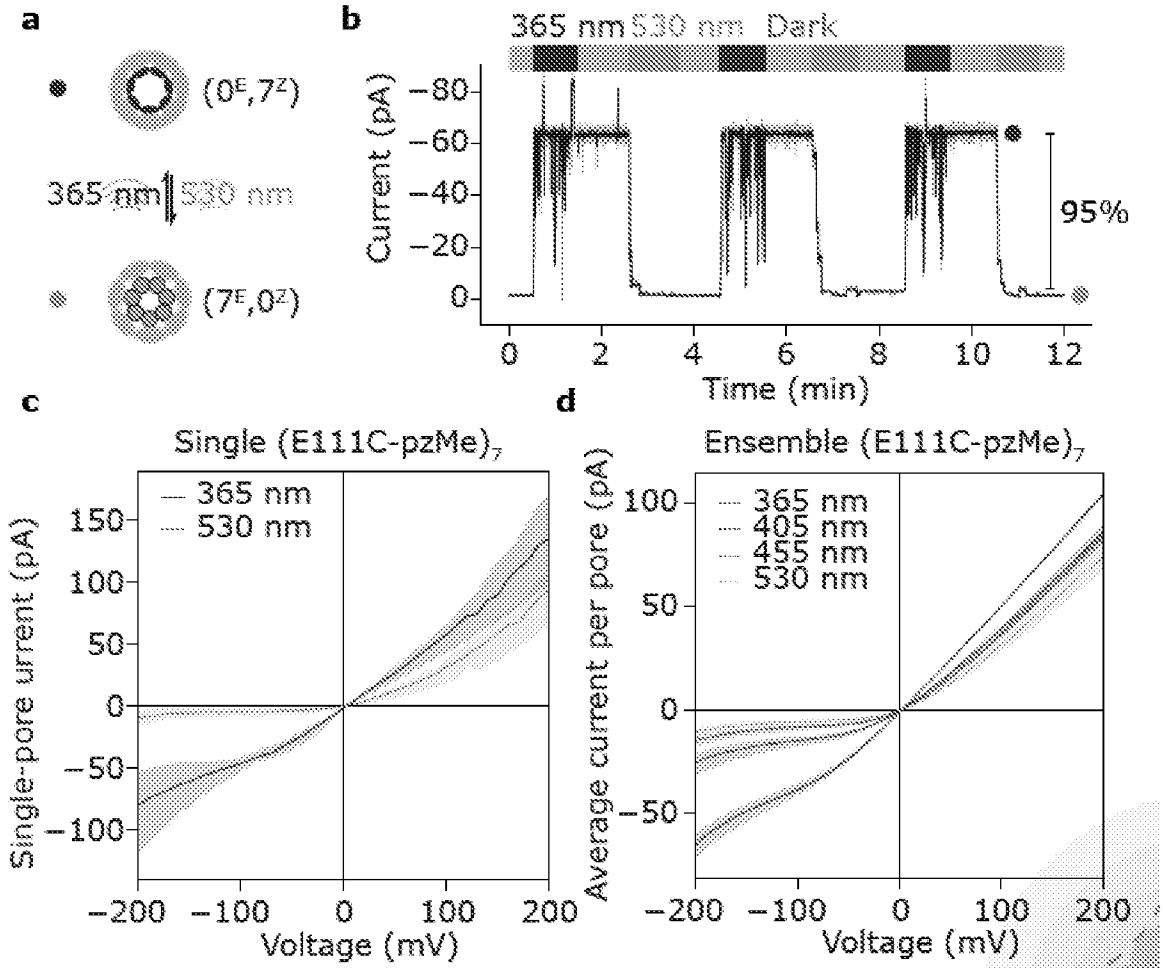
a
(0E,7Z)
365 nm
530 nm
(7E,0Z)
b
365 nm
530 nm
Dark
Current (pA)
−80
−60
−40
−20
0
95%
0
2
4
6
8
10
12
Time (min)
c
Single (E111C-pzMe)7
365 nm
530 nm
Single-pore urrent (pA)
150
100
50
0
−50
−100
−200
−100
0
100
200
Voltage (mV)
d
Ensemble (E111C-pzMe)7
365 nm
405 nm
455 nm
530 nm
Average current per pore (pA)
100
50
0
−50
−200
−100
0
100
200
Voltage (mV)

Fig. 7

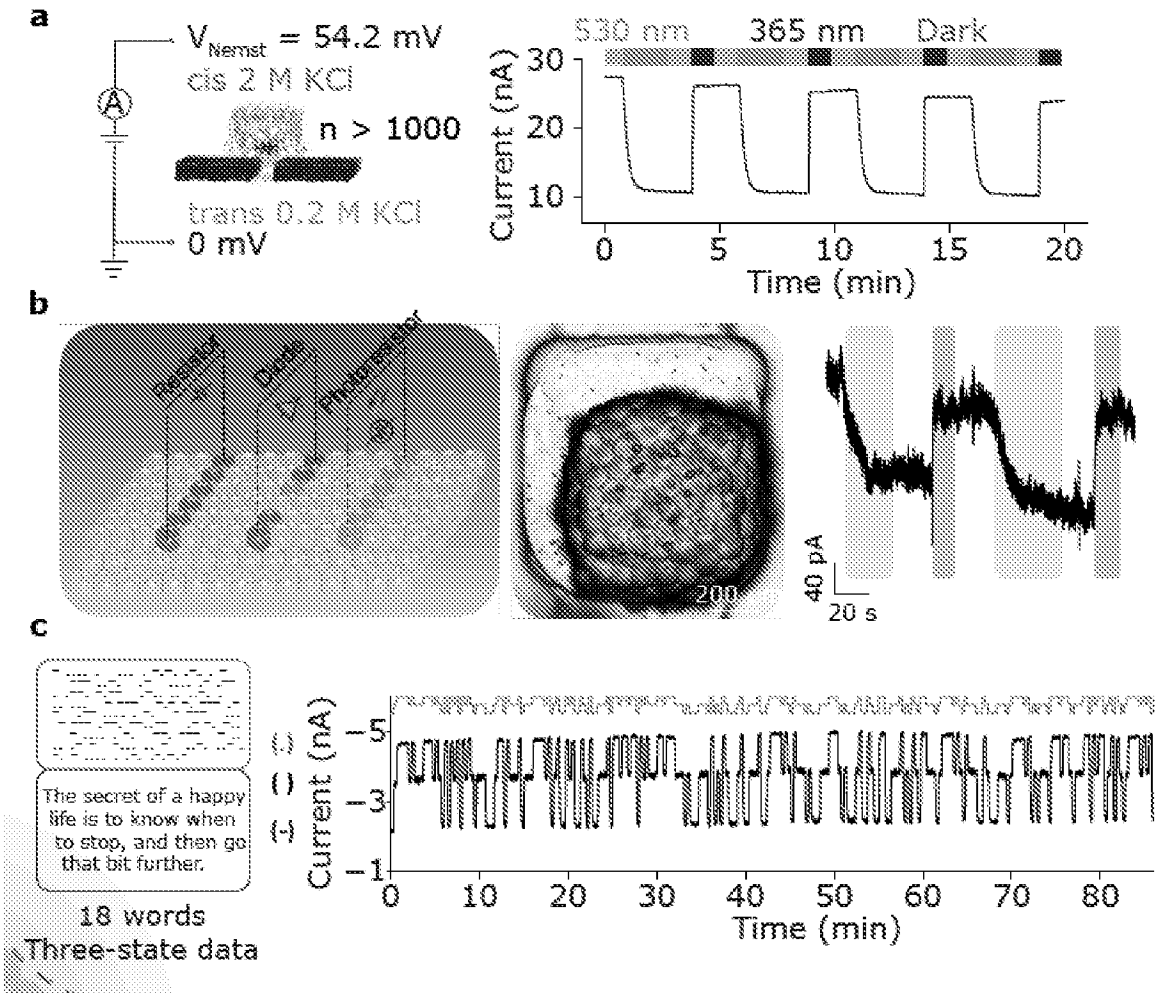
a
V_{Nernst} = 54.2 mV
cis 2 M KCl
n > 1000
trans 0.2 M KCl
0 mV
530 nm
365 nm
Dark
Current (nA)
Time (min)
b
40 pA
20 s
c
The secret of a happy life is to know when to stop, and then go that bit further.
18 words
Three-state data
Current (nA)
Time (min)

Fig. 8

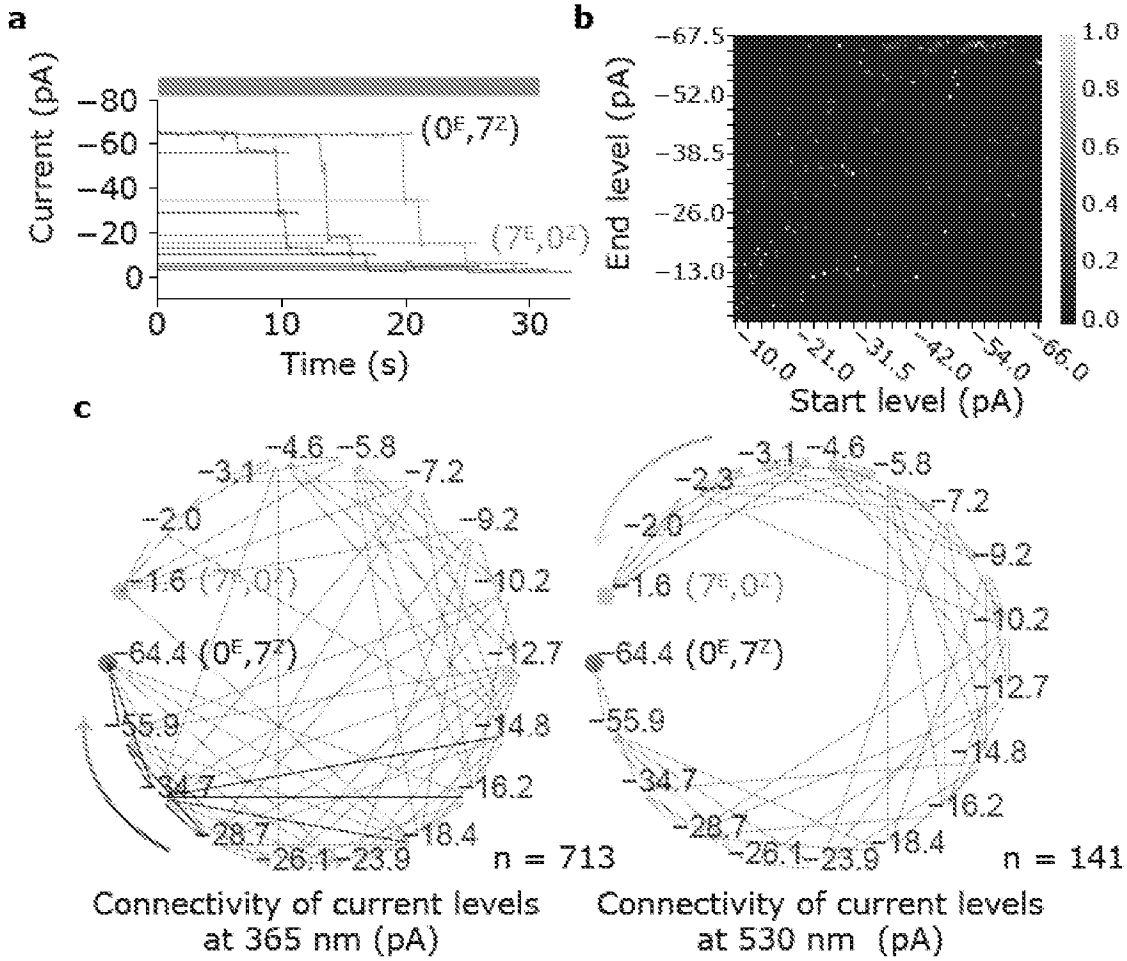
a
Current (pA)
−80
−60
−40
−20
0
(0E,7Z)
(7E,0Z)
0
10
20
30
Time (s)
b
End level (pA)
−67.5
−52.0
−38.5
−26.0
−13.0
1.0
0.8
0.6
0.4
0.2
0.0
−10.0
−21.0
−31.5
−42.0
−54.0
−66.0
Start level (pA)
c
−4.6
−5.8
−3.1
−7.2
−2.0
−9.2
−1.6 (7E,0Z)
−10.2
−64.4 (0E,7Z)
−12.7
−55.9
−14.8
−34.7
−16.2
−28.7
−18.4
−26.1
−23.9
n = 713
Connectivity of current levels at 365 nm (pA)
−3.1
−4.6
−5.8
−2.3
−7.2
−2.0
−9.2
−1.6 (7E,0Z)
−10.2
−64.4 (0E,7Z)
−12.7
−55.9
−14.8
−34.7
−16.2
−28.7
−18.4
−26.1
−23.9
n = 141
Connectivity of current levels at 530 nm (pA)

Fig. 9

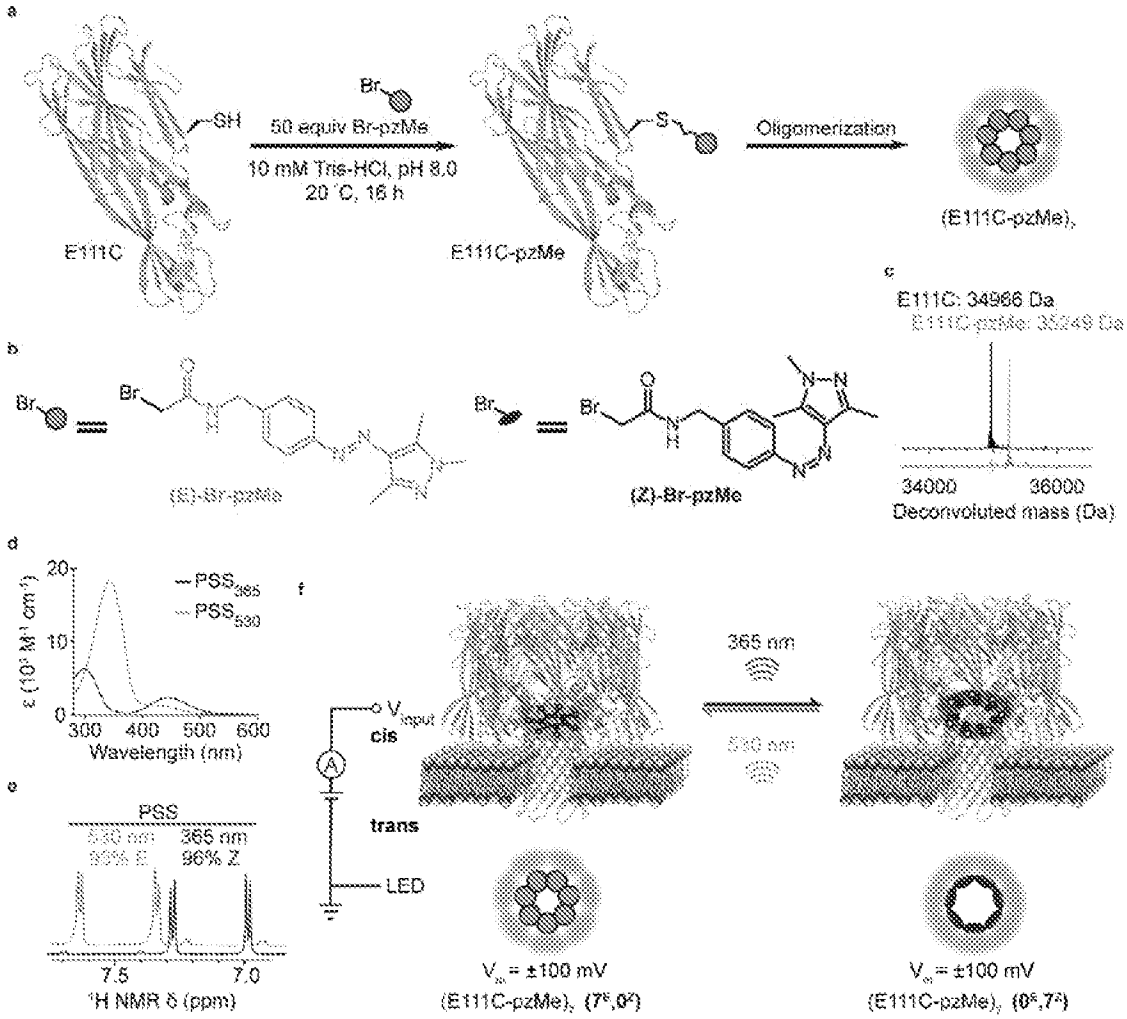
a
SH
E111C
Br
50 equiv Br-pzMe
10 mM Tris-HCl, pH 8.0
20 °C, 16 h
S
E111C-pzMe
Oligomerization
(E111C-pzMe)n
b
Br
Br
(E)-Br-pzMe
Br
Br
(Z)-Br-pzMe
c
E111C: 34966 Da
E111C-pzMe: 35249 Da
34000
36000
Deconvoluted mass (Da)
d
20
10
0
ε (10³ M⁻¹ cm⁻¹)
PSS365
PSS530
300
400
500
600
Wavelength (nm)
e
PSS
530 nm
95% E
365 nm
96% Z
7.5
7.0
¹H NMR δ (ppm)
f
V input
cis
trans
LED
365 nm
530 nm
Vm = ±100 mV
(E111C-pzMe)n (7E,0Z)
Vm = ±100 mV
(E111C-pzMe)n (0E,7Z)

Fig. 10

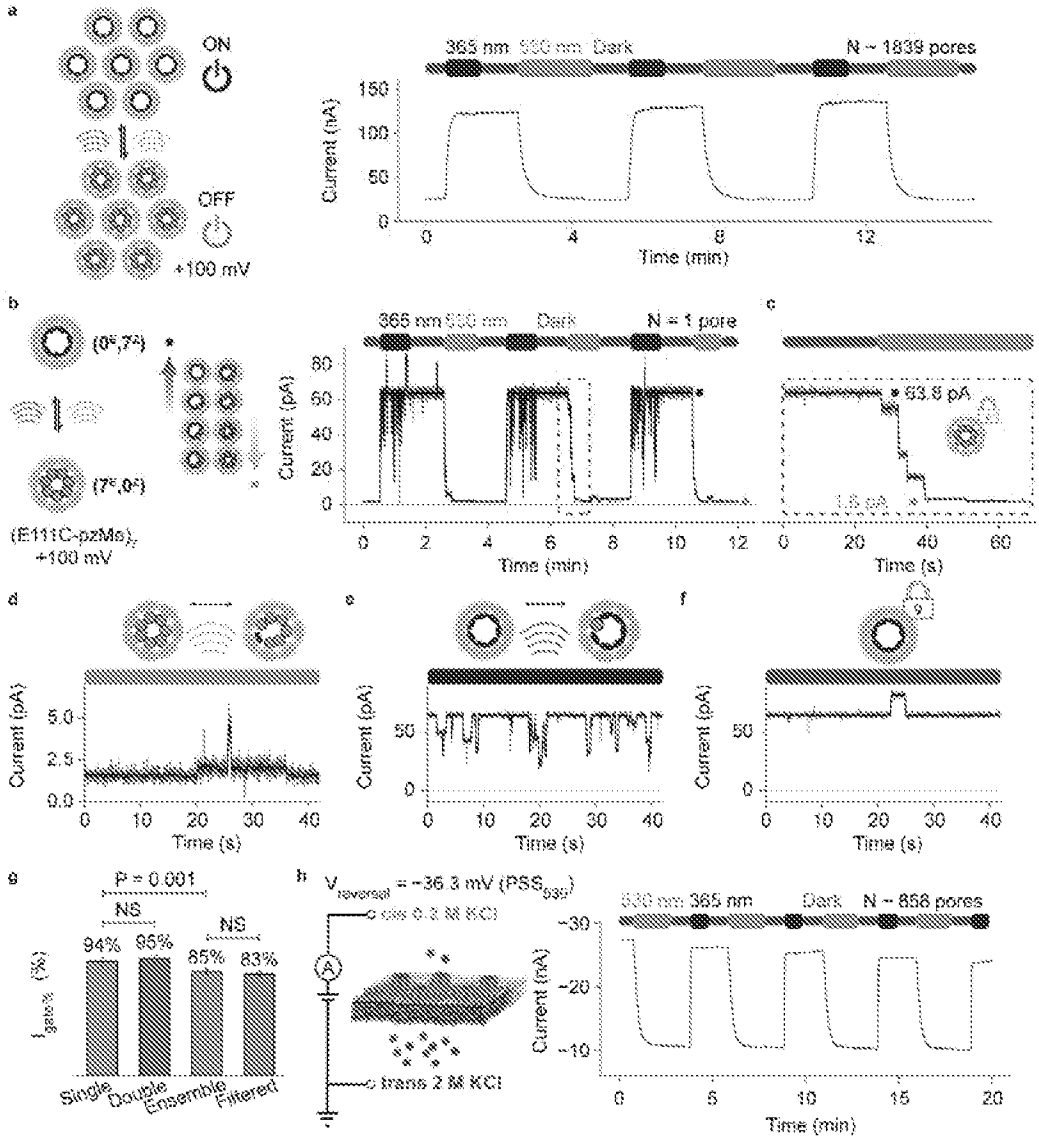
a
ON
OFF
+100 mV
365 nm 530 nm Dark
N ~ 1839 pores
Current (nA)
Time (min)
b
(6E,7A)
(7E,0A)
(E111C-pzMa)2
+100 mV
365 nm 530 nm Dark
N = 1 pore
Current (pA)
Time (min)
c
63.6 pA
1.8 pA
Time (s)
d
e
f
Current (pA)
Time (s)
g
P = 0.001
NS
NS
94%
95%
85%
83%
Single
Double
Ensemble
Filtered
h
V reversal = −36.3 mV (PSS530)
cis 0.3 M KCl
trans 2 M KCl
530 nm 365 nm Dark N ~ 858 pores
Current (nA)
Time (min)

Fig. 11

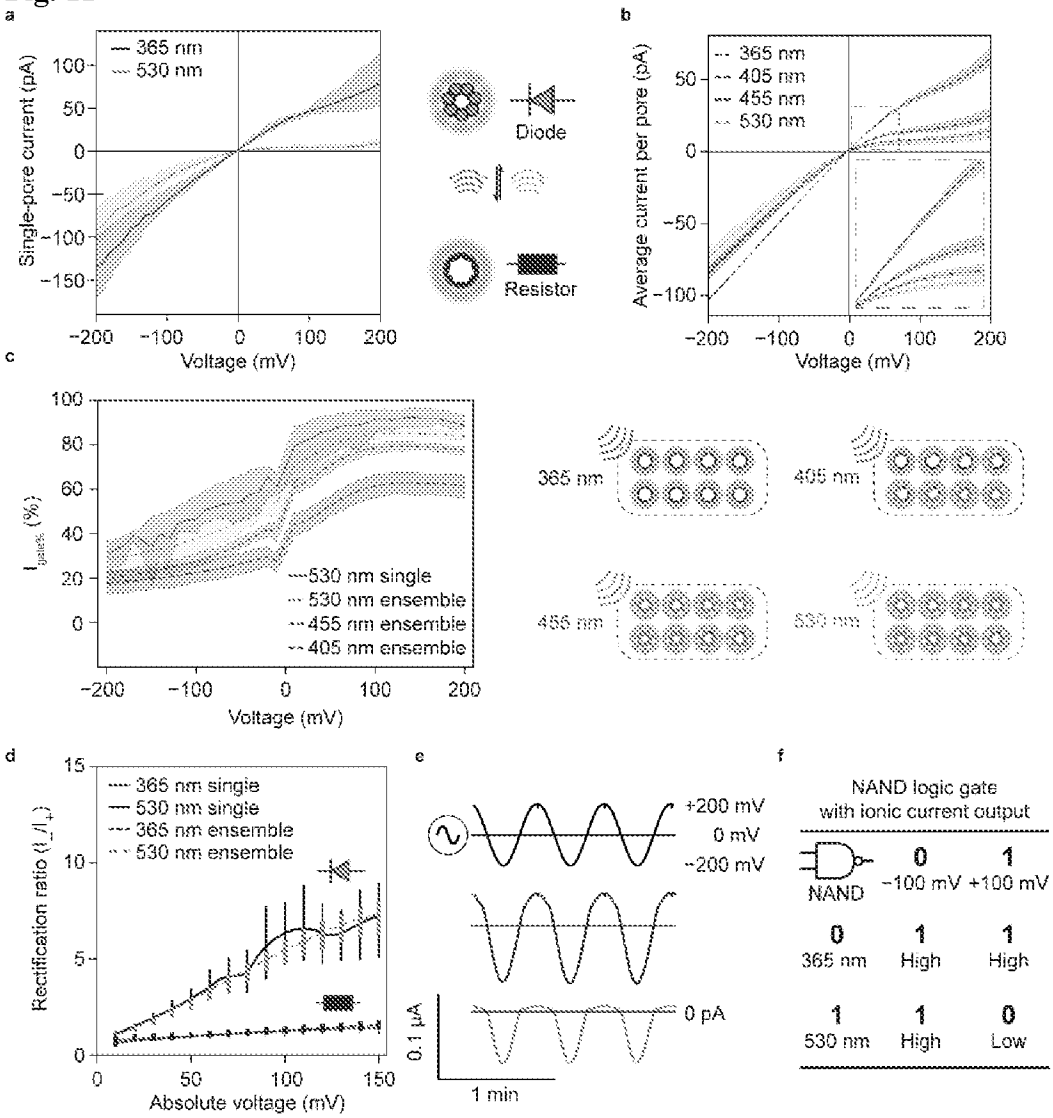
a
365 nm
530 nm
Single-pore current (pA)
Voltage (mV)
Diode
Resistor
b
365 nm
405 nm
455 nm
530 nm
Average current per pore (pA)
Voltage (mV)
c
530 nm single
530 nm ensemble
455 nm ensemble
405 nm ensemble
Voltage (mV)
365 nm
405 nm
455 nm
530 nm
d
365 nm single
530 nm single
365 nm ensemble
530 nm ensemble
Absolute voltage (mV)
e
+200 mV
0 mV
−200 mV
0 pA
0.1 µA
1 min
f
NAND logic gate
with ionic current output
NAND
0
−100 mV
1
+100 mV
0
365 nm
1
High
1
High
1
530 nm
1
High
0
Low

Fig, 12

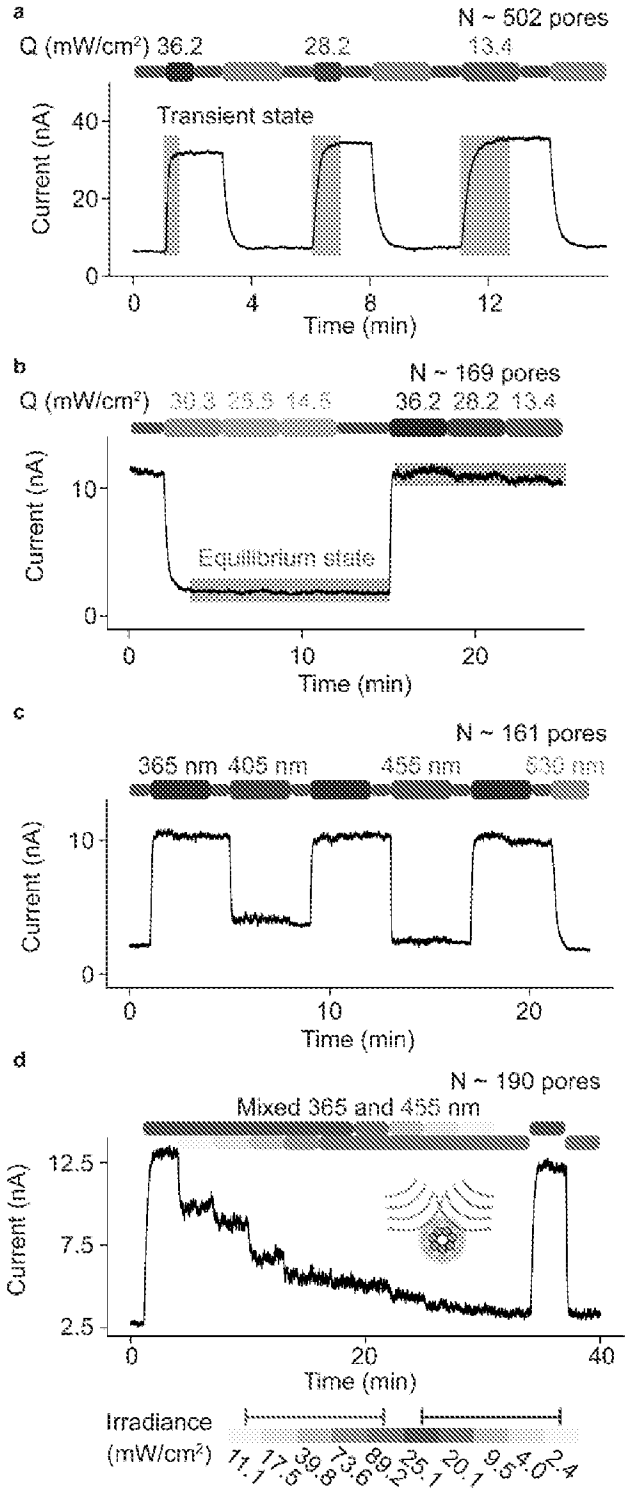
a
N ~ 502 pores
Q (mW/cm²) 36.2
28.2
13.4
Transient state
Current (nA)
40
20
0
0
4
8
12
Time (min)
b
N ~ 169 pores
Q (mW/cm²) 36.2 28.2 13.4
Equilibrium state
Current (nA)
10
0
0
10
20
Time (min)
c
N ~ 161 pores
365 nm 405 nm 455 nm 530 nm
Current (nA)
10
0
0
10
20
Time (min)
d
N ~ 190 pores
Mixed 365 and 455 nm
Current (nA)
12.5
7.5
2.5
0
20
40
Time (min)
Irradiance
(mW/cm²)
11.1 17.5 39.8 13.6 89.5 25.1 20.1 9.5 4.0 2.4

Fig, 13

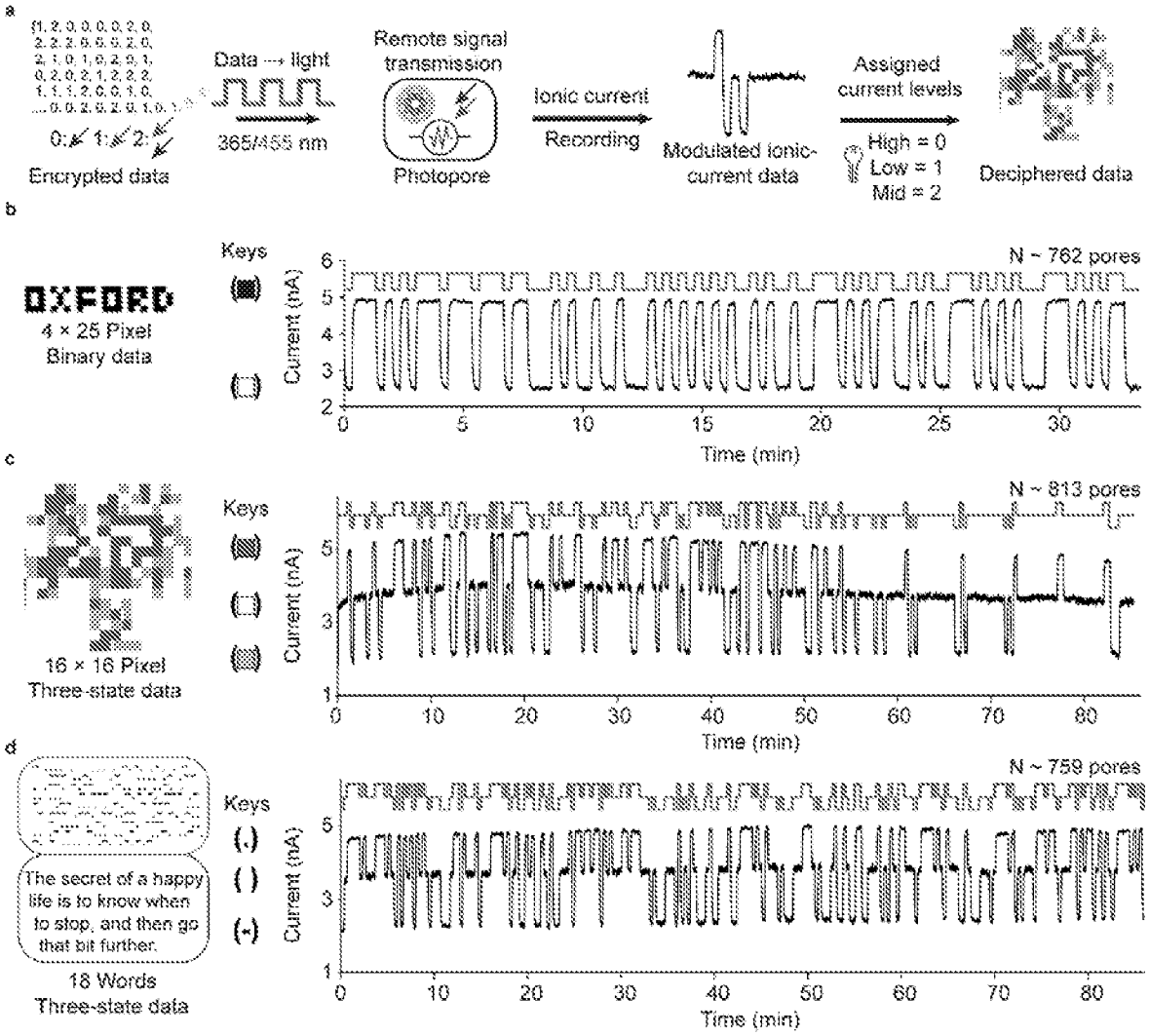
a
Encrypted data
0: 1: 2:
Data → light
365/455 nm
Remote signal transmission
Photopore
Ionic current
Recording
Modulated ionic-current data
Assigned current levels
High = 0
Low = 1
Mid = 2
Deciphered data
b
OXFORD
4 × 25 Pixel
Binary data
Keys
Current (nA)
N ~ 762 pores
Time (min)
c
16 × 16 Pixel
Three-state data
Keys
Current (nA)
N ~ 813 pores
Time (min)
d
The secret of a happy life is to know when to stop, and then go that bit further.
18 Words
Three-state data
Keys
(.)
( )
(-)
Current (nA)
N ~ 759 pores
Time (min)

Fig. 14

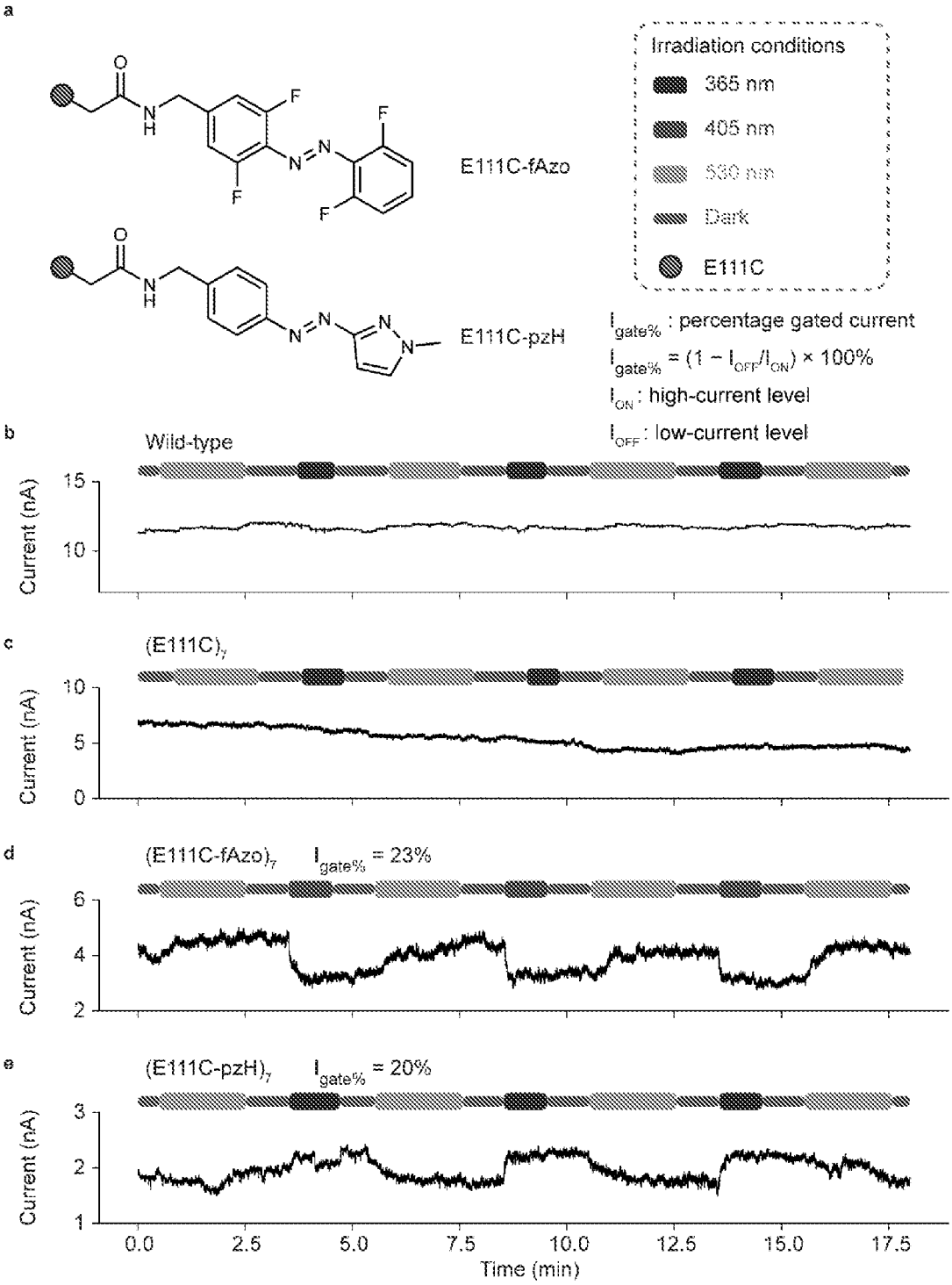
a
E111C-fAzo
E111C-pzH
Irradiation conditions
365 nm
405 nm
530 nm
Dark
E111C
$I_{gate\%}$: percentage gated current
$I_{gate\%} = (1 - I_{OFF}/I_{ON}) \times 100\%$
I_{ON} : high-current level
I_{OFF} : low-current level
b
Wild-type
c
$(E111C)_7$
d
$(E111C\text{-}fAzo)_7$ $I_{gate\%}$ = 23%
e
$(E111C\text{-}pzH)_7$ $I_{gate\%}$ = 20%
Current (nA)
Time (min)

Fig. 15

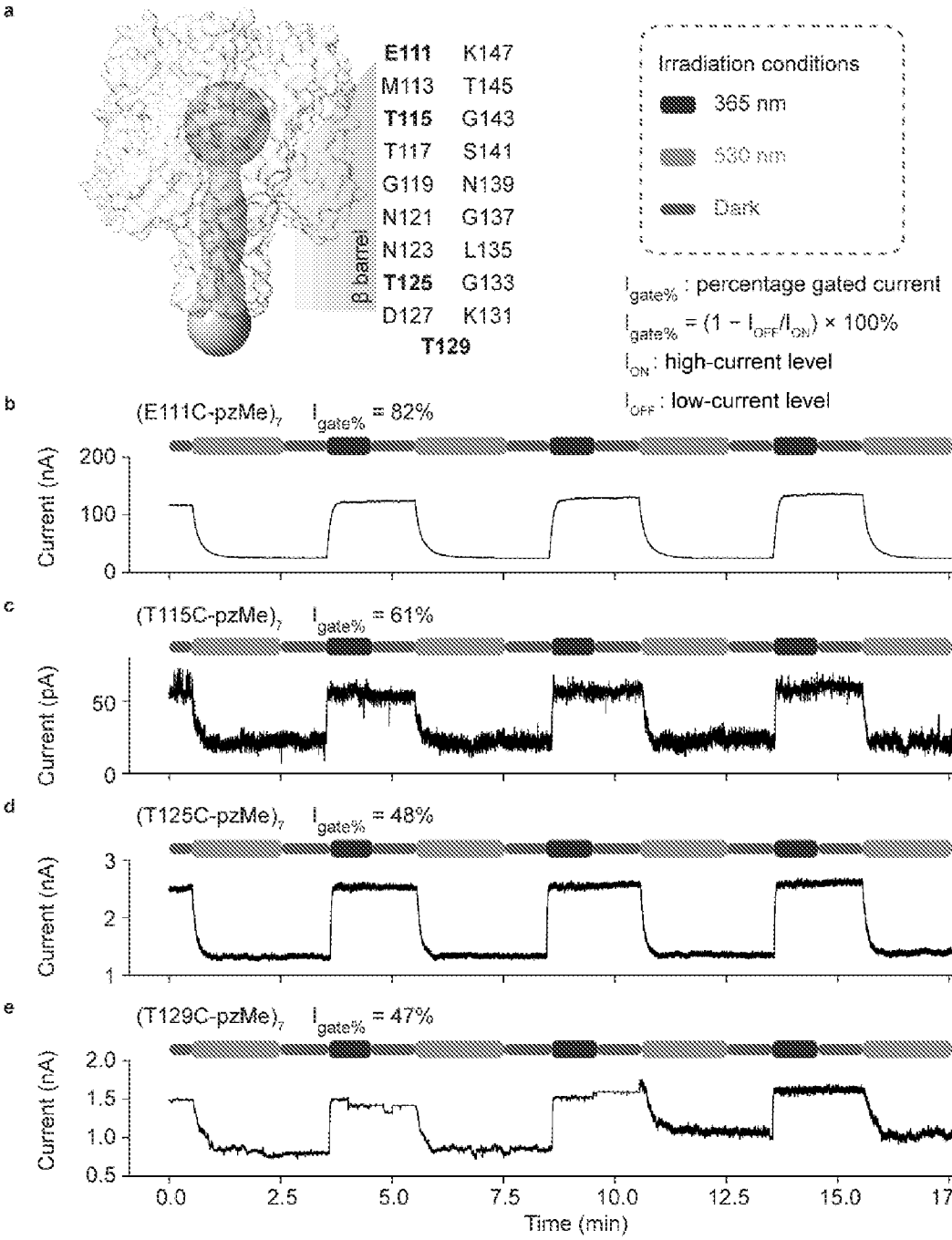
a
β barrel
E111 K147
M113 T145
T115 G143
T117 S141
G119 N139
N121 G137
N123 L135
T125 G133
D127 K131
T129
Irradiation conditions
365 nm
530 nm
Dark
$I_{gate\%}$: percentage gated current
$I_{gate\%} = (1 - I_{OFF}/I_{ON}) \times 100\%$
I_{ON} : high-current level
I_{OFF} : low-current level
b
(E111C-pzMe)$_7$ $I_{gate\%}$ = 82%
Current (nA)
200
100
0
c
(T115C-pzMe)$_7$ $I_{gate\%}$ = 61%
Current (pA)
50
0
d
(T125C-pzMe)$_7$ $I_{gate\%}$ = 48%
Current (nA)
3
2
1
e
(T129C-pzMe)$_7$ $I_{gate\%}$ = 47%
Current (nA)
2.0
1.5
1.0
0.5
0.0
2.5
5.0
7.5
10.0
12.5
15.0
17.5
Time (min)

Fig. 16

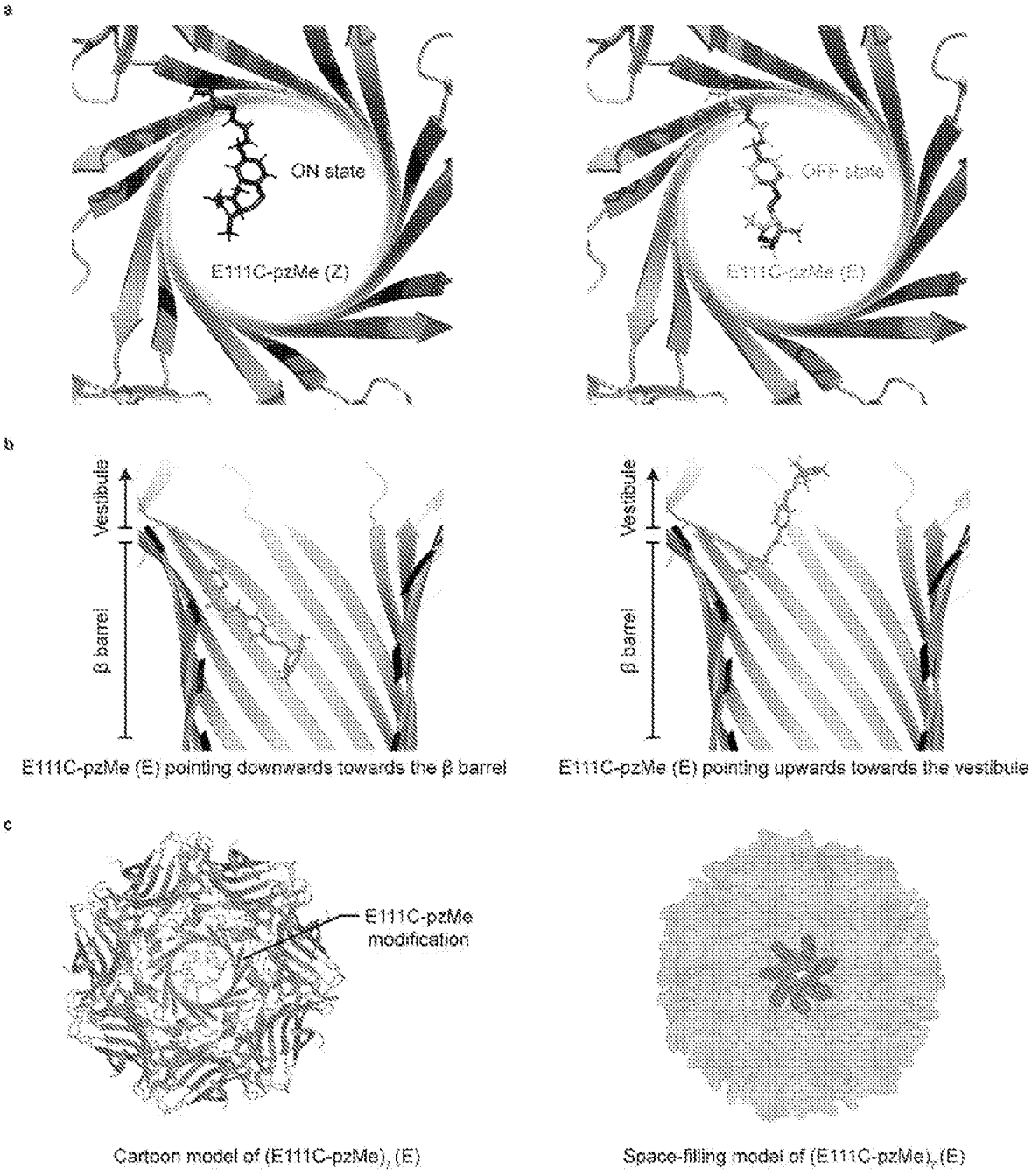
a
ON state
E111C-pzMe (Z)
OFF state
E111C-pzMe (E)
b
Vestibule
β barrel
E111C-pzMe (E) pointing downwards towards the β barrel
Vestibule
β barrel
E111C-pzMe (E) pointing upwards towards the vestibule
c
E111C-pzMe modification
Cartoon model of (E111C-pzMe), (E)
Space-filling model of (E111C-pzMe), (E)

Fig. 17

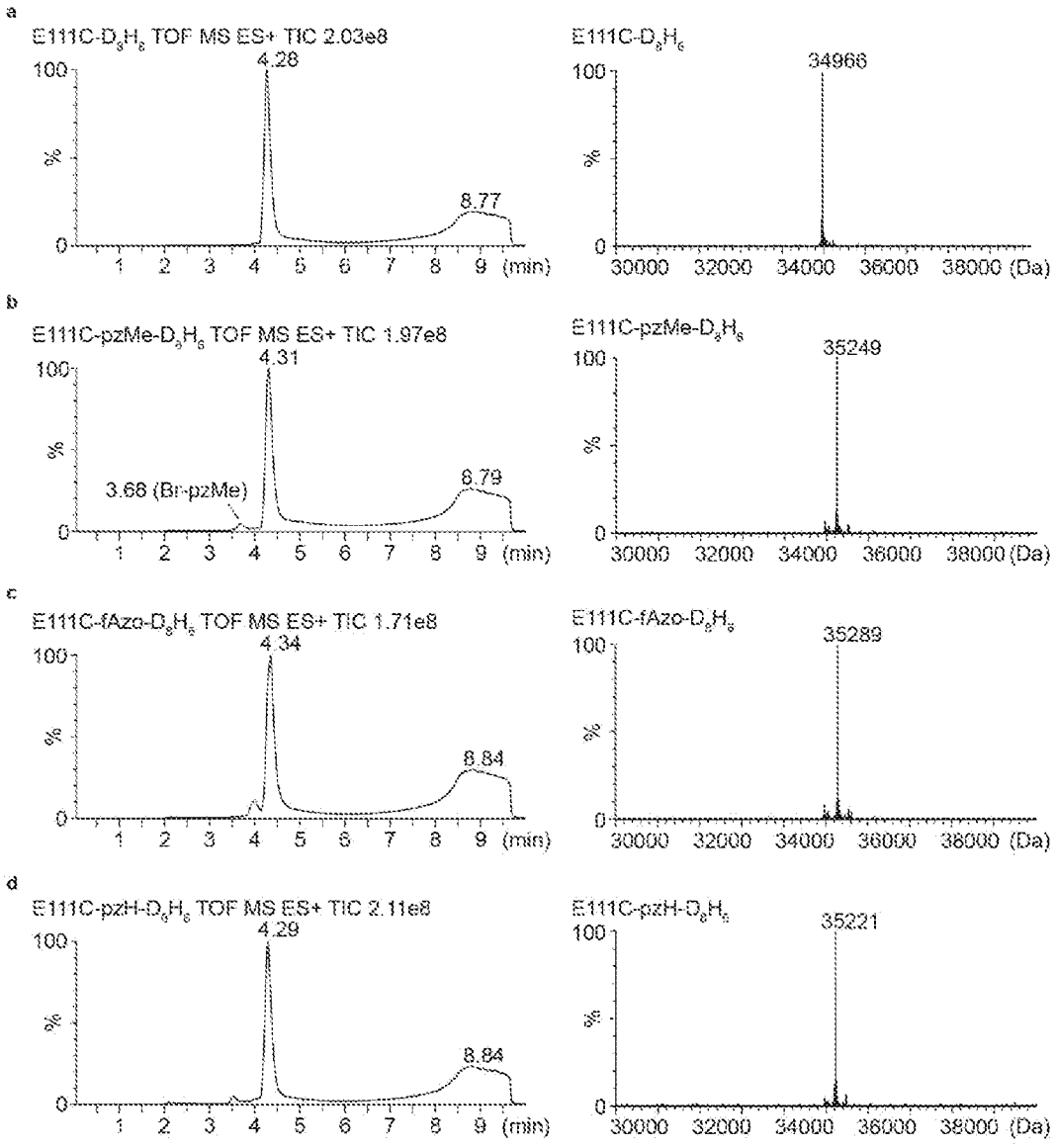
a
E111C-D8H6 TOF MS ES+ TIC 2.03e8
4.28
8.77
E111C-D8H6
34966
b
E111C-pzMe-D8H6 TOF MS ES+ TIC 1.97e8
4.31
3.68 (Br-pzMe)
8.79
E111C-pzMe-D8H6
35249
c
E111C-fAzo-D8H6 TOF MS ES+ TIC 1.71e8
4.34
8.84
E111C-fAzo-D8H6
35289
d
E111C-pzH-D8H6 TOF MS ES+ TIC 2.11e8
4.29
8.84
E111C-pzH-D8H6
35221
100
%
0
1 2 3 4 5 6 7 8 9 (min)
30000 32000 34000 36000 38000 (Da)

Fig. 18

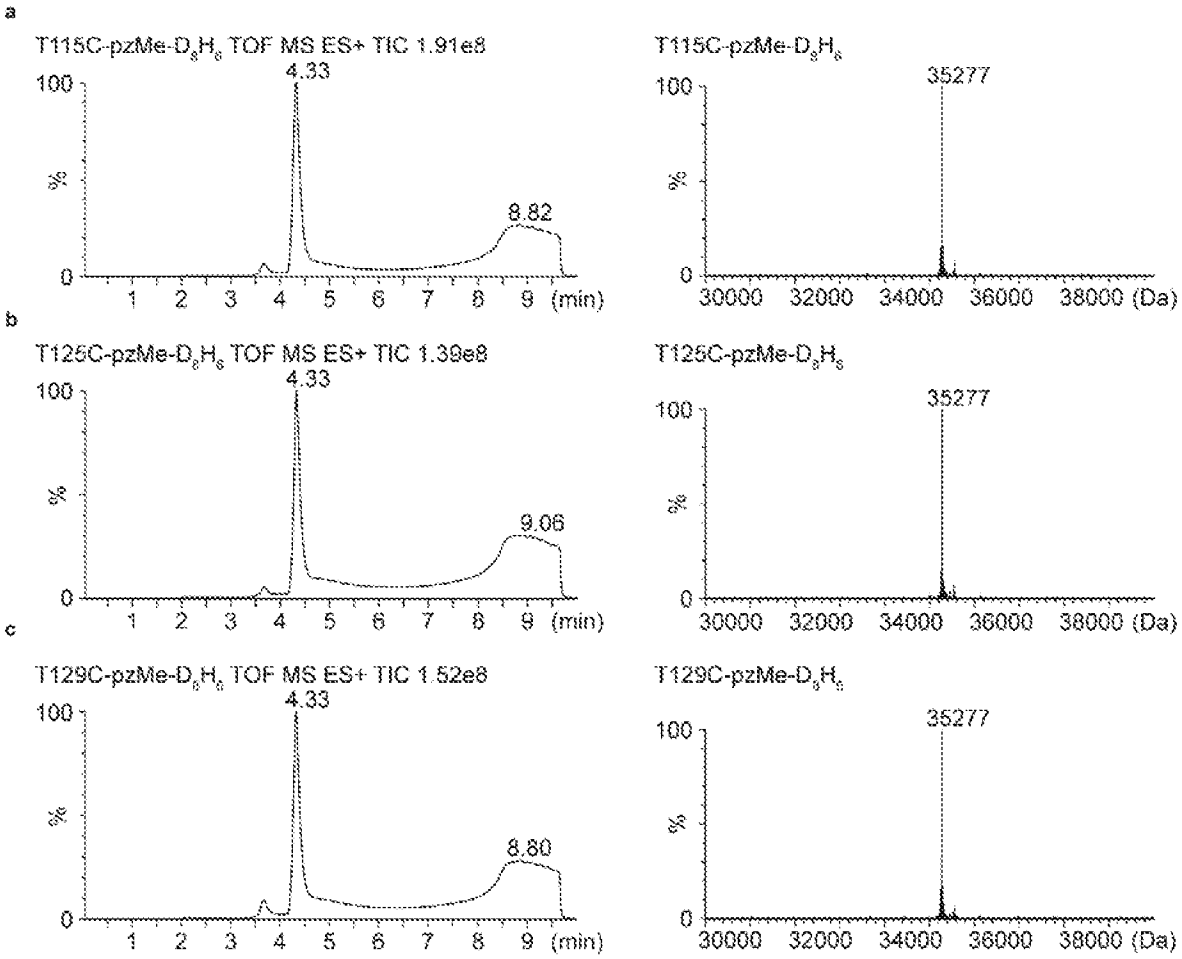
a
T115C-pzMe-D8H6 TOF MS ES+ TIC 1.91e8
4.33
8.82
100
%
0
1 2 3 4 5 6 7 8 9 (min)
T115C-pzMe-D8H6
35277
30000 32000 34000 36000 38000 (Da)
b
T125C-pzMe-D8H6 TOF MS ES+ TIC 1.39e8
4.33
9.06
T125C-pzMe-D8H6
35277
c
T129C-pzMe-D8H6 TOF MS ES+ TIC 1.52e8
4.33
8.80
T129C-pzMe-D8H6
35277

Fig. 19

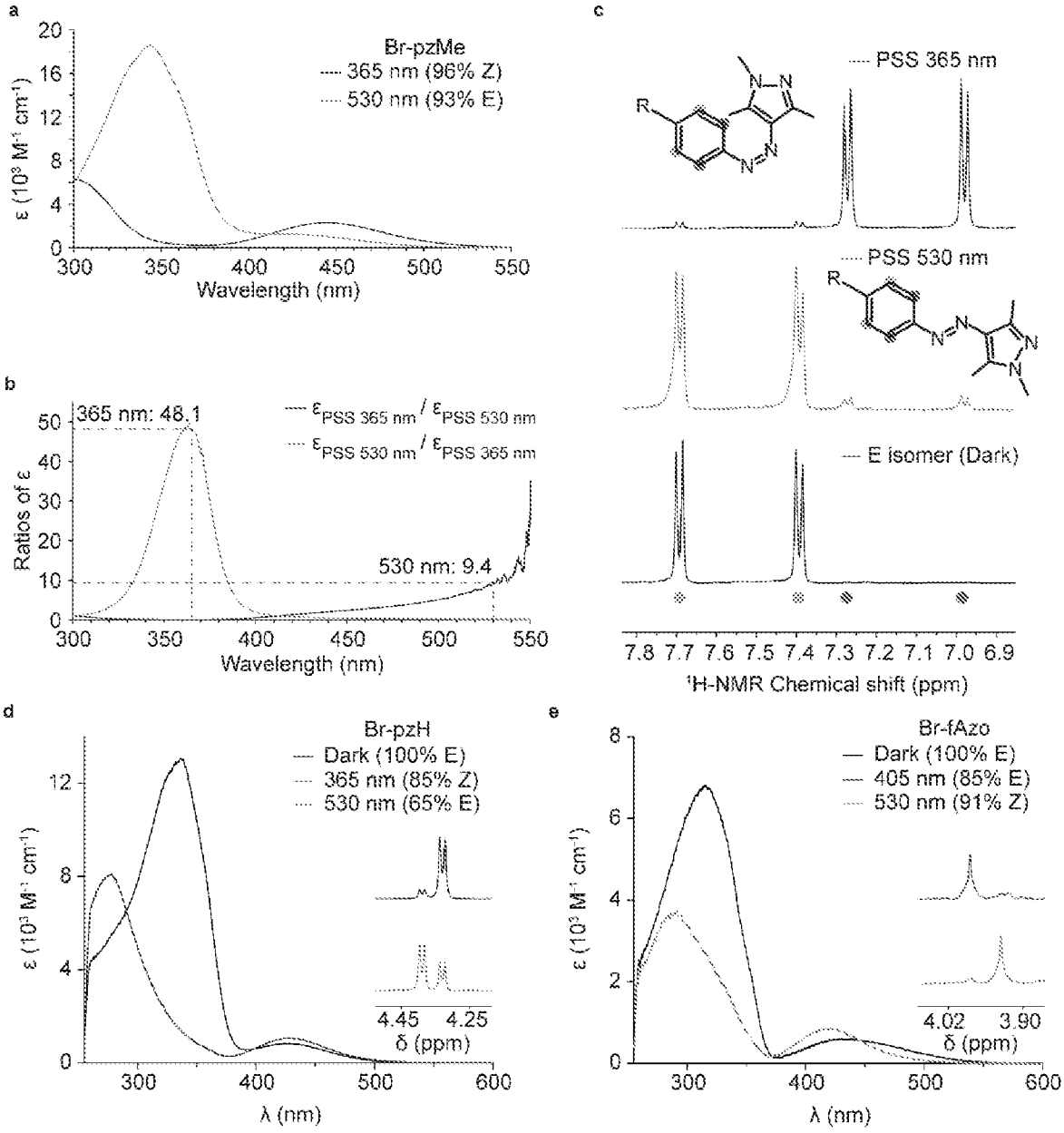
a
Br-pzMe
365 nm (96% Z)
530 nm (93% E)
ε (10³ M⁻¹ cm⁻¹)
Wavelength (nm)
b
365 nm: 48.1
530 nm: 9.4
Ratios of ε
Wavelength (nm)
c
PSS 365 nm
PSS 530 nm
E isomer (Dark)
¹H-NMR Chemical shift (ppm)
d
Br-pzH
Dark (100% E)
365 nm (85% Z)
530 nm (65% E)
ε (10³ M⁻¹ cm⁻¹)
δ (ppm)
λ (nm)
e
Br-fAzo
Dark (100% E)
405 nm (85% E)
530 nm (91% Z)
ε (10³ M⁻¹ cm⁻¹)
δ (ppm)
λ (nm)

Fig. 20

a

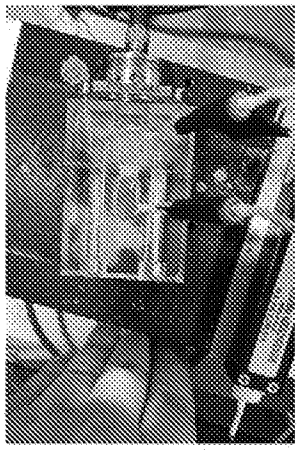

Recording chamber

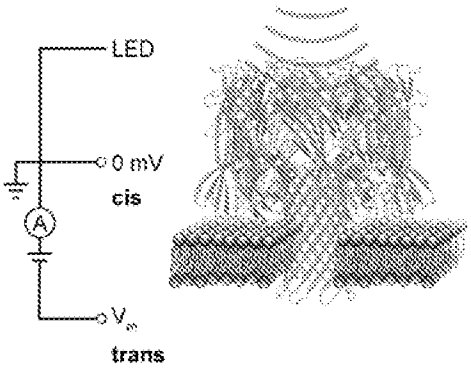

b

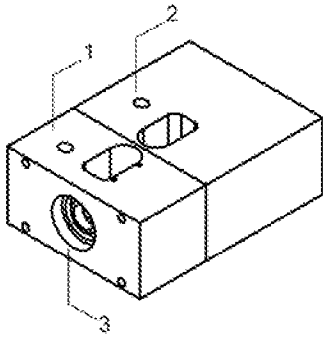

1. For the cis electrode
2. For the trans electrode
3. For the collimator

c

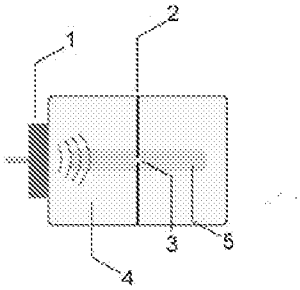

1. LED and Collimator
2. Teflon film
3. Ø 100 µm aperture
4. PMMA chamber
5. Buffer sink

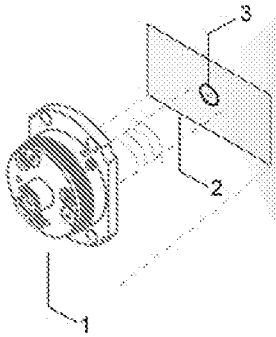

Collimation

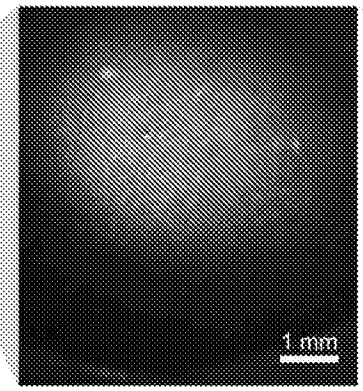

Irradiation on the Teflon film

d

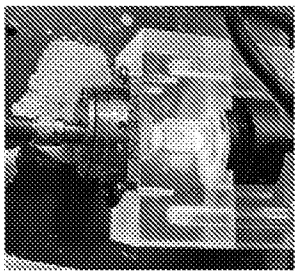

Power meter chamber

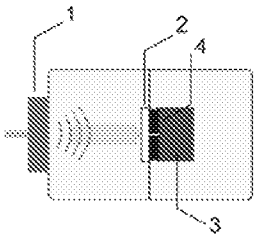

1. LED and Collimator
2. Optical window
3. LED powermeter
4. Ø 300 µm pin hole

e

Irradiance of LED on the planar lipid bilayer

Wavelength (nm)	Irradiance (mW/cm²)
365	36.2
405	75.5
455	126.2
530	30.3

Fig. 21

a

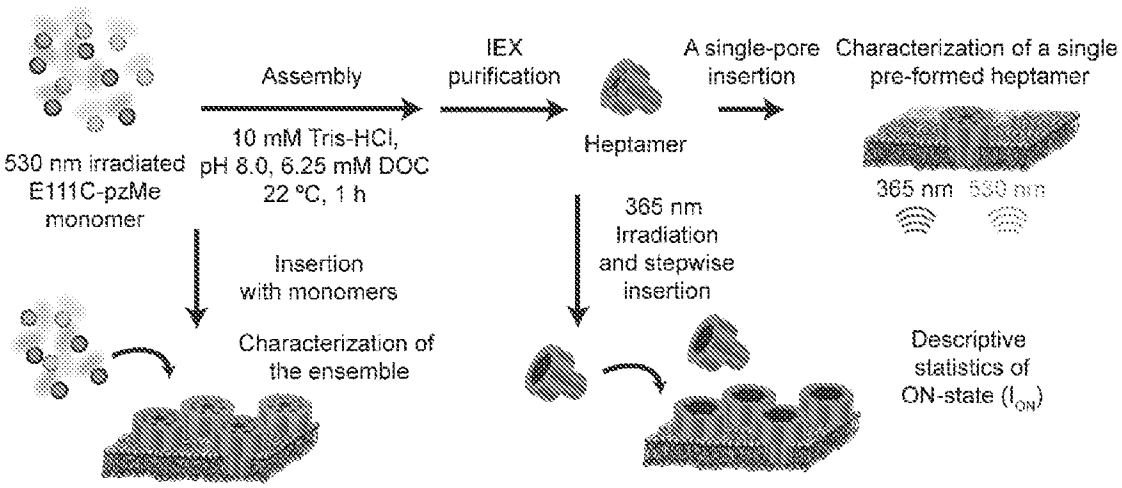
530 nm irradiated
E111C-pzMe
monomer
Assembly
10 mM Tris-HCl,
pH 8.0, 6.25 mM DOC
22 °C, 1 h
IEX
purification
Heptamer
A single-pore
insertion
Characterization of a single
pre-formed heptamer
365 nm
530 nm
Insertion
with monomers
Characterization of
the ensemble
365 nm
Irradiation
and stepwise
insertion
Descriptive
statistics of
ON-state (I_{ON})

b

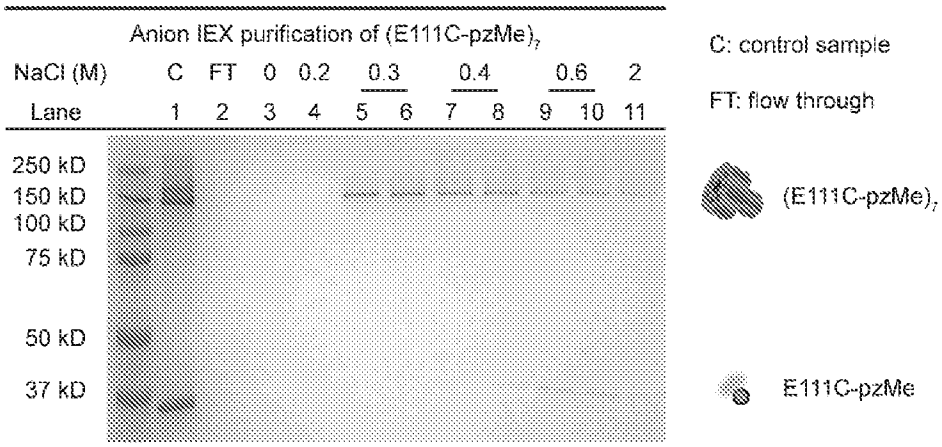
Anion IEX purification of (E111C-pzMe)7
NaCl (M) C FT 0 0.2 0.3 0.4 0.6 2
Lane 1 2 3 4 5 6 7 8 9 10 11
250 kD
150 kD
100 kD
75 kD
50 kD
37 kD
C: control sample
FT: flow through
(E111C-pzMe)7
E111C-pzMe

Fig. 22

a

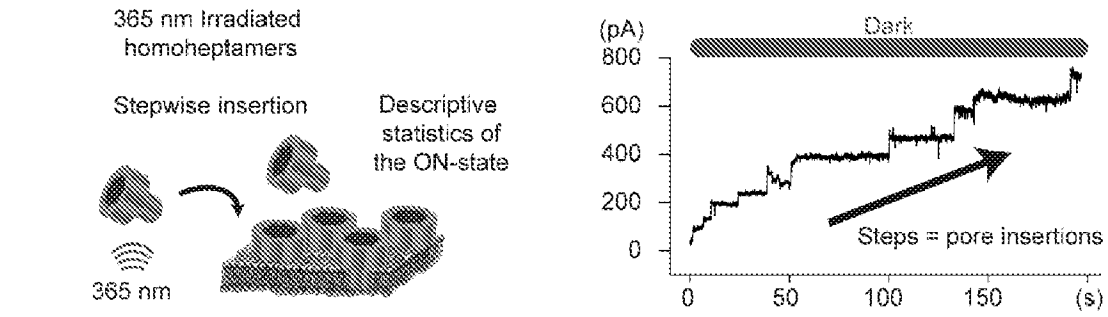

b

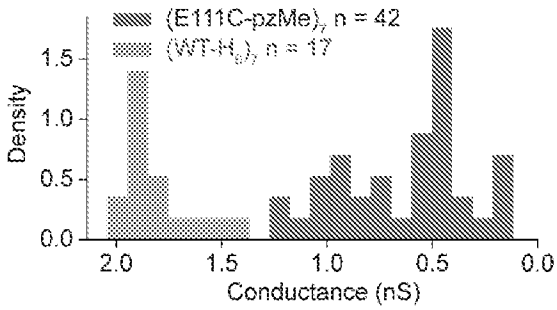

c

Conductance of ON-state by stepwise insertion

Species	g (nS)
$(E111C\text{-}pzMe)_7$	0.62 ± 0.30
$(E111C\text{-}pzMe)_7$ max	1.27
$(E111C\text{-}pzMe)_7$ min	0.12
$(WT\text{-}H_8)_7$	1.81 ± 0.17

Fig. 23

a

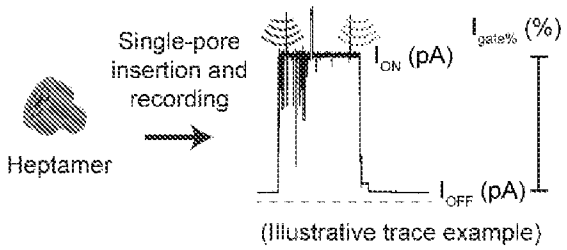

b

ON-OFF switching of $(E111C\text{-}pzMe)_7$
Single pre-heptamerised pore insertion

Repeat	I_{ON} (pA)	I_{OFF} (pA)	$I_{gate\%}$ (%)
1	98.7	1.5	98.5
2	98.5	4.1	95.8
3	95.6	8.7	90.9
4	93.4	2.5	97.4
5	92.8	3.4	96.3
6	85.7	2.7	96.8
7	64.0	1.7	97.4
8	55.5	1.3	97.7
9	50.1	4.3	91.4
10	49.7	3.2	93.6
11	49.3	3.9	92.1
12	48.8	5.1	89.5
13	40.8	3.0	92.5
14	26.0	0.9	96.4
15	24.5	1.4	94.3
16	21.9	0.5	97.7
17	20.6	1.6	92.3
18	15.9	0.5	96.9
19	14.0	0.6	95.7
20	13.3	0.5	96.2
21	9.9	0.4	96.0

$I_{gate\%}$ (%) = 95.0 ± 2.5

c

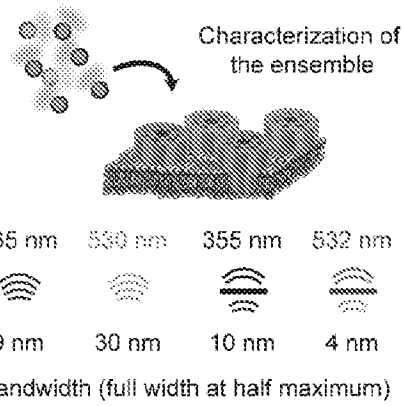

d

ON-OFF switching of
$(E111C\text{-}pzMe)_7$ ensemble

Number of pores	I_{ON} (pA)	I_{OFF} (pA)	$I_{gate\%}$ (%)
120	7692	1167	84.8
106	6808	961	85.9
113	7256	892	87.8
46	2977	550	81.5
161	10297	1649	84.0

$I_{gate\%}$ (%) = 84.8 ± 2.1

e

ON-OFF switching of
$(E111C\text{-}pzMe)_7$ ensemble with in-line filter

Number of pores	I_{ON} (pA)	I_{OFF} (pA)	$I_{gate\%}$ (%)
535	34259	5421	84.2
337	21585	3639	83.1
706	45225	6986	84.6
173	11057	2178	80.3

$I_{gate\%}$ (%) = 83.0 ± 1.7

Fig. 24

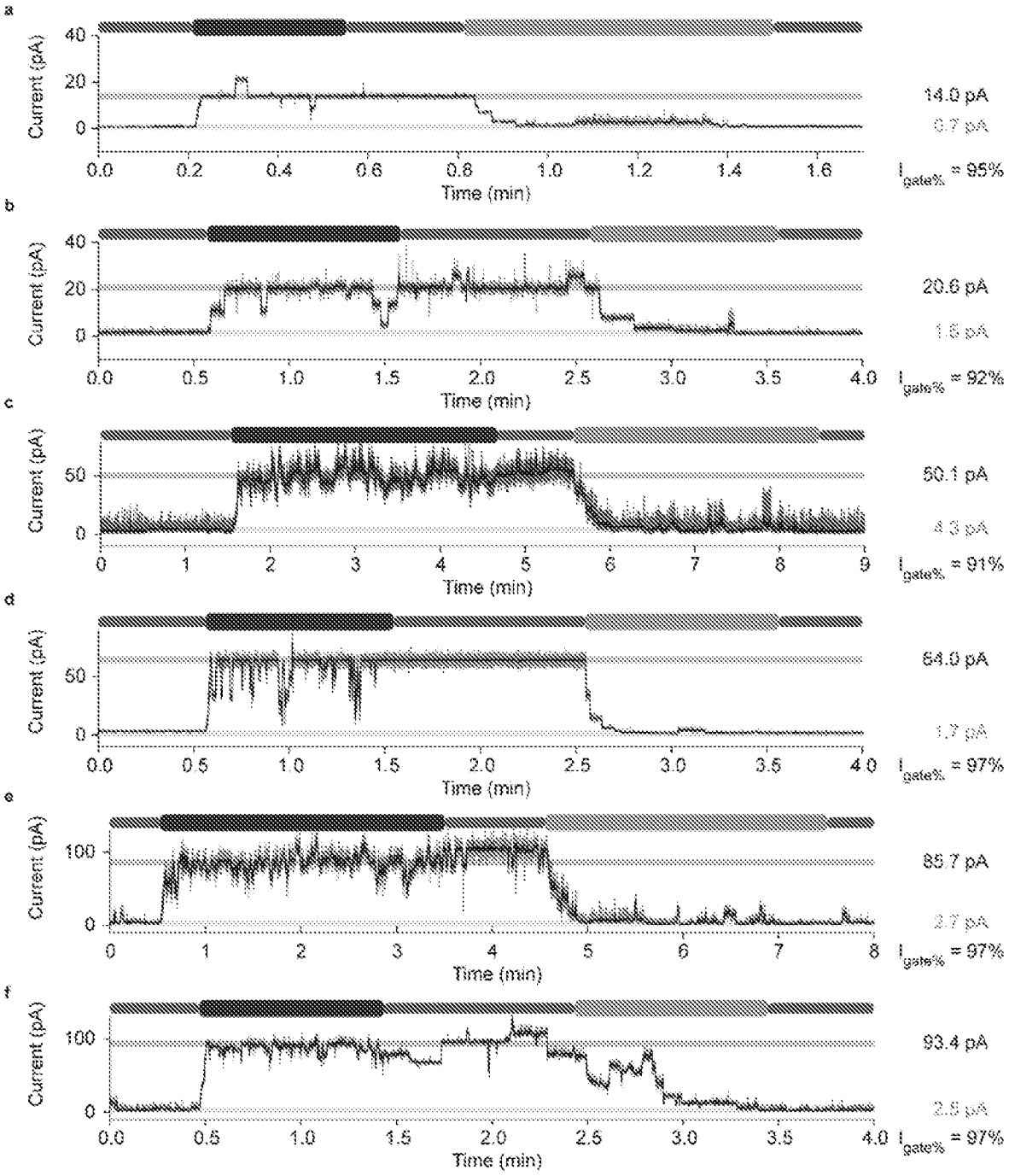
a
Current (pA)
40
20
0
0.0
0.2
0.4
0.6
0.8
1.0
1.2
1.4
1.6
Time (min)
14.0 pA
6.7 pA
$I_{gate\%}$ = 95%
b
Current (pA)
40
20
0
0.0
0.5
1.0
1.5
2.0
2.5
3.0
3.5
4.0
Time (min)
20.6 pA
1.6 pA
$I_{gate\%}$ = 92%
c
Current (pA)
50
0
0
1
2
3
4
5
6
7
8
9
Time (min)
50.1 pA
4.3 pA
$I_{gate\%}$ = 91%
d
Current (pA)
50
0
0.0
0.5
1.0
1.5
2.0
2.5
3.0
3.5
4.0
Time (min)
64.0 pA
1.7 pA
$I_{gate\%}$ = 97%
e
Current (pA)
100
0
0
1
2
3
4
5
6
7
8
Time (min)
85.7 pA
2.7 pA
$I_{gate\%}$ = 97%
f
Current (pA)
100
0
0.0
0.5
1.0
1.5
2.0
2.5
3.0
3.5
4.0
Time (min)
93.4 pA
2.5 pA
$I_{gate\%}$ = 97%

Fig. 25

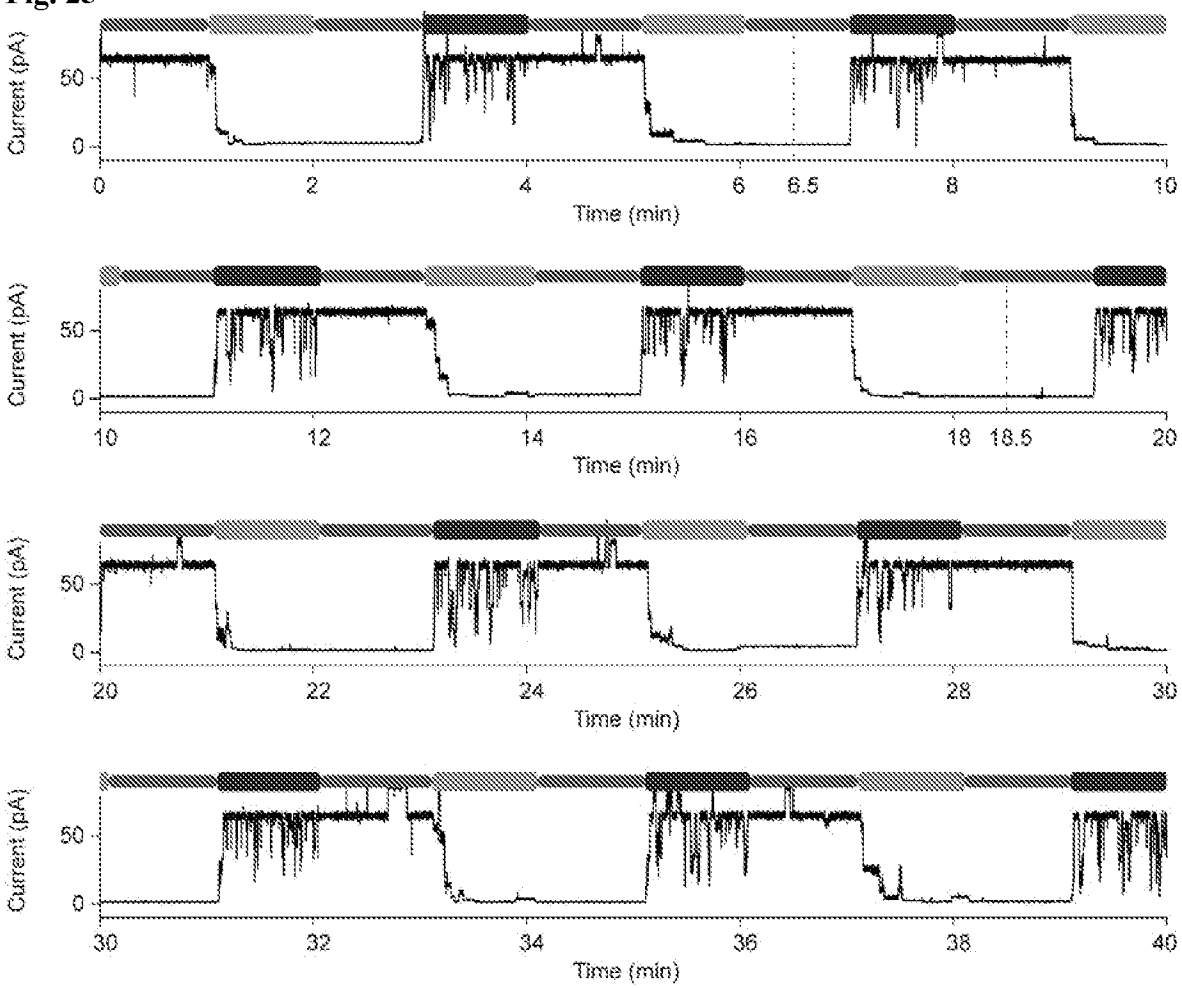
Current (pA)
50
0
0
2
4
6
6.5
8
10
Time (min)
Current (pA)
50
0
10
12
14
16
18
18.5
20
Time (min)
Current (pA)
50
0
20
22
24
26
28
30
Time (min)
Current (pA)
50
0
30
32
34
36
38
40
Time (min)

Fig. 26

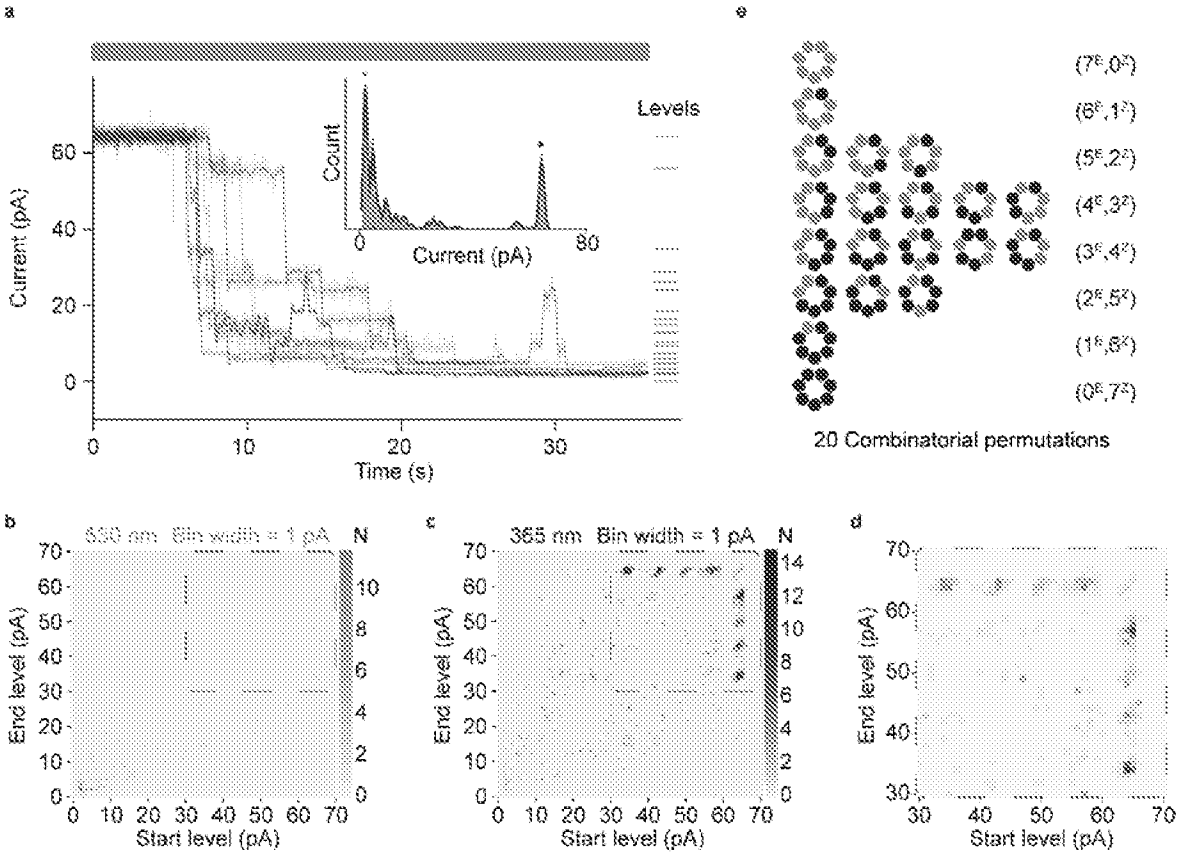
a
Current (pA)
Time (s)
Levels
Count
Current (pA)
e
20 Combinatorial permutations
b
630 nm Bin width = 1 pA
End level (pA)
Start level (pA)
N
c
365 nm Bin width = 1 pA
End level (pA)
Start level (pA)
N
d
End level (pA)
Start level (pA)

Fig. 27

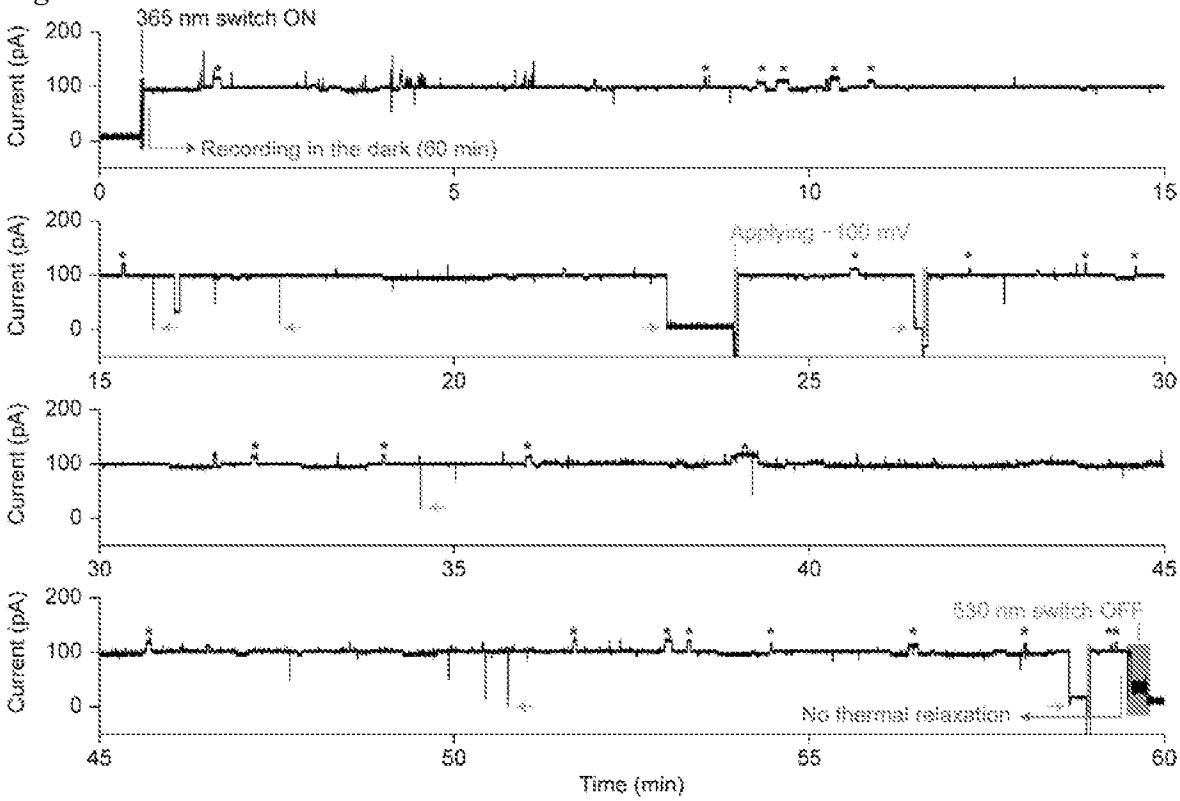
365 nm switch ON
Recording in the dark (60 min)
Applying −100 mV
530 nm switch OFF
No thermal relaxation
Current (pA)
200
100
0
0
5
10
15
20
25
30
35
40
45
50
55
60
Time (min)

Fig. 28

a

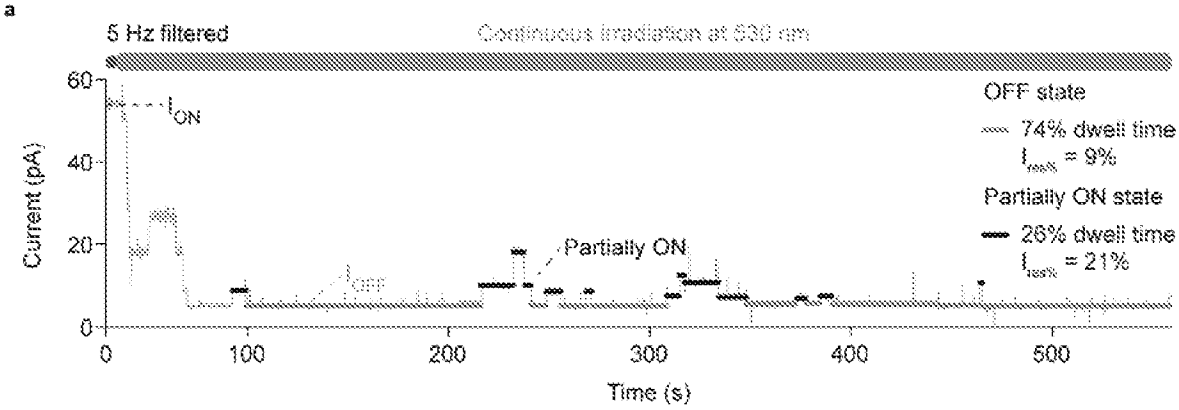

b

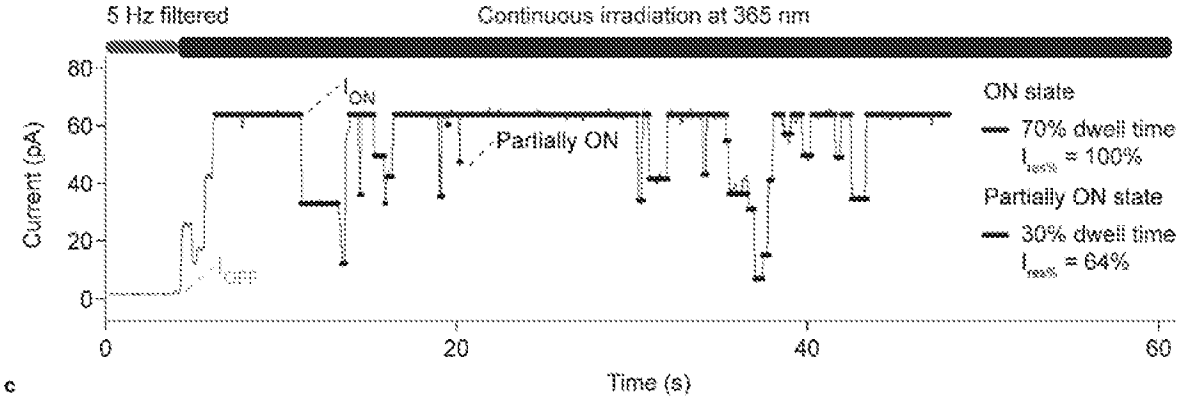

c

Wavelength	Fractional time in complete OFF state ($I_{res\%}$ = 9%)	Fractional time in partially ON state ($I_{res\%}$ = 21%)	Macroscopic OFF-state current
530 nm	74%	26%	74% × 9% + 26% × 21% = 12%

Wavelength	Fractional time in complete ON state ($I_{res\%}$ = 100%)	Fractional time in partially ON state ($I_{res\%}$ = 64%)	Macroscopic ON-state current
365 nm	70%	30%	70% × 100% + 30% × 64% = 89%

Fig. 29

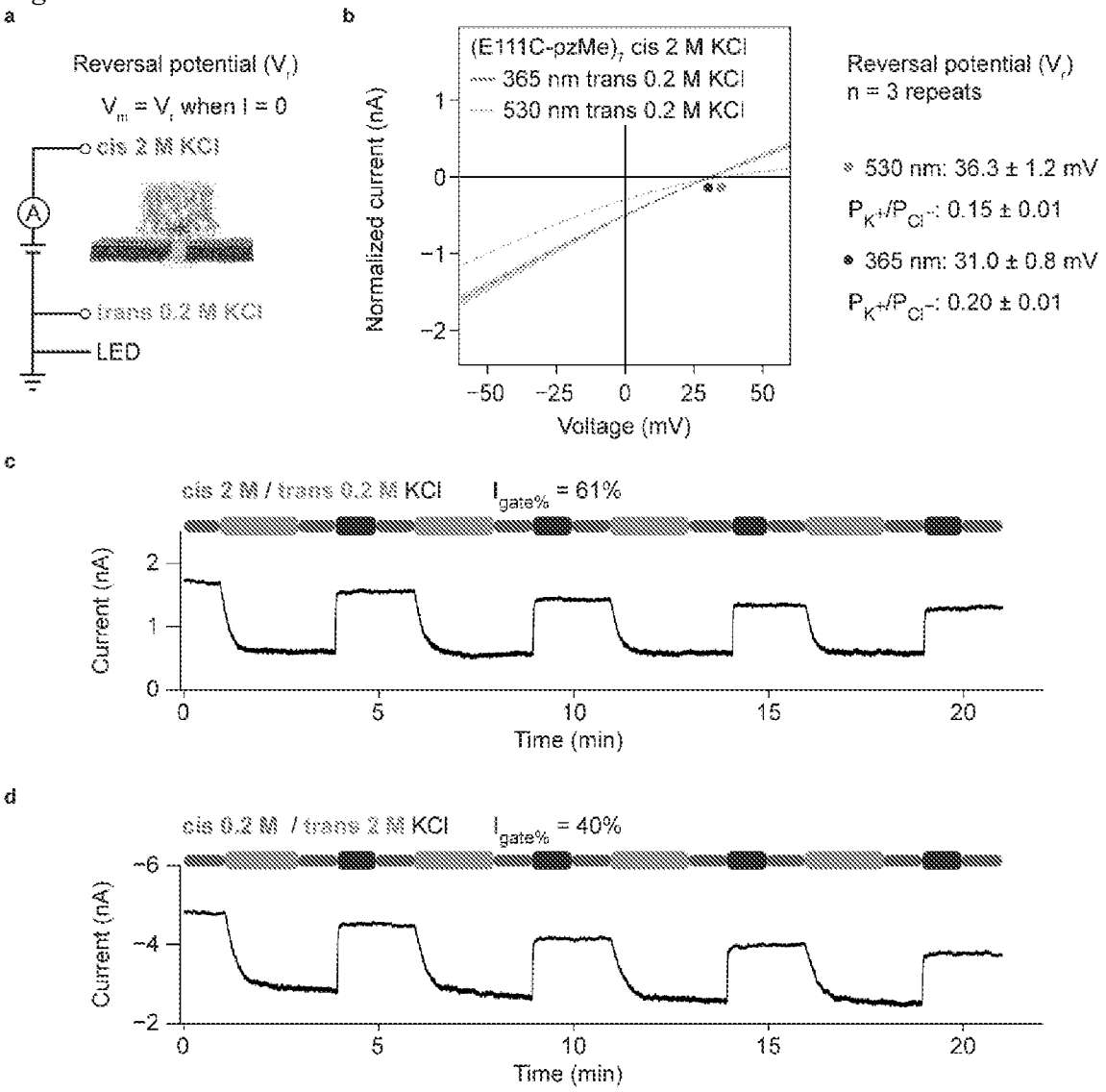
a
Reversal potential (V_r)
$V_m = V_r$ when I = 0
cis 2 M KCl
trans 0.2 M KCl
LED
b
(E111C-pzMe)$_7$ cis 2 M KCl
365 nm trans 0.2 M KCl
530 nm trans 0.2 M KCl
Normalized current (nA)
Voltage (mV)
Reversal potential (V_r)
n = 3 repeats
530 nm: 36.3 ± 1.2 mV
P_{K^+}/P_{Cl^-}: 0.15 ± 0.01
365 nm: 31.0 ± 0.8 mV
P_{K^+}/P_{Cl^-}: 0.20 ± 0.01
c
cis 2 M / trans 0.2 M KCl
$I_{gate\%}$ = 61%
Current (nA)
Time (min)
d
cis 0.2 M / trans 2 M KCl
$I_{gate\%}$ = 40%
Current (nA)
Time (min)

Fig. 30

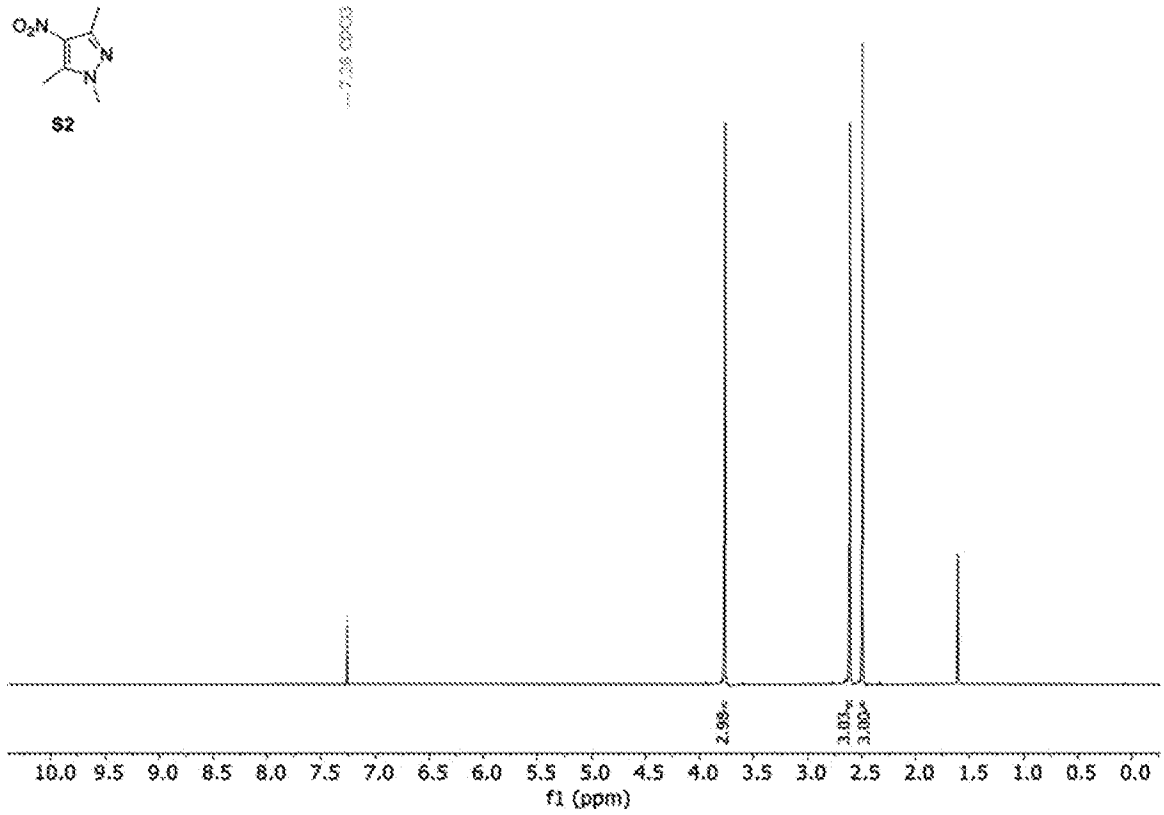
S2
10.0 9.5 9.0 8.5 8.0 7.5 7.0 6.5 6.0 5.5 5.0 4.5 4.0 3.5 3.0 2.5 2.0 1.5 1.0 0.5 0.0
f1 (ppm)

Fig. 31

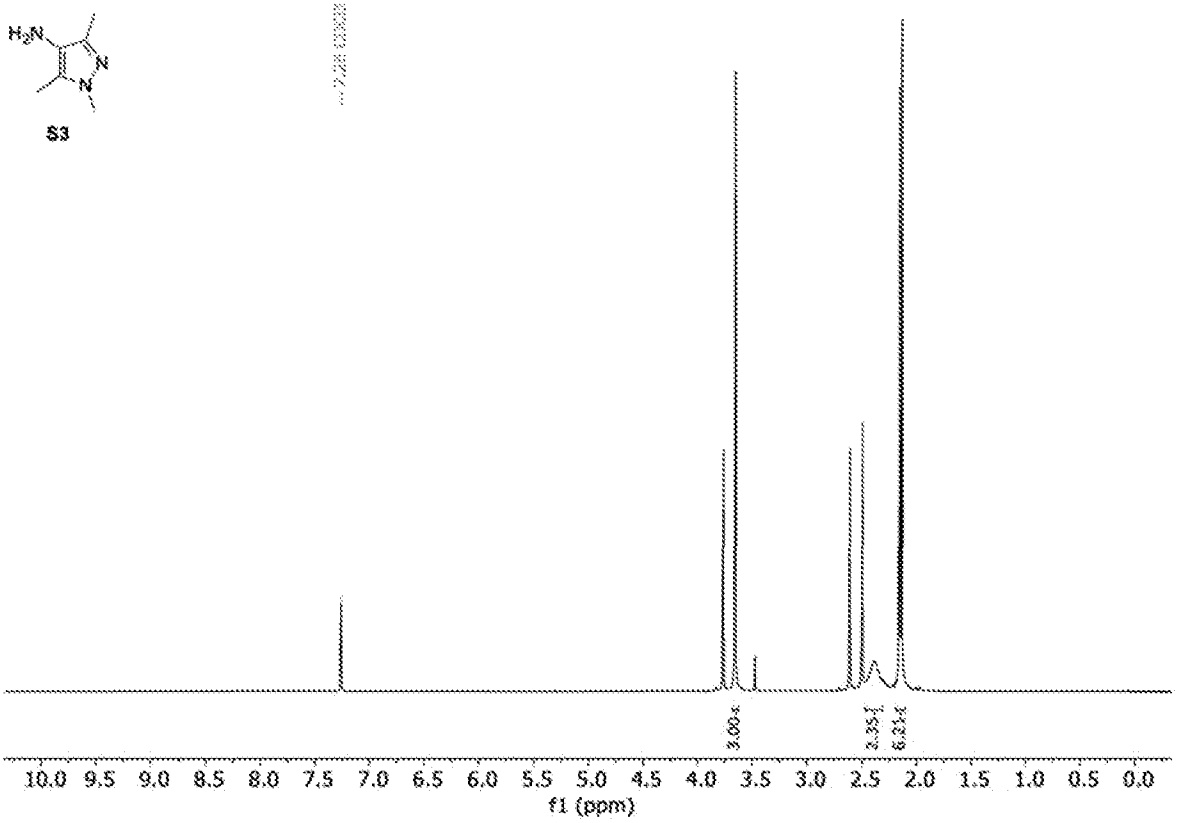
S3
10.0 9.5 9.0 8.5 8.0 7.5 7.0 6.5 6.0 5.5 5.0 4.5 4.0 3.5 3.0 2.5 2.0 1.5 1.0 0.5 0.0
f1 (ppm)

Fig. 32

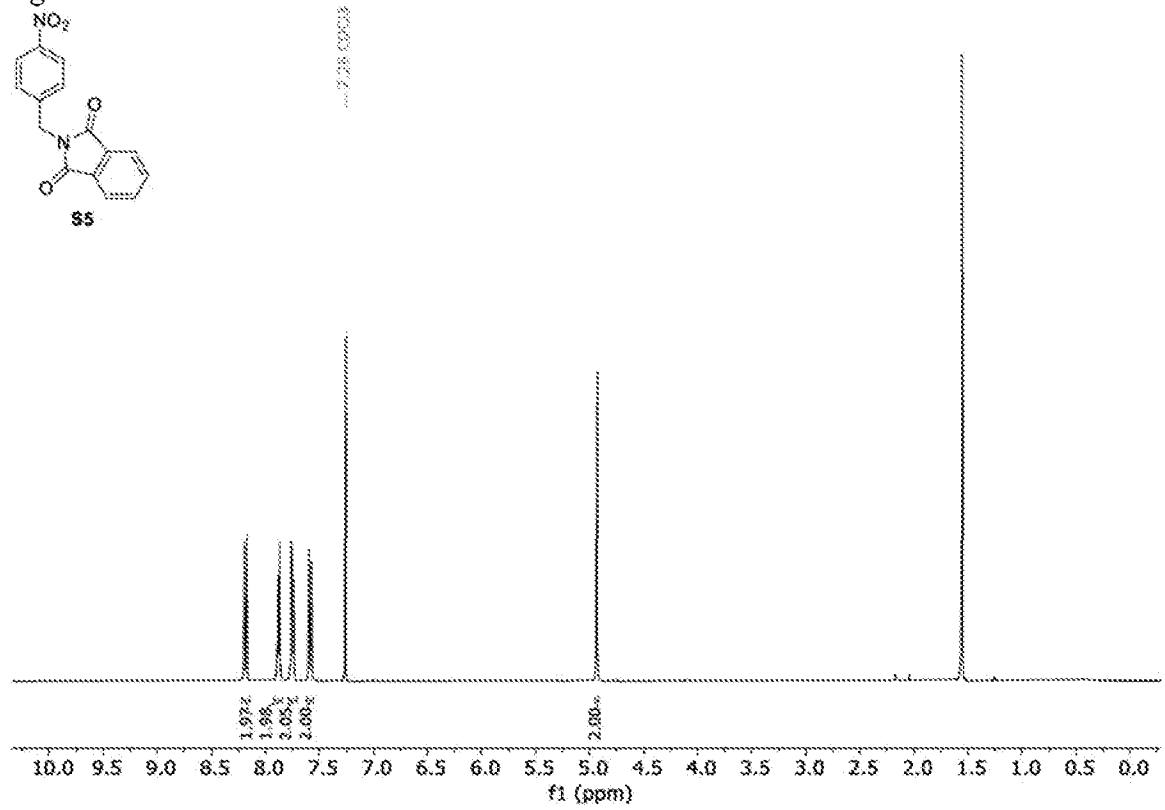
NO2
O
N
O
S5
1.97
1.98
2.05
2.08
2.00
10.0 9.5 9.0 8.5 8.0 7.5 7.0 6.5 6.0 5.5 5.0 4.5 4.0 3.5 3.0 2.5 2.0 1.5 1.0 0.5 0.0
f1 (ppm)

Fig. 33

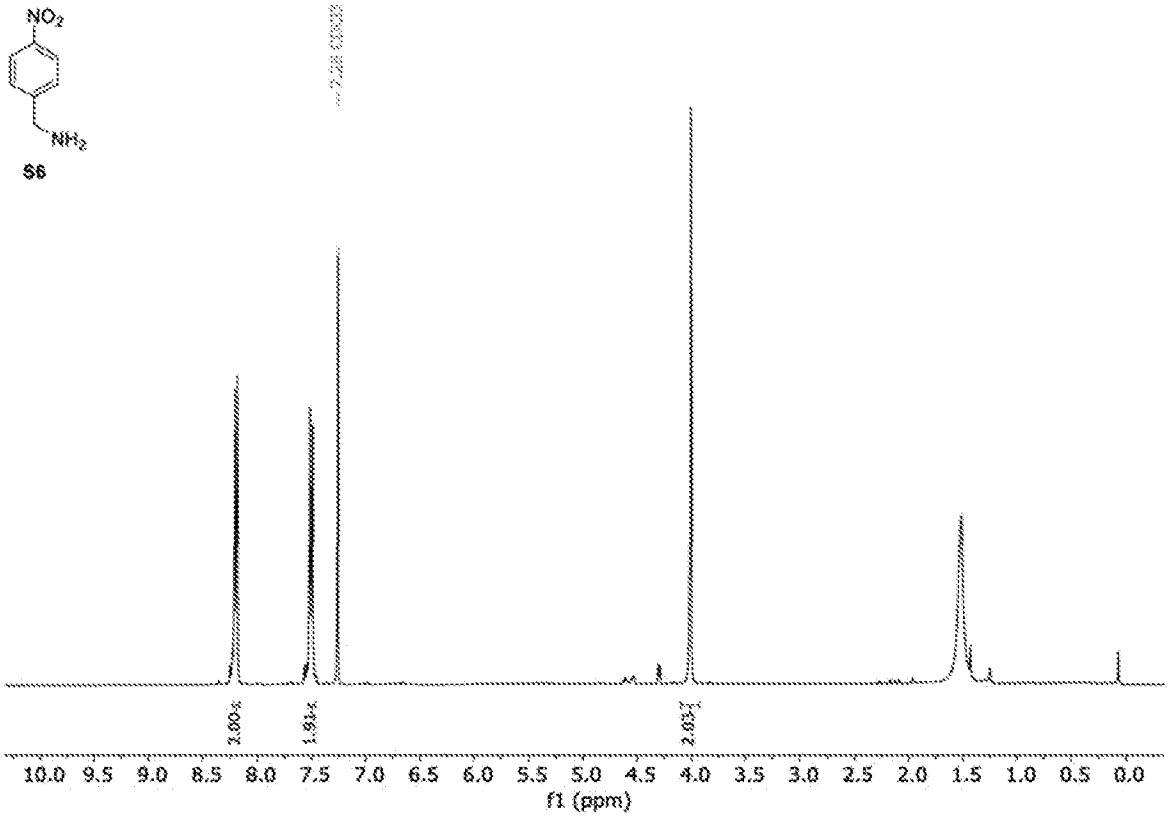
NO2
NH2
S6
1.00
1.91
2.03
10.0 9.5 9.0 8.5 8.0 7.5 7.0 6.5 6.0 5.5 5.0 4.5 4.0 3.5 3.0 2.5 2.0 1.5 1.0 0.5 0.0
f1 (ppm)

Fig. 34

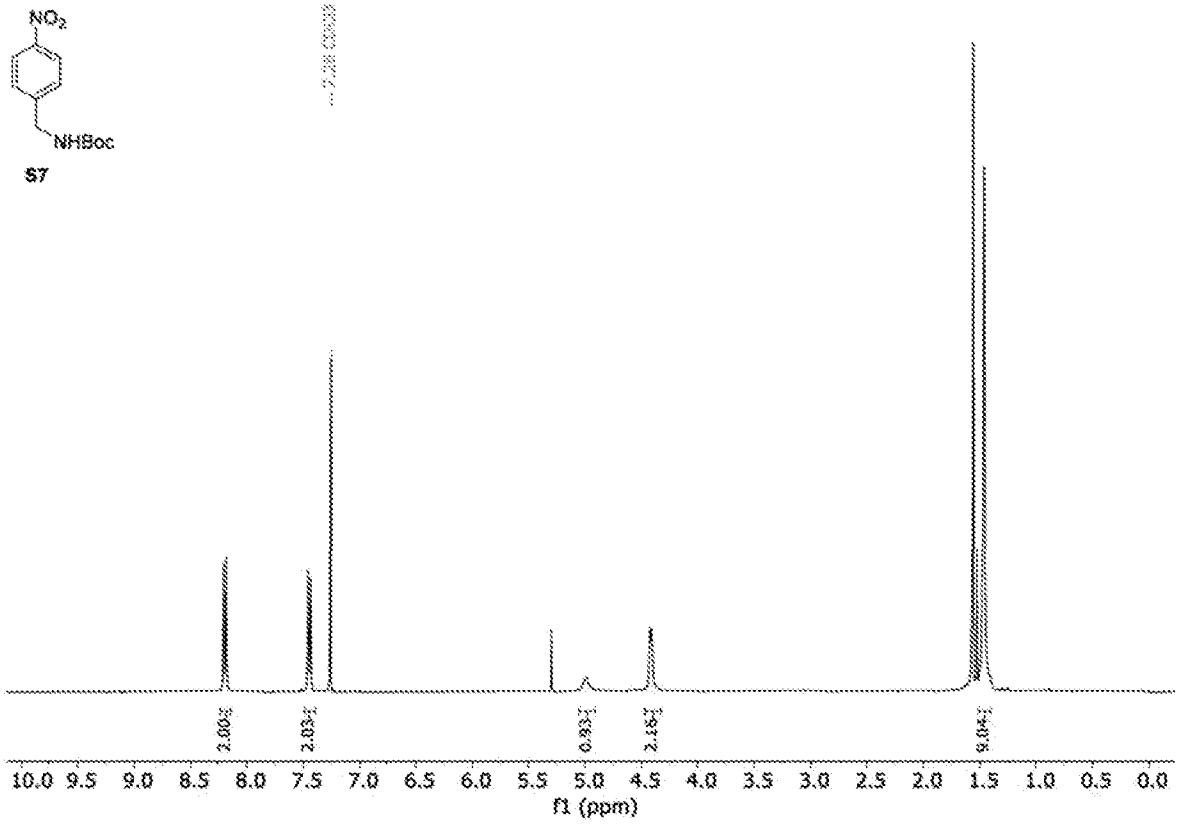
NO2
NHBoc
S7
2.005
2.031
0.933
2.167
9.094
10.0 9.5 9.0 8.5 8.0 7.5 7.0 6.5 6.0 5.5 5.0 4.5 4.0 3.5 3.0 2.5 2.0 1.5 1.0 0.5 0.0
f1 (ppm)

Fig. 35

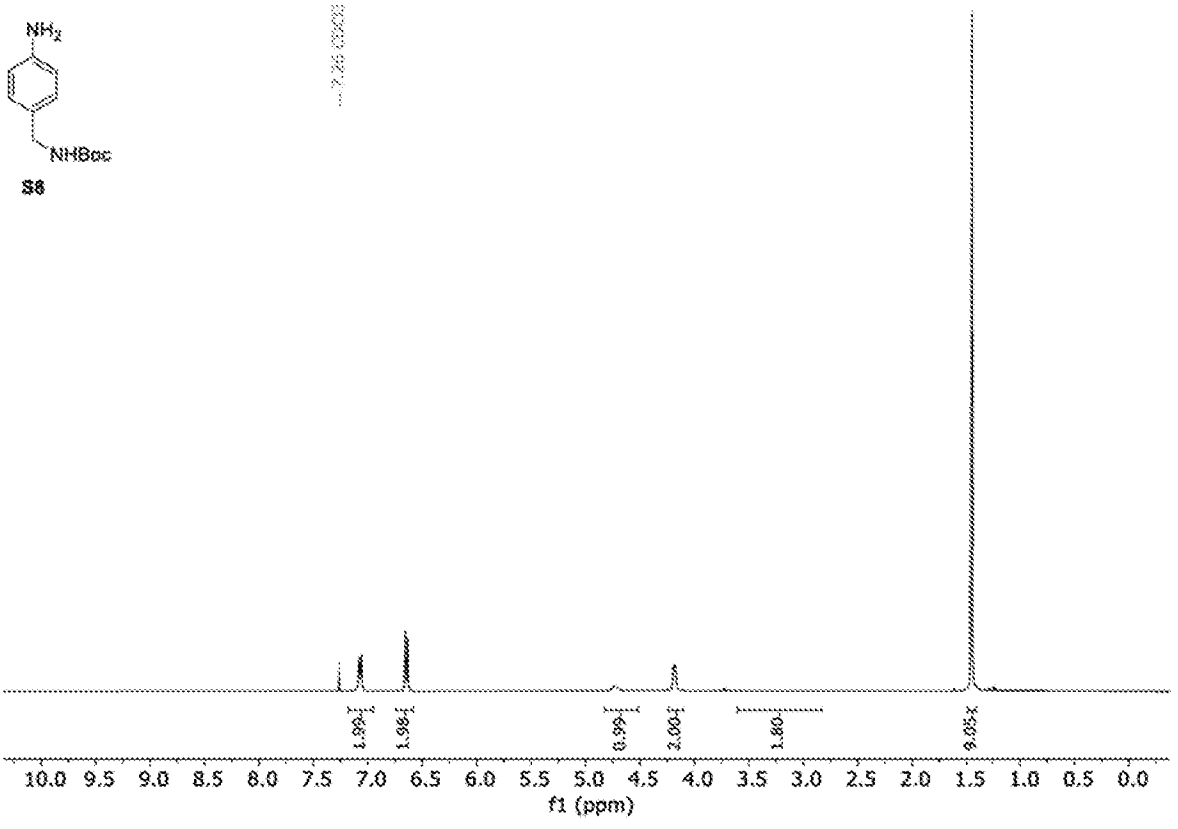
NH2
NHBoc
S8
1.067
1.964
0.990
2.000
1.860
9.035
10.0 9.5 9.0 8.5 8.0 7.5 7.0 6.5 6.0 5.5 5.0 4.5 4.0 3.5 3.0 2.5 2.0 1.5 1.0 0.5 0.0
f1 (ppm)

Fig. 36

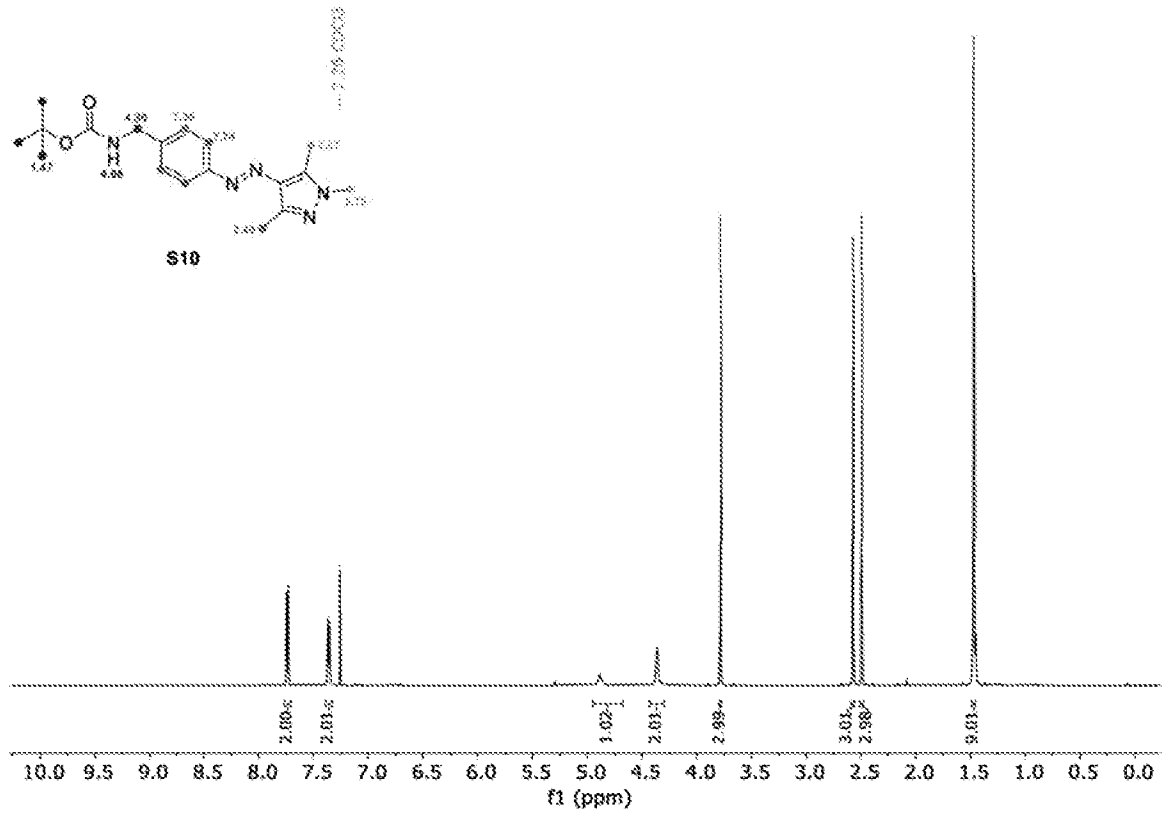
S10
2.00
2.03
1.02
2.01
2.98
3.01
2.98
9.03
10.0 9.5 9.0 8.5 8.0 7.5 7.0 6.5 6.0 5.5 5.0 4.5 4.0 3.5 3.0 2.5 2.0 1.5 1.0 0.5 0.0
f1 (ppm)

Fig. 37

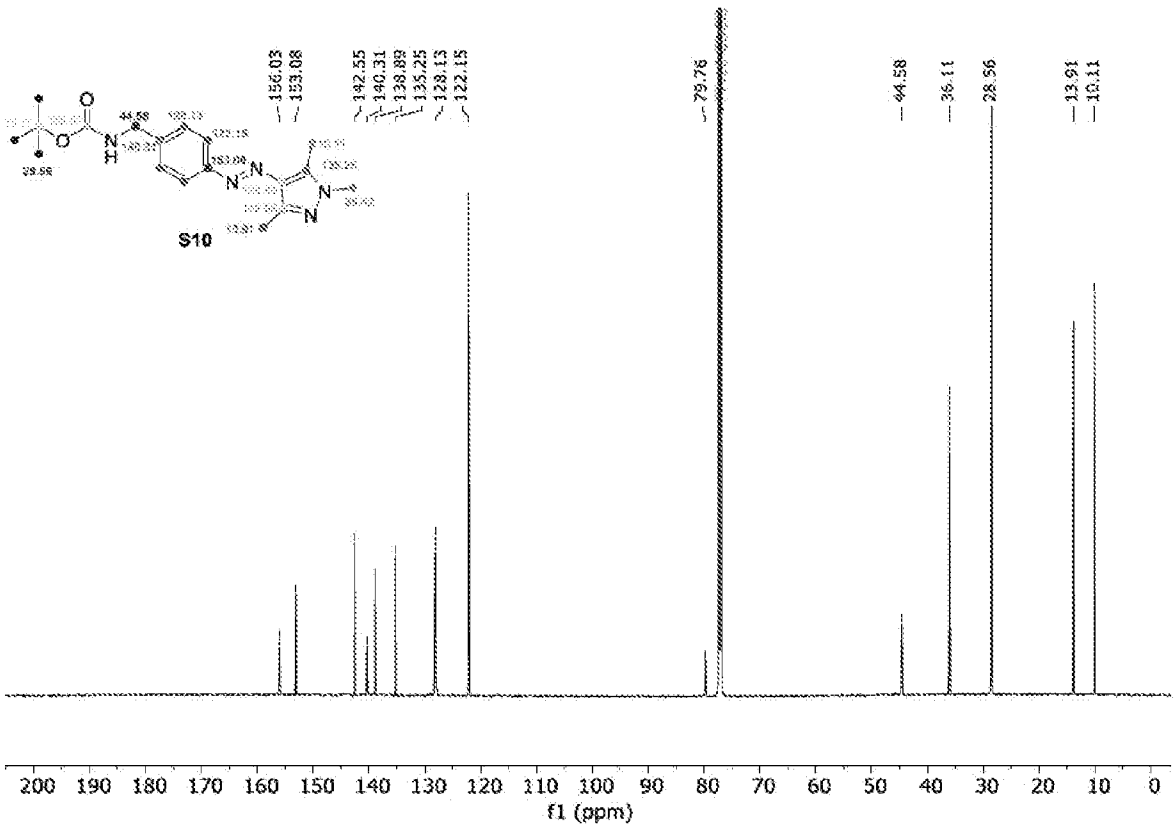
S10
156.03
153.08
142.55
140.31
138.89
135.25
128.13
122.15
79.76
44.58
36.11
28.56
13.91
10.11
200 190 180 170 160 150 140 130 120 110 100 90 80 70 60 50 40 30 20 10 0
f1 (ppm)

Fig. 38

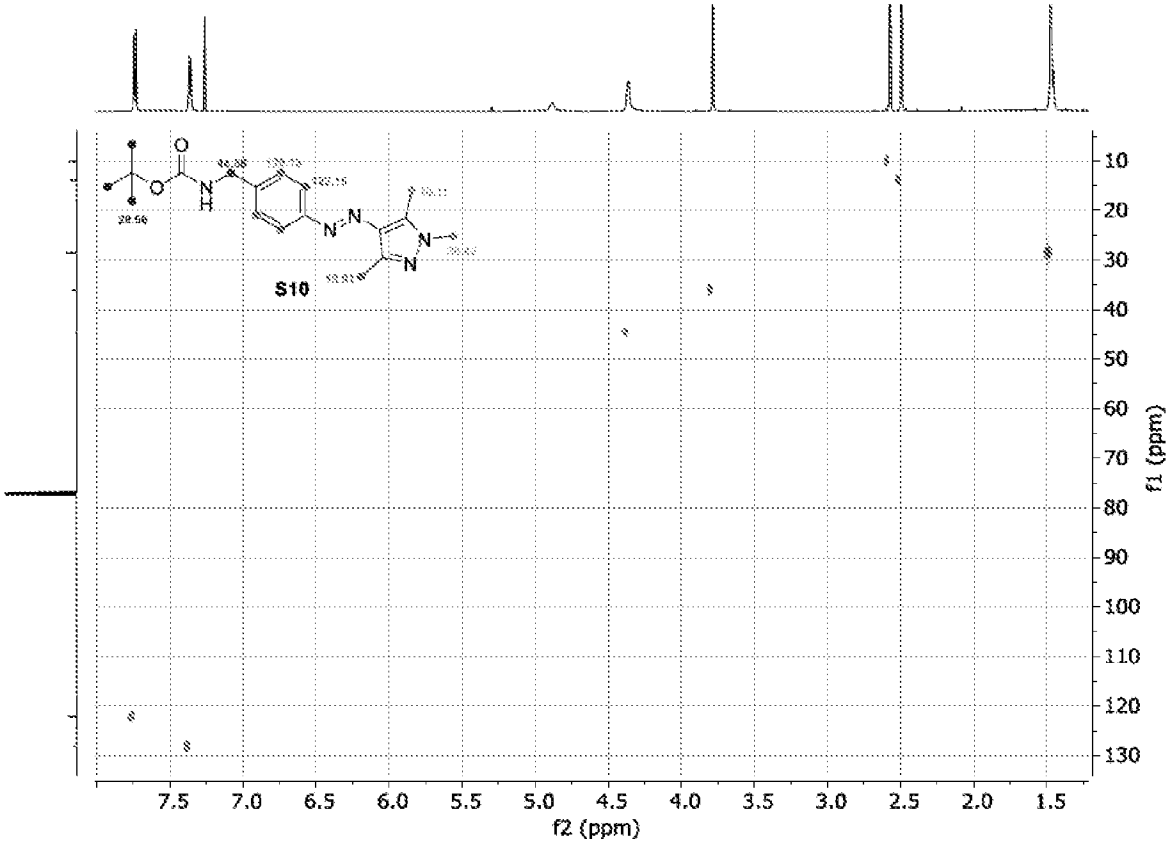

Fig. 39

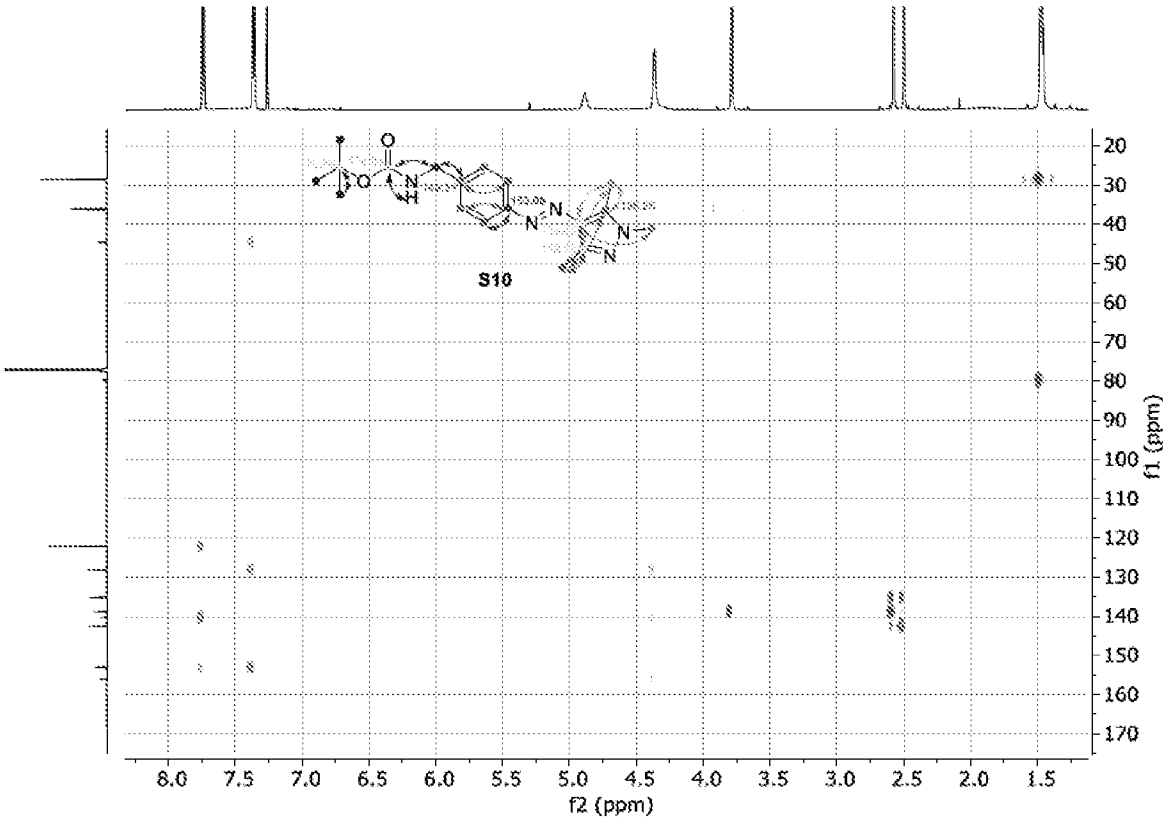

Fig. 40

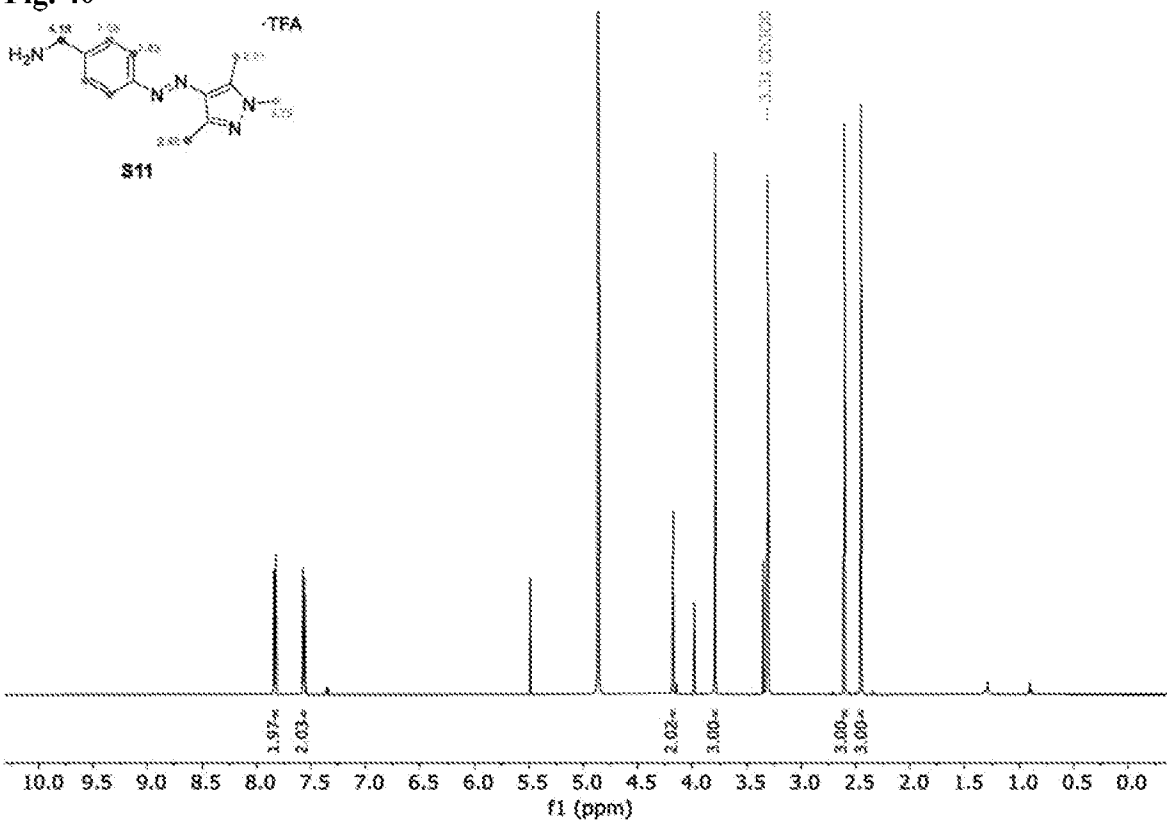
TFA
S11
1.97
2.03
2.02
3.00
3.00
3.00
10.0 9.5 9.0 8.5 8.0 7.5 7.0 6.5 6.0 5.5 5.0 4.5 4.0 3.5 3.0 2.5 2.0 1.5 1.0 0.5 0.0
f1 (ppm)

Fig. 41

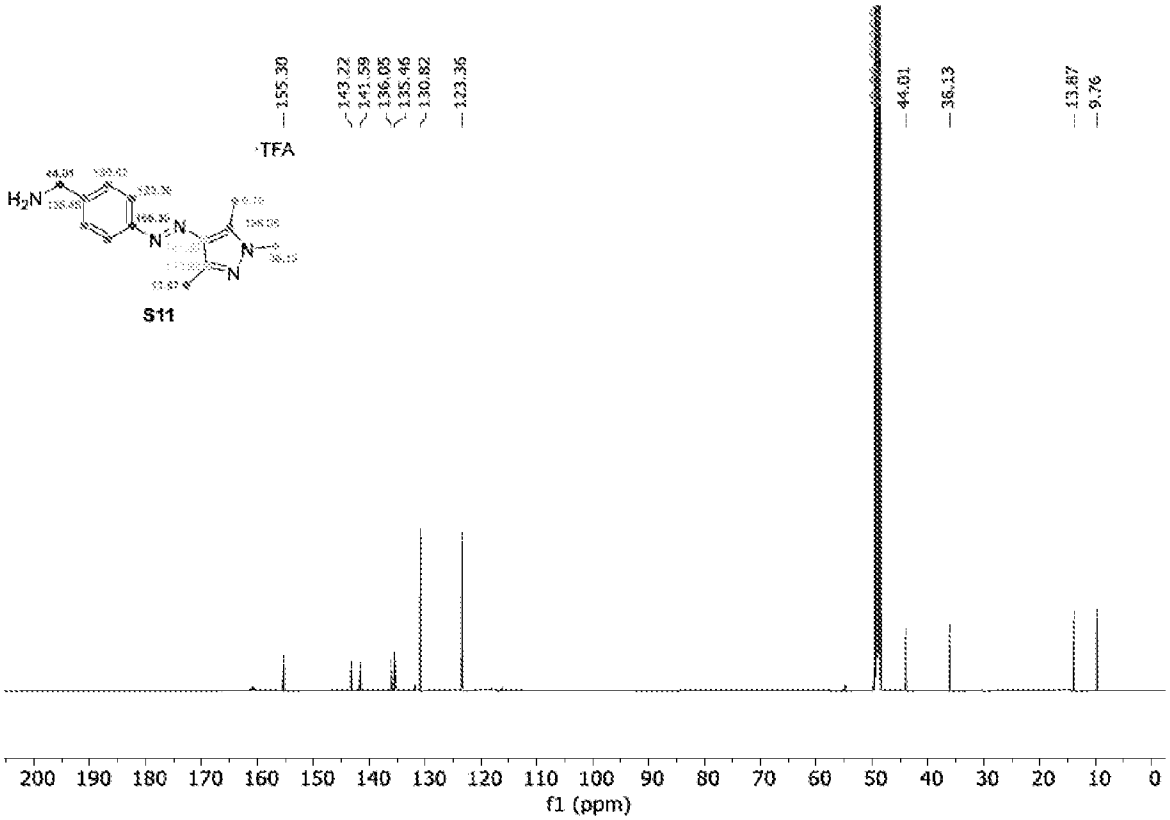
155.30
143.22
141.59
136.05
135.46
130.82
123.36
44.01
36.13
13.87
9.76
TFA
S11
200 190 180 170 160 150 140 130 120 110 100 90 80 70 60 50 40 30 20 10 0
f1 (ppm)

Fig. 42

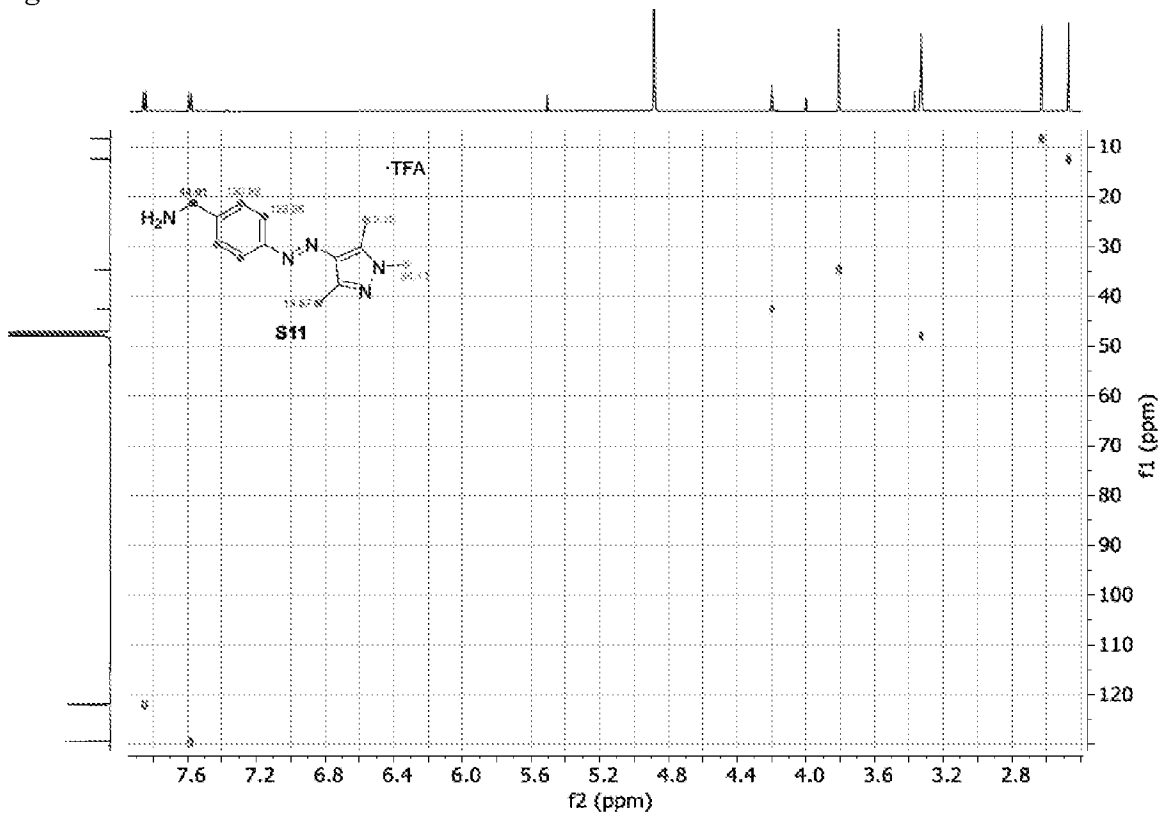

Fig. 43

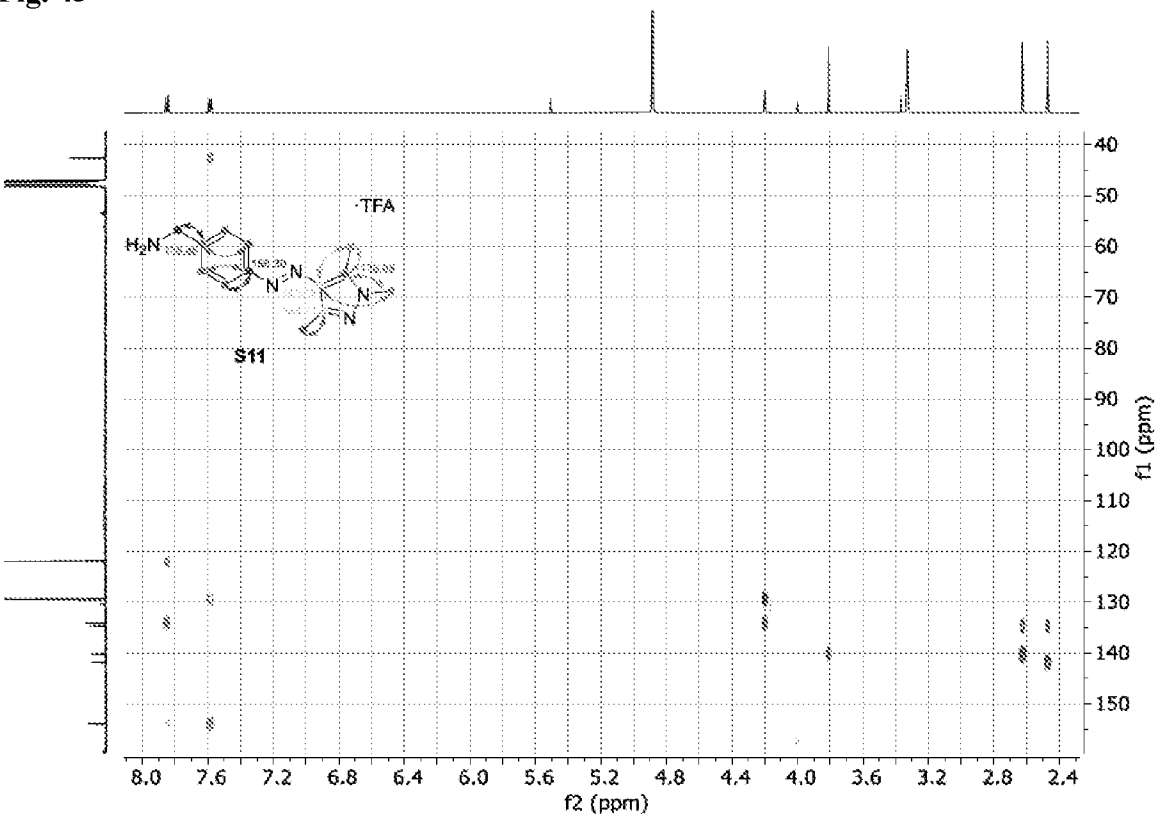

Fig. 44

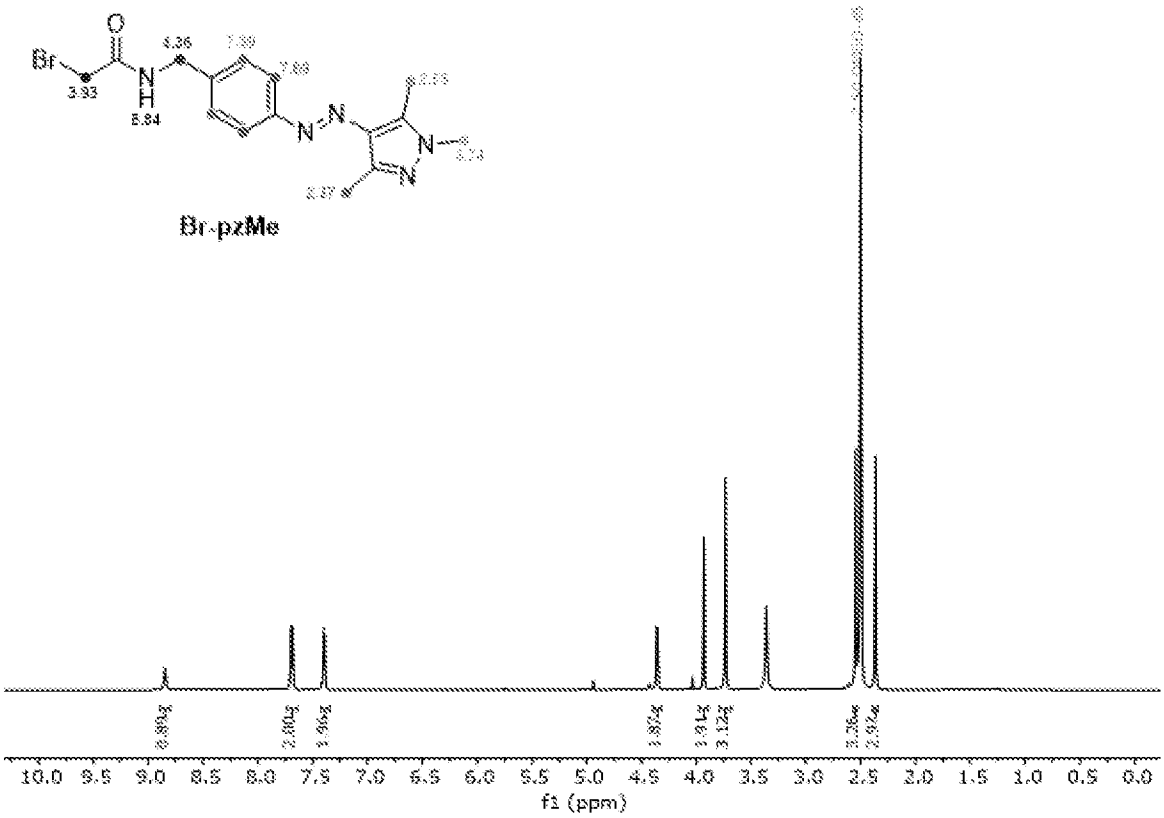

Fig. 45

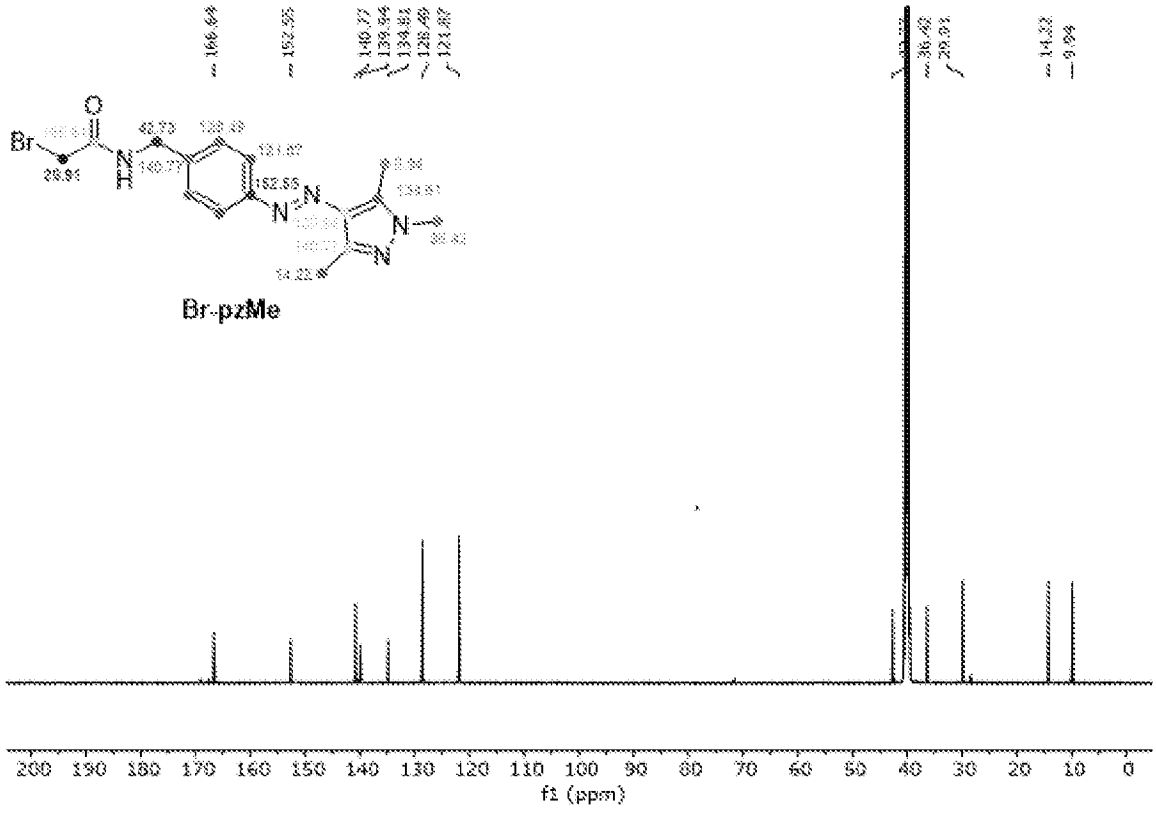

Fig. 46

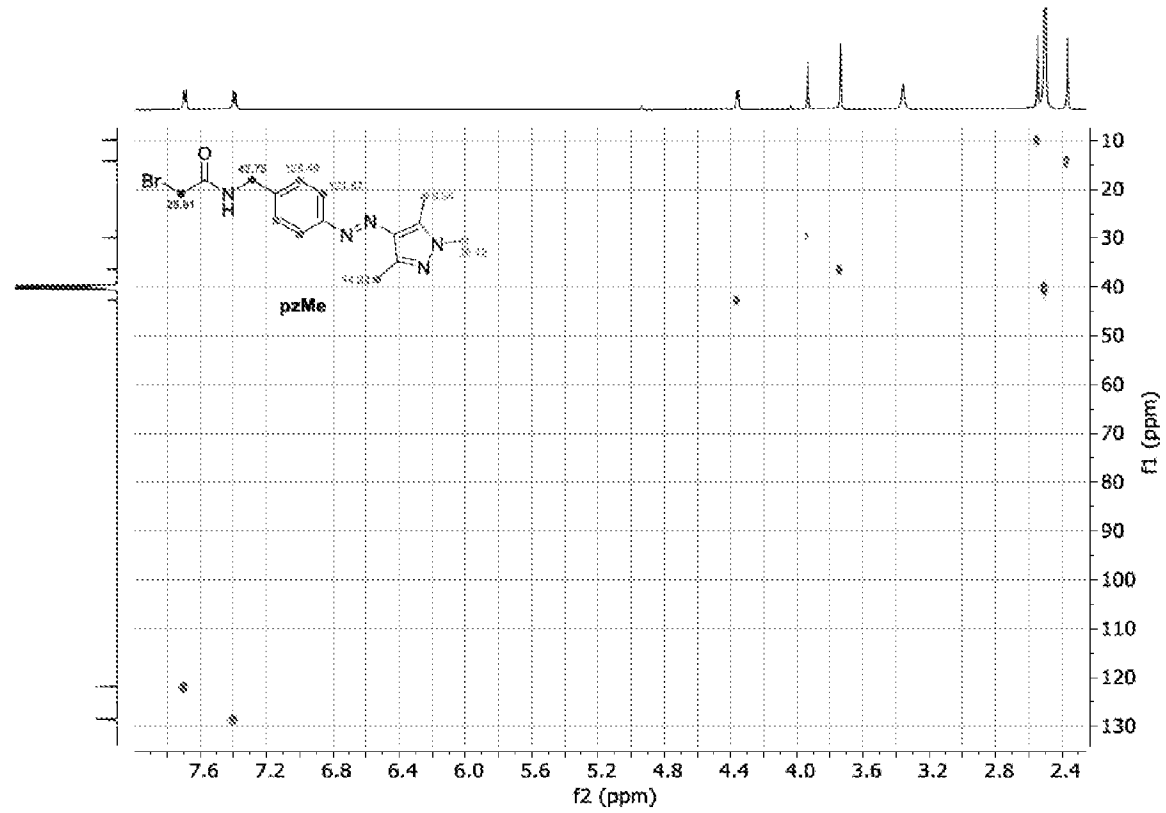

Fig. 47

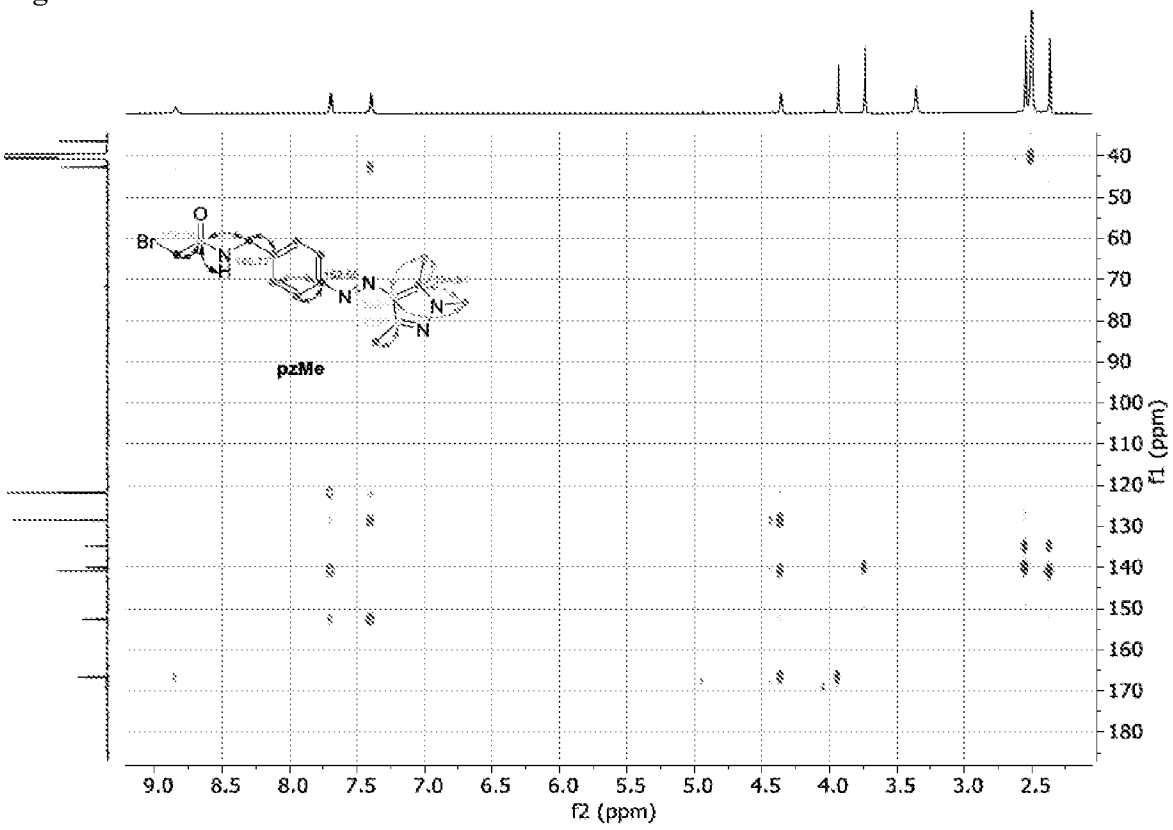

Fig. 48

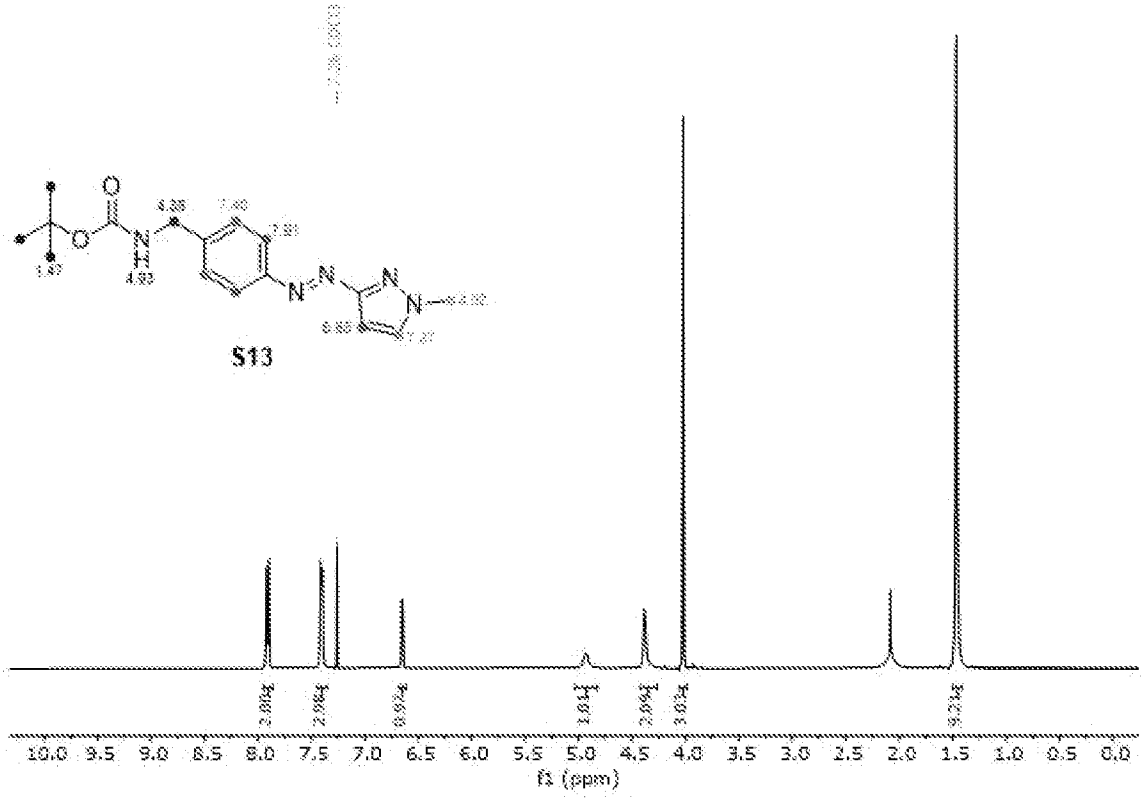
S13
10.0 9.5 9.0 8.5 8.0 7.5 7.0 6.5 6.0 5.5 5.0 4.5 4.0 3.5 3.0 2.5 2.0 1.5 1.0 0.5 0.0
f1 (ppm)

Fig. 49

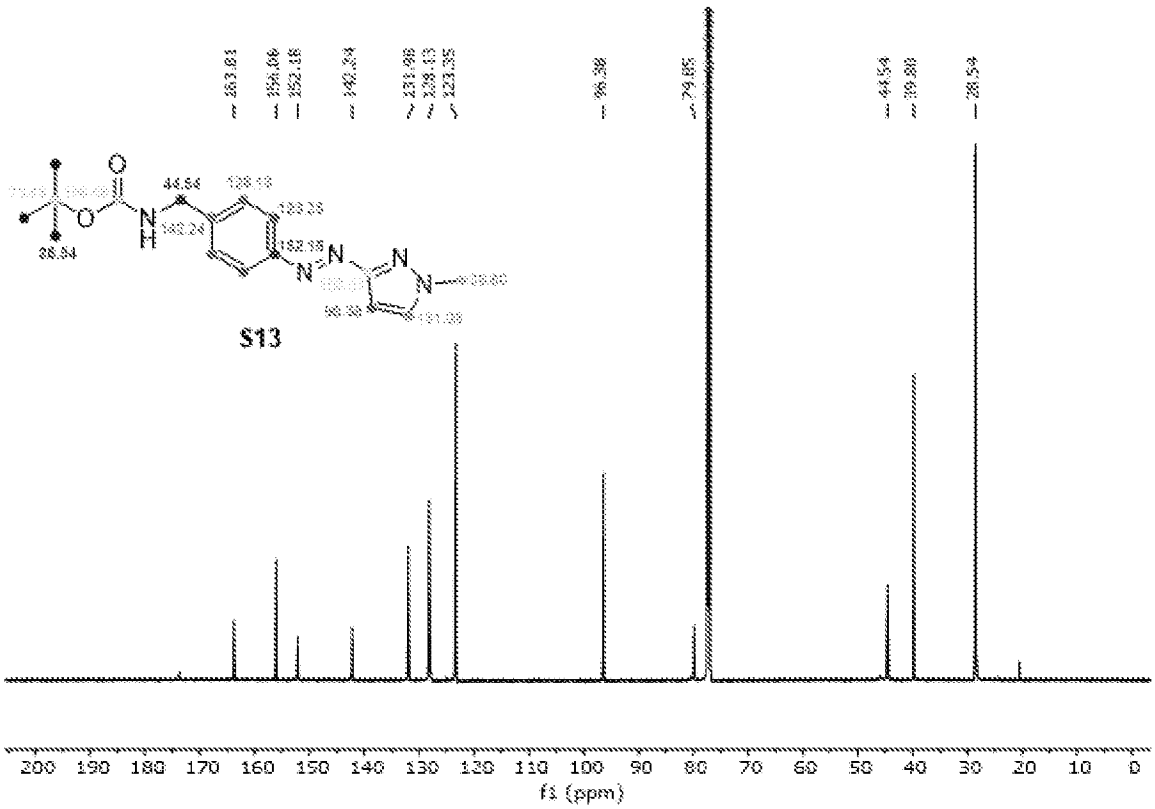
S13
200 190 180 170 160 150 140 130 120 110 100 90 80 70 60 50 40 30 20 10 0
f1 (ppm)

Fig. 50

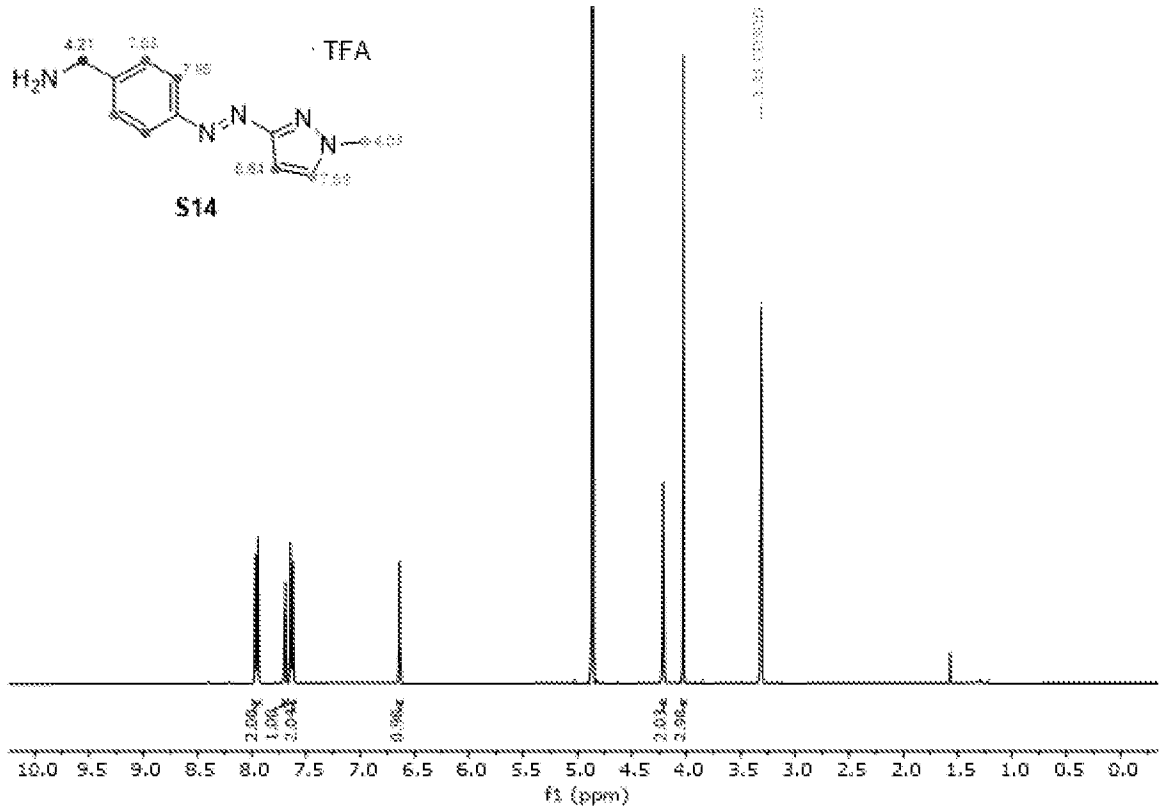

Fig. 51

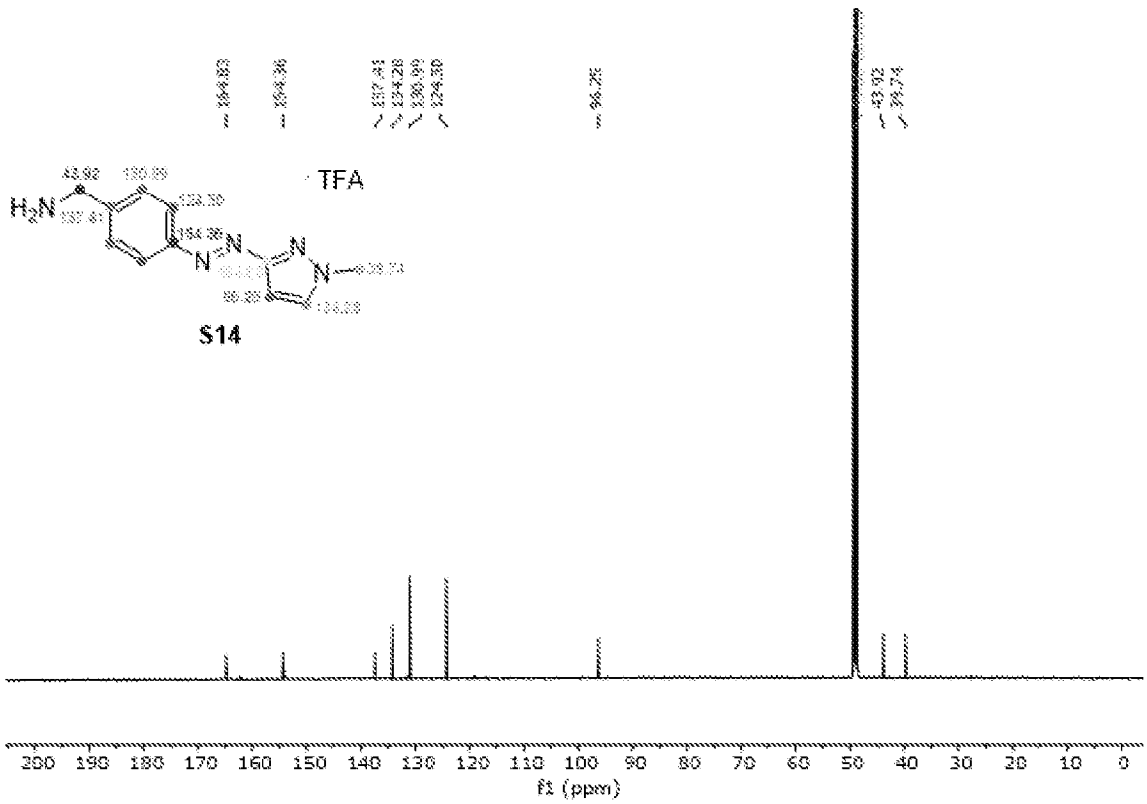

Fig. 52

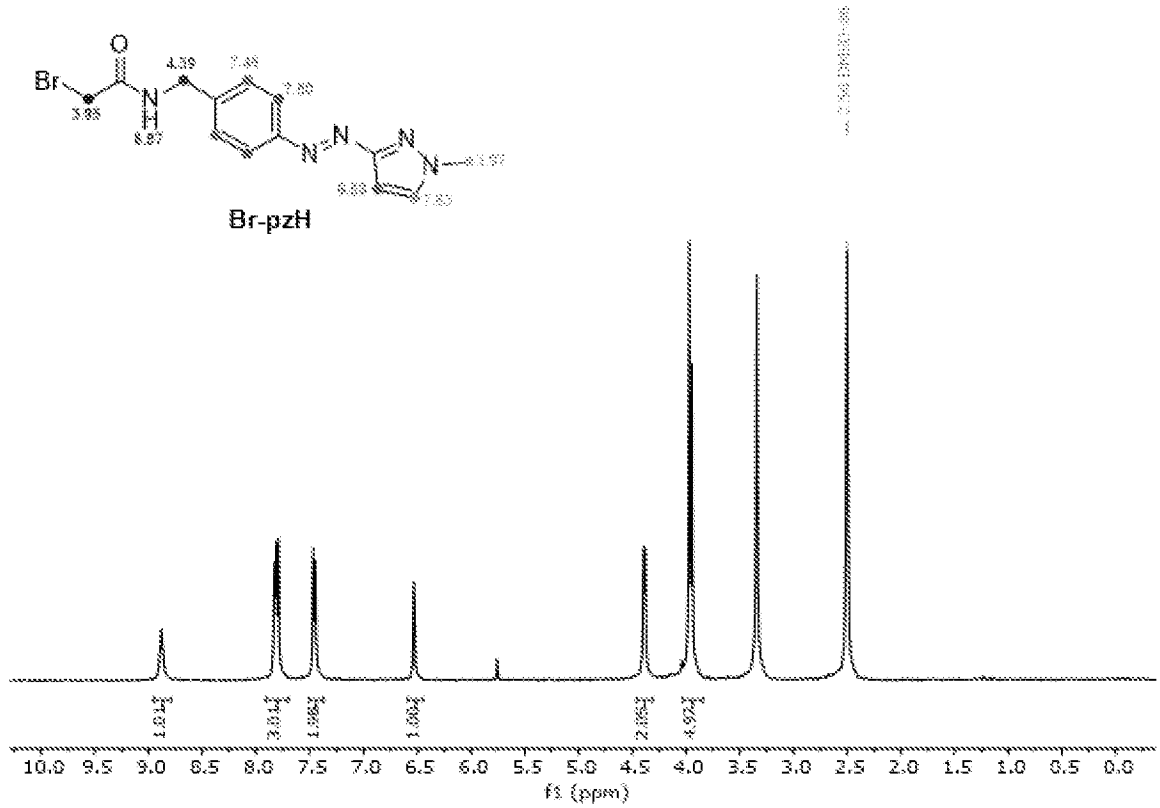
Br-pzH
10.0 9.5 9.0 8.5 8.0 7.5 7.0 6.5 6.0 5.5 5.0 4.5 4.0 3.5 3.0 2.5 2.0 1.5 1.0 0.5 0.0
f1 (ppm)

Fig. 53

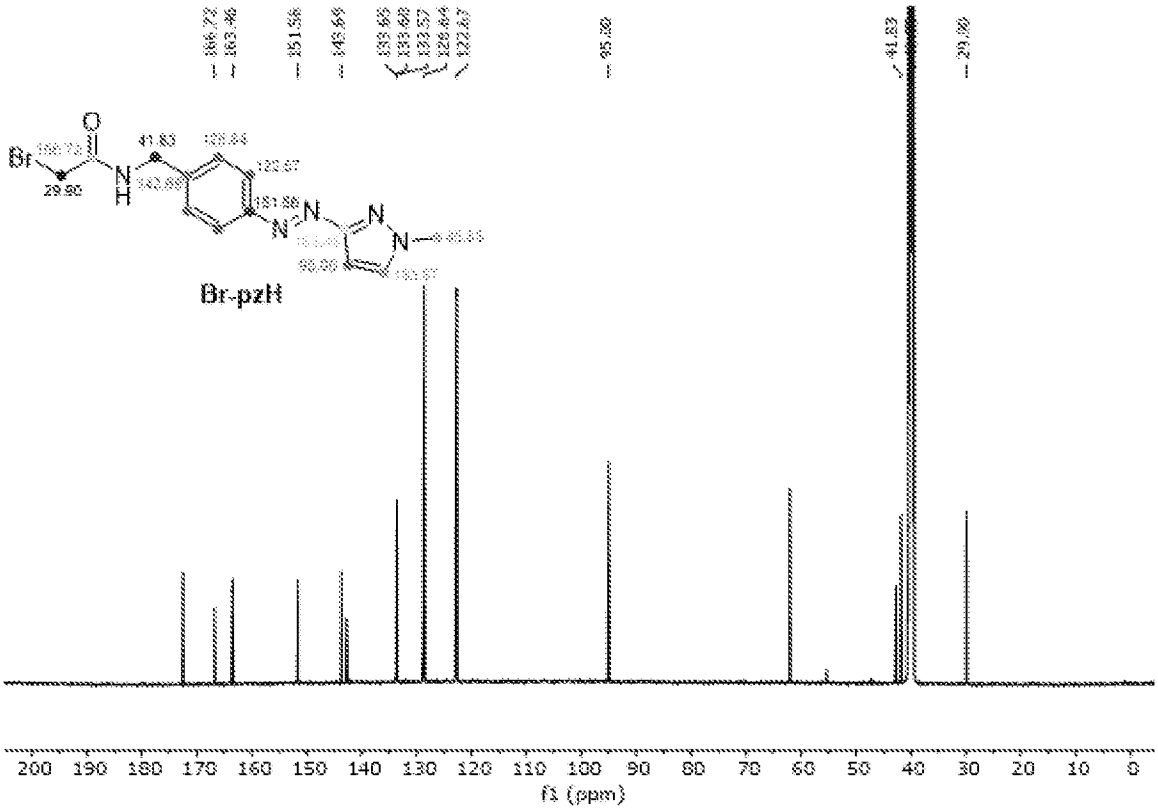
Br-pzH
200 190 180 170 160 150 140 130 120 110 100 90 80 70 60 50 40 30 20 10 0
f1 (ppm)

Fig. 54

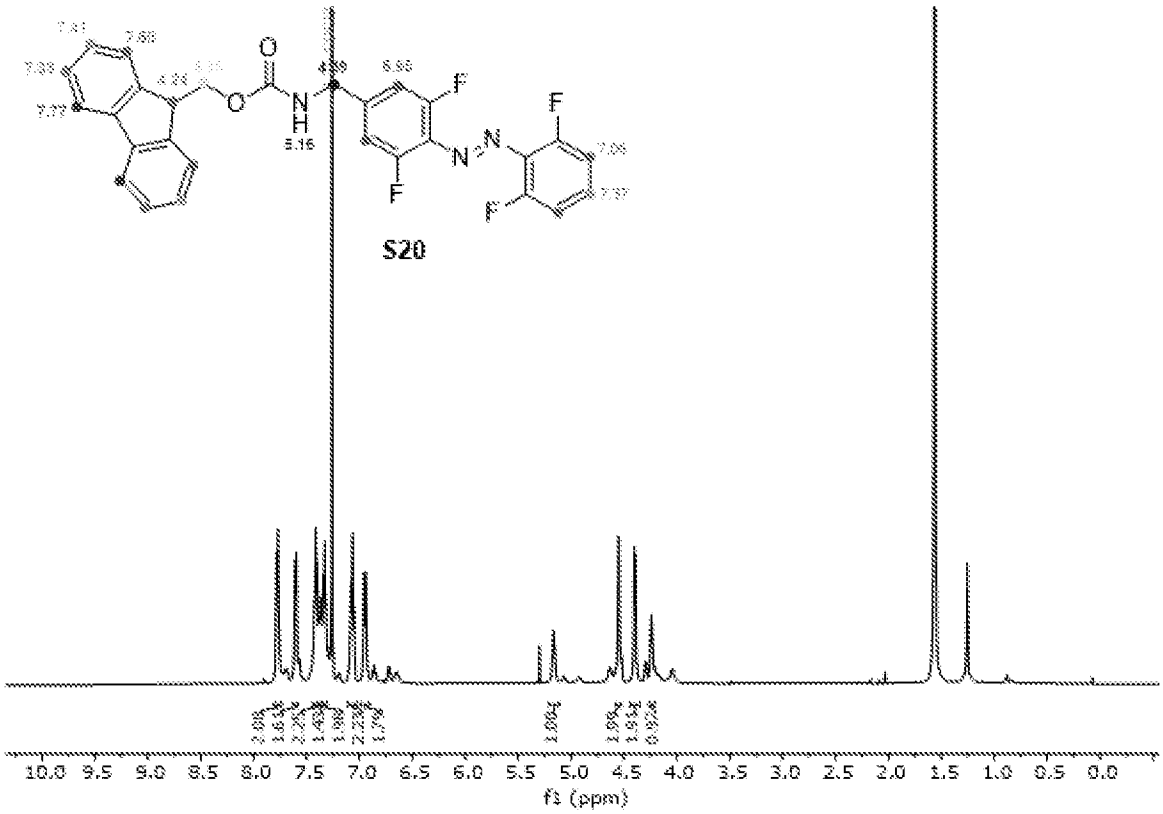
S20
10.0 9.5 9.0 8.5 8.0 7.5 7.0 6.5 6.0 5.5 5.0 4.5 4.0 3.5 3.0 2.5 2.0 1.5 1.0 0.5 0.0
f1 (ppm)

Fig. 55

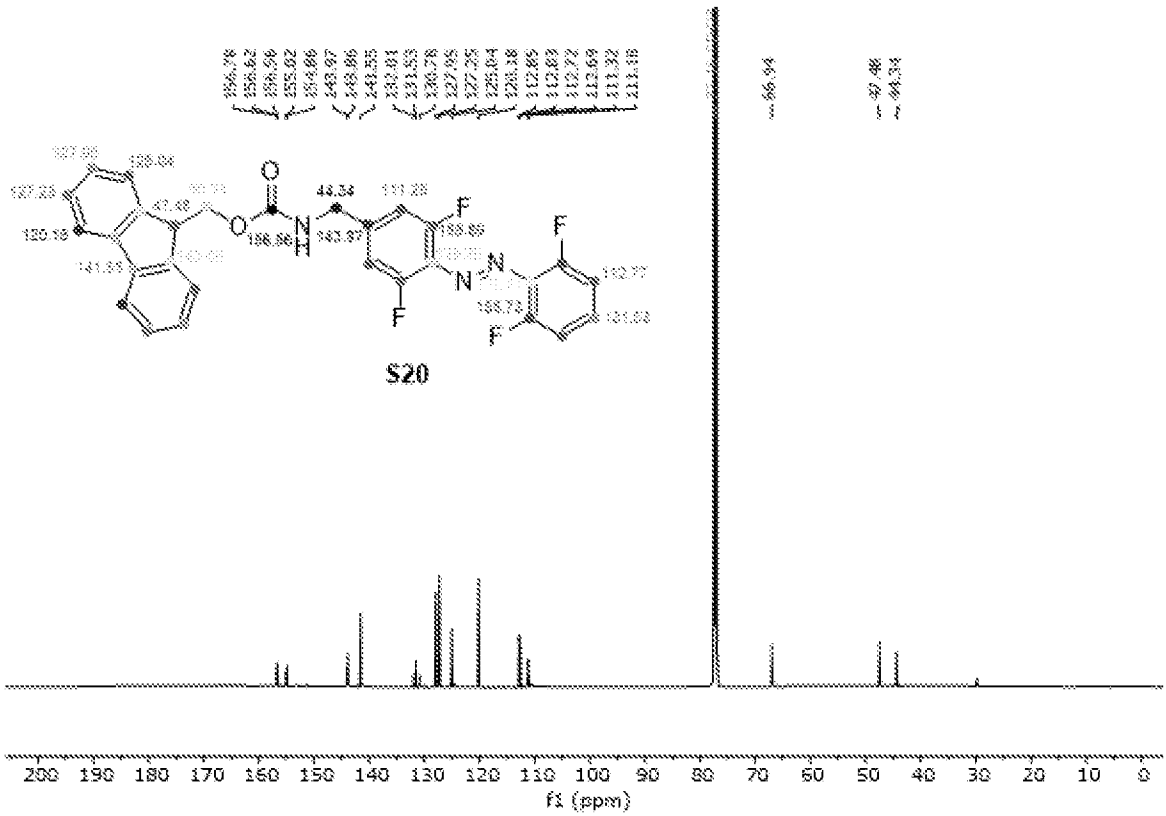
S20
200 190 180 170 160 150 140 130 120 110 100 90 80 70 60 50 40 30 20 10 0
f1 (ppm)

Fig. 56

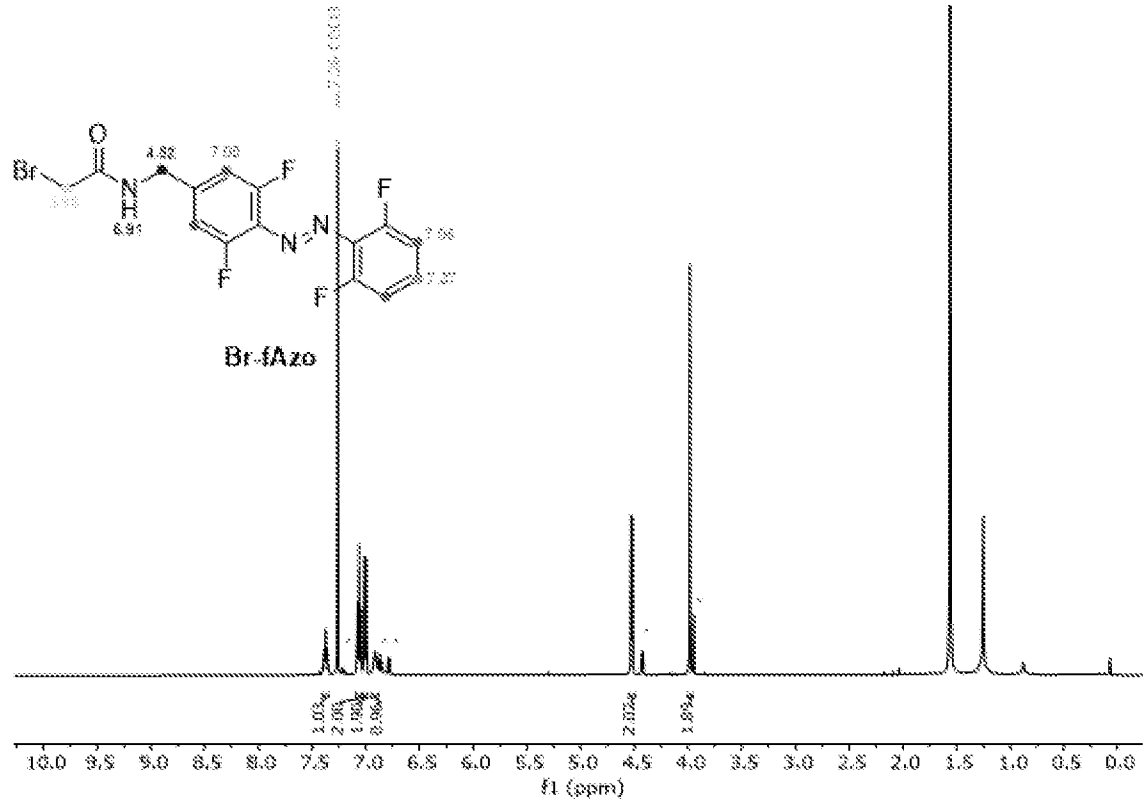

Fig. 57

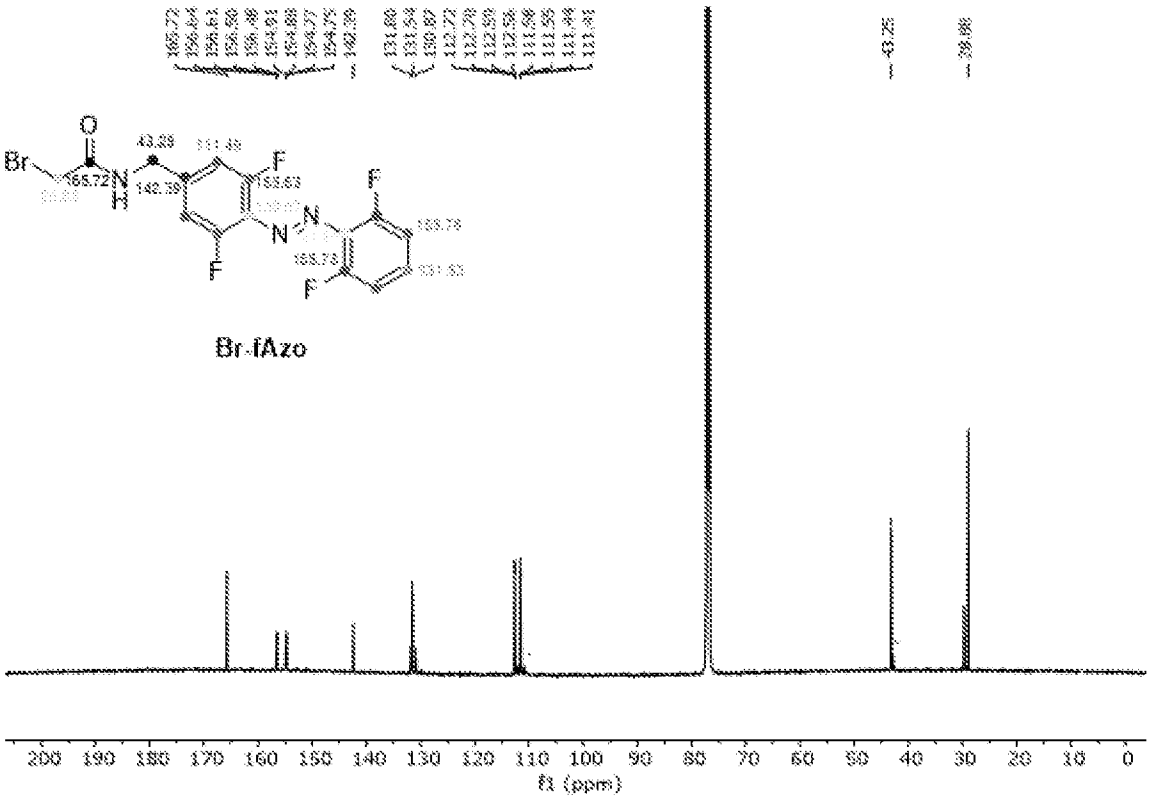

Fig. 58

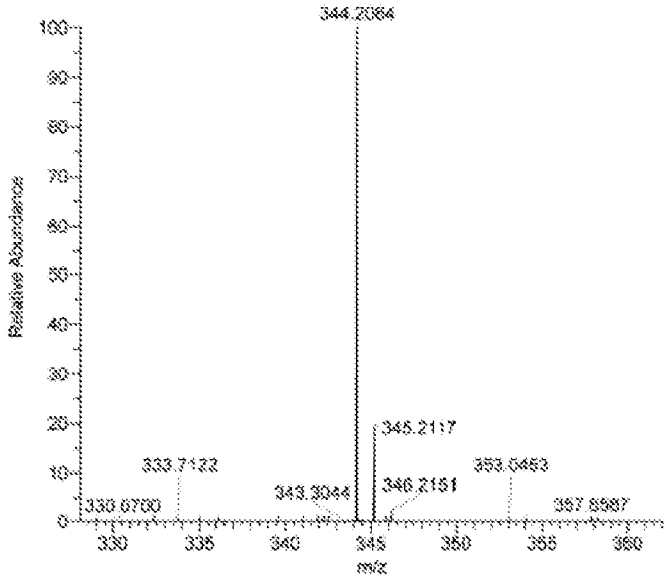

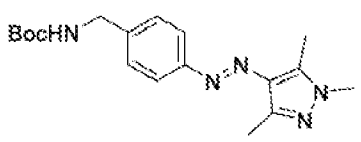

S10

Fig. 59

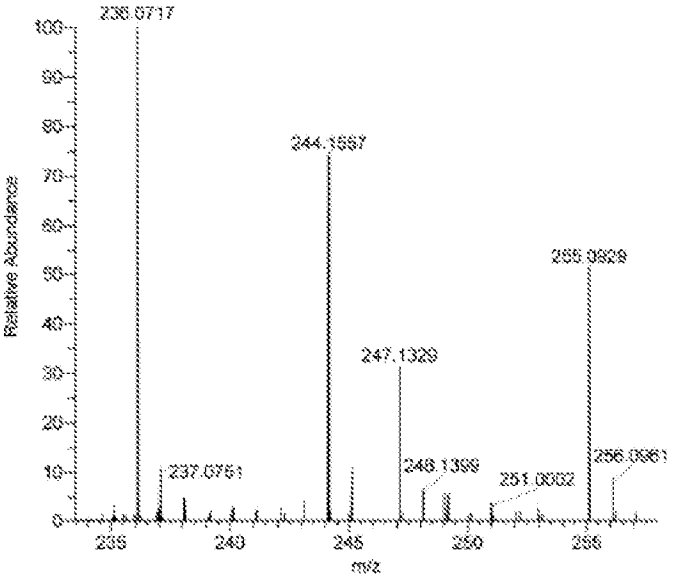

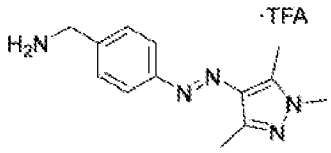

S11

Fig. 60

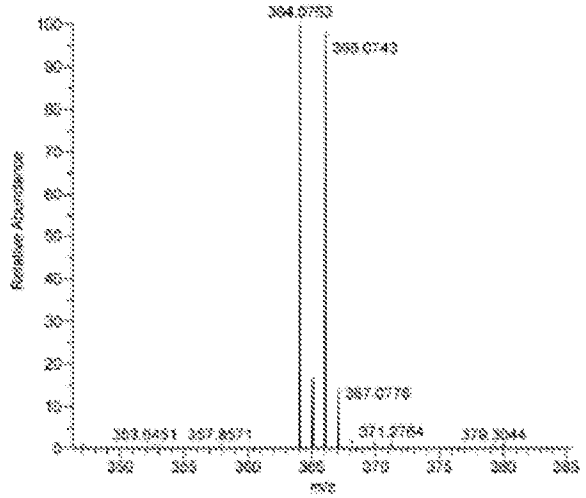

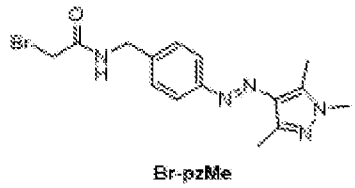

Br-pzMe

Fig. 61

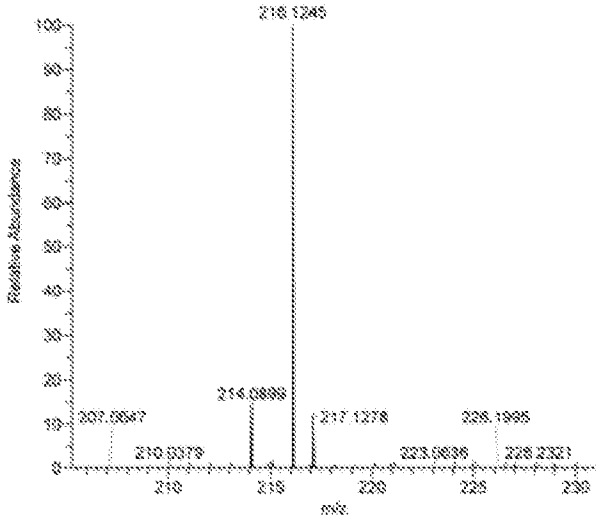

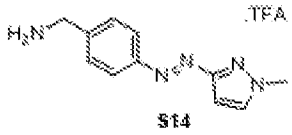

S14

Fig. 62

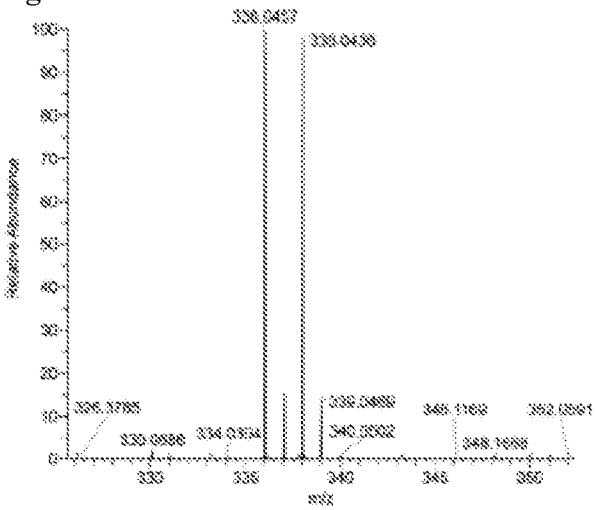

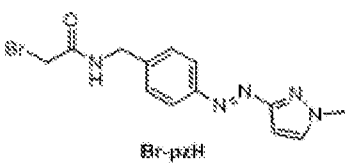

Br-pzH

Fig. 63

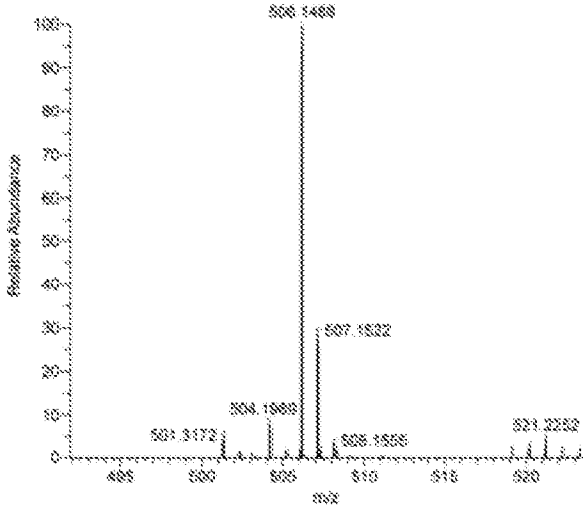

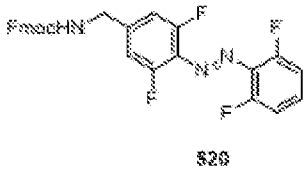

S20

Fig. 64

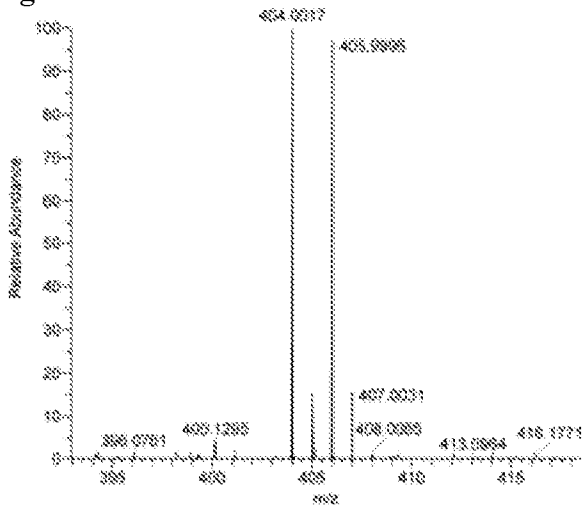

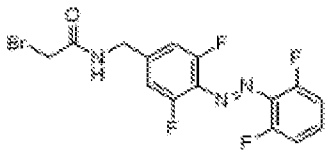

Br-fAzo

Fig. 65

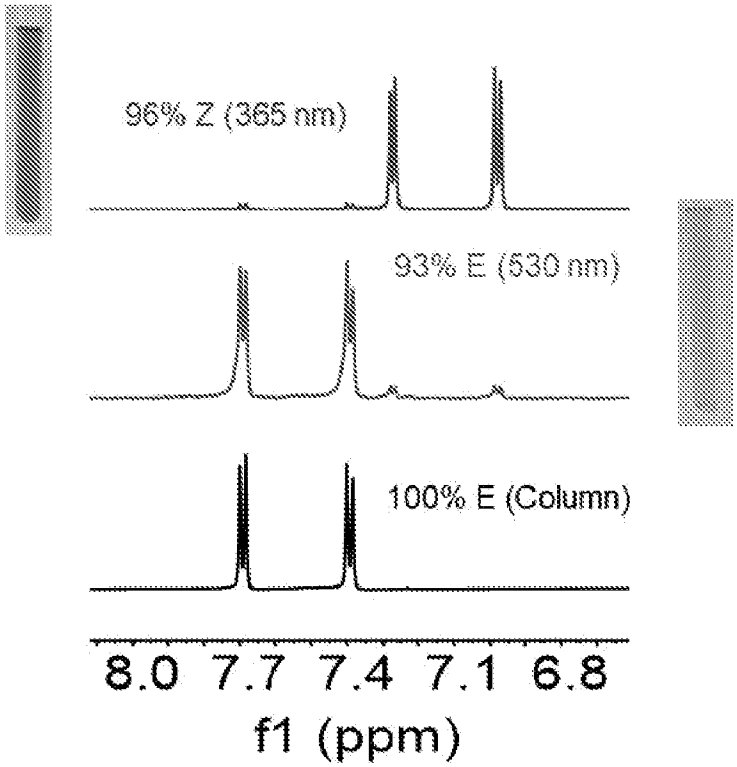
96% Z (365 nm)
93% E (530 nm)
100% E (Column)
8.0 7.7 7.4 7.1 6.8
f1 (ppm)

Fig. 66

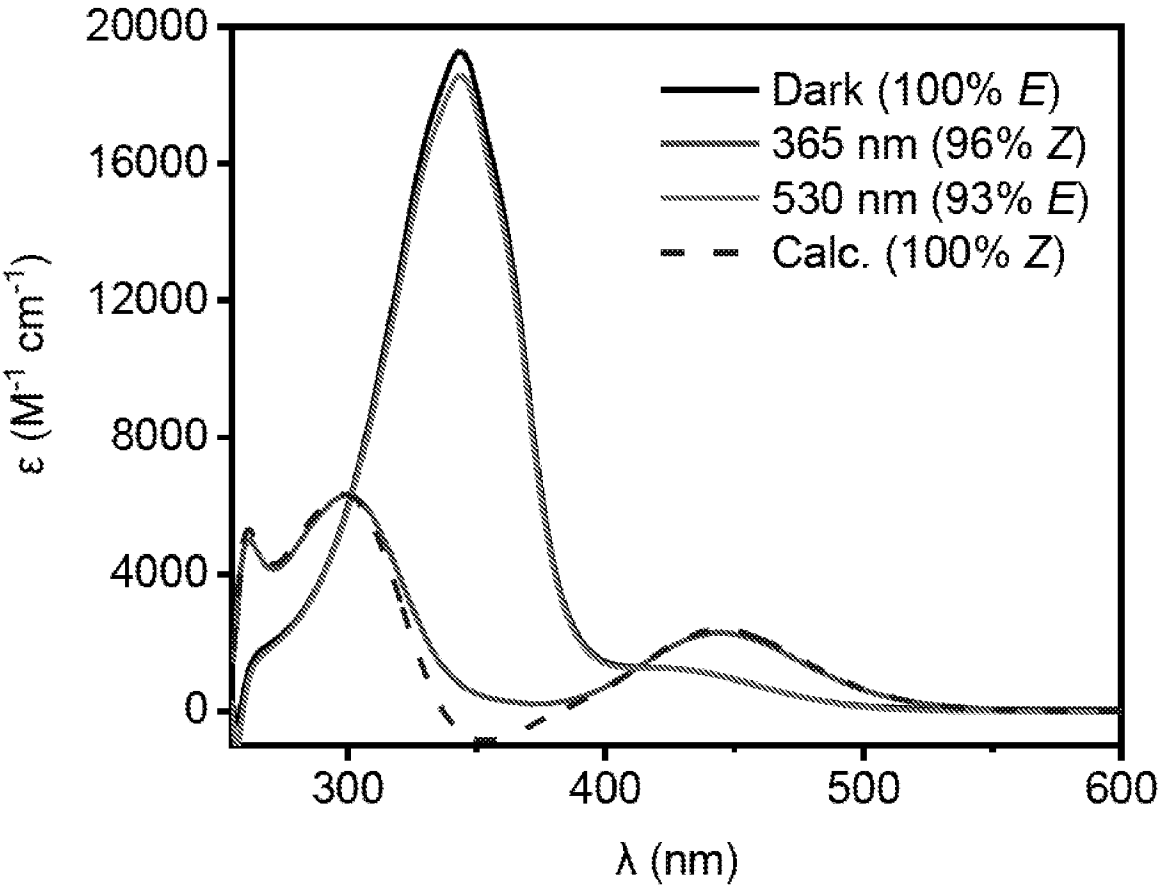
20000
16000
12000
8000
4000
0
ε (M-1 cm-1)
300
400
500
600
λ (nm)
Dark (100% E)
365 nm (96% Z)
530 nm (93% E)
Calc. (100% Z)

Fig. 67

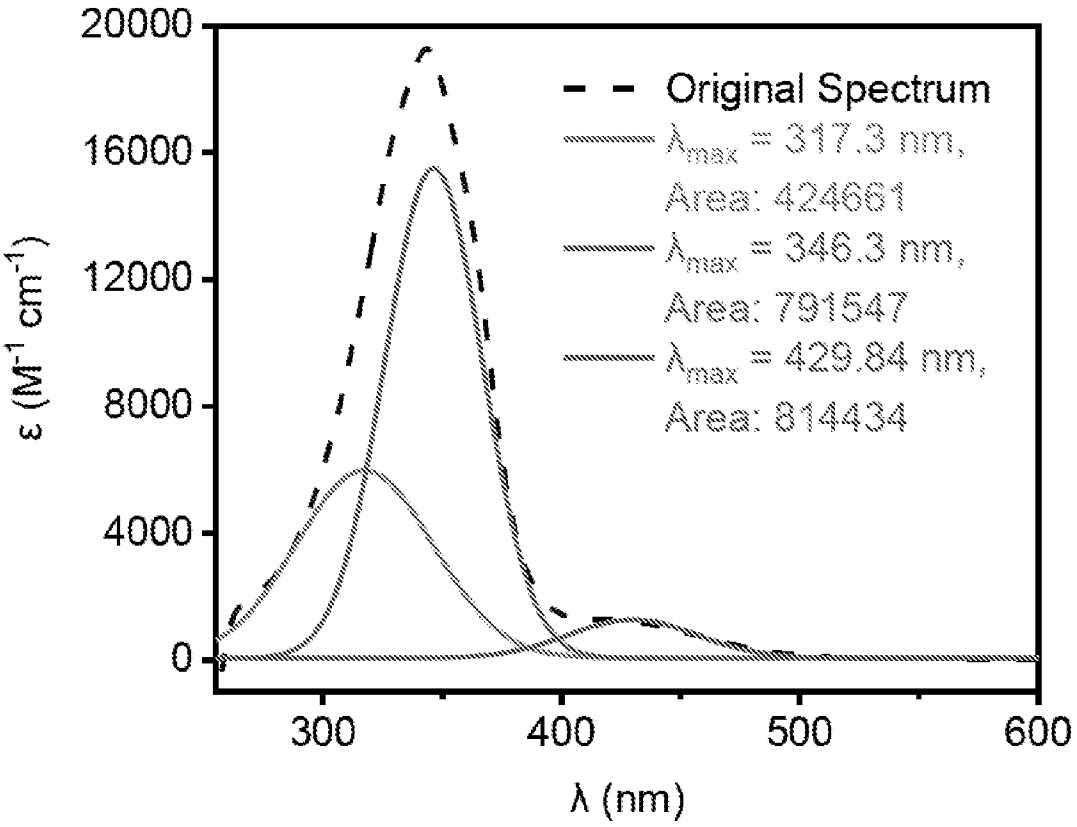
Original Spectrum
λmax = 317.3 nm, Area: 424661
λmax = 346.3 nm, Area: 791547
λmax = 429.84 nm, Area: 814434
ε (M-1 cm-1)
λ (nm)
20000
16000
12000
8000
4000
0
300
400
500
600

Fig. 68

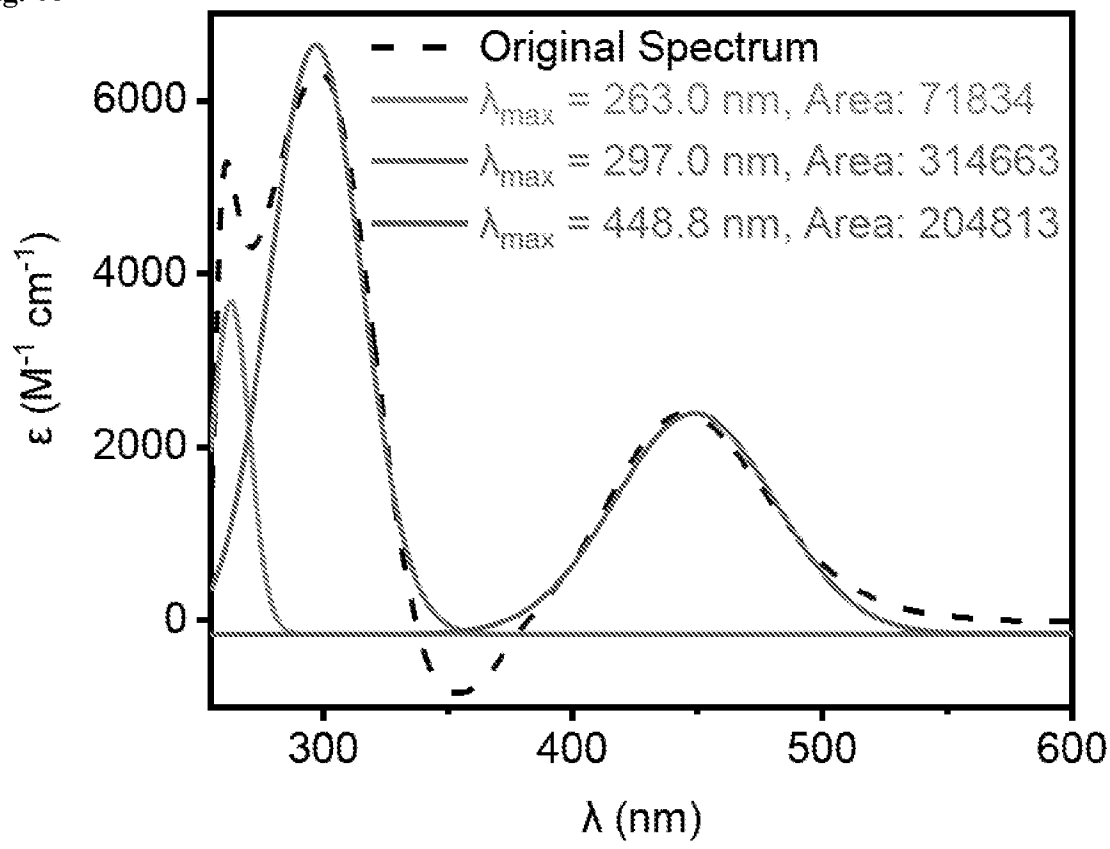
Original Spectrum
λmax = 263.0 nm, Area: 71834
λmax = 297.0 nm, Area: 314663
λmax = 448.8 nm, Area: 204813
ε (M-1 cm-1)
λ (nm)
6000
4000
2000
0
300
400
500
600

INTERNATIONAL SEARCH REPORT

International application No
PCT/GB2024/052165

A. CLASSIFICATION OF SUBJECT MATTER

INV. A61K47/54 B82Y5/00 B82Y10/00 C07D401/14 C12Q1/68
C12Q1/6869 G06N3/00

ADD.

According to International Patent Classification (IPC) or to both national classification and IPC

B. FIELDS SEARCHED

Minimum documentation searched (classification system followed by classification symbols)

A61K G06N B82Y C07D C12Q

Documentation searched other than minimum documentation to the extent that such documents are included in the fields searched

Electronic data base consulted during the international search (name of data base and, where practicable, search terms used)

EPO-Internal, BIOSIS, WPI Data, Sequence Search, EMBASE

C. DOCUMENTS CONSIDERED TO BE RELEVANT

Category*	Citation of document, with indication, where appropriate, of the relevant passages	Relevant to claim No.
X	CHANDRAMOULI BALASUBRAMANIAN ET AL: "Introducing an artificial photo-switch into a biological pore: A model study of an engineered [alpha]-hemolysin", BIOCHIMICA ET BIOPHYSICA ACTA, ELSEVIER, AMSTERDAM, NL, vol. 1858, no. 4, 29 December 2015 (2015-12-29), pages 689-697, XP029451772, ISSN: 0005-2736, DOI: 10.1016/J.BBAMEM.2015.12.030 the whole document ----- -/--	1-23

[x] Further documents are listed in the continuation of Box C.

[x] See patent family annex.

* Special categories of cited documents :

"A" document defining the general state of the art which is not considered to be of particular relevance

"E" earlier application or patent but published on or after the international filing date

"L" document which may throw doubts on priority claim(s) or which is cited to establish the publication date of another citation or other special reason (as specified)

"O" document referring to an oral disclosure, use, exhibition or other means

"P" document published prior to the international filing date but later than the priority date claimed

"T" later document published after the international filing date or priority date and not in conflict with the application but cited to understand the principle or theory underlying the invention

"X" document of particular relevance;; the claimed invention cannot be considered novel or cannot be considered to involve an inventive step when the document is taken alone

"Y" document of particular relevance;; the claimed invention cannot be considered to involve an inventive step when the document is combined with one or more other such documents, such combination being obvious to a person skilled in the art

"&" document member of the same patent family

Date of the actual completion of the international search	Date of mailing of the international search report
30 October 2024	12/11/2024

Name and mailing address of the ISA/	Authorized officer
European Patent Office, P.B. 5818 Patentlaan 2 NL - 2280 HV Rijswijk Tel. (+31-70) 340-2040, Fax: (+31-70) 340-3016	Gabriels, Jan

1

Form PCT/ISA/210 (second sheet) (April 2005)

INTERNATIONAL SEARCH REPORT

International application No
PCT/GB2024/052165

C(Continuation). DOCUMENTS CONSIDERED TO BE RELEVANT

Category*	Citation of document, with indication, where appropriate, of the relevant passages	Relevant to claim No.
X	DANIEL OFFENBARTL-STIEGERT ET AL: "A Light-Triggered Synthetic Nanopore for Controlling Molecular Transport Across Biological Membranes", ANGEWANDTE CHEMIE, WILEY - V C H VERLAG GMBH & CO. KGAA, DE, vol. 134, no. 52, 29 November 2022 (2022-11-29), page n/a, XP072612801, ISSN: 0044-8249, DOI: 10.1002/ANGE.202210886 figures 1A,1B; table S1	1,10, 14-16, 20-24
X	BREGESTOVSKI P D ET AL: "Photopharmacology: A Brief Review Using the Control of Potassium Channels as an Example", NEUROSCIENCE AND BEHAVIORAL PHYSIOLOGY, CONSULTANTS BUREAU, NEW YORK, NY, US, vol. 49, no. 2, 31 January 2019 (2019-01-31), pages 184-191, XP036710534, ISSN: 0097-0549, DOI: 10.1007/S11055-019-00713-3 [retrieved on 2019-01-31] figure 3	1,10, 14-16, 20-23
A	EP 3 771 687 A1 (UNIV GRONINGEN [NL]; ACADEMISCH ZIEKENHUIS GRONINGEN [NL]) 3 February 2021 (2021-02-03) claims 1-7	1
A	ALFORD A. JOHN ET AL: "Synthesis and Site-Specific Incorporation of Red-Shifted Azobenzene Amino Acids into Proteins", ORGANIC LETTERS, vol. 17, no. 24, 9 December 2015 (2015-12-09), pages 6258-6261, XP055606135, US ISSN: 1523-7060, DOI: 10.1021/acs.orglett.5b03268	1-21

1

INTERNATIONAL SEARCH REPORT

International application No.

PCT/GB2024/052165

Box No. I Nucleotide and/or amino acid sequence(s) (Continuation of item 1.c of the first sheet)

1. With regard to any nucleotide and/or amino acid sequence disclosed in the international application, the international search was carried out on the basis of a sequence listing:

   a. [X] forming part of the international application as filed.

   b. [ ] furnished subsequent to the international filing date for the purposes of international search (Rule 13*ter*.1(a)).

      [ ] accompanied by a statement to the effect that the sequence listing does not go beyond the disclosure in the international application as filed.

2. [ ] With regard to any nucleotide and/or amino acid sequence disclosed in the international application, this report has been established to the extent that a meaningful search could be carried out without a WIPO Standard ST.26 compliant sequence listing.

3. Additional comments:

INTERNATIONAL SEARCH REPORT

Information on patent family members

International application No
PCT/GB2024/052165

Patent document cited in search report	Publication date	Patent family member(s)	Publication date
EP 3771687 A1	03-02-2021	NONE	